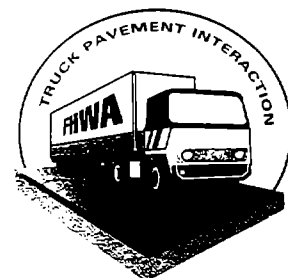# Road Simulator Study of Heavy-Vehicle Wheel Forces

U.S. Department of Transportation

Federal Highway Administration

Research and Development
Turner-Fairbank Highway Research Center
6300 Georgetown Pike
McLean, VA 22101-2296

FOREWORD

This report summarized the findings of a road simulator study performed by the Pennsylvania Transportation Institute. In this study, the effects of pertinent vehicle and road characteristics on the magnitude of dynamic tire forces generated by a two-axle truck under a variety of road and vehicle operating conditions were investigated. The influence of vehicle suspension type, tire type, tire inflation pressure, travel speed, axle static load, and road roughness on dynamic tire forces was examined. The results from this study may be used to assess the pavement damaging potential.

Charles J. Nemmers, P.E.
Director, Office of Engineering
Research and Development

NOTICE

This document is disseminated under the sponsorship of the Department of Transportation in the interest of information exchange. The United States Government assumes no liability for its contents or use thereof. This report does not constitute a standard, specification, or regulation.

The United States Government does not endorse products or manufacturers. Trade and manufacturers' names appear in this report only because they are considered essential to the object of the document.

1. Report No. FHWA-RD-98-019	2. Government Accession No.	3. Recipient's Catalog No.	
4. Title and Subtitle ROAD SIMULATOR STUDY OF HEAVY-VEHICLE WHEEL FORCES		5. Report Date September 1998	
		6. Performing Organization Code	
7. Author(s) Donald A. Streit, Bohdan T. Kulakowski, Peter E. Sebaaly, and Robert J. Wollyung		8. Performing Organization Report No. PTI 9712	
9. Performing Organization Name and Address The Pennsylvania Transportation Institute Research Office Building The Pennsylvania State University University Park, PA 16802-4710		10. Work Unit No. (TRAIS) 3C4A	
		11. Contract or Grant No. DTFH61-90-C-00084	
12. Sponsoring Agency Name and Address Office of Engineering Research and Development Federal Highway Administration 6300 Georgetown Pike McLean, VA 22101-2296		13. Type of Report and Period Covered Final Report 10/15/90-11/01/97	
		14. Sponsoring Agency Code	

15. Supplementary Notes
Contracting Officer's Technical Representative (COTR): William J. Kenis, HNR-30

16. Abstract

The main objective of the study was to investigate the effects of vehicle and road characteristics on dynamic forces applied by heavy vehicles on pavement. The work conducted under this contract can be divided into three major areas: (1) development of equipment necessary for the testing program, (2) performance of the tests, and (3) analysis of the test results. The three main pieces of equipment used in this study were a road simulator, a two-axle truck, and a wheel force transducer. The road simulator was not operational when the project began, and a major effort was devoted to first make the simulator operational and then to improve its performance to the level dictated by the research objectives of this study. A new wheel force transducer was designed, fabricated, and tested. It was demonstrated that the transducer provides a reliable and accurate tool for measuring dynamic tire forces generated by heavy trucks. The tests involving the two-axle truck were conducted on the road simulator, on three road sites in Virginia, and on an instrumented test road section. In addition, three tire types, including two popular dual tire types and a wide-base single tire, were tested. The test variables in the road simulator experiments included suspension type (steel leaf spring and air bag), tire type, vehicle speed, road roughness, axle static load, and tire inflation pressure. The air suspension generated lower dynamic loads in tests conducted on low- to medium-roughness roads at low to medium speeds. There were no benefits from using air suspension when the vehicle was traveling at higher speeds on high roughness roads. The differences between dynamic loads produced by the three tire types were relatively small. Furthermore, it was found that the dynamic tire forces were strongly affected by vehicle speed and road roughness and moderately affected by axle static loads. The effects of tire inflation pressure were very small. The results of the tests further demonstrated that the magnitude of dynamic loads is significant in comparison to static loads applied by heavy trucks to pavements. The standard deviation of the dynamic loads was over 20 percent of the static loads, whereas the peak dynamic loads measured on in-service roads exceeded the static loads by more than 200 percent.

17. Key Words Tire forces, suspension, road simulator, pavement, wheel force transducer, tire types.		18. Distribution Statement No restrictions. This document is available to the public through the National Technical Information Service, Springfield, Virginia 22161.	
19. Security Classif. (of this report) Unclassified	20. Security Classif. (of this page) Unclassified	21. No. of Pages 272	22. Price

Form DOT F 1700.7   (8-72)   Reproduction of completed page authorized

SI* (MODERN METRIC) CONVERSION FACTORS

APPROXIMATE CONVERSIONS TO SI UNITS

Symbol	When You Know	Multiply By	To Find	Symbol
LENGTH				
in	inches	25.4	millimeters	mm
ft	feet	0.305	meters	m
yd	yards	0.914	meters	m
mi	miles	1.61	kilometers	km
AREA				
in^2	square inches	645.2	square millimeters	mm^2
ft^2	square feet	0.093	square meters	m^2
yd^2	square yards	0.836	square meters	m^2
ac	acres	0.405	hectares	ha
mi^2	square miles	2.59	square kilometers	km^2
VOLUME				
fl oz	fluid ounces	29.57	milliliters	mL
gal	gallons	3.785	liters	L
ft^3	cubic feet	0.028	cubic meters	m^3
yd^3	cubic yards	0.765	cubic meters	m^3

NOTE: Volumes greater than 1000 l shall be shown in m^3.

Symbol	When You Know	Multiply By	To Find	Symbol
MASS				
oz	ounces	28.35	grams	g
lb	pounds	0.454	kilograms	kg
T	short tons (2000 lb)	0.907	megagrams (or "metric ton")	Mg (or "t")
TEMPERATURE (exact)				
°F	Fahrenheit temperature	5(F-32)/9 or (F-32)/1.8	Celcius temperature	°C
ILLUMINATION				
fc	foot-candles	10.76	lux	lx
fl	foot-Lamberts	3.426	candela/m^2	cd/m^2
FORCE and PRESSURE or STRESS				
lbf	poundforce	4.45	newtons	N
lbf/in^2	poundforce per square inch	6.89	kilopascals	kPa

APPROXIMATE CONVERSIONS FROM SI UNITS

Symbol	When You Know	Multiply By	To Find	Symbol
LENGTH				
mm	millimeters	0.039	inches	in
m	meters	3.28	feet	ft
m	meters	1.09	yards	yd
km	kilometers	0.621	miles	mi
AREA				
mm^2	square millimeters	0.0016	square inches	in^2
m^2	square meters	10.764	square feet	ft^2
m^2	square meters	1.195	square yards	yd^2
ha	hectares	2.47	acres	ac
km^2	square kilometers	0.386	square miles	mi^2
VOLUME				
mL	milliliters	0.034	fluid ounces	fl oz
L	liters	0.264	gallons	gal
m^3	cubic meters	35.71	cubic feet	ft^3
m^3	cubic meters	1.307	cubic yards	yd^3
MASS				
g	grams	0.035	ounces	oz
kg	kilograms	2.202	pounds	lb
Mg (or "t")	megagrams (or "metric ton")	1.103	short tons (2000 lb)	T
TEMPERATURE (exact)				
°C	Celcius temperature	1.8C + 32	Fahrenheit temperature	°F
ILLUMINATION				
lx	lux	0.0929	foot-candles	fc
cd/m^2	candela/m^2	0.2919	foot-Lamberts	fl
FORCE and PRESSURE or STRESS				
N	newtons	0.225	poundforce	lbf
kPa	kilopascals	0.145	poundforce per square inch	lbf/in^2

(Revised September 1993)

TABLE OF CONTENTS

TABLE OF CONTENTS

(continued)

TABLE OF CONTENTS

(continued)

LIST OF FIGURES

LIST OF FIGURES

(continued)

LIST OF FIGURES

(continued)

LIST OF FIGURES

(continued)

LIST OF TABLES

CHAPTER 1. INTRODUCTION

The progressive deterioration of civil infrastructure has become an increasingly critical area in government-sponsored research in the United States and around the world because of its strategic importance for regional and national economies and because of the immense financial resources consumed by the construction and maintenance of roads, bridges, and airport runways. As road wear is inevitable, the extent of the wear and the rate at which it progresses may vary considerably depending on many factors determined by both traffic and road characteristics and on the manner in which vehicles and roads interact. One of the main factors contributing to road damage is the dynamic loading applied by the tires of heavy vehicles to road pavements.

The main objective of this study was to investigate the effects of pertinent vehicle and road characteristics on the magnitude of dynamic tire forces generated by a two-axle truck under a variety of road and vehicle operating conditions. The test variables included the vehicle's suspension type, tire type, tire inflation pressure, travel speed, axle static load, and road roughness. To accomplish the objectives of the study, the following tasks were performed:

A. Development of a test program.
B. Conduct of the test program.
C. Analysis of test data and calibration.
D. Preparation of interim reports.
E. Preparation of draft final report and technical summary.
F. Submission of final report and technical summary.

The research tasks delineated in the initial contract were modified several times in response to unexpected problems and additional research needs identified in the course of the study. The most substantial modifications included the addition of the

work that was necessary to make the vehicle hydraulic shaker system fully operational and the design of the new wheel-force transducer.

This report describes all of the research performed and all of the principal research results obtained in this study. Additional information can be found in two Interim Reports[1,2] and in the Equipment Report.[3] The contents of this final report are organized into nine chapters. Chapter 2 describes the test equipment, including a two-axle truck instrumented with accelerometers, linear-variable displacement transducers (LVDT's), strain gauges, and an on-board computer data acquisition system; the servo-hydraulic shaker system (road simulator), called DYNTRAC; the additional equipment used in tests conducted on in-service roads in Virginia; and the equipment used in tests conducted on a section of pavement instrumented with strain gauges to measure pavement response to dynamic tire forces. Chapter 3 presents the test program followed in tests conducted on DYNTRAC, on in-service roads, and on an instrumented road section. Chapter 4 describes the design, development, and testing of wheel-force transducers. Chapter 5 is devoted to the measurement and identification of parameters of several linear and nonlinear mathematical models of truck dynamics. In chapter 6, the experimental characteristics of the three tire types, including two types of dual tires and a wide-base single tire, are presented. The measurements of tire characteristics were performed by the Goodyear Tire and Rubber Company. The results of the DYNTRAC and field tests are presented in chapter 7. Chapter 8 describes the results of data analysis performed to determine the effects of the test variables on dynamic tire forces and to assess the pavement damaging potential of the test vehicle. Finally, the principal research accomplishments of this study, as well as conclusions and recommendations for future research, are summarized in chapter 9.

CHAPTER 2. TEST EQUIPMENT

A wide variety of equipment was required to pursue this study. The major items provided by the Federal Highway Administration (FHWA) at the beginning of the project included:

- DYNamic TRuck ACtuator System (DYNTRAC).
- Single-axle flat bed truck.
- Test pavement with instrumentation.
- Wheel-force transducer (WFT) prototype.

In addition to the procurement of equipment, considerable effort was expended to improve the performance and capabilities of the systems associated with this project. This work involved redesigning and retrofitting mechanical and electrical systems, developing new software, and creating procedures for performing complex test plans. Some of the more significant tasks included:

- Changing the test vehicle wheel configuration from cast spoke to disk wheels.
- Changing the test vehicle leaf spring suspension to air suspension, and then back to leaf spring.
- Continuous upkeep and improvement of DYNTRAC operation, including hydraulic, mechanical, and electrical system modification.
- Rewriting major portions of the DYNTRAC control computer program to facilitate real-time profile simulation.
- Completely redesigning and testing the WFT prototype.

The following major items were purchased or fabricated in order to complete the project tasks:

- Four dynamic wheel scales for DYNTRAC.
- Longitudinal and lateral restraint systems for DYNTRAC.

- Data acquisition systems for vehicle, DYNTRAC, and instrumented pavement testing.
- Air compressor and accessories for changing/inflating truck tires.
- Three additional WFT's based on the prototype redesign.
- Sensors, signal conditioners, and power supplies for vehicle instrumentation.

More detailed descriptions of equipment, system improvements, and design modifications can be found in the two Interim Reports[1,2] that were submitted through the course of the project and in the Equipment Report.[3] The subsequent sections of this chapter describe the operation, performance, and major work associated with the test vehicle, DYNTRAC, and the instrumented pavement. WFT development is discussed separately in chapter 4.

2.1 TEST VEHICLE AND ASSOCIATED INSTRUMENTATION

The vehicle used for dynamic wheel-force research was a Navistar International S series, flat-bed, single-axle truck, model 1957, assembled in 1980. A side-view schematic of the truck is shown in figure 2-1. The front suspension is a constant-rate leaf spring assembly. A sketch of the assembly is shown in figure 2-2. A progressive-rate leaf spring assembly is used on the rear axle. Table 2-1 contains the basic geometric characteristics and load limits of the test vehicle.
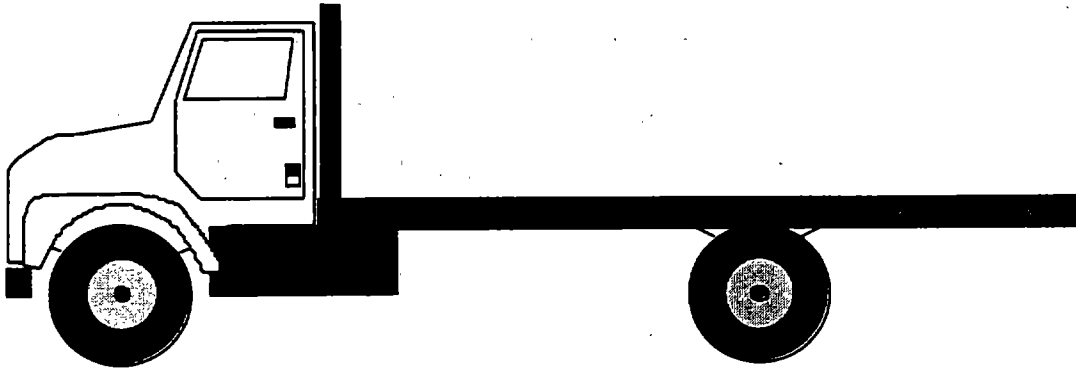
Figure 2-1. Single-axle flat-bed truck used in the study.

MT-23336
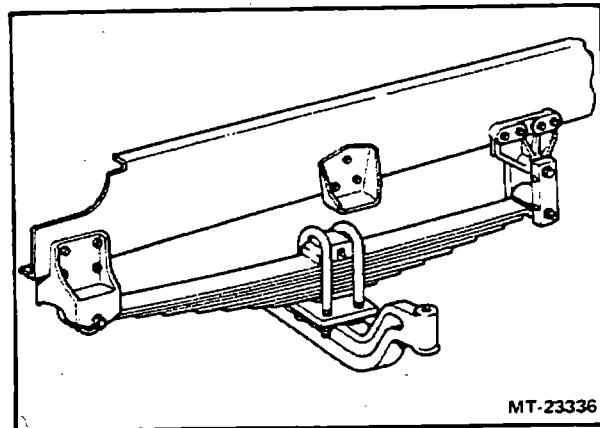
Figure 2-2. Constant-rate leaf spring assembly (front axle).

Table 2-1. Geometry and load limits of test vehicle.

Wheel Base	6.48 m (21.25 ft)
Wheel Track	2.05 m (6.71 ft)
Truck Length	10.00 m (32.83 ft)
Bed Length	7.39 m (24.25 ft)
Bed Width	2.44 m (8.0 ft)
Gross Vehicle Weight	150,677 N (33,680 lb)
Empty Weight	71,067 N (15,970 lb)
Manufacturer Allowable Load	79,611 N (17,890 lb)
DOT Allowable Load	50,018 N (14,890 lb)

Hardware and instrumentation associated with the vehicle testing configuration are briefly discussed below. Such items include suspension type, tire type, vehicle-mounted sensors, and the vehicle's data acquisition system.

2.1.1 Suspension

Two suspension types were tested using the rear axle of the truck: progressive rate-leaf springs and air suspension with tapered leaf springs. The original suspension configuration is the progressive-rate spring, which is shown in figure 2-3. The springs are shown in loaded and unloaded conditions. The spring rate of this suspension changes with the effective length of the assembly. This is accomplished by a sliding contact on one end of the spring. As the vehicle is loaded, the effective leaf length is shortened when the point of contact moves toward the center of the spring.
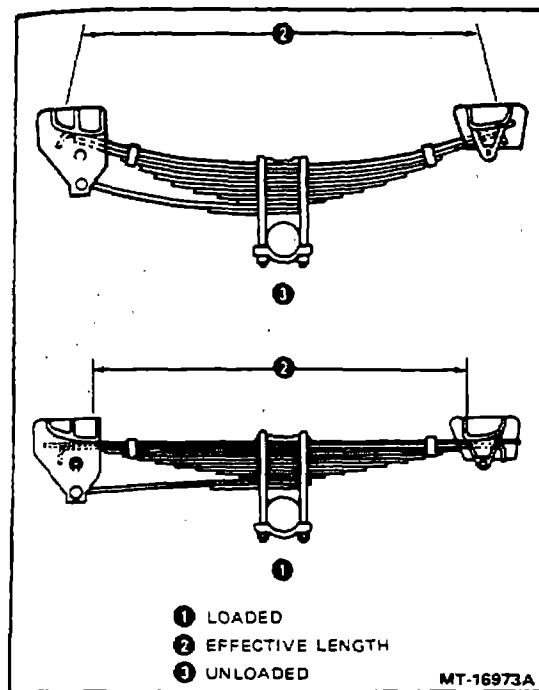
Figure 2-3. Progressive-rate leaf spring assembly.

After all tests were performed with the leaf spring configuration, the rear-axle suspension was converted to an air suspension. Figure 2-4 is a drawing of the air spring assembly. The suspension consists of the following major components:

- Air spring (bag) - replaces the steel leaf springs (typically filled to 689.5 kPa [100 psi]).

- Height control valve - automatically fills and empties the air bag, keeping the ride height constant.

- Tapered leaf spring - transfers load directly to the axle; absorbs road shock and horizontal loads.

- Shock absorbers - assist the air bags with ride comfort and damping.

- Torque rods - minimize axle windup caused by loads transferred by driveline torque and braking.

7
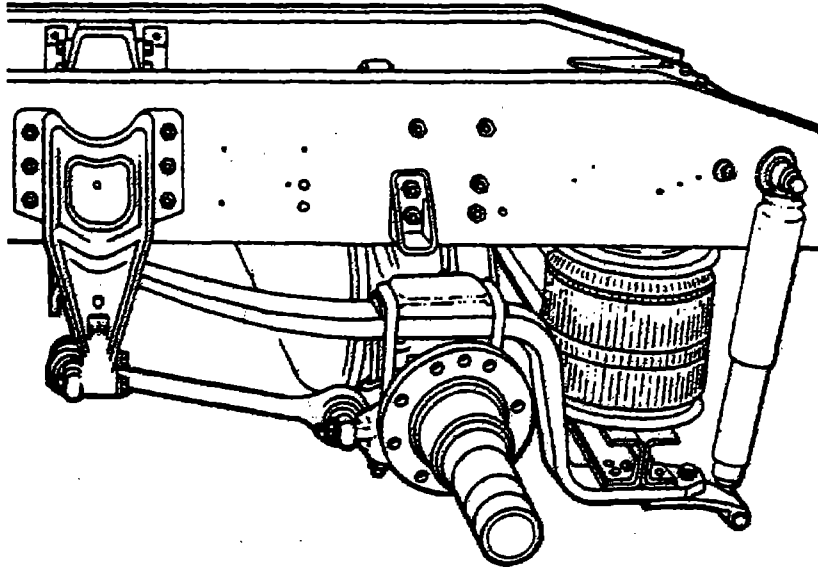
Figure 2-4. Air suspension configuration.

2.1.2 Tires

A literature review and market evaluation were conducted to determine the current market share distribution of the various truck tire types and sizes. As a part of this survey, several tire manufacturers were contacted, including Goodyear, Michelin, and Firestone. The Rubber Manufacturers Association was also contacted. The information gathered from these sources is summarized in table 2-2.

Table 2-2. Market share distribution for various tire types.

		Percentage of the Market		
Tire Size	Tire Description	1987	1989	Percentage Change *
295/75R22.5 275/80R22.5	Low-Profile Radial	24.2	30.8	27.3
11R22.5	Conventional Radial	23.0	19.7	-14.3
185/75R22.5 275/80R24.5	Low-Profile Radial	23.3	19.4	-16.7

*Percentage Change = Percentage of Market (1989) - Percentage of Market (1987) *100
Percentage of Market (1987)

8

As a result of the survey, three tire types were selected for the testing program. Table 2-2 indicates that low-profile radials represent the most common truck tire type that is in use today. One of these low-profile radials, the 295/75R22.5, was chosen for use in this study. The second most common tire type, the 11R22.5 conventional radial, was also chosen for testing. The third tire that was included in the study was not chosen on the basis of popularity or market share, but rather, because of its recent increase in market share and also because of its distinct differences from the conventional and low-profile radial, dual-wheel configuration. This third tire type, wide-base or super-single radials, is generally considered to be particularly damaging to pavement. In fact, many States are currently considering legislation to either allow or ban the use of wide-base tires on highways.

2.1.3 Vehicle Instrumentation

The test vehicle was instrumented with sensors to measure axle strain, axle acceleration, truck chassis acceleration, and suspension deflection. Criteria used for specifying instrumentation included hardware/software compatibility, price, performance characteristics, data acquisition speed, flexibility, number of channels, and system reliability and history. The power supply, signal conditioning equipment, and data acquisition equipment were mounted in the cab of the truck.

The typical vehicle configuration used during tests included the following sensors:

- LVDT's measuring the displacement between the end of each axle and the body of the truck.

- Accelerometers located at the end of each axle.

- Accelerometers mounted under each corner and under the center of the truck bed.

- Redundant, thermally isolated accelerometer mounted on the right end of the rear axle.

- Half bridge strain gauge circuits placed at the end of each axle.

Displacement transducers were selected for measuring the relative movement between the axle and chassis. A displacement range of 254 mm (10 in) was required to measure the dynamic suspension deflection. Although string potentiometers were considered, the cycle life requirements exceeded the cycle life ratings of such instruments. LVDT's accommodated the required cycle life.

The thermally isolated accelerometer was included to identify any potential temperature effects on acceleration measurements. No significant temperature influences on acceleration measurement were observed during this study. The location of axle instrumentation is shown in figure 2-5 and figure 2-6.

An infrared (IR) emitter-receiver was also used during field tests for vehicle position and velocity measurement.
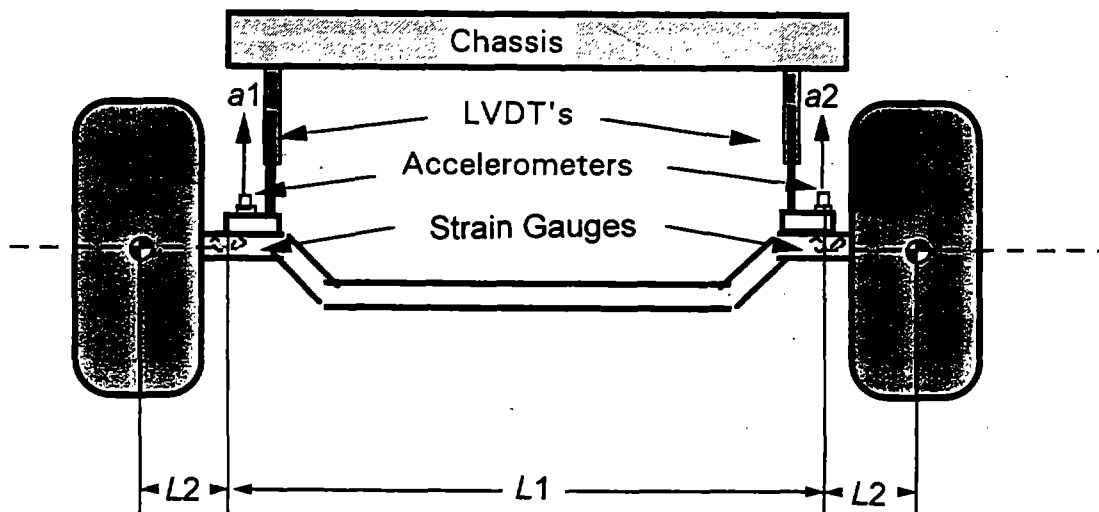
Figure 2-5. Front-axle instrumentation.
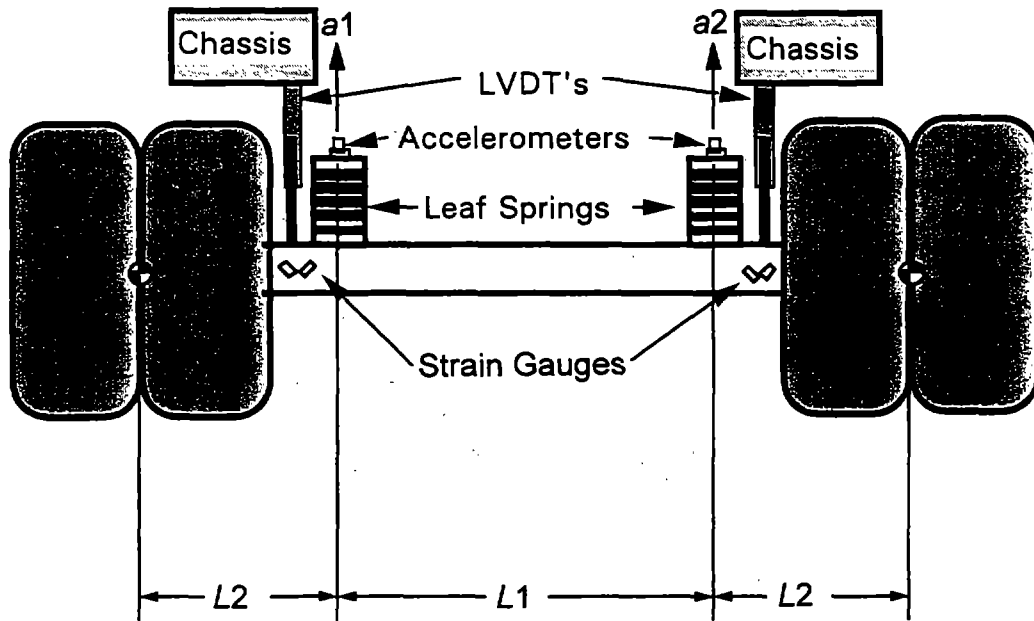
Figure 2-6. Rear-axle instrumentation.

Data acquisition was accomplished using a portable computer with a 48-channel analog input board and data acquisition software. The vehicle data acquisition system is shown schematically in figure 2-7.
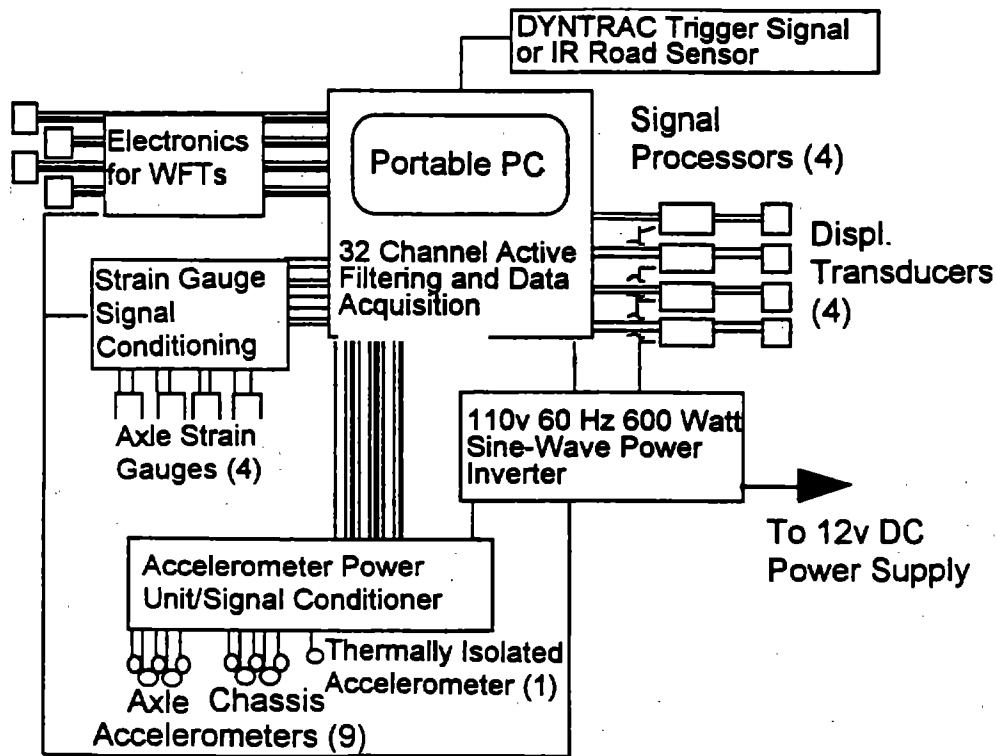
Figure 2-7. Vehicle data acquisition system schematic.

During most dynamic tests, data were recorded from all vehicle sensors. Two exceptions occurred early in the testing program and during the last set of tests. In the first exception, data from the LVDT sensors were unavailable during the December 1994 tests due to damaged cables. In the second exception, only data pertaining to the dynamics of the left side of the vehicle were recorded during testing in the summer of 1993. This was due to data acquisition system limitations at that time.

Typical static strain gage calibrations are shown in figures 2-8 and 2-9. These calibrations changed during the testing program due to changes in strain gage conditioning equipment and the replacement of the rear-axle gages after the suspension was changed. Note that, in figure 2-4, the front-right-axle strain increased with increasing load, while the front-left-axle strain decreased with increasing load. This difference reflects the way in which the strain gages were wired to the strain gage conditioners. Calibration values for other vehicle sensors are shown in table 2-3.
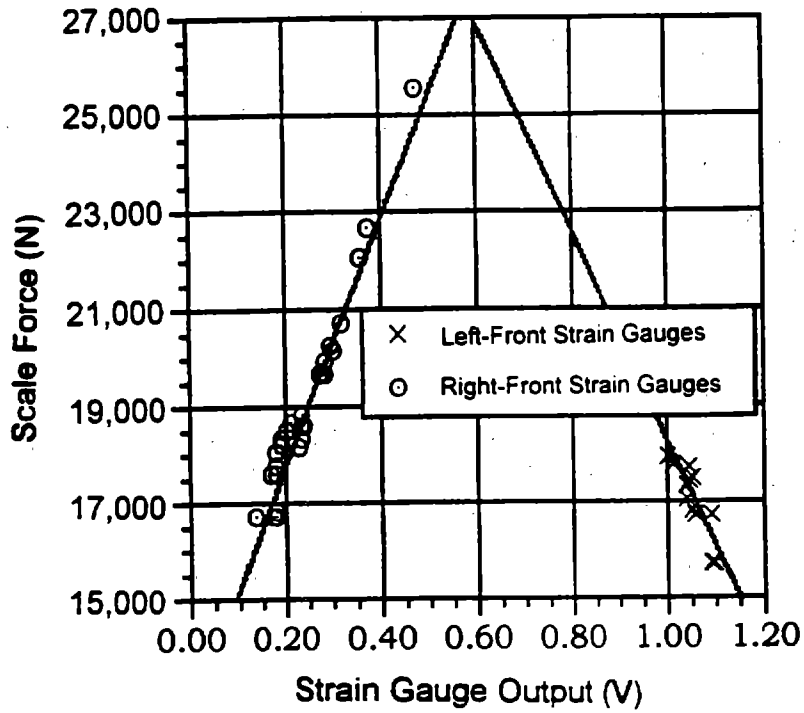
Figure 2-8. Front-axle strain-gauge calibration.
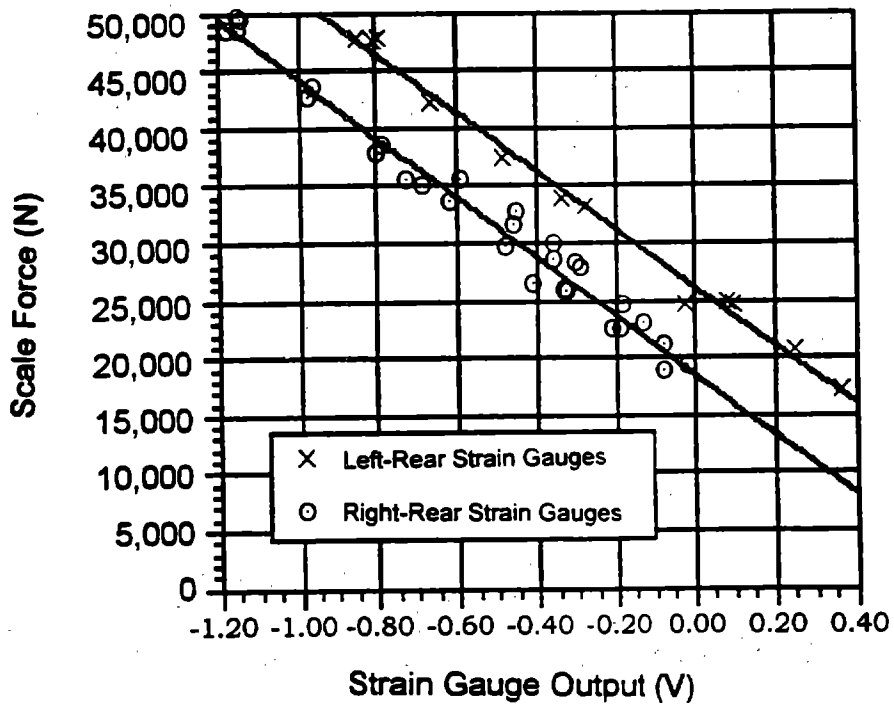
Figure 2-9. Rear-axle strain-gauge calibration.

13

Table 2-3. Vehicle sensor calibrations.

Sensor Type	Calibration Value	Output Units	Notes
Piezo Crystal Accelerometer	90 mV/g	g's	1 g = 9.81 m/s²
Linear-Variable Differential Transducer (LVDT)	25.4 mm/V	millimeters	Position measurement
Strain Gauges Arranged to Measure Shear	see figure 2-8 and figure 2-9	Newtons	For wheel force, outboard mass inertia must be added

Dynamic wheel forces were calculated using axle strain, wheel mass, and wheel acceleration data. Strain gauges were bonded near the ends of the front and rear axles. The gauges were mounted on the axle between the wheel and the location of suspension attachment, as shown in figure 2-6. The gauges were oriented to measure shearing strain in the axle. Axle strain was calibrated to indicate shearing force, F_g, at the gauge location. To calculate the force between the tire and pavement, it is necessary to first calculate the inertial force due to acceleration of outboard mass. Outboard mass, m, includes a portion of the axle, brake drum, wheel assembly, and tires.

Outboard mass acceleration was calculated with the use of data from two axle-mounted accelerometers. To illustrate this process, consider the front-axle assembly (see figure 2-5). The outboard mass center of gravity location is estimated to be at the center of the wheel assembly. The distance between the tire center of gravity location and strain gauge/accelerometer location is $L2$, and the distance between accelerometers is $L1$. Measurements from the left and right accelerometers are $a1$ and $a2$, respectively. The vertical acceleration of the left outboard mass is given by:

$$a_{wheel} = a2 + \frac{L1 + L2}{L1} \cdot (a1 - a2) \qquad (2\text{-}1)$$

The force between the tire and pavement, F_p, is then estimated as

$$F_p = m \cdot a_{wheel} + F_g \qquad (2\text{-}2)$$

2.2 DYNTRAC AND ASSOCIATED INSTRUMENTATION

Experimental data were obtained using a DYNTRAC road simulator located at the Turner-Fairbank Highway Research Center in McLean, Virginia. The simulator consists of a four-post servo-hydraulic system; position, acceleration, and force sensors with data acquisition system; and a control computer capable of inputting road profiles to the servo-hydraulic controllers. A schematic drawing of the DYNTRAC system is shown in figure 2-10.
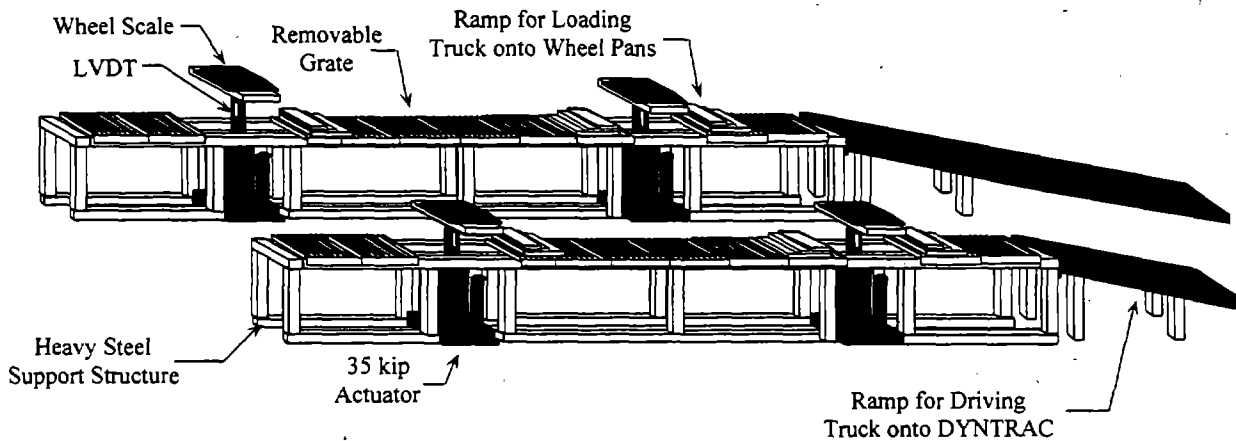
Figure 2-10. DYNTRAC system.

2.2.1 Mechanical, Servo-Hydraulic, and Control Systems

The DYNTRAC system includes a steel frame so vehicles can drive up onto hydraulic actuators. The frame is constructed such that hydraulic actuators can be moved to accommodate several axle configurations. The frame was attached to the floor of the lab by rebar "bolts" that extended through the laboratory floor. Using a forklift, steel ramps were temporarily positioned in front of DYNTRAC for mounting and

removing vehicles. Removable steel grates on top of the frame provided vehicle support. Wooden ramps were used to step the vehicle up from the grates to the actuator wheel pans. The wheel pans, on which the wheels of a vehicle are positioned during testing, were rigidly connected to actuator pistons.

A wheel-restraint system was used to keep the vehicle properly positioned on the actuators. A fore/aft wheel restraint consisted of a heavy steel bracket bolted to the front and rear of each wheel pan. Restraint brackets were adjustable to tire size and wheel position. The heavy fore/aft restraint system occasionally stripped out the threaded holes in the wheel pans. Periodic inspection and replacement of fasteners addressed this problem. The original lateral restraint consisted of a steel bracket bolted to the top surface of each wheel pan and adjacent to the outside of each tire set. This bracket interfered with the placement of retrofitted dynamic wheel scales. Additionally, front wheel pans rotated as much as 45° during dynamic testing. Because of these limitations, a new lateral restraint system was designed and implemented. The new lateral restraint supported a disk that contacted a tire sidewall. The replacement lateral restraint system worked effectively; it allowed mounting of dynamic wheel scales onto the wheel pan assembly and reduced wheel pan rotation.

The DYNTRAC servo-hydraulic components were powered by hydraulic pumps located in the basement of the lab. The pumps supplied hydraulic fluid at a pressure of 20,670 kPa (3 kip) to two service manifolds that filtered and distributed fluid to the servovalves. The manifolds also moderated pressure fluctuations in the fluid supply. The servovalves in each of the four actuators controlled the volume and direction of the fluid that was delivered to the actuators. The servovalves were controlled by electronic signals from the control console.

All four actuators were 160-kN (35-kip) rated with a 31.3-cm^2 (4.85-in^2) piston area. An internal LVDT measured piston rod position. The LVDT signal was used in actuator control. The LVDT signal was recorded during testing as a measure of the actual road profile input to a vehicle. Rear actuators were augmented with a static weight equilibrator system. Nitrogen accumulators provided a supporting force that was

approximately equal to static wheel load. Rear-wheel actuators, therefore, were needed only to provide the dynamic force component during testing.

The control computer sent an analog voltage signal representing the simulated road profile to the control console. The control console operated the servovalve on the basis of the computer input and on console operational settings. Console operational settings for each actuator are described in table 2-4.

Table 2-4. Actuator controls.

Control	Description
Set Point	Controls the static mean level offset to the actuator. Can also be used to manually raise and lower the actuators.
Span	Scales the amplitude of the actuator output with respect to the dynamic input (0 - 100% scale).
Gain	Adjusts the forward gain of the servo control loop.
ΔP	Controls the amount of control signal correction relative to the differential pressure in the actuator.
Rate	Adjusts the amplitude of the first derivative of the feedback signal.
Controller Card	Contains potentiometers for gain, symmetry, and phase of transducer output (can be adjusted by manufacturer representative only).

The performance of each actuator is determined by a control loop that uses piston position and differential pressure as feedback signals to the controller. These settings can be used to tune the system so that piston displacement closely approximates the road profiles generated by the control computer. A flow chart of the operation of a single actuator is shown in figure 2-11. Figure 2-12 illustrates the performance of the left-rear actuator. The two signals shown in figure 2-12 are the desired road profile as generated by the control computer (actuator input) and the actual displacement of the actuator piston (actuator output). This test simulated a 48-km/h (30-mi/h) run over a medium-roughness road with an international road roughness index (IRI) (further discussed in chapter 3) of 2.6 mm/m (164 in/mi). No correction has

17

been applied to achieve the actuator response shown in figure 2-12. Ideally, the actuator output should be the same as the road profile. Figures 2-13 through 2-15 show actuator frequency response characteristics given a white noise input with a frequency cutoff of 50 Hz. The frequency response plots demonstrate that actual DYNTRAC wheel pan displacement (actuator output) closely resembles the desired road profile (actuator input). The transfer function indicates good performance out to approximately 20 Hz.
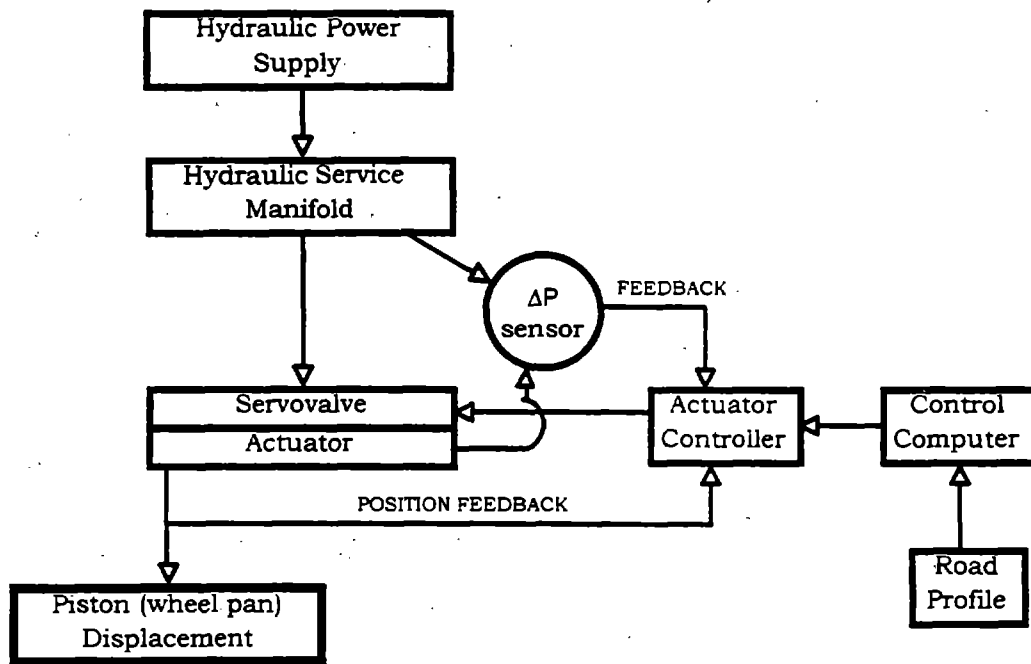
Figure 2-11. Flow chart of actuator control.
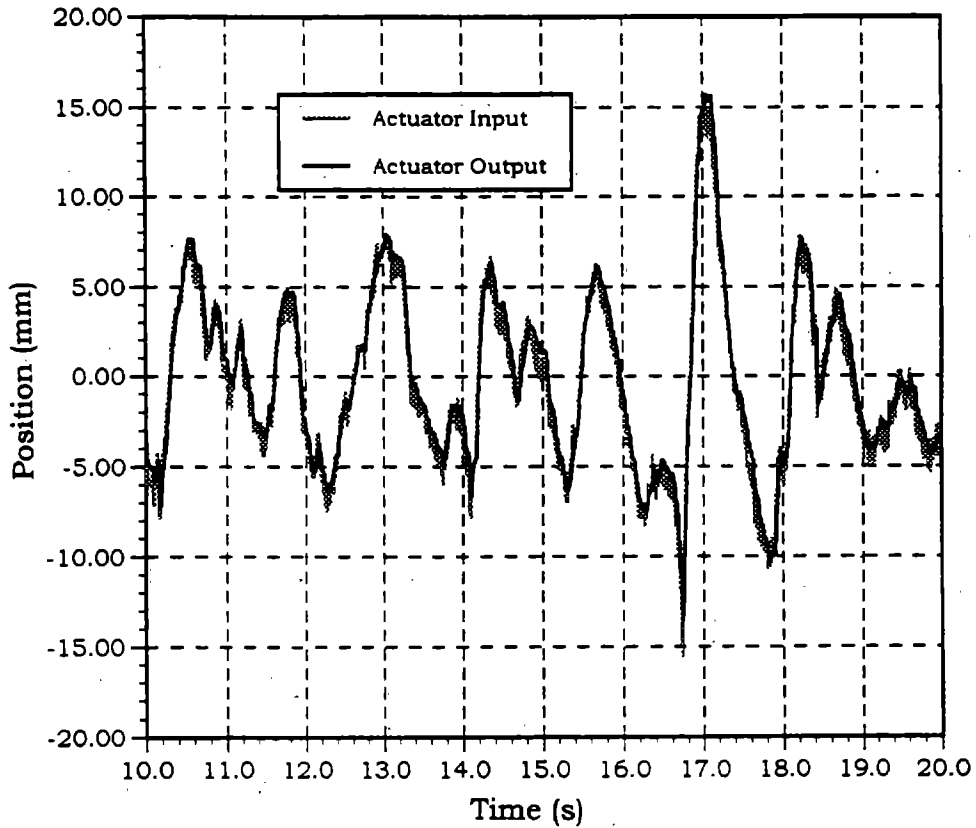
Figure 2-12. Actuator performance for simulated 48-km/h (30-mi/h) run over a medium-roughness road with an IRI of 2.6 mm/m (163 in/m).
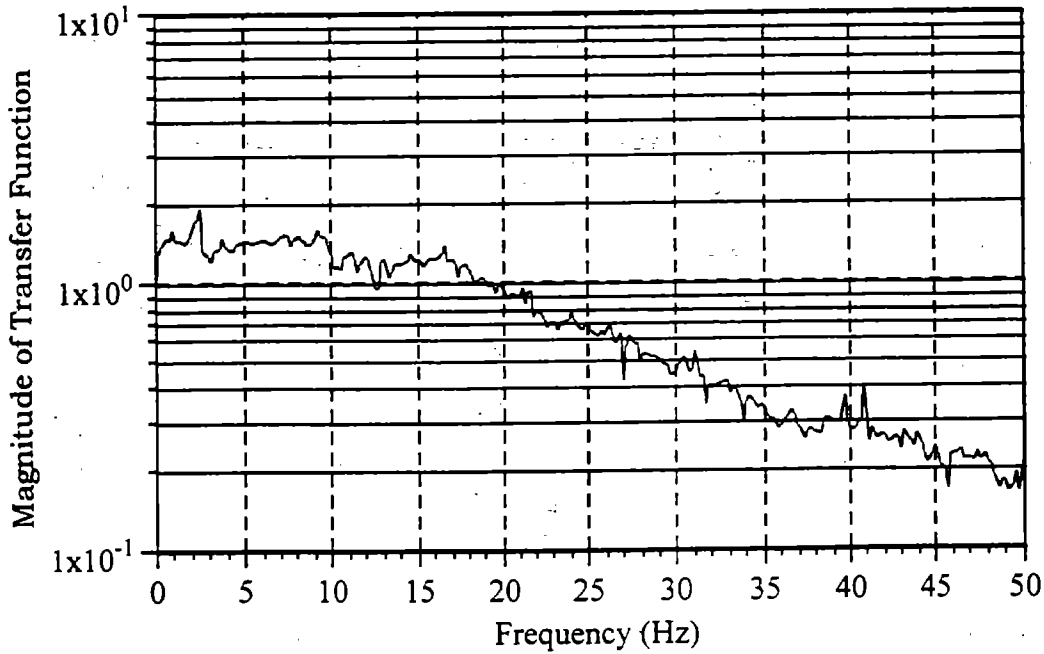
Figure 2-13. Magnitude of left-rear actuator transfer function obtained using white-noise input.
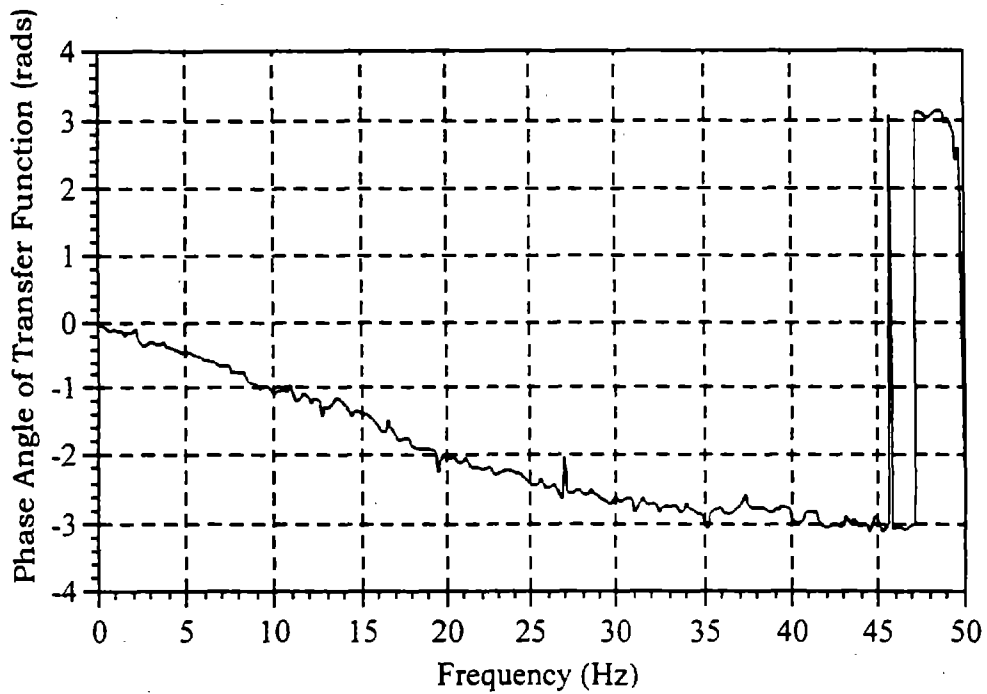
Figure 2-14. Phase shift of left-rear actuator transfer function obtained using white-noise input.
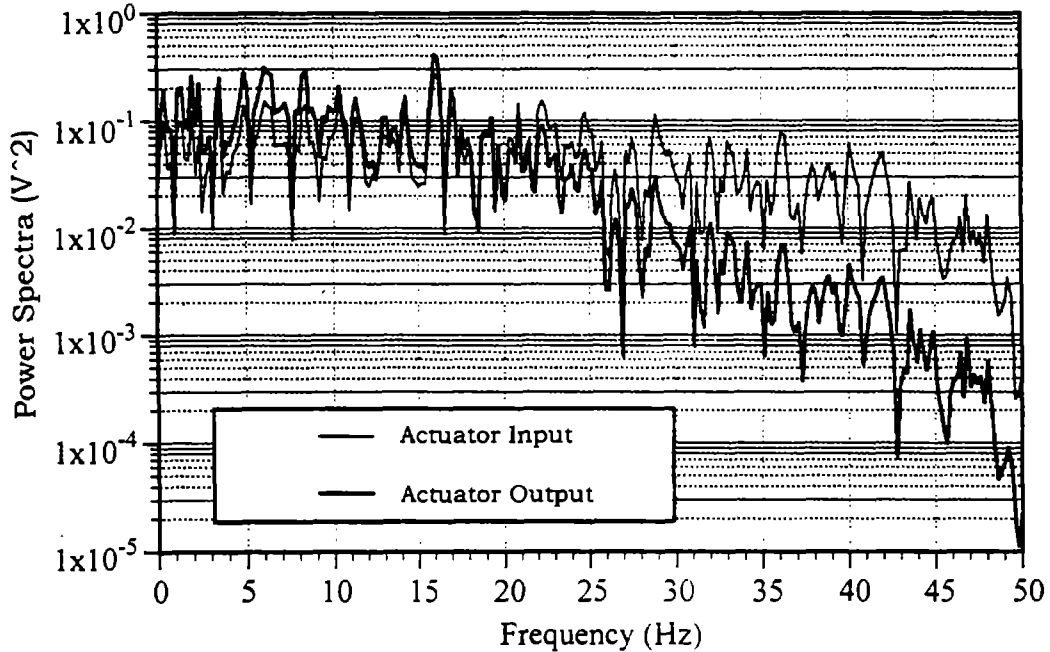
Figure 2-15. Power spectrums of actuator input and output from white-noise signal.

Actuator response was further studied using a high-roughness IRI of 3.1 mm/m (198 in/m). In the plots shown in figure 2-16, the speed is 72 km/h (45 mi/h), and the three lines represent road profile field data (left track), input to the left-front actuator controller, and displacement of the left-front actuator. Some small differences can be observed between the field data and actuator input. These differences arise because road profile field data were collected every 15 cm (6 in) of vehicle travel. Actuator input was generated using field data by interpolating between field data points, such that data were provided to the actuators at a rate of 200 Hz. Actuator output data reproduced the road profile data well, except that the output data did not track some of the small-amplitude, high-frequency input data characteristics.
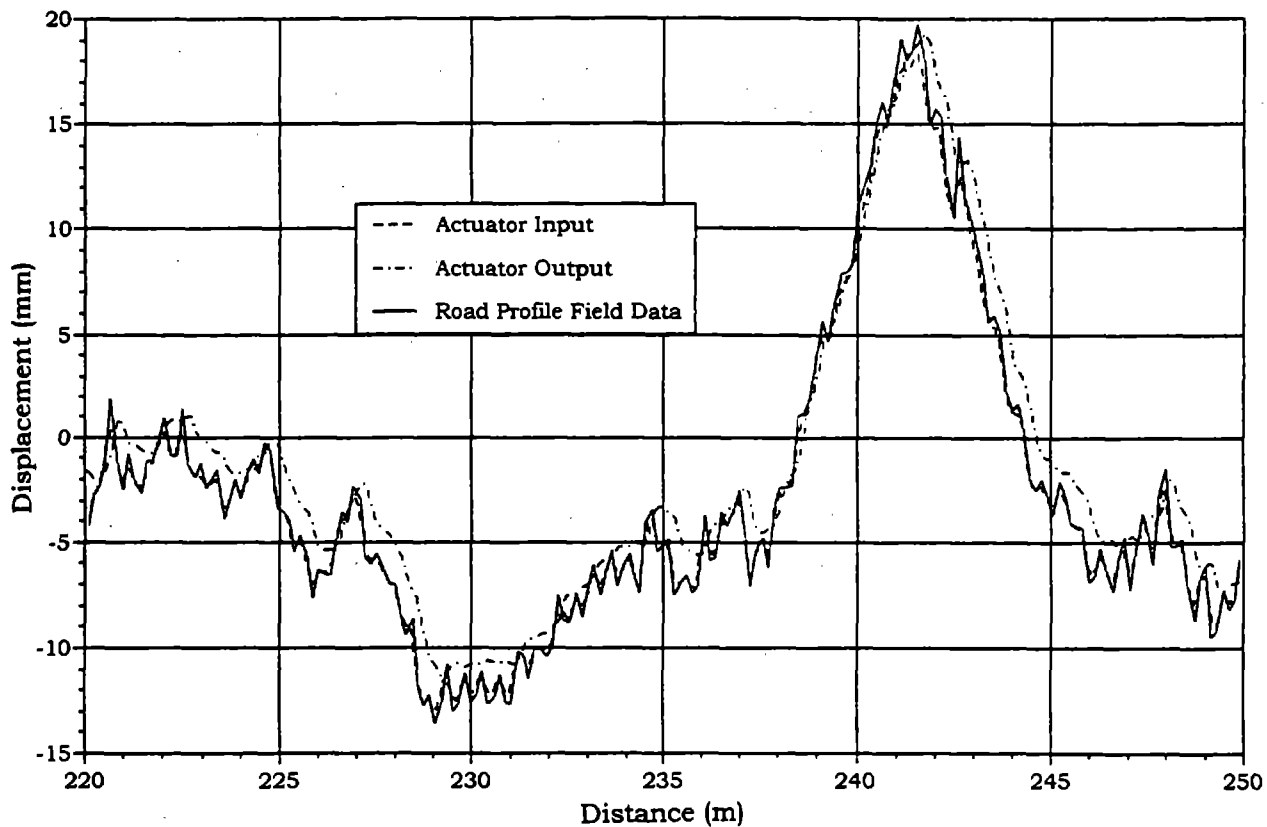
Figure 2-16. Portion of Penn18 simulation (72 km/h [45 mi/h]).

21

The power spectrum densities (PSD) of the right-front actuator displacement are shown in figure 2-17. Actuator performance is shown to be very good up to about 20 Hz.
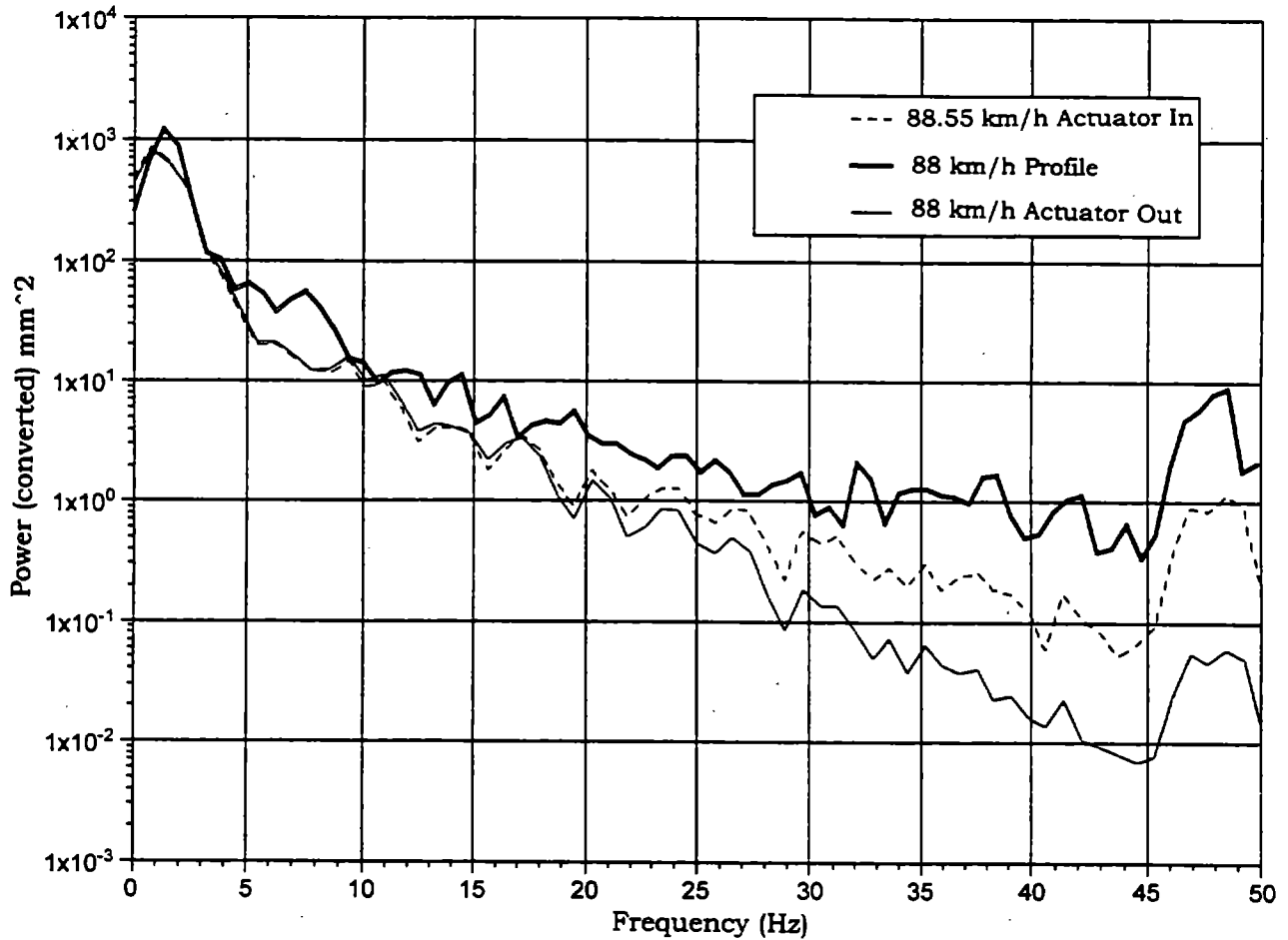
Figure 2-17. Right-front profile and actuator signal PSD's at 88 km/h (55 mi/h).

Figure 2-18 compares the PSD's of high-roughness simulations (IRI of 3.1 mm/m [198 in/mi]) at the 17.6-kN (4-kip) payload for various speeds. As speed increases, a slight decrease in overall magnitude of the spectra is observed. One reason for this slight decrease is the change in input profile used for each simulation. In every case, a 200-Hz input signal was generated from road profile field data. As simulation speed changed, the spatial spacing of these data changed.

22

As shown in figure 2-19, little change in PSD was observed when vehicle load is changed but speed remains constant.
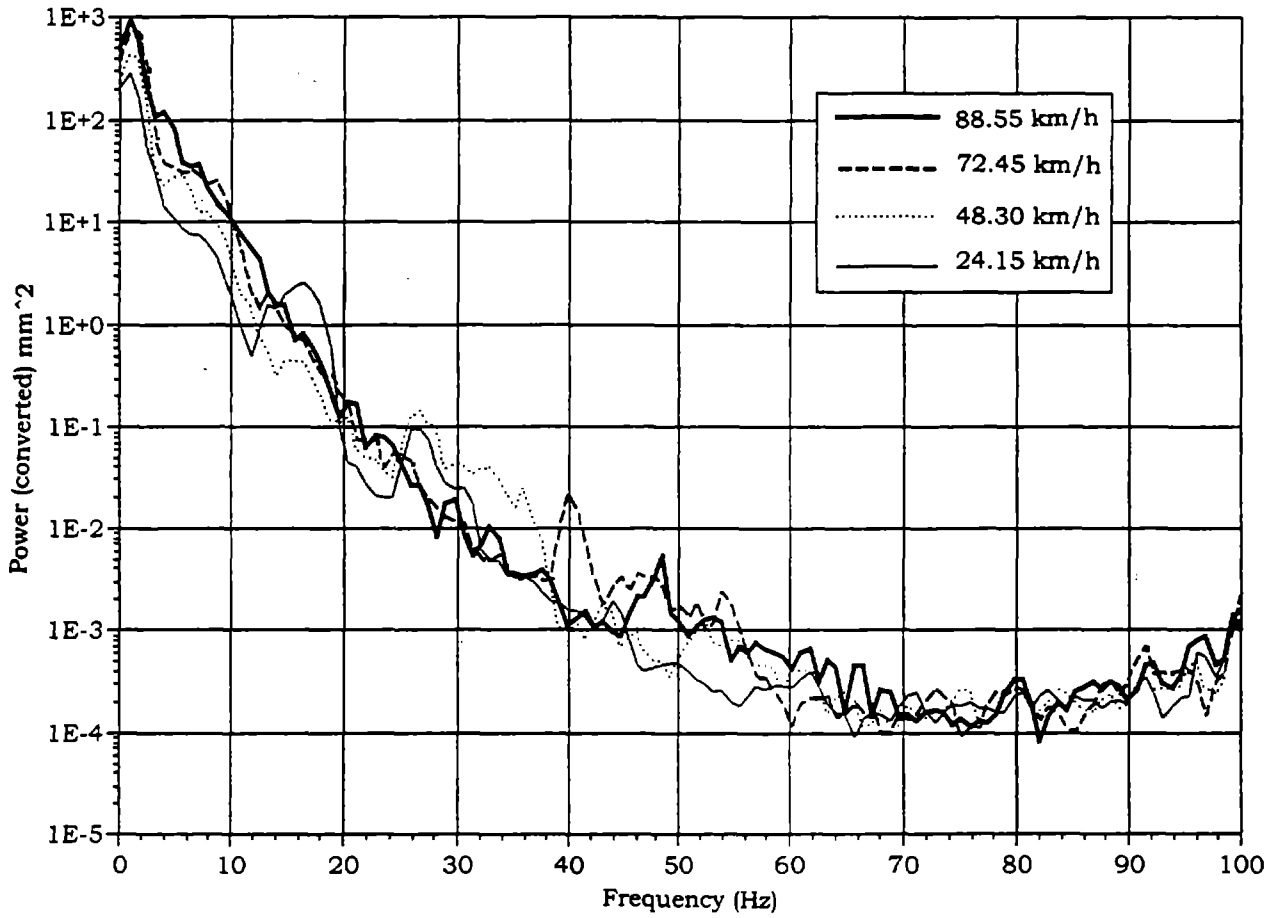
Figure 2-18. Right-rear actuator output power spectrum at various speeds.
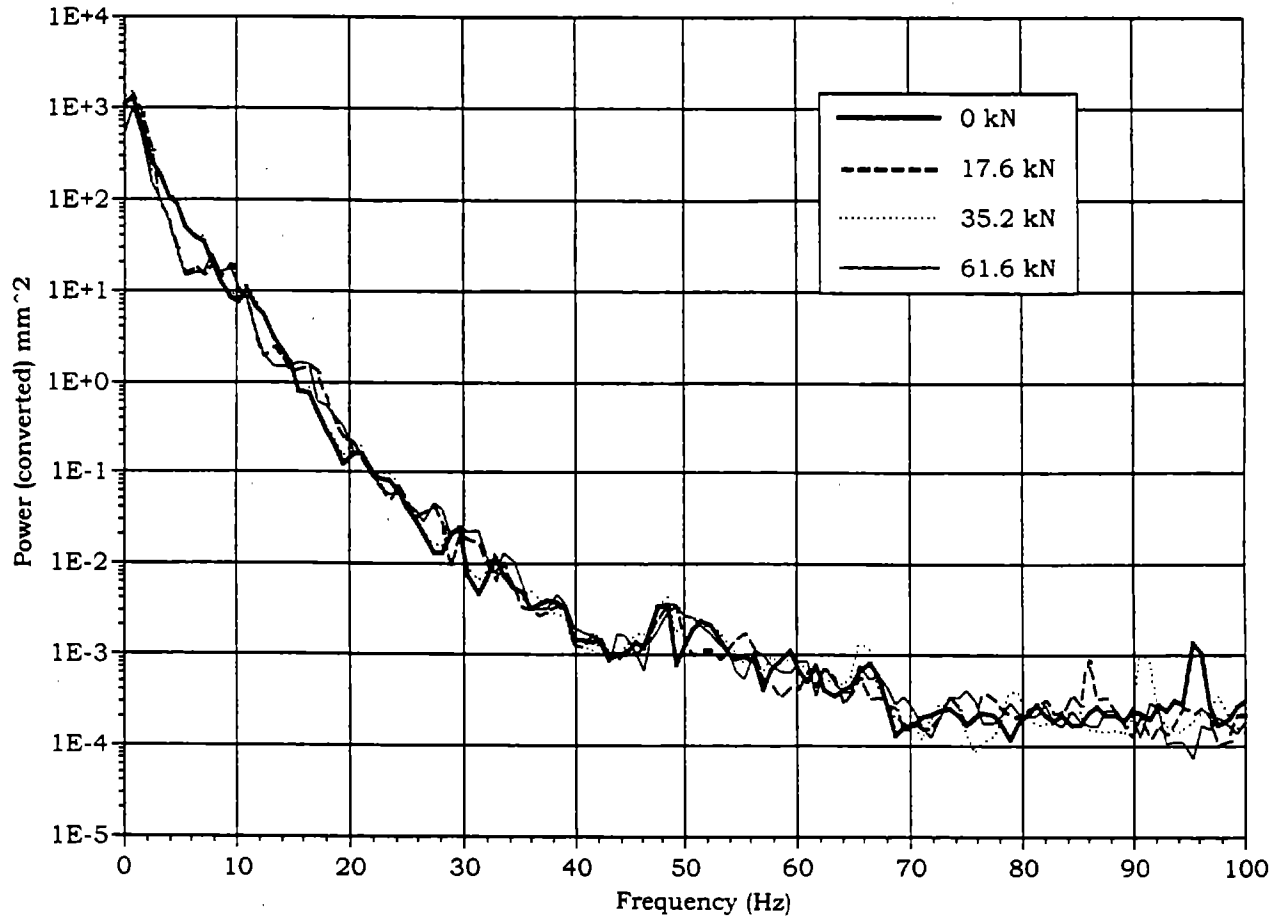
Figure 2-19. Right-rear actuator output power spectrum at various loads.

In summary, the following conclusions can be made from analyzing the profile simulations on DYNTRAC.

- Vehicle payload does not significantly affect actuator performance.
- Vehicle speed results in some small changes in profile data.
- Actuator performance is acceptable in the 0- to 20-Hz range.

The control computer, a 386 PC, interacted with a digital-to-analog output board. Analog outputs included voltage signals representing generated road profiles and a trigger to the data acquisition computer to start collecting data.

A computer program was used to generate actuator input data from measured road profile data. The program user specified the following information:

24

- Field-measured road profile data.
- Number of times the profile is to be repeated.
- Simulated speed.
- Output gain setting.
- Vehicle wheelbase.
- Profile roll and step limits.

The field-measured road profile data were stored in an ASCII file containing a header and a two-column matrix of road elevations. The header contained information such as distance between elevation measurements, measurement units, and matrix length. The computer modified the field data so that they did not exceed actuator capabilities (±7.5 cm [±3 in]) or specified step and roll amplitude limits. The step limit specified a maximum allowable road profile step change amplitude (7.62 cm [3 in]). The roll limit specifies a maximum allowable difference (10.16 cm [4 in]) in road profile amplitude between left- and right-track profile data at any given time. The computer program then converted the distance-based road profile data into time-based actuator input data. The program allowed a profile to be run repeatedly; the user could specify the number of times to repeat a given program.

Several DYNTRAC modifications and repairs were made to improve system performance; these are listed in detail in the second-year interim report. The system was tuned and inspected by technical service representatives. Controller circuitry was modified to improve the feedback control loop. ΔP sensor hydraulic lines were connected to the correct manifold ports, providing an improved signal for feedback control. The system control computer program was rewritten to improve the dynamic capabilities of road simulation and to add a digital trigger to start and stop the data acquisition system.

2.2.2 Sensors and Data Acquisition

At the start of the project, the DYNTRAC sensors included the actuator LVDT's and the wheel pan-mounted accelerometers. Additional sensors were required to measure dynamic wheel forces. Also, a data acquisition system capable of recording data from both DYNTRAC and vehicle sensors had to be assembled. These DYNTRAC-related activities are described in the following subsections.

2.2.2.1 Dynamic Wheel Scale Development

Five systems were surveyed for dynamic wheel scale application:

- Tire deflection.
- Piezoelectric load cells.
- Force or pressure capacitive sensors.
- Resistance-varying polymers.
- Strain-gauged sensors.

Determining dynamic wheel forces on the basis of tire deflection requires *a priori* knowledge of tire properties. Piezoelectric load cells are not capable of measuring static loads for long periods of time. Both capacitive and resistance-varying polymers have limitations in accuracy and linearity. In light of these limitations, the strain-gauged sensors were chosen as the most viable technology for a dynamic wheel scale.

Three strain-gauged sensor systems were studied for use with DYNTRAC: a standard load cell, a bending-plate law enforcement wheel scale, and a shear beam law enforcement wheel scale. Each of these systems was mounted on a hydraulic test frame to study static and/or dynamic sensor response.

Both static and dynamic characteristics of the 445-kN (10-kip) load cell were well documented by the manufacturer. However, documentation on the effects of off-axis loading was not available. Off-axis loading was considered a possibility on DYNTRAC in the event that wheels were not placed directly over the center of a wheel pan. Since the center of rear dual tires does not align with the center of single front tires, and since front and rear DYNTRAC wheel pans were in-line (facilitating drive-on mounting of

26

vehicles), off-axis loading of wheel pans normally occurred. Off-axis loading was checked using the arrangement shown in figure 2-20.
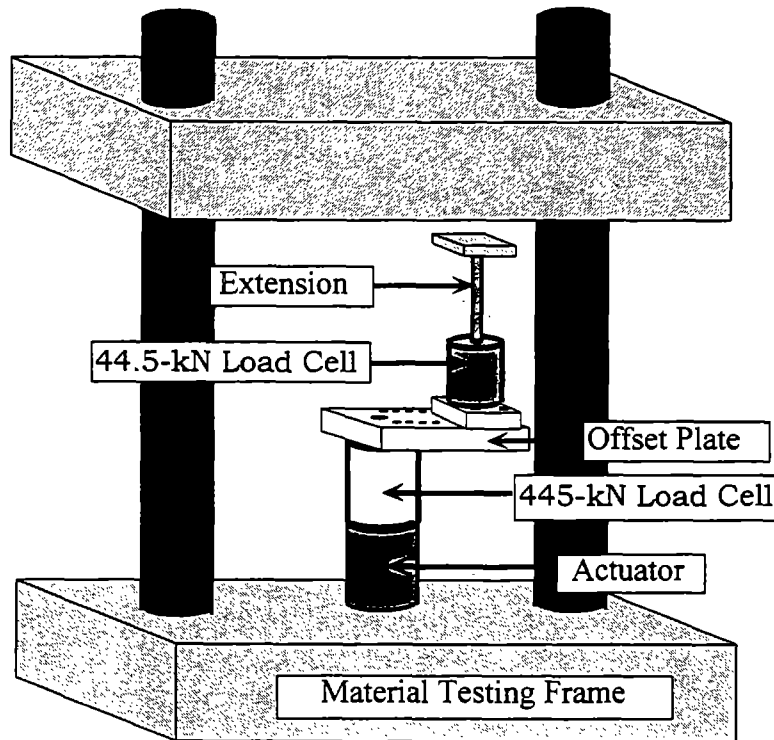
Figure 2-20. Load cell off-axis test setup.[4]

In figure 2-20, the 44.5-kN (10-kip) load cell is always loaded axially. As the offset between the central axis of the two load cells is increased, the bending moment applied to the 445-kN (100-kip) load cell is also increased. The difference in measurement between the reference (44.5-kN [10-kip]) load cell and the 445-kN (100-kip) load cell is affected by offset distance. After about 13.5 kN (3.03 kip) of applied load, the difference calculations fall into two groups. When offset is 0 to 7.62 cm (0 to 3 in), force measurements differ by less than 200 N (45 lbf). When offset is 10.16 to 15.24 cm (4 to 6 in), however, the difference in force measurement between the two load cells increases linearly with applied load. It is interesting to observe that, even though the difference in measurement increases with applied load, the error between the reference load cell and the 445-kN (100-kip) load cell remains less than 1.5 percent.

On the basis of these tests, it was concluded that the error in off-axis loading of a 445-kN (100-kip) load cell would remain within tolerable limits for DYNTRAC application. Load cell measurements would have to be corrected for inertial loading of the wheel pan in order to determine wheel forces.

The second system analyzed for DYNTRAC use was a lightweight, portable heavy-vehicle, law enforcement scale (a SAW 10 C Portable Wheel Load Weigher, PAT Equipment Corporation, 1665 Orchard Drive, Chambersburg, PA 17201). The scale was made of aluminum and was instrumented to measure bending strain. The scale had a manufacturer's rating of 100 kg (221 lb) for a 10,000-kg (22,100-lb) applied load. Figure 2-21 depicts the test setup used for this scale. The scale performed well in static tests, although in dynamic tests, the scale stiffness was found to be too low for DYNTRAC use.[4]
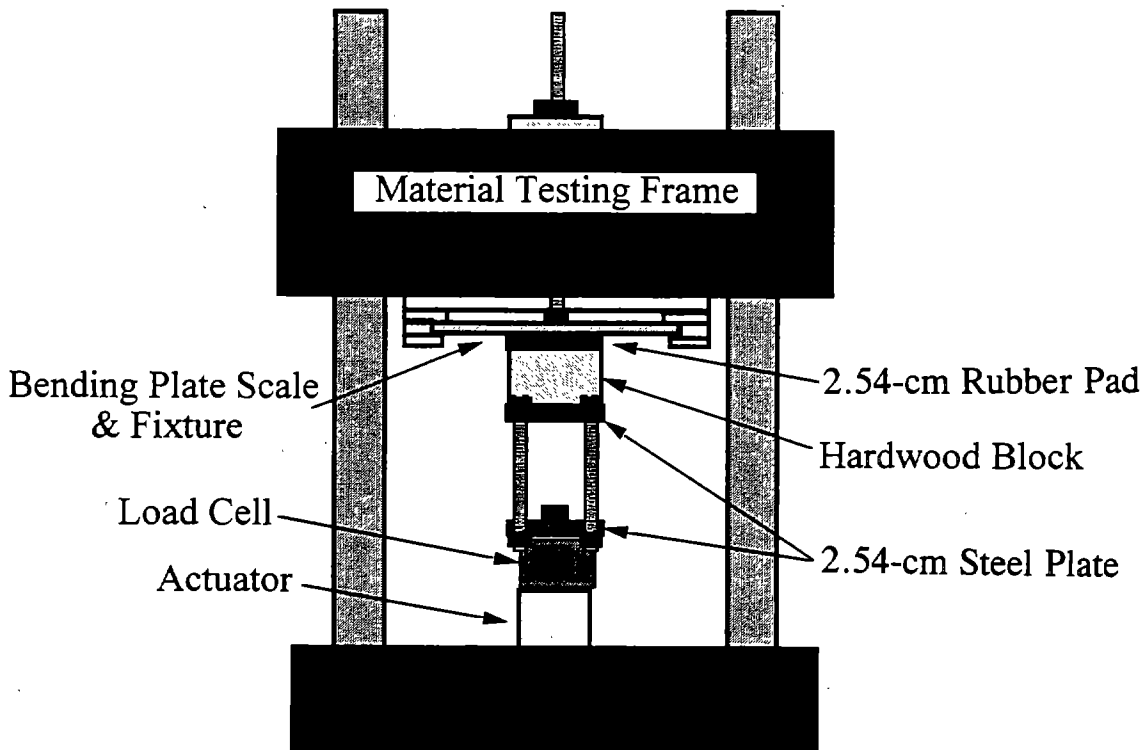
Figure 2-21. Test setup for law enforcement wheel scales.[4]

The third system considered for DYNTRAC was a second law enforcement wheel scale. This system used two shear-beam load cells inside the platform to

support a relatively rigid wheel platform (Intercomp PT 300 DW Wheel Load Scale, Intercomp Corporation, 14465 23rd Ave. North, Minneapolis, MN 55447). The test setup for this scale was similar to that shown in figure 2-21. In static tests, the square of the correlation coefficient (R^2) between load cell and wheel scale measurements was 0.9999. Results of dynamic tests are presented in table 2-5.

Table 2-5. Correlation results between wheel scale and load cell.[4]

Test Description	R^2
2-Hz sine input	0.9989
4-Hz sine input	0.9983
8-Hz sine input	0.9956
20-Hz sine input	0.9747
0.5-Hz sine input for 2 hours	0.9987
Sine sweep from 0.5 to 0.9 Hz	0.9994
Sine sweep from 1 to 6 Hz	0.9990
Sine sweep from 6 to 9.5 Hz	0.9970
0.5-Hz square wave input	0.9992

Both the static and dynamic performance of the shear gauge wheel scale were sufficient to meet DYNTRAC operational requirements. Because the top plate of this wheel scale was aluminum and relatively lightweight, wheel-scale measurement did not have to be corrected for inertial loading. Also, the wheel scale did not introduce a large increase in wheel pan height, allowing for "drive on" mounting of vehicles. For these reasons, the shear-beam wheel scale was chosen over the load cell for implementation on DYNTRAC.

Four shear-beam law enforcement scales were modified for use with DYNTRAC. Each scale contained two shear-beam load cells with bridge excitation and digital display electronics. The scale electronics were modified so that a continuous signal from the load cells could be recorded. The scale structure was modified to permit its mounting onto a wheel pan. Figure 2-22 depicts the right-front wheel scale. Much of

the scale electronics were moved off the scale and onto the frame of DYNTRAC. This minimized the risk of electronics failure due to vibration. Upon installation, the scale digital electronic display was used to calibrate its analog output signal.

Scale calibration was statically checked before each test sequence and when the scale electronics were modified. Figure 2-23 is an example of the calibration results. Scale measurements were also checked against test vehicle instrumentation. The force measured by the left-rear scale and the force calculated from left-rear axle strain data and inertial effects are plotted in figure 2-24. Further discussion of scale performance for this dynamic application is given by Wollyung et al.[4]
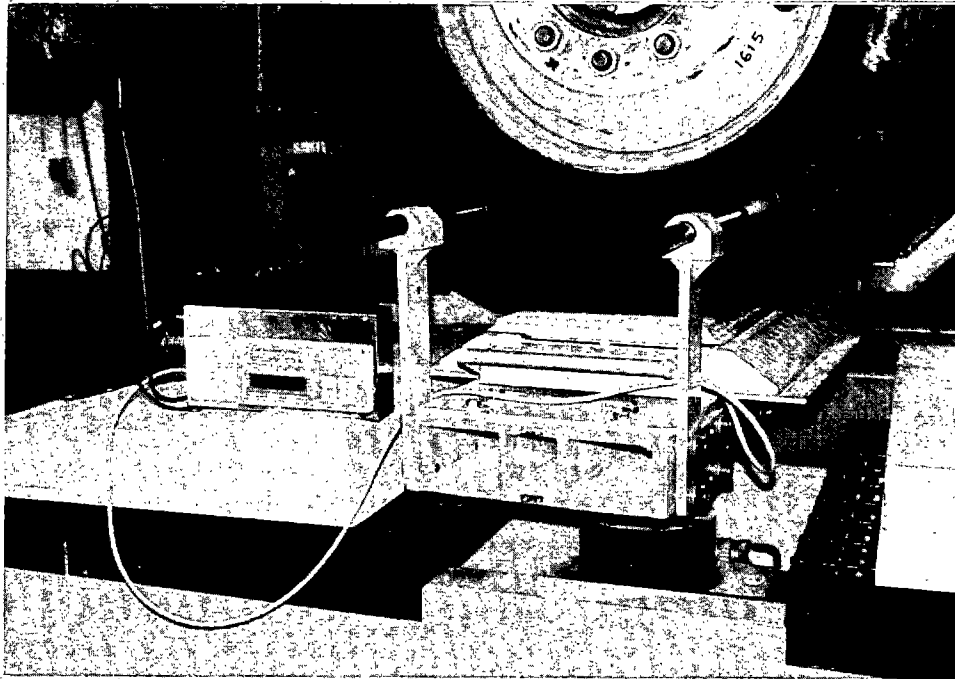
Figure 2-22. Dynamic wheel scale installed on DYNTRAC.
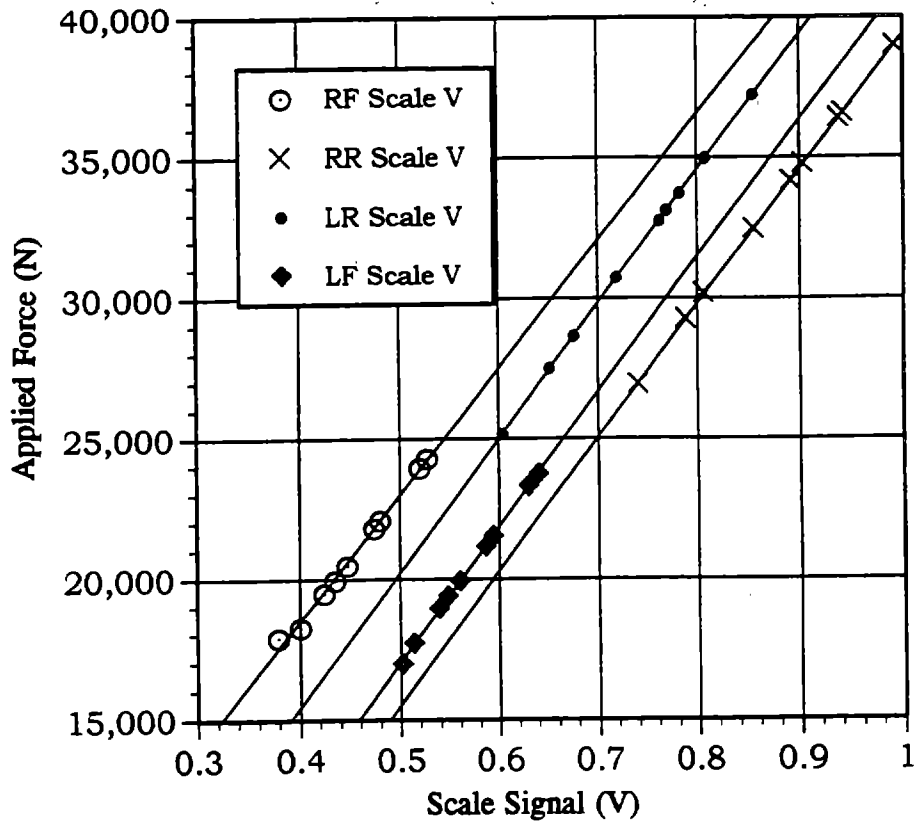
Figure 2-23. Typical scale calibration chart.
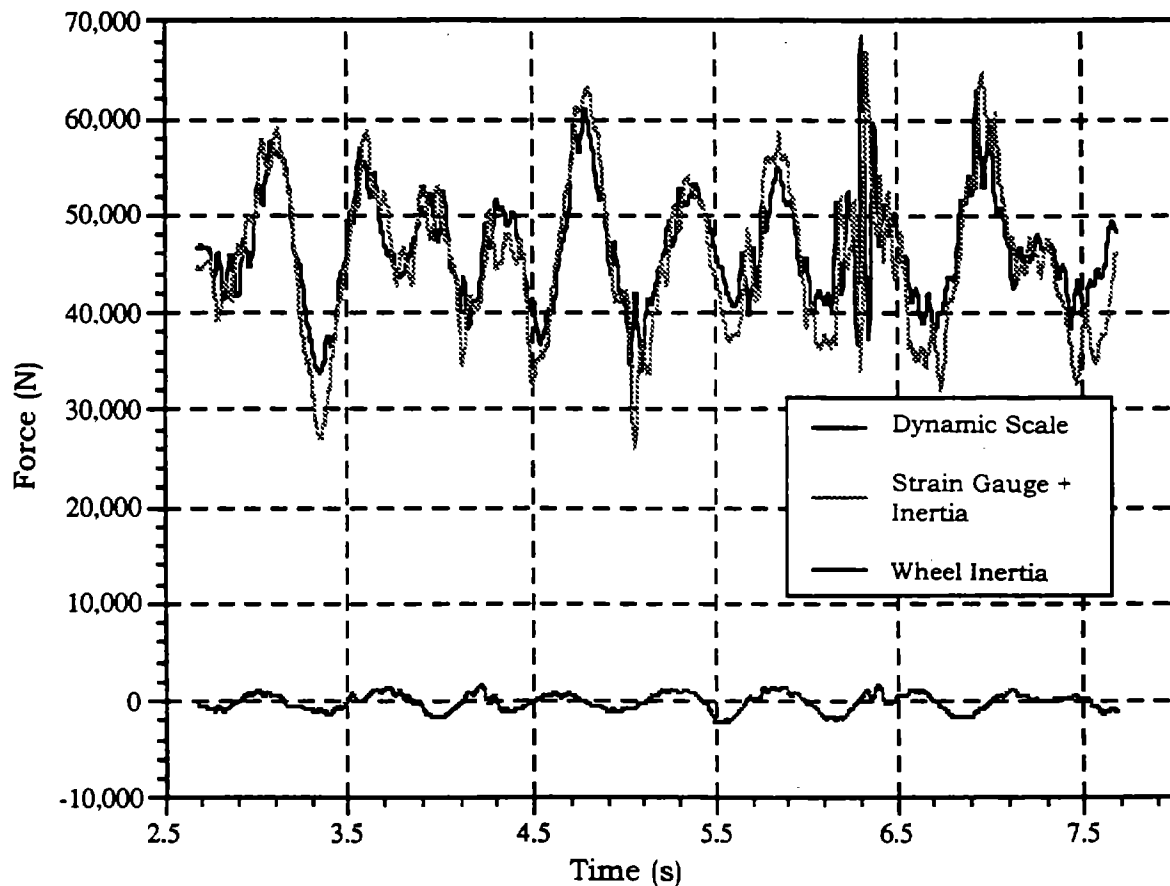
Figure 2-24. Force measurement by dynamic wheel scale and inertially compensated axle-strain gauges, for standard dual tires, air suspension, medium-roughness road profile (Penn5a), a payload of 61.6 kN (14 kip), and a speed of 88.6 km/h (55 mi/h).

2.2.2.2 DYNTRAC Data Acquisition

During laboratory testing, the 48-channel data acquisition system was removed from the vehicle and placed beside the DYNTRAC. This system was then used to simultaneously collect both vehicle and DYNTRAC data. This system was triggered in the laboratory by a digital line coming from the DYNTRAC control computer so that data acquisition began at the same time as DYNTRAC actuation.

Three sets of information were collected from the DYNTRAC system during testing. The control signal sent from the computer to each actuator controller (actuator input) was recorded as a history of the desired actuator output. The calibration for the actuator inputs is the actuator LVDT calibration multiplied by the span setting. The

actuator LVDT response (actuator output) was recorded, identifying the actual input experienced by the test vehicle. Dynamic wheel scale data provided a time history of dynamic forces generated between the tire and the actuator. Table 2-6 is a list of calibration factors associated with the recorded data.

Table 2-6. DYNTRAC sensor calibrations.

Sensor	Calibration	Offset
Actuator Inputs	7.62 mm/V	0 mm
Actuator Output (LVDT)	12.7 mm/V	0 mm
Right-Front Scale	10,736 N/V	-185 N
Right-Rear Scale	10,376 N/V	-1436 N
Left-Rear Scale	11,029 N/V	-1549 N
Left-Front Scale	11,682 N/V	-1974 N

2.3 INSTRUMENTED TEST PAVEMENT

Original plans for testing included driving the test vehicle over a section of pavement instrumented with subsurface pavement strain gauges. Periodic tests revealed that many of the pavement strain gauges had failed and were not usable. For this reason, the intended tests using instrumented pavement could not be completed.

Supporting equipment and procedures for instrumented pavement tests were developed for future projects. These include:

- Effective and repeatable triggering of the pavement data acquisition (DAQ) system.
- Synchronization of pavement and vehicle data acquisition systems.
- Accurate measurement of vehicle position with respect to pavement strain gauges.

IR sensors were selected for triggering the DAQ's. The sensors contained an IR emitter as well as a receiver. The time constant of the retroreflective IR sensors was 1

ms. One such sensor was mounted to the vehicle bumper looking downward. This sensor was used to trigger the onboard data acquisition system. A strip of reflective tape was placed across the pavement surface. The vehicle DAQ was triggered when the IR sensor encountered this reflective tape. A second retroreflective IR sensor was ground-mounted and directed laterally toward the passing vehicle. Reflective tape was placed on the outside edge of the vehicle bumper, thereby triggering the ground-based DAQ at nearly the same instant as the vehicle DAQ trigger.

The vehicle-based retroreflective IR sensor was also used to locate the vehicle longitudinal position. Reflective tape was placed at known locations along the roadway. When the vehicle-mounted IR sensor responded to the reflective tape, a positive vehicle location was achieved. Anstrom and Streit[13] demonstrated that the same sensor can be used to measure the lateral position of a vehicle.

CHAPTER 3. TEST PROGRAM

The study of dynamic forces in this project involves measurements associated with the variation of several vehicle-based parameters. All vehicle-parameter variations were made using a Model 1957 International, two-axle, flat-bed truck. This chapter first presents a brief discussion of each test variable. A summary of how these variables were combined for both DYNTRAC and field tests follows.

3.1 TEST VARIABLES

Test variables that were considered in this study of dynamic wheel forces on pavement include rear suspension, payload, tire type, tire pressure, vehicle speed, and road profile. A brief discussion of each of these variables follows.

3.1.1 Vehicle Suspension

Heavy vehicle suspensions have been the subject of many studies involving dynamic wheel forces. Researchers such as Cole and Cebon,[5,6] Cebon,[7] Gillespie and Karamihas,[8] Mitchell and Gyenes,[9] and Sweatman[10] have shown that suspension type affects pavement damage and dynamic wheel-force generation. These studies involve various vehicle models and axle configurations. Mitchell and Gyenes used a trailer with a removable subframe, allowing for multiple suspension types.[9] In the present study, two rear suspensions and one front suspension were investigated using a two-axle truck. Both configurations were specified by the vehicle manufacturer and all suspension modifications were done by a manufacturer-approved service facility.

3.1.1.1 Front Axle

The front-axle suspension was a constant-rate leaf spring assembly. A plot of the right-front suspension deflection during static loading is shown in figure 3-1. The deflection was measured using the right-front LVDT mounted between the vehicle axle and the chassis.
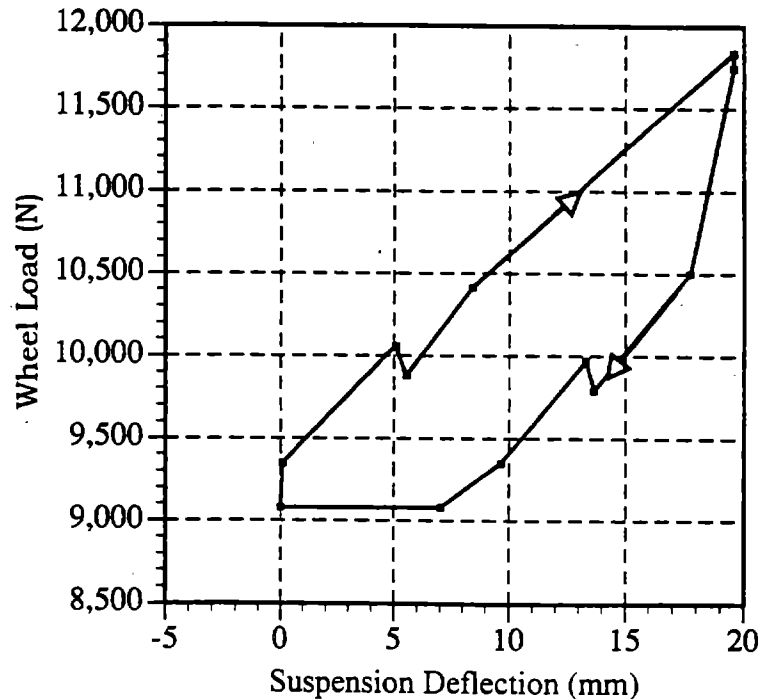
Figure 3-1. Right-front suspension deflection versus load.

The area in the hysteresis loop in figure 3-1 identifies the energy-dissipating properties of leaf springs. The difference in loading and unloading is due in part to the friction between the leaves of the spring. Because friction varies between static and dynamic loading, the static response of figure 3-1 cannot be equated to the dynamic response of the springs. The effective spring rate is a function of the applied load and the magnitude of the suspension deflection.[11]

3.1.1.2. Rear Axle

Two rear-suspension types were studied: a progressive-rate leaf spring and an air suspension. Both configurations were original-equipment manufacturer (OEM) options and all suspension modifications were done by a manufacturer-approved service facility. Testing was first conducted using the progressive-rate leaf springs. The static load versus deflection characteristics of the right-rear suspension are shown in figure 3-2.
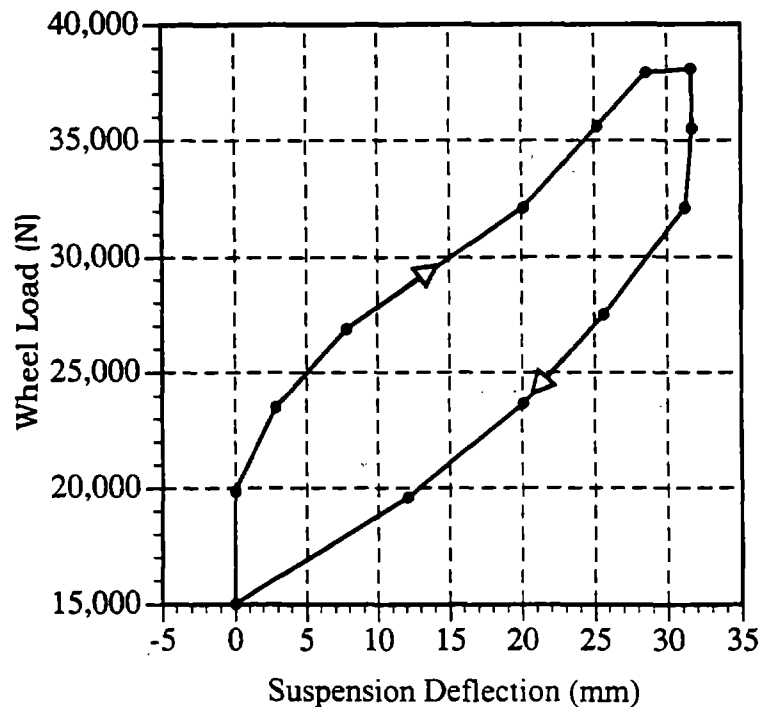
Figure 3-2. Load versus deflection for right-rear leaf spring suspension.

After tests were performed using the leaf spring configuration, the rear-axle suspension was converted to an air suspension. A second battery of tests was then conducted to study the effects of air suspension on dynamic wheel forces. Load versus deflection information was unavailable because of sensor problems resulting from the suspension conversion.

3.1.2 Tire Type

Three different tire types were tested using the steel suspension configuration: the standard dual tire designated 11R22.5, the low-profile dual tire designated 295/75R22.5, and the wide-base single tire designated 425/65R22.5. Tire-type selection was based on a literature review and market evaluation study. All tires were provided by the Goodyear Tire and Rubber Company. Static testing of each tire type was accomplished through a subcontract with the University of Nevada, Reno. Tire tests involved the following measurements:

- Net contact area.
- Gross contact area.
- Tire deflection versus load.
- Contact pressure distribution.

Tire test results are presented in detail in chapter 6.

After analysis of the results of the steel-suspension tests on DYNTRAC, it was determined that tire type did not significantly affect dynamic wheel forces. Further discussion of this point is presented in chapter 8, section 8.1.2. After the first sequence of DYNTRAC tests, low-profile and wide-base tires were not used in subsequent tests.

It should be noted that pavement damage depends on both wheel force and tire footprint area. The statement that tire type did not significantly affect dynamic wheel load does not conflict with previous pavement damage conclusions. When footprint area is considered and when force distribution under a tire footprint is also considered, then it can be expected that different tires will result in increased or decreased pavement damage. The assessment of the pavement-damaging potential of the three tire types used in this study is presented in section 8.2.

3.1.3 Tire Inflation Pressure

Tire inflation pressures were varied in the first set of DYNTRAC tests and during field tests on the medium-roughness road. The three tire pressures used were 482 kPa (70 psi), 655 kPa (95 psi), and 827 kPa (120 psi).

While tire pressure affected tire footprint area and stiffness, little effect was observed on dynamic wheel force. After analysis of the first set of DYNTRAC tests, tire pressure was not used as a variable in subsequent DYNTRAC and field tests.

3.1.4 Road Roughness

Road profile clearly plays an important role in the generation of dynamic wheel forces. Four sets of road profile data were used during DYNTRAC tests. The first was

a set of three profiles collected in the vicinity of State College, Pennsylvania. The profiles were selected to represent low- (Penn21), medium- (Penn5a), and high- (Penn18) roughness roads.

A second set of three roads was selected for the field-test portion of the study in the area surrounding McLean, Virginia. The roads were selected on the basis of their road roughness, proximity to the laboratory, and acceptable traffic pattern to facilitate heavy vehicle testing. The road selected for low roughness was a section of Virginia State Route 15 North (RT15N). The medium-roughness road was a section of the Clara Barton Parkway off of Interstate 270 (Clarab). Virginia State Route 659 (RT659) was selected as the high-roughness road. Profiles of each road were collected using FHWA's profilometer, PRORUT.

Two mathematically generated white-noise profiles (WN25 and WN50) represent the third set of road profile data used in this study.

The fourth data set of two medium-roughness road profiles was obtained from the road leading into the Turner-Fairbank Highway Research Center (TFHRC) (TRNOBMP2 and TRBMP4).

All profiles were filtered to specific limits set by the DYNTRAC control computer. The maximum allowable step was ±7.62 cm (±3 in). Short-duration road profile steps larger than this limit were removed from the data. The DYNTRAC actuator stroke limitation was ±7.62 cm (±3 in), and low-frequency road profile components were removed via high-pass filtering in order to meet this limitation. The limit placed on roll was a maximum of ±3.81 cm (±1.5 in) difference between left and right profiles. This limitation was met by a combination of manual inspection of data and high-pass filtering.

3.1.4.1 IRI Values

The most accepted method for quantifying road roughness is based on the IRI. Calculation of IRI is based on the suspension deflection of a standard quarter-car numerical model. The number is usually reported in mm/m or in/mi. The IRI is

explained in detail, and computer source code for calculating IRI is provided, by Sayers et al.[12] The algorithm used in the present study provided an IRI value that was within 1 percent of that reported by Sayers et al. for their standard test profile data.[12] The IRI values calculated for each set of road profile data are given in table 3-1. Figure 3-3 provides a graphical presentation of this data, for the first profiles listed in table 3-1. Note that the IRI of the Virginia high-roughness road, RT659, is almost twice that of the next roughest road, Penn18.

Table 3-1. IRI of input profile for DYNTRAC.

Profile fname.PRO	Designation	Left Track mm/m	Left Track in/mi	Right Track mm/m	Right Track in/mi
Penn21	Low	1.19	75.6	1.22	77.2
RT15N	Low	1.52	96.2	1.50	95.4
Penn5a	Medium	2.87	182.0	2.67	169.4
Clarab	Medium	2.31	146.6	2.78	176.3
Penn18	High	3.92	248.5	3.68	233.5
RT659	High	6.47	410.4	7.04	446.5
WN25*	White Noise	14.39	910.7	14.59	924.9
WN50*	White Noise	15.99	1,013.5	16.34	1,035.8
TRNOBMP2	Test Road	1.83	116.3	2.14	135.9
TRBMP4	Test Road	2.54	161.1	2.76	175.1

* Note: These profiles were mathematically generated and were run on DYNTRAC with a gain setting of 0.25.
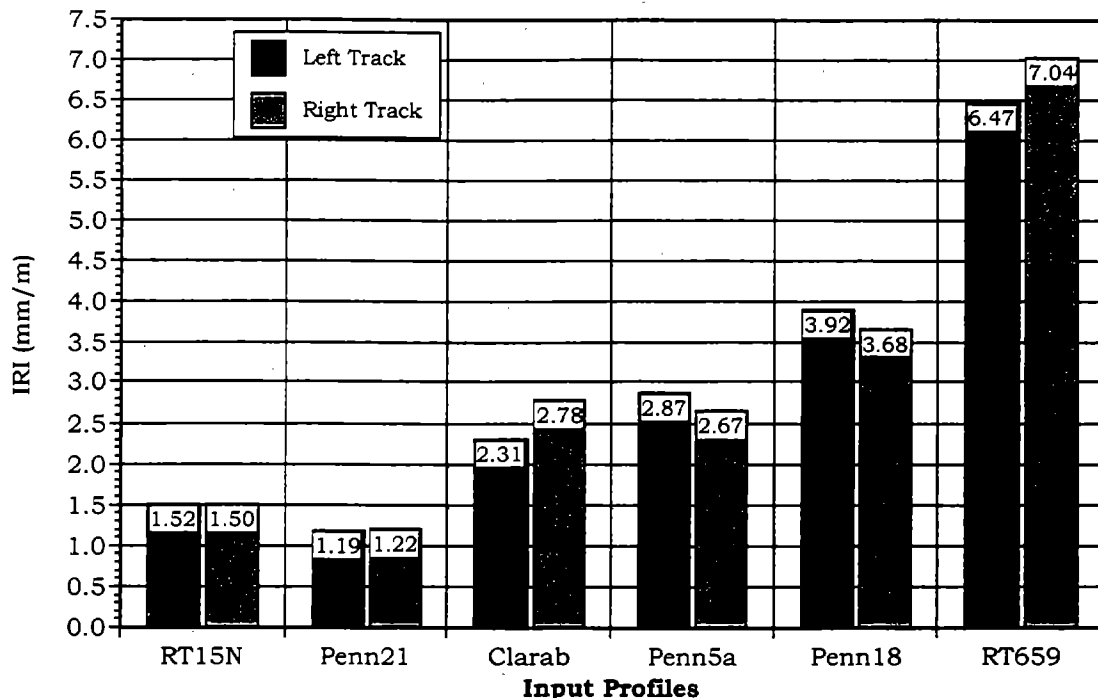
Figure 3-3. IRI of DYNTRAC road profile field data.

40

3.1.4.2 Road Profiles

Plots of the left track of the Virginia road profile field data are shown in figures 3-4 through 3-6.
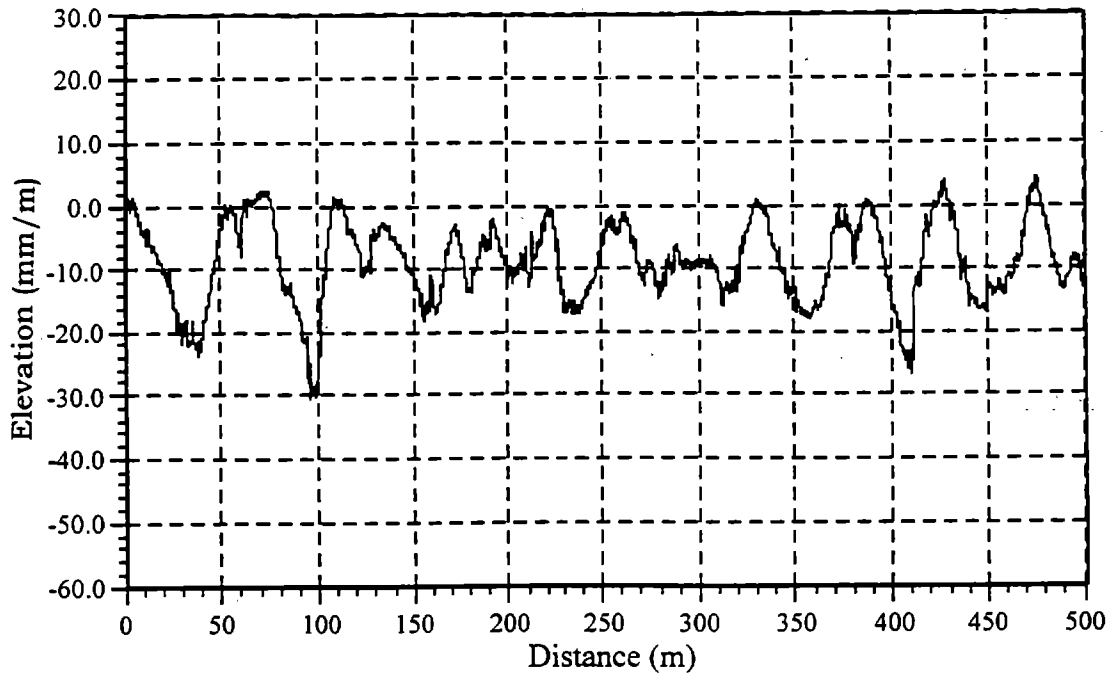
Figure 3-4. Left track of RT 15 N profile.
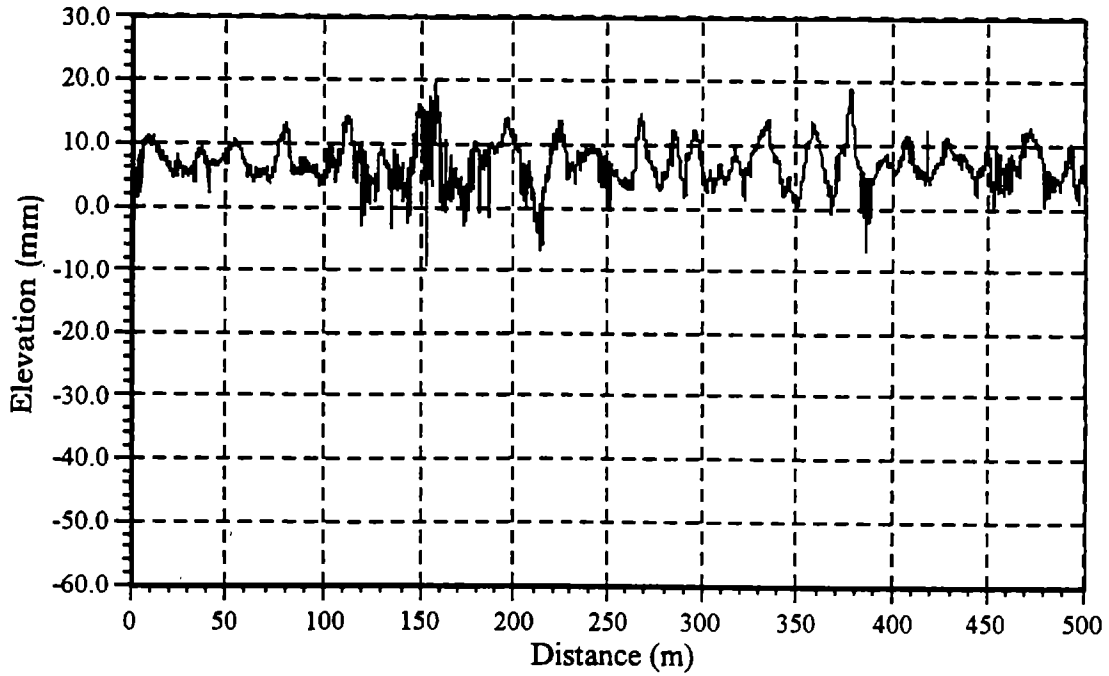
Figure 3-5. Left track of Clara Barton Parkway.
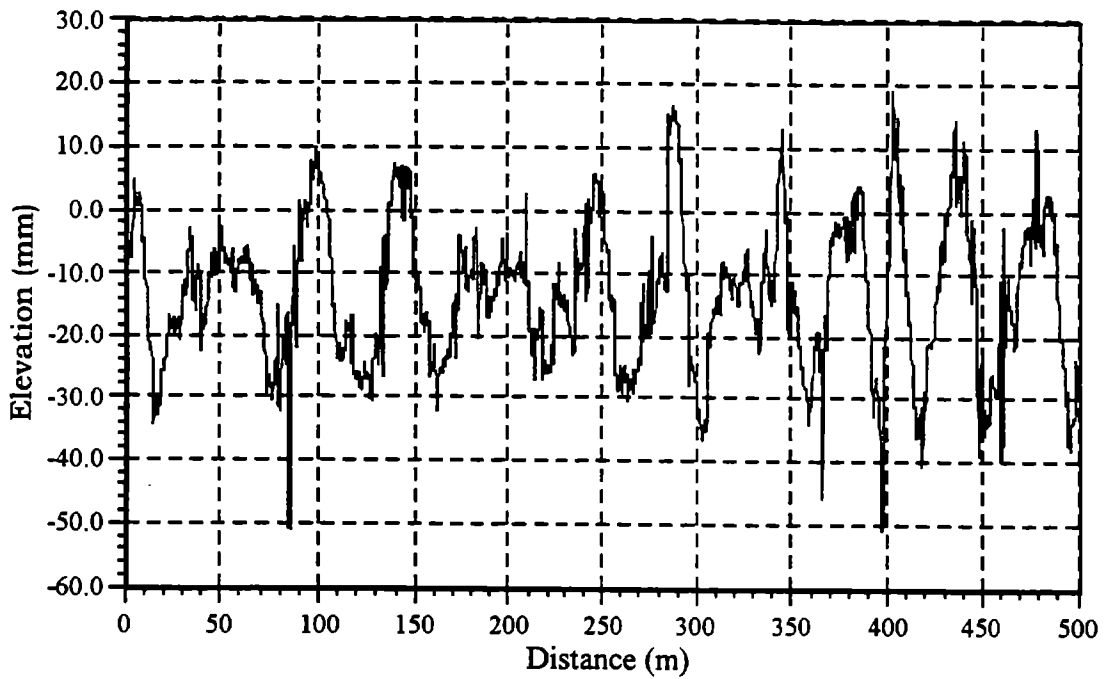
Figure 3-6. Left track of RT 659.

Left-track road profile field data from the three central Pennsylvania roads are plotted in figures 3-7 through 3-9.

42
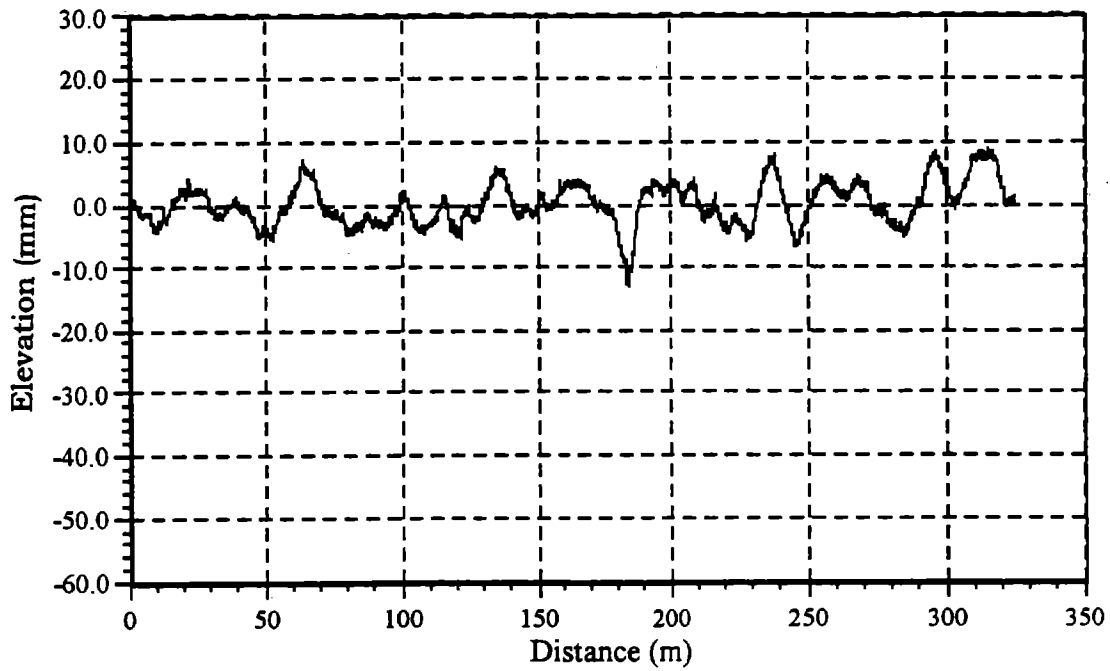
Figure 3-7. Left track of Penn21 profile.
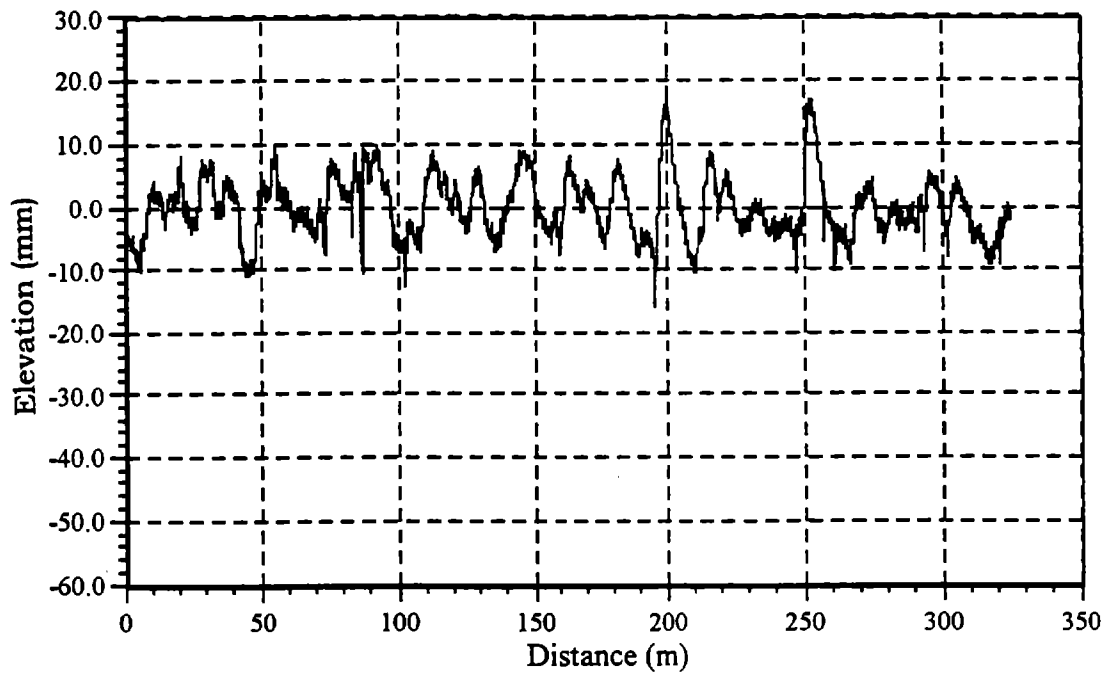
Figure 3-8. Left track of Penn5a profile.

43
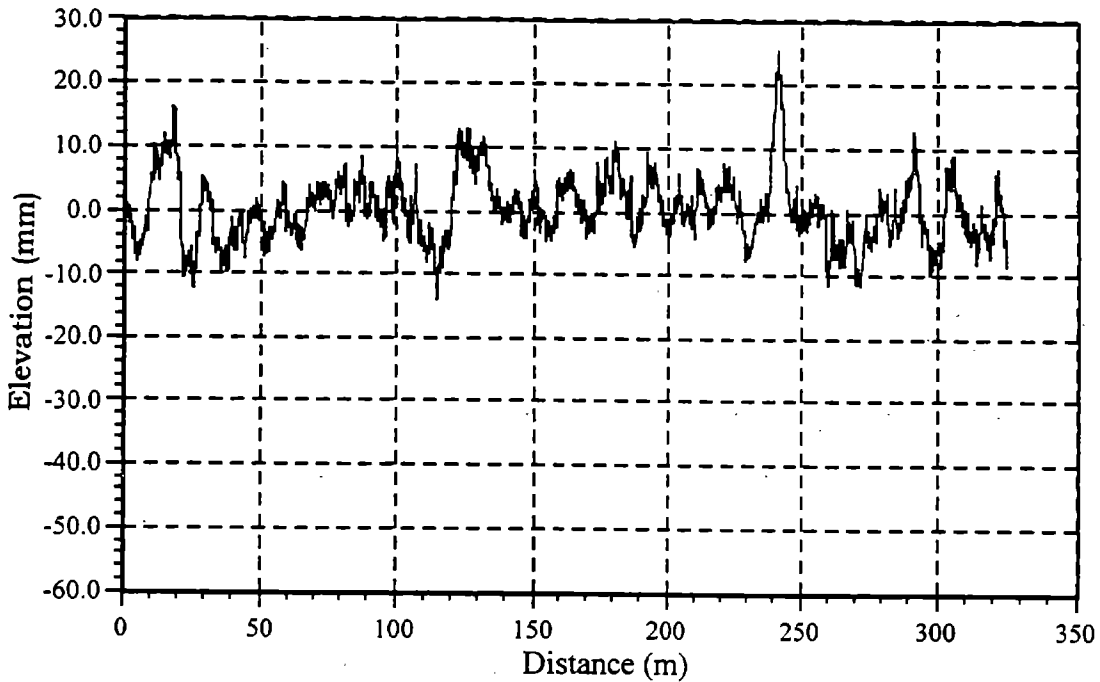
Figure 3-9. Left track of Penn18 profile.

3.1.4.3 Processing of Road Profiles

Road profile data were collected from the field and processed by the DYNTRAC control computer program. The actual DYNTRAC actuator motion then approximated the desired road profile. Table 3-2 provides a short description of terminology associated with the processing of road profile data and DYNTRAC response.

Table 3-2. Road profile terminology.

Term	Source	Comments
Road Profile Field Data	Actual road profile field data. These data are an input to the DYNTRAC control computer program.	Profile data are collected every 152.4 mm (6 in) along a road.
Actuator Input Profile	The control computer program sends a new profile amplitude to the actuator every .005 s. This signal is recorded by the data acquisition system at a sampling rate of 200 Hz.	The simulated distance between sampled data is a function of simulation speed and DAQ sample rate.
Actuator Output Profile	The output signal from each actuator is sampled by the data acquisition system at a rate of 200 Hz.	The LVDT signal reports actual actuator displacement. The simulated distance between sampled data is a function of simulation speed and DAQ sample rate.

44

3.1.4.4 Road Profile Field Data

The field data collected using a profilometer are called the road profile field data. Data are collected every 152.4 mm (6 in) along a given road section. These data are used directly to calculate an IRI for a given road section.

3.1.4.5 Actuator Input Profile

Care must be taken so that actuators will not introduce artificial dynamic effects into the system simulation. For example, in the case of an 8-km/h (5-mi/h) simulation, if actuators were to receive profile data that were spaced 152.4 mm (6 in) apart, then the actuator update rate would be approximately 14 Hz. This, however, is very close to the suspension resonance frequency and can therefore result in atypical vehicle dynamic response. To ensure that actuator motion frequency remains significantly above vehicle primary resonant frequencies, an actuator update frequency of 200 Hz was chosen. To this end, road profile field data were interpolated using a polynomial curve-fitting algorithm such that the simulated travel distance between profile data points was a function of vehicle speed, as shown in table 3-3.

Table 3-3. Distance between profile data points as a function of vehicle speed.

Speed (km/h [mi/h])	Speed (m/s [ft/s])	Distance between data points (mm [in])
24.1 (15)	6.7 (22)	33.5 (1.32)
48.3 (30)	13.4 (44)	67.0 (2.64)
72.4 (45)	20.1 (66)	100.6 (3.96)
96.6 (60)	26.8 (88)	134.1 (5.28)
field data	field data	152.4 (6.00)

The digital road profile data were changed to an analog signal via the digital-analog (D/A) converter. The analog signal was sent to the DYNTRAC control console and is simultaneously sampled (along with all other data channels) at a rate of 200 Hz by the data acquisition system.

3.1.4.6 Actuator Output Profile

The control computer converted an ASCII file of discrete road elevations to an analog signal sent to the actuator controller. This analog signal was then sent to the individual actuator controllers. The actuator controller used the analog input along with feedback to generate a signal to control a servovalve. The servovalve determined the hydraulic fluid flow that drove the actuator piston. The physical characteristics of the actuator and its control loop dictated the effectiveness of the road simulation. The actuator frequency and time domain performance were discussed in chapter 2. Now, the effects of test parameters on actuator output IRI are presented.

Figure 3-10 demonstrates how IRI calculations are affected by load. The IRI of the input profiles are shown in figure 3-3. There is no clear reduction of IRI when load is varied (see figure 3-10). The response of the other three actuators was found to be similar.
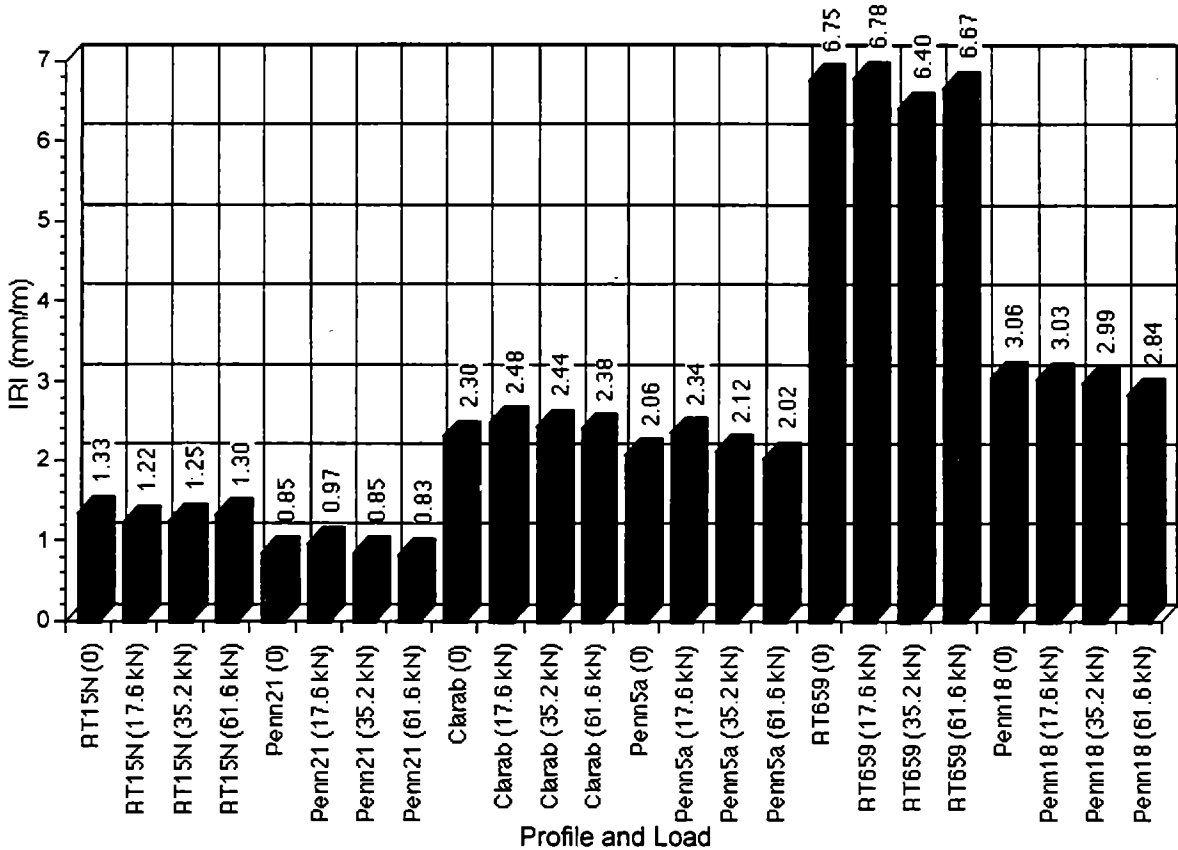
Figure 3-10. Actuator IRI's versus profile and load.

Data presented in chapter 2 demonstrated that vehicle speed and load had little effect on actuator output PSD over this frequency range of 0 to 20 Hz. Since high-frequency data are of relatively small amplitude, the conclusions in chapter 2 are consistent with those made here that vehicle speed and load only minimally affect actuator output IRI.

3.1.5 Load

Four values of vehicle load were used for both DYNTRAC and field tests. The different load configurations were achieved using seven concrete blocks, each weighing 8.8 kN (2,000 lb). Placement of the weights was designed to achieve large rear-axle loads. Figure 3-11 shows the test vehicle in each loading condition. Table 3-4 shows typical static wheel, axle, and vehicle forces for each load configuration.
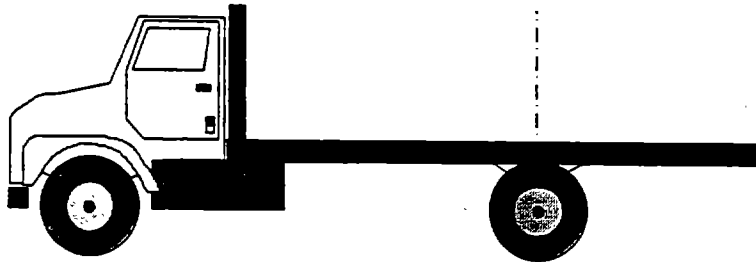
1st Loading Condition
Empty Truck

Approx. Total Weight: 71,067 N
(15,970 lb)
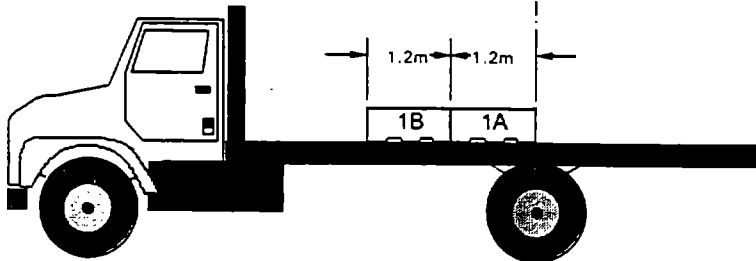
2nd Loading Condition
2 - 8.8 kN weights
2 - 2,000 lb
17.6 kN total weight
4,000 lb

Approx. Total Weight: 88,867 N
(19,970 lb)
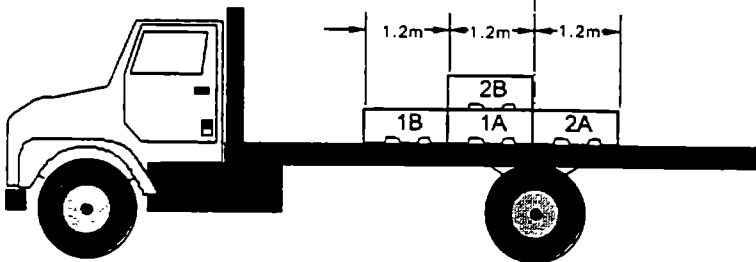
3rd Loading Condition
4 - 8.8 kN weights
4 - 2,000 lb
35.2 kN total weight
8,000 lb

Approx. Total Weight: 106,667 N
(23,970 lb)
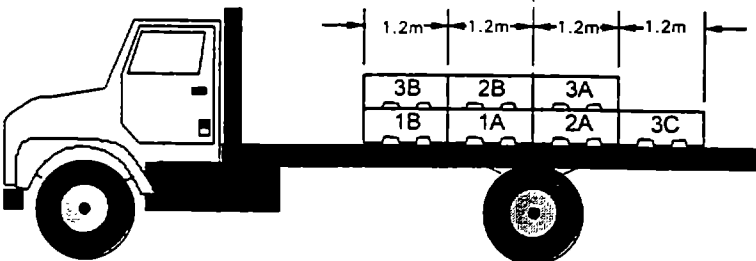
4th Loading Condition
7 - 8.8 kN weights
7 - 2,000 lb
61.6 kN total weight
14,000 lb

Approx. Total Weight: 133,367 N
(29,970 lb)

Figure 3-11. Vehicle loading configurations.

48

Table 3-4. Typical wheel and axle weights for loading conditions.

Configuration	Right-Front Wheel N (lb)	Right-Rear Wheel N (lb)	Left-Rear Wheel N (lb)	Left-Front Wheel N (lb)	Front Axle N (lb)	Rear Axle N (lb)	Vehicle N (lb)
1	16,380 (3,680)	18,870 (4,240)	17,980 (4,040)	16,020 (3,600)	32,400 (7,280)	36,670 (8,240)	69,060 (15,520)
2	18,250 (4,100)	26,970 (6,060)	25,190 (5,660)	16,910 (3,800)	35,160 (7,900)	52,150 (11,720)	87,300 (19,620)
3	17,890 (4,020)	36,400 (8,180)	33,730 (7,580)	17,000 (3,820)	34,890 (7,840)	70,130 (15,760)	105,020 (23,600)
4	17,270 (3,880)	50,640 (11,380)	47,170 (10,600)	16,550 (3,720)	33,820 (7,600)	97,810 (21,980)	131,630 (29,580)

3.1.6 Speed

Three vehicle speeds, 48, 72, and 97 km/h (30, 45, and 60 mi/h), were used for the first set of DYNTRAC tests. All subsequent DYNTRAC test sequences included a fourth speed, 24 km/h (15 mi/h). Field tests included all four speeds, with one exception. For safety reasons it was not possible to travel at the highest speed of 88 km/h (55 mi/h) on the high-roughness road. Table 3-5 is a list of test speeds in various units.

During DYNTRAC tests, speed is a user input for the control program. However, during field tests, the vehicle operator controls the speed. Actual vehicle speed and position were measured using a vehicle-mounted, retroreflective IR sensor. The sensor was mounted to point downward at the pavement and to respond to the presence of reflective tape. Two strips of tape spaced 2 m (6.6 ft) apart were applied across the road surface at 100-m (328-ft) intervals along the test road. Sensor response was used to measure the travel time between tape strips, thereby facilitating velocity measurement. Further detail related to this process is given by Anstrom and Streit.[13]

Table 3-5. Vehicle test speeds.

mi/h	km/h	ft/s	m/s
15	24	22	6.7
30	48	44	13
45	72	66	20
55	89	80	25
60	97	88	27

3.2 DYNTRAC TESTS

Three different major sets of DYNTRAC tests were used to study dynamic wheel forces. The first set involved testing the vehicle steel suspension and the Pennsylvania profiles. The second set took place after the field tests were completed. This set involved simulations with profiles taken during the field tests. Both sets of profiles were used in the third set of DYNTRAC tests. The third set of tests took place after the vehicle rear suspension was changed to air.

Table 3-6 lists the test configurations investigated during DYNTRAC tests.

Table 3-6. Test configurations for DYNTRAC simulations.

Set #1 324 Tests	Leaf Spring Suspension
	3 Tire Types: 11R22.5, 295/75R22.5, 425/65R22.5
	4 Loads: 0-, 17.6-, 35.2-, 61.6-kN payloads
	3 Tire Pressures: 482, 655, 827 kPa
	3 Profiles: Penn21, Penn5a, Penn18
	3 Speeds: 48, 72, 97 km/h
Set #2 48 Tests	**Leaf Spring Suspension**
	1 Tire Type: 11R22.5
	4 Loads: 0-, 17.6-, 35.2-, 61.6-kN payloads
	1 Tire Pressure: 655 kPa
	3 Profiles: RT15N, Clarab, RT659
	4 Speeds: 24, 48, 72, 89 km/h
Set #3 192 Tests	**Air Suspension**
	2 Tire Types: 11R22.5, 425/65R22.5
	4 Load Configurations: 0-, 17.6-, 35.2-, 61.6-kN payloads
	1 Tire Pressure: 655 kPa for 11R22.5, 758 kPA for 425/65R22.5
	6 Profiles: RT15N, Penn21, Clarab, Penn5a, RT659, Penn18
	4 Speeds: 24, 48, 72, 89 km/h

In addition to the tests noted in table 3-6, 56 replicate tests were conducted to check the repeatability of DYNTRAC response. DYNTRAC tests were also performed to support the following activities:

- Measure and improve the performance of DYNTRAC.
- Evaluate dynamic wheel scale designs.
- Measure test-vehicle parameters.
- Test the WFT prototype.

- Calibrate vehicle- and DYNTRAC-based sensors.
- Provide experimental data for validating computer simulations of vehicle dynamics.

Test procedures for using DYNTRAC were developed and improved during the course of testing. A brief description of these procedures is presented in the following section.

3.2.1 Test Procedures

Extensive planning and preparation were needed to collect data from over 20 sensors; set up a system of computers, electronics, hydraulics, and mechanical fixtures capable of shaking a fully loaded truck; and systematically test various combinations of parameters. This section briefly describes the activities required to perform tests using DYNTRAC. These procedures arise from manufacturer recommendations, experience from testing, and standard engineering practice.

Procedures for DYNTRAC startup

1. Inspect the system.
2. Place truck on DYNTRAC.
3. Activate static support of rear actuators (nitrogen accumulators).
4. Install wheel restraints.
5. Connect sensors to DAQ system.
6. Perform static calibration of sensors.
7. Warm up hydraulic system.

Procedures for each load condition

1. Load/unload weights.
2. Acquire static sensor measurements.
3. Check scale digital displays.
4. Perform dynamic calibration of axle strain gauges.
5. Perform random profile tests.

6. Perform profile simulations.

7. Check scale digital displays.

These activities are briefly discussed below.

As mentioned in chapter 2, DYNTRAC is a complex system of mechanical, electronic, and hydraulic components. Vibrations and dynamic forces can loosen mechanical and electrical connections. Before startup and periodically during testing, the mechanical and electrical connections are checked. This visual inspection identified potential problems involving the restraint fixtures, rebar bolts connecting DYNTRAC to the foundation, and electrical connections to the actuators.

Mounting a vehicle on DYNTRAC involves using a forklift to place ramps in front of DYNTRAC. A vehicle is then backed up onto the DYNTRAC frames and onto the actuators. Once the truck is in place, the lateral and longitudinal wheel restraints are installed and the nitrogen static support is engaged on the rear actuators. To isolate the DAQ computer from vehicle dynamics and vibrations, the computer is placed outside the vehicle cab during DYNTRAC testing. Sensors from both the vehicle and DYNTRAC are then connected to the DAQ system.

Static calibration of both DYNTRAC- and vehicle-mounted sensors is performed whenever sensors have been modified or when there has been a long period without testing. Calibration requires the loading of 8.8-kN (2-kip) concrete block weights onto the vehicle bed. After each load change, the digital output of the wheel scales was recorded manually and the analog output from all signals of the sensors was recorded using the DAQ system. Typically, seven to ten different loads are used for calibration. Figures 2-4, 2-5, 2-12, 2-13, 3-1, and 3-2 were obtained from static calibration data.

Once preparation steps were completed, hydraulic pumps were turned on, actuators and manifolds were brought to full pressure, and wheel pans were raised to their zero position. This zero position, determined by the set point control, was the midpoint of the piston's 152.4-mm (6-in) stroke. The actuators were then warmed up by sending a low amplitude (25.4 to 50.8 mm [1 to 2 in] peak to peak) sine wave control signal of about 0.5 Hz to the actuators. All actuators moved together. The control

signal was generated by a signal generator connected to the actuators' control console. This warm-up period typically lasted 30 min and served several purposes:

- Hydraulic oil was brought to an optimum operating temperature.
- Seals and valves became completely lubricated before more demanding road profiles were run.
- Hoses and fittings could be checked for any leaks.
- Operation of sensors and actuators could be checked for any problems before testing begins.

After the warm-up period, profile simulations were started. In addition to profile tests, dynamic calibration and random input profile tests were conducted with each load change. These tests are explained later in this chapter.

The test order was designed for operational efficiency. Test set #1, for example, involved changing all program variables except vehicle suspension. Changing tires required removing the vehicle from DYNTRAC, so all other variables were tested with the individual tire type. These tests were sequenced so that movement of the concrete weights and changing of tire pressure was minimized. Changing simulation speed and road profile simply involved software changes and was therefore easily performed. Therefore, these variables were changed before the payload or tire pressure.

Table 3-7. Ranking of parameter changes with respect to time required.

	Parameter Change
Most time-consuming	Suspension
	Tire Type
↓	Concrete Weights
	Tire Pressure
	Road Profile
Least time-consuming	Simulator Speed

3.2.2 Dynamic Calibration of Axle-Strain Gauges

Dynamic wheel force measurement utilizing axle-strain gauges and axle accelerometers was explained in detail in chapter 2. During field tests, static calibration of the axle-strain gauges was necessary to determine the force measured by the gauges. DYNTRAC provided another method for calibrating the vehicle-based force measurement system. Sine wave inputs were used to generate data for dynamic calibration. The amplitude and frequency of the wave were tuned manually to avoid vehicle pitch, heave, and roll modes. Two such tests were recorded after each load change. The dynamic wheel scales installed on DYNTRAC allowed continuous measurement of the resulting dynamic wheel forces. Axle accelerations and strain gauge voltages were also collected using the DAQ system. Slope and offset values for calibrating the axle-strain gauges could be determined by using the dynamic wheel forces measured by the scales.

Inertial wheel force was calculated using axle accelerometer data. Two methods were used to accomplish dynamic calibration during the project. The first method involved a MATLAB™ program that used numerical optimization routines to minimize the error between wheel-scale and vehicle-based measurements. Initial values for slope and offset were systematically varied until the error between measurements reached a satisfactory level (44.5 N [10 lb]). The second method, also a MATLAB™ routine, used linear regression to directly find slope and offset for the axle-strain gauges. The inertial force measured by the axle accelerometers was subtracted from the dynamic force measured by the wheel scales. The resulting forces were the axle loads used to calibrate the strain gauges. A linear regression was used to correlate the resultant force (dependent variable) with strain gauge voltage (independent variable). The regression result was a first-degree polynomial containing the slope (strain gauge sensitivity or calibration constant) and offset values. Correlation coefficients were then used to judge the quality of the calibration. Figure 2-24 in chapter 2 provides a good example of the agreement between vehicle-based and wheel-scale measurements.

3.2.3 Special Input Tests

Two additional tests were performed after dynamic calibration. They were used to characterize the system's dynamic response and to provide experimental data for comparison with planar vehicle simulation models.

3.2.3.1 White-Noise Input Tests

After dynamic calibration, DYNTRAC was run using two mathematically generated road profiles. These tests were run using a modified version of the DYNTRAC control program. The modified program sent the front- and rear-actuator command signals to the actuators at the same time regardless of wheel base. The first profile contained white noise with a cutoff frequency of 25 Hz. The second white-noise profile had a cutoff frequency of 50 Hz. These tests consisted of identical and simultaneous actuation of all four actuators. The gain in the control program was set to 0.25 during these runs because of the violent nature of the profiles.

There were two main objectives of these tests. The first was to characterize the dynamic performance of the actuators (see chapter 2). Data from these tests assisted in the system tuning process, thereby improving the frequency range of acceptable DYNTRAC response. The second objective was to provide a broad band of excitation for system natural frequency identification. The frequency information from the actuators was useful in designing a computer model of DYNTRAC, which was accomplished by Gore.[14] Examination of the test vehicle's natural frequencies is discussed in chapter 5. Third, the frequency information from the actuators was used by Gore to design a computer model of DYNTRAC.[14] Finally, these tests served to act as the final system "shake down." Sensor performance was checked during these tests, and the violent nature of these tests also quickly revealed any loose electrical or mechanical connections.

3.2.3.2 Identical Track Tests

In addition to the standard profile tests, special tests were performed to help verify vehicle computer simulations. These tests involved identical profiles, as only one

56

track is sent to both the left and right actuators. This test minimized roll in the vehicle dynamic response, thereby providing good comparison with simplified, planar, half-truck computer simulation models. Some computer models of vehicle dynamics did not consider the entire vehicle, but only a quarter-truck or half-truck. These simulations cannot measure vehicle roll if only the left or right half of the vehicle was being modeled. Therefore, experimental data with minimized vehicle roll could be useful in verifying the quality of the computer simulations.

3.2.4 Data Storage

Three different DAQ systems/programs were used during DYNTRAC tests. All systems were capable of storing the data in standard ASCII format. This format was used for archiving the data and was the working format for data processing. ASCII format allowed for easy import to data processing and plotting software packages such as MATLAB™, MINITAB™, and Deltagraph™. This format was also used for data archiving. Because of the relatively large size of the ASCII files, DYNTRAC tests alone consumed nearly 1 Gb of storage. Table 3-8 presents a list of sizes for several typical data files that were collected as a part of DYNTRAC simulation set #3 (set #3 is identified in table 3-6).

Table 3-8. Select DYNTRAC data file sizes.

Speed of Simulation km/h (mi/h)	Size of ASCII File 1,000's of bytes
24 (15)	3,923
48 (30)	1,322
72 (45)	972
89 (55)	702

For DYNTRAC tests alone, this requires 975,579,000 bytes (approximately 1 Gb) of storage. To ensure safe storage, two separate copies of the ASCII data files were made, thereby doubling the data storage requirements. Most of the binary versions of

57

the data were also kept. Before considering the data from the field tests, the required storage size was now approximately 3 Gb.

Removable storage media were used to satisfy the storage needs for this project. Magneto-optical disks capable of storing 650 Mb of data (325 Mb per side) on each disk were selected for the project. The magneto-optical disk drive was connected to the computer via an SCSI connection, allowing the drive to be quickly connected to the data acquisition computer for downloading test data during a break in the test sequence. The read/write speeds of the portable drive permitted easy manipulation and processing of large amounts of data. In addition, the computer resources at the TFHRC allowed easy transfer of test data to FHWA personnel.

A comprehensive guide to the file names used, location of data files, and a description of the ASCII files themselves are contained in the appendix.

3.3 FIELD TESTS

Field-test roads were selected by FHWA personnel on the basis of profilometer measurements, location with regard to travel time from TFHRC, and ease of vehicle access with regard to traffic and maneuverability. Analysis of the first set of DYNTRAC data indicated that tire type did not significantly affect dynamic wheel forces. Therefore, only one tire type was used for field tests. Tire pressure was only varied on the medium-roughness road, providing field validation of DYNTRAC tests. Tire pressure was shown to have little effect on vertical wheel forces. Table 3-9 lists the variables used during field tests.

58

Table 3-9. Field-test parameters.

Low Roughness RT15N	Leaf spring suspension 1 Tire Type: 11R22.5 4 Load Configurations: 0-, 17.6-, 35.2-, 61.6-kN payloads 4 Speeds: 24, 48, 72, 88 km/h
Medium Roughness Clara Barton Parkway (Clarab)	Leaf spring suspension 1 Tire Type: 11R22.5 4 Load Configurations: 0-, 17.6-, 35.2-, 61.6-kN payloads 3 Tire Pressures: 482, 655, 827 kPa 4 Speeds: 24, 48, 72, 88 km/h
High Roughness RT659	Leaf spring suspension 1 Tire Type: 11R22.5 4 Load Configurations: 0-, 17.6-, 35.2-, 61.6-kN payloads 3 Speeds: 24, 48, 72 km/h

Two tests were conducted for each parameter combination. Additional tests were conducted if an insufficient number of pavement markers (reflective tape position and velocity markers) were sensed by the vehicle-mounted, retroreflective IR sensor.

At least two test-road profiles were collected on each test day. One measured profile of each road was selected for filtering for conversion into a DYNTRAC input profile. On average, about two load configurations were tested per day. Factors influencing this schedule included the following:

- Round-trip time to RT659 was over 50 min.
- Late afternoon rain showers often caused tests to be delayed.
- Morning and evening rush hour affected traffic patterns for RT15 and the Clara Barton Parkway.

After each load change, static axle loads were measured, and a complete static calibration of the axle-strain gauges was performed. The following sections discuss the

general procedure used for field tests, problems encountered with axle-strain gauges, and storage of test data.

3.3.1 Test Procedures

Field tests were accomplished with support provided by FHWA personnel. On the morning of a field test, FHWA personnel would measure the profiles of the selected roads and then mark the roads with reflective tape. The two reflective strips were spaced every 100 m (328 ft). The two strips would be placed 2 m (6.6 ft) apart. The entire length of each test road is 700 m (2,295 ft). Therefore, eight sets of road markers were used. These strips would appear as spikes on the retroreflective, IR sensor output. These spikes were used to determine position along the road and to verify vehicle speed.

While the roads were being measured and marked, the test vehicle was prepared for testing. The DAQ system was installed in the vehicle and tested. Static calibration of the axle-strain gauges was performed and a final static wheel weight was recorded before leaving for the test sites.

Data acquisition was manually triggered upon commencement of testing at the selected test road. When the end of the test road was reached, the data from the IR sensors was quickly replayed to determine the acceptability of the test. Test acceptance criteria included: (1) at least one of the two strips must have been recorded at both the beginning and end of the test, and (2) at least five full sets of markers must have been sensed.

3.3.2 Performance of Axle-Strain Gauges

Figure 3-12 presents axle-strain gauge data from several axle-strain gauge calibration tests, collected at various times and on various days. It was obvious that axle-strain gauge sensitivity (or associated electronics) was affected by temperature and/or humidity. Similar sensitivity variations were observed with the right-rear axle gauges. Because the vehicle was scheduled for a suspension change, and because at

60

least one of the test roads was scheduled to be resurfaced, field tests had to continue without replacing the strain gauges. No significant drifts were detected during actual tests, and new calibration tests were made at every opportunity. The processed results revealed expected trends in dynamic load coefficients.
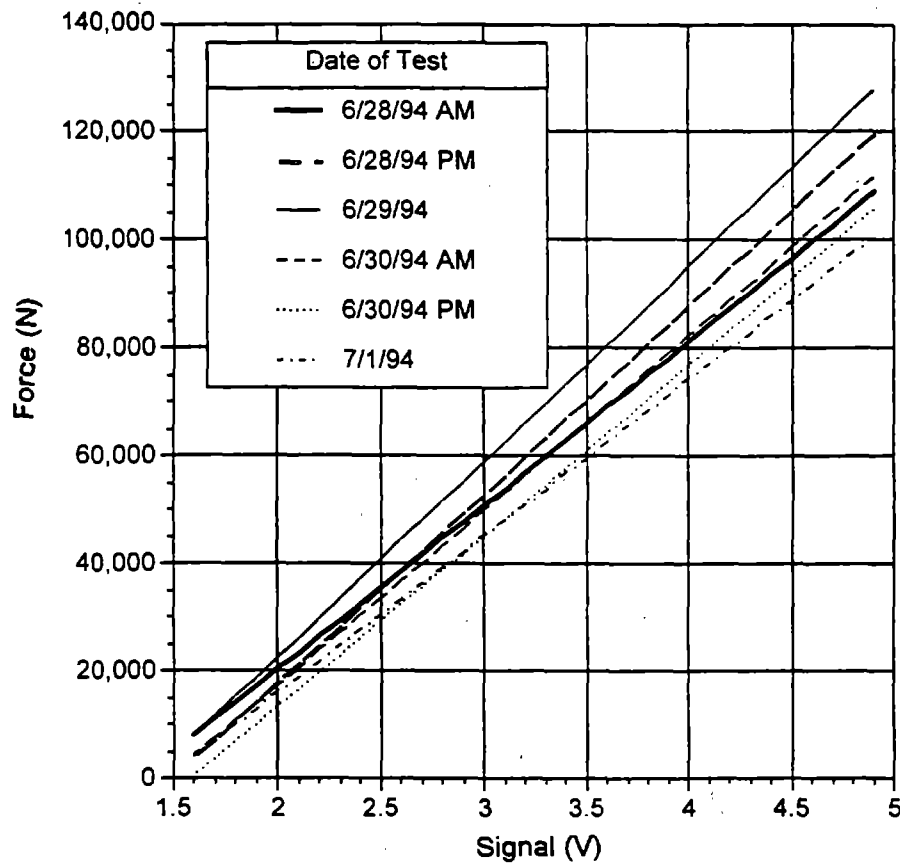
Figure 3-12. Slope drift of left-rear axle-strain gauges.

During the suspension change from leaf spring to air, new axle-strain gauges were installed on the rear axle. The new gauges performed with constant calibration values during the third set of DYNTRAC tests.

3.3.3 Data Storage

The same data storage system used for DYNTRAC tests was employed for the field tests. A comprehensive guide to the file names used, location of data files, and a description of the ASCII files themselves are contained in the appendix.

3.4 TESTS ON INSTRUMENTED ROAD

As mentioned in chapter 2, problems with the internal gauges of the instrumented road prevented extensive testing as originally planned. Sensors and processing procedures are also described in that chapter. Figure 3-13 is a plot of both the pavement-based and the vehicle-based triggers. Note that the third peak of the vehicle-based sensor matches the pavement-based sensor. These peaks would provide a common starting point in time for the pavement-sensor data files and for the vehicle-sensor data files. The three spikes from the vehicle-based sensor would be used to determine the position of the vehicle with respect to the instrumented road, as discussed in chapter 2.
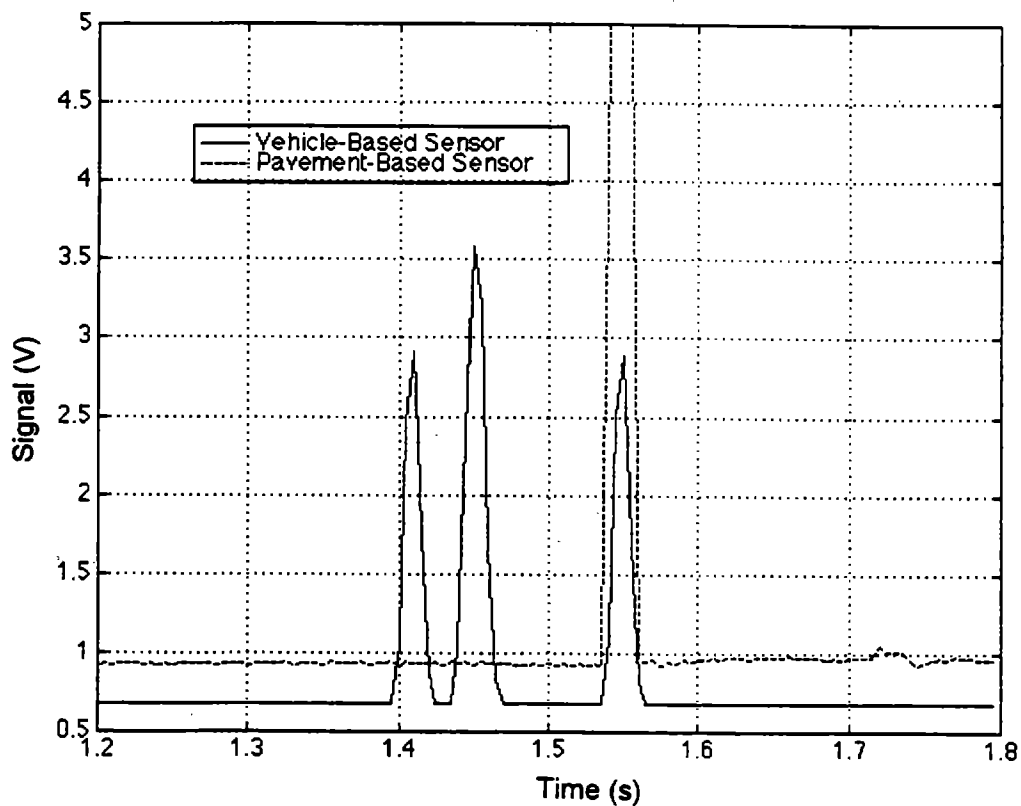
Figure 3-13. Example of pavement trigger and lateral position sensors.

CHAPTER 4. DEVELOPMENT OF WHEEL-FORCE TRANSDUCERS

4.1 INTRODUCTION

There has been a continual search for means to measure dynamic tire forces on pavement. Particularly when dealing with heavy vehicles, the interest is in identifying a tool that is useful in studying both the effect of vehicle dynamics on dynamic pavement forces and the effect of road profile on vehicle response. It is reasonable to expect that the closer the measurement is made to the point of interest (at the tire/pavement contact patch), the better will be the measurement. Ideally, an instrument would be mounted to the surface of the tire and, as the vehicle traveled, the instrument would report the dynamic forces between the tire and the road. Because an instrument such as this does not exist, other measurement locations have been considered. For example, one standard approach is to mount strain gauges on the axles of vehicles to determine dynamic axle loads. By estimating the mass outboard from the strain gauge location and using accelerometer data, inertial loading can be approximately determined and dynamic wheel loads on pavement can be back-calculated. Several difficulties exist with this approach. First, it is very difficult to accurately estimate the mass that is outboard from the axle-strain gauge. Accurate determination of this parameter can require disassembly of the axle. Second, depending on the configuration of an axle and suspension, it is often difficult to mount gauges in appropriate locations on the axle housing.

To address these difficulties, a new wheel-force transducer was designed. The transducer was mounted between the wheel and its hub. In the following sections, design criteria are presented, the WFT design that met these criteria is described, system mounting and operations are discussed, and WFT performance is compared against axle-strain gauge data.

4.2 DESIGN AND MODIFICATIONS

4.2.1 WFT Design Requirements

WFT design criteria include the following:

1. Weight should be kept below 445 N (100 lbf). Simulations have demonstrated that if weight is kept below 1,340 N (300 lbf), dynamic wheel forces will change by less than 5 percent.

2. System stresses must be low enough to provide fatigue life of better than 10^6 cycles. This is often correlated with infinite life when considering fatigue loading of steel.

3. Vertical and forward/backward horizontal wheel forces should be measured.

4. Wheel offset should be at a minimum.

5. The WFT should be mountable to a heavy vehicle without making any modifications to the vehicle or wheel.

6. The transducer and wheel should be mountable using a standard impact wrench and socket.

7. Standard wheel-bolt torque specifications should be achievable for mounting of both the transducer and the wheel.

8. On-wheel electronics must be rugged enough to withstand operating conditions.

9. Slip rings should not corrupt strain-gauge data.

10. The WFT and electronics housing should be easily transportable.

11. The WFT should be able to be conveniently mounted and dismounted by one person.

12. Acceleration must be measured to allow inertial correction to WFT measurements.

13. Wheel orientation must be measured to within 0.5° accuracy.

A discussion of the original wheel-force transducer is presented in the next section.

4.2.2 Evaluation of Original WFT, Modifications to Original Transducer, and Design of New Transducers

FHWA delivered a WFT to the Pennsylvania Transportation Institute (PTI) with accompanying machine drawings. The machine drawings differed in both features and dimensions from the WFT that was delivered to PTI. The actual hardware delivered included features and dimensions as indicated in table 4-1. No explanation regarding discrepancies between drawings and hardware were provided. The original WFT delivered to PTI will be referred to as WFT0. Changes were made to WFT0, and this transducer, after modifications, will be referred to as WFT1. The three new transducers will be referred to as WFT2, WFT3, and WFT4. The new WFT2, WFT3, and WFT4 designs are shown in figures 4-1 through 4-3.

WFT0 as delivered to PTI did not work for a number of reasons. Two obvious items that were missing from the WFT0 were wheel orientation measurement and wheel acceleration measurement. Without these two measurements, it was impossible to accurately resolve bridge voltage into horizontal and vertical force components. It was also impossible to correct for inertial loads resulting from wheel acceleration. These inertial loads had to be accommodated to relate axle force measurements from WFT's to vertical wheel/pavement forces.

In addition to the two obvious omissions in WFT0 design, table 4-1 identifies several other problems and disadvantages associated with the original WFT0 design. For each WFT0 problem item, table 4-1 identifies modifications that were made to achieve the working WFT1, and solutions that were implemented in construction of WFT2, WFT3, and WFT4.

Table 4-1. Problems with WFT0 and modifications that were made to achieve functionality.

1	WFT0 Item:	No wheel orientation instrumentation was included in the WFT.
	Modification to achieve WFT1 functionality:	A resolver with a 7-min accuracy was employed with associated resolver to digital converter and D/A chip.
	WFT2, WFT3, WFT4 design:	A resolver with a 7-min accuracy was employed with associated resolver to digital converter and D/A chip.
2	WFT0 Item:	No wheel acceleration instrumentation was included in the WFT.
	Modification to achieve WFT1 functionality:	An accelerometer was mounted on WFT1.
	WFT2, WFT3, WFT4 design:	An accelerometer was mounted in each of the new WFT electronics housings.
3	WFT0 Item:	The required 612 N-m (450 ft-lb) torque could not be applied with an open-end wrench. This necessitated an extension bar, which was nearly impossible to use because of limited space inside the wheel well. When the required torque was introduced, the open-end wrench was destroyed. This item rendered the WFT unsafe for highway use.
	Modification to achieve WFT1 functionality:	Clearance holes were drilled through the outer ring, allowing inner nut cups to be used to fasten the WFT to the axle hub. The inner nut cup heads were shortened so as not to protrude outside of the outer ring. An impact socket could then be used to torque the WFT mounting nuts (inner nut cups) to specs.
	WFT2, WFT3, WFT4 design:	Clearance holes were provided in the outer ring to allow inner nut cups to be used to fasten the WFT to the axle hub. The new WFT's were slightly wider than WFT0 so that full-length inner nut cups could be used to fasten the WFT's to the wheel hub. An impact socket could then be used to torque the WFT mounting nuts (inner nut cups) to specs.
4	WFT0 Item:	Mounting of the WFT could not be done by one person. A minimum of two people was required. One person was needed to align the WFT while one or two others attempted to simultaneously align 10 lug nuts between the inside and outside WFT rings, and to start threading each of those nuts on respective studs.

Table 4-1. Problems with WFT0 and modifications that were made to achieve functionality (continued).

	Modification to achieve WFT1 functionality:	WFT1 was mounted to the hub via clearance holes in the outside ring. This allowed system mounting by one person.
	WFT2, WFT3, WFT4 design:	New WFT's were mounted to a hub via clearance holes in the outside ring. This allowed system mounting by one person.
5	WFT0 Item:	Mounting the WFT required releasing the rear brakes and rotating the wheel to allow access to lug nuts with an open-end wrench and an extension bar.
	Modification to achieve WFT1 functionality:	Access holes for impact sockets allowed WFT mounting without releasing rear brakes.
	WFT2, WFT3, WFT4 design:	Access holes for impact sockets allowed WFT mounting without releasing rear brakes.
6	WFT0 Item:	Mounting of WFT0 was extremely tedious. It required small, sequential turns of each of 10 lug nuts using an open-end wrench while inside the wheel well.
	Modification to achieve WFT1 functionality:	An impact wrench could be used to mount WFT1 to a hub.
	WFT2, WFT3, WFT4 design:	An impact wrench could be used to mount the new WFT's to a hub.
7	WFT0 Item:	Strain gauges and associated wiring were easily damaged with the open-end wrench when lug nuts were mounted and tightened. If more than a very limited rotation range (approximately 1/6 turn) of a lug nut was executed with the open-end wrench, the end of that wrench would bear on the inner ring of the WFT and crush either strain gauges or attached wiring.
	Modification to achieve WFT1 functionality:	By using an impact socket through the outer ring, all risk of strain gauge damage from mounting tools was eliminated.
	WFT2, WFT3, WFT4 design:	By using an impact socket through the outer ring, all risk of strain gauge damage from mounting tools was eliminated.

Table 4-1. Problems with WFT0 and modifications that were made to achieve functionality (continued).

8	WFT0 Item:	Lugs mounted in the outer ring were specified as being press-fit from the back of the ring. Actual hardware execution included studs that were threaded into the outer ring. When specified torque of 748 N-m (550 ft-lb) for mounting bud wheels was applied to the WFT studs, they unscrewed from their threaded attachment to the WFT. The purpose of this design change was not discussed in the original WFT report. As to the reason for this change, it appears that the head of the stud that was specified in the prints would have interfered with the open-end wrench clearance requirements. This might have motivated elimination of the head in favor of the threaded-stud attachment. The threaded-stud design increases WFT manufacturing costs. It is not known if a strength comparison was made between a standard press-fit stud and a turned stud.
	Modification to achieve WFT1 functionality:	No modification was possible. WFT1 was functional, but the full torque of 748 N-m (550 ft-lb) could unseat the threaded stud heads.
	WFT2, WFT3, WFT4 design:	Press-fit studs were used in the new WFT design.
9	WFT0 Item:	Mounting of the inner wheel of doubles was accomplished with inner nut cups that were through-drilled to traverse extra-long WFT studs. The resulting thin wall square head of these inner nut cups was not strong enough to sustain torque requirements and cracked when used.
	Modification to achieve WFT1 functionality:	No modification was possible. WFT1 was functional, but it was not possible to apply full torque specs to the inner nut cups used to secure the inner wheel of duals.
	WFT2, WFT3, WFT4 design:	Regular-length studs were used in the new WFT design. This allowed use of standard inner nut cups without the need to through-drill those nut cups.
10	WFT0 Item:	Five 0.34-kg (3/4-lb) mounting brackets were attached outside the outer wheel. This hardware was used in the mounting of the wheel electronics to the rotating wheel. This item adds additional unnecessary weight to the wheel, increases WFT manufacturing costs, and adds unnecessary complexity to the WFT mounting arrangement.

	Modification to achieve WFT1 functionality:	No modification was possible. WFT1 was functional, but additional hardware was needed to fasten the electronics housing to the wheel.
	WFT2, WFT3, WFT4 design:	Extra-long inner nut cups were used in the new WFT design. This allowed mounting of the electronics housing directly to the inner nut cups, thereby eliminating the need for additional mounting brackets.
11	WFT0 Item:	Unshielded wires were used to connect the strain gauges to the slip rings. This choice introduced the unnecessary potential for noise in the strain data.
	Modification to achieve WFT1 functionality:	All wires used were high temperature shielded.
	WFT2, WFT3, WFT4 design:	All wires used were high temperature shielded.
12	WFT0 Item:	Studs were through-drilled to allow wires to be pulled through them. This resulted in a weakening of the studs.
	Modification to achieve WFT1 functionality:	No modification was made. Through-drilled studs are functional, but not as strong as the new WFT design.
	WFT2, WFT3, WFT4 design:	The new WFT design used standard solid studs.
13	WFT0 Item:	The unshielded wires were brought through the hollow studs and into the electronics housing. These wires were easily damaged during handling, mounting, and in-service use of the WFT. Wire fatigue at the exit point of the stud was common.
	Modification to achieve WFT1 functionality:	Connection between strain gauges and slip rings, in the new WFT design, was achieved via a replaceable cable between the hub and the WFT electronics housing.
	WFT2, WFT3, WFT4 design:	The new WFT design brought strain-gauge wires through the wheel valve access hole. Impact sockets will then be usable on all 10 lug nuts.
14	WFT0 Item:	Electronics used inside the WFT caused cross talk between bridge signals. This rendered strain/load information useless.

Table 4-1. Problems with WFT0 and modifications that were made to achieve functionality (continued).

	Modification to achieve WFT1 functionality:	WFT1 used independent electronics for each strain gauge bridge to bring current signals through the slip rings.
	WFT2, WFT3, WFT4 design:	Independent electronics for each strain gauge bridge were used to bring current signals through the slip rings.
15	WFT0 Item:	WFT power supplies were much larger than necessary.
	Modification to achieve WFT1 functionality:	Smaller and lighter power supplies were used with WFT1.
	WFT2, WFT3, WFT4 design:	Smaller and lighter power supplies were used with the new WFT's.
16	WFT0 Item:	WFT electronics filtering was set at a corner frequency of 10 Hz. Output data were therefore rendered useless.
	Modification to achieve WFT1 functionality:	All filtering was removed from WFT electronics. Filtering is done via 7-pole elliptical, low-pass filters with 40-Hz corner frequency inside the DAQ system.
	WFT2, WFT3, WFT4 design:	Filtering was done via 7-pole elliptical, low-pass filters with 40-Hz corner frequency inside the DAQ system.
17	WFT0 Item:	No provision was made to reduce electronics housing dimensions for use of front wheels. The original system protruded 406 mm (16 in) outside the truck tire when mounted on a front wheel.
	Modification to achieve WFT1 functionality:	No modification was made. WFT1 was functional but not convenient for front-wheel use.
	WFT2, WFT3, WFT4 design:	Electronics housings were designed to facilitate easy modification for front-wheel use.
18	WFT0 Item:	Screw terminals provided a less-than-convenient means for connecting the cables, which protruded from the WFT studs to the slip rings.
	Modification to achieve WFT1 functionality:	Mil spec. plugs and sockets were used.
	WFT2, WFT3, WFT4 design:	Mil spec. plugs and sockets were used.

Table 4-1. Problems with WFT0 and modifications that were made to achieve functionality (continued).

19	WFT0 Item:	No consideration was given to the fatigue from wheel rotation and vibration of excess wire lengths inside the WFT housing.
	Modification to achieve WFT1 functionality:	Excess wire length was eliminated.
	WFT2, WFT3, WFT4 design:	Excess wire length was eliminated in the new design. The gauge-to-housing cable was strain reinforced at both ends.
20	WFT0 Item:	WFT electronics located on the wheel included a microprocessor chip in a surface mount base. This presented the possibility of the chip vibrating loose during operation.
	Modification to achieve WFT1 functionality:	The surface-mount base was removed.
	WFT2, WFT3, WFT4 design:	No surface-mount base was used.

Safety associated with WFT use was studied with the use of a finite element analysis. Finite element analyses of both the original transducer as delivered to PTI and the new design incorporating the above-mentioned modifications were completed. These models did not predict any problems in terms of yield strength or fatigue strength of the WFT.

4.2.3 New WFT Design

WFT force ring schematics are given in figure 4-1 through figure 4-3. Only nominal dimensions are shown in these figures.

r 0.25 typ between rings and tube for smooth transition.

NOTES:
All units in inches except where noted.

Inner ring, outer ring, and tube are made of one piece of stainless steel.

This surface polished

Clearance Holes (10) for Ø1 5/16 Diameter Press Fit Stud Head
Ø1 3/8

Ø13-1/2
Ø11-1/4
Ø9-1/8
Ø8-3/4

A

Conical Seat
Ø26.7 mm
Ø21.8 mm
Wheel Stud Clearance
A

Det A-A

Inner Ring   Outer Ring

1-3/4

21.8 mm   26.7 mm

1 in=25.4 mm

Figure 4-1. Edge view of WFT strain-gauged force ring.
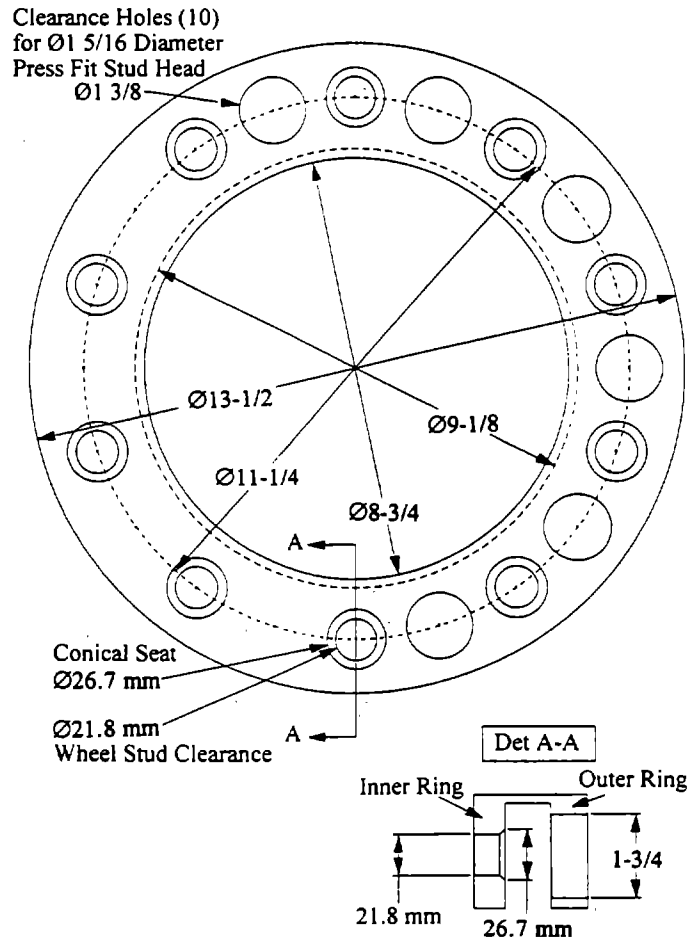
Figure 4-2. WFT inside ring.

72

Clearance Holes (10)
for Impact Socket
Ø1 3/4

Ø13-1/2

Ø9-1/8

Ø1-1/4

Ø8-3/4

Ø for press fit on wheel stud
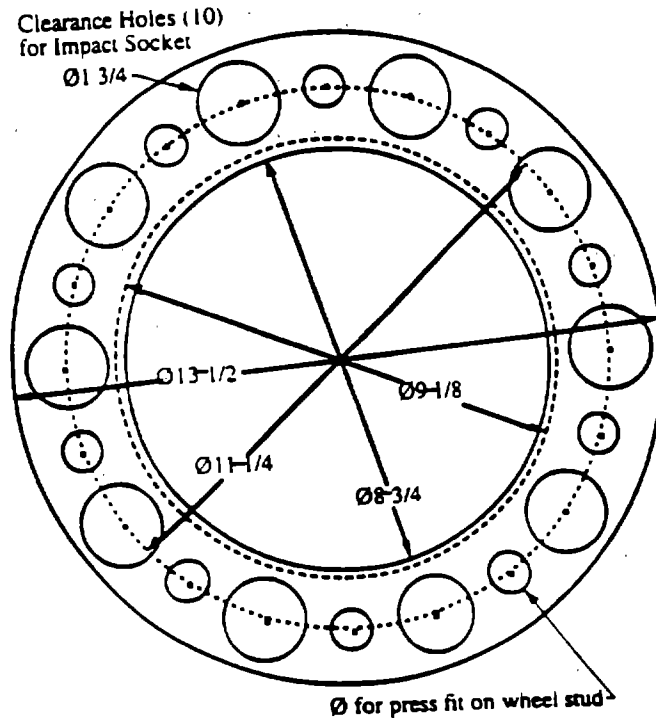
1 in = 25.4 mm

Figure 4-3. WFT outside ring.

The overall width of the force ring was determined by both ring thickness and tube-length requirements. A finite element method (FEM) of this strain-gauged force ring was performed to identify stress concentrators that might arise from holes in the inner ring, holes in the outer ring, tube thickness, or tube-to-ring radius. The tube length of 24 mm (15/16 in) provided a uniform strain field that responded linearly to applied loads.

The inside ring was designed to slide over the studs of standard Budd wheels. The inner ring was secured to the hub using inner nut cups. Because the square head of an inner nut is relatively small, a stock impact socket was available with an outside diameter that would fit through the 44-mm (1-3/4-in) clearance hole in the outside ring. Inner/outer-ring hole alignment for inner nut cup fastening is given as detail A-A in figure 4-2. This arrangement allows the use of standard pneumatic tools for WFT mounting and dismounting.

73

Studs are attached to the outside ring of the WFT to allow mounting of a wheel. To provide enough strength to withstand the 1,020-N-m (750-ft-lbf) bolt-torque mounting specifications, the studs had to be press-fit into the outer ring. This required clearance holes in the inner ring through which the studs were pressed. Single or dual Budd wheels could then be mounted to the WFT in the usual manner.

Two full strain-gauge bridges were mounted onto the tube, which is shown in the figure 4-1 schematic. The bridges were 90° apart and were mounted such that strain arising from axial, torsional, and bending wheel loads was canceled out. Theoretically, the strain-gauge bridges measure shear force only. Shear force is generated by either vertical wheel forces or fore/aft horizontal wheel forces.

4.2.4 WFT Electronics

After the wheels were mounted to the WFT, an electronics housing was mounted to the outside wheel. Strain-gauge bridge wiring was brought into this housing for signal conditioning. Because voltage signals can be affected when passing through slip rings, strain-gauge amplifiers that provide current output were chosen. After these signals were brought through the slip rings, voltage across a precision resistor was monitored. The voltage signals were brought through a low-pass, anti-aliasing filter.

A resolver was also mounted in the electronics housing and an accelerometer was mounted on the nonrotating portion of the WFT. The resolver provided angular position resolution. All data were collected using a personal computer through an analog-to-digital converter board at a sampling rate of 200 Hz.

4.3 TESTING AND ANALYSIS

4.3.1 Axle-Strain Measurements

To compare WFT performance in the field, strain gauges were mounted to the rear axle of a truck. Shear gauges were mounted to the front and back sides of the axle housing.

4.3.2 Test Procedure

The wheel-force transducer was mounted on a vehicle. The static wheel load was measured using a wheel scale. Care was taken when measuring the static wheel load so that the truck remained horizontal. This was accomplished with the use of wooden blocks under the other wheels, with height equal to the wheel-scale height. The vehicle was driven slowly on a level surface. When the clutch was free, and the vehicle was coasting slowly, horizontal forces were minimal and dynamic vehicle oscillations were relatively small. WFT data were collected. These data were used to identify a zero-angle reference position, and also to generate error-correction data to be applied to high-speed tests.

4.3.3 WFT Algorithms

Vertical force Fv and horizontal force Fh on the wheel-force transducer can be calculated as follows:

$$Fv = Fa \sin q + Fb \cos q \qquad (4\text{-}1)$$

$$Fh = Fa \cos q - Fb \sin q \qquad (4\text{-}2)$$

where

$$Fa = Ca * Va + Cao$$
$$Fb = Cb * Vb + Cbo$$

and

Ca, Cao	= calibration factor slope and offset for strain-gauge bridge "a."
Cb, Cbo	= calibration factor slope and offset for strain-gauge bridge "b."
Va	= bridge "a" output voltage.
Vb	= bridge "b" output voltage.
q	= wheel angle given by resolver.

The total dynamic forces at the interface between the tire and the road can be calculated using equations 4-1 and 4-2 with inertial force compensation. Then the

vertical and horizontal forces at the tire/pavement contact, Fvw and Fhw, respectively, are given by

$$Fvw = Fv + W + Fvi \qquad (4\text{-}3)$$

$$Fhw = Fh + Fhi \qquad (4\text{-}4)$$

where

$$Fvi = \_ M * Avi$$
$$Fhi = \_ M * Ahi$$

and

W = static wheel and tire weight.

Fvi = all vertical inertial forces from mass outboard from the WFT.

Fhi = all horizontal inertial forces from mass outboard from the WFT.

M = mass outboard from WFT.

Avi = vertical acceleration of center of gravity of wheel(s).

Ahi = horizontal acceleration of center of gravity of wheel(s).

4.3.4 Data Processing

If the WFT were a perfect measurement instrument, if the vehicle were rolling on a flat, horizontal surface, and if the vehicle were not vibrating or bouncing at all, then the output for bridge "a" and bridge "b" should be a perfect sine and cosine wave, respectively, for one wheel rotation. Since this was not the case, error was observed in the WFT signals. It is helpful to recognize that a large portion of the error in this instrument was periodic in one wheel rotation, $\theta = 0$ to $360°$. This was true for any imperfection in WFT material homogeneity, strain-gauge mounting, and strain-gauge bridge response. A Fourier series was ideally suited to provide an error-correction algorithm for the WFT. The error correction can be explained in terms of the bridge "a" and bridge "b" voltage reported in figures 4-4 and 4-5.
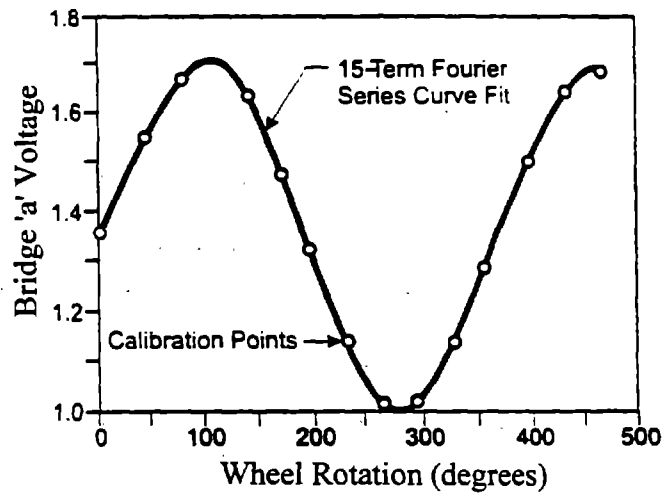
Figure 4-4. Bridge "a" calibration data.
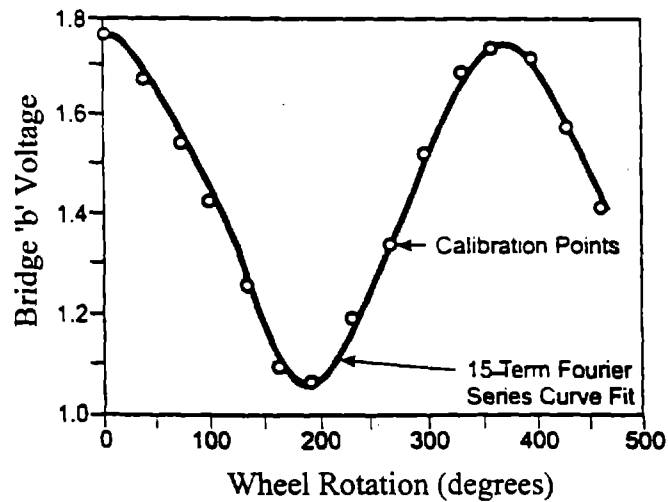
Figure 4-5. Bridge "b" calibration data.

The data from figures 4-4 and 4-5 were obtained by incrementally moving the truck forward by approximately 30° of wheel rotation for slightly more than one complete wheel revolution. At each wheel-rotation increment, the vehicle was stationary and, without any applied brake force, WFT data were collected from strain-gauge bridges "a" and "b." The bridge data collected were purely static data arising from vertical wheel loads, with negligible horizontal forces applied. Fifteen data points are presented in figures 4-4 and 4-5. From these figures, it can be observed that bridge "a" produced a

signal that was close to the expected sine wave, but the bridge "b" response deviated noticeably from the expected cosine wave.

The data from this static testing were not equally spaced. To generate equally spaced data for Fourier transform algorithms, a cubic spline curve-fitting algorithm was applied to the 15 experimental points shown in figures 4-4 and 4-5. Equally spaced data in θ were then obtained from these cubic curves and a 15-term Fourier series expansion of each of these curves was generated. The Fourier series expansion of a periodic signal is given by:

$$
\begin{aligned}
V(\theta) = \ & C_0 \cos \phi_0 \\
& + C_1 \cos(\theta + \phi_1) \\
& + C_2 \cos(2\theta + \phi_2) \\
& + C_3 \cos(3\theta + \phi_3) \\
& + ...
\end{aligned}
\tag{4-5}
$$

or

$$
\begin{aligned}
V(\theta) = \ & C_0 \cos \phi_0 \\
& + C_1 (\cos \phi_1 \cos \theta - \sin \phi_1 \sin \theta) \\
& + C_2 \cos(2\theta + \phi_2) \\
& + C_3 \cos(3\theta + \phi_3) \\
& + ...
\end{aligned}
\tag{4-6}
$$

Theoretically, in the perfect WFT, bridge "a" should be a sine wave. Therefore, for static measurements, the error in the bridge "a" measurement is known to be the difference between the actual bridge "a" response and a perfect sine wave. If bridge "a" responded perfectly as a sine wave, then $V(\theta)$ in equation 4-6 would equal $C_1 \sin \theta$. Therefore, all terms in equation 4-6 besides $C_1 \sin \theta$ could be considered inaccurate. Bridge voltage V_a could therefore be corrected. Let the corrected voltage be called V_{anew}. Since V_{anew} should be a perfect sine wave, let $V_{anew} = C_1 \sin \theta$. Then, solving equation 4-6 for $C_1 \sin \theta$,

$$V_{anew}(\theta) = [-V_a(\theta) + C_{a0} \cos \phi_{a0}$$
$$+ C_{a1} \cos \phi_{a1} \cos \theta$$
$$+ C_{a2} \cos(2\theta + \phi_{a2})$$
$$+ C_{a3} \cos(3\theta + \phi_{a3})$$
$$+ ...]/\sin \phi_{a1} \qquad (4\text{-}7)$$

Similarly, if bridge "b" responded perfectly as a cosine wave, then $V(\theta)$ in equation 4-6 would equal $C_1 \cos \theta$. Therefore, all terms in equation 4-6 besides **$C_1 \cos \theta$** can be considered inaccurate. V_b can therefore be corrected by:

$$V_{bnew}(\theta) = [V_b(\theta) - C_{b0} \cos \phi_{b0}$$
$$+ C_{B1} \sin \phi_{b1} \sin \theta$$
$$- C_{b2} \cos(2\theta + \phi_{b2})$$
$$- C_{b3} \cos(3\theta + \phi_{b3})$$
$$- ...]/\cos \phi_{b1} \qquad (4\text{-}8)$$

It should be noted that the corrections of equations 4-7 and 4-8 shift the bridge "a" and bridge "b" voltage signals through phase angles ϕ_{a1} and ϕ_{b1}, respectively. These phase angles arise because one wheel position was assigned the $\theta = 0°$. However, when bridges "a" and "b" are combined to obtain vertical wheel force, an arbitrary choice of $\theta = 0°$ results in degradation of measurement accuracy. Bridge "a" and "b" maximum sensitivity occurred when the respective bridge was in its horizontal position. However, an arbitrary $\theta = 0°$ position forces a less sensitive bridge position to provide a peak V_{anew} and V_{bnew} signal. To avoid this undesirable consequence, the $\theta = 0°$ wheel orientation was carefully chosen. For perfect bridge "a" and bridge "b" response, then $\theta = 0°$ when the bridge "b" (cosine) response is maximum and $\theta = 90°$ when the bridge "a" (sine) response is maximum. Because the bridge "a" and "b" peaks were not 90° apart, an averaged value of θ corresponding to peak response of bridges "a" and "b" was used, as follows:

$$\theta_0 = \theta(V_{bmax}) + \{90° - [\theta(V_{amax}) - \theta(V_{bmax})]\}/2 \qquad (4\text{-}9)$$

79

where $\theta(V_{amax})$ corresponds to the value of θ when V is maximum for bridge "a" in equation 4-7 and $\theta(V_{bmax})$ corresponds to the value of θ when V is maximum for bridge "b" in equation 4-8. The values of ϕ_{a1} and ϕ_{b1} angles in equations 4-7 and 4-8 should be reasonably close to the value of θ corresponding to maximum bridge "a" and "b" voltages, respectively. The value of θ_0 in equation 4-9 is then taken as the zero wheel orientation, and V_{anew} and V_{bnew} are obtained from equations 4-7 and 4-8.

4.3.5 WFT Performance

Calibration data were collected and error correction was applied to slow-rolling vehicle tests. After inertial correction for both WFT and axle housing strain-gauge data, vertical wheel force was calculated, and both signals were plotted in figure 4-5. WFT response was shown to correlate very well with axle-strain data. Force peaks between the two curves typically differed by less than 2,200 N (500 lbf) or about 7 percent of the nominal signal.

Higher-speed test data are shown in figure 4-7. At 56 km/h (35 mi/h), peak forces reported by WFT and axle strain both indicated that similar vehicle dynamics were being captured.
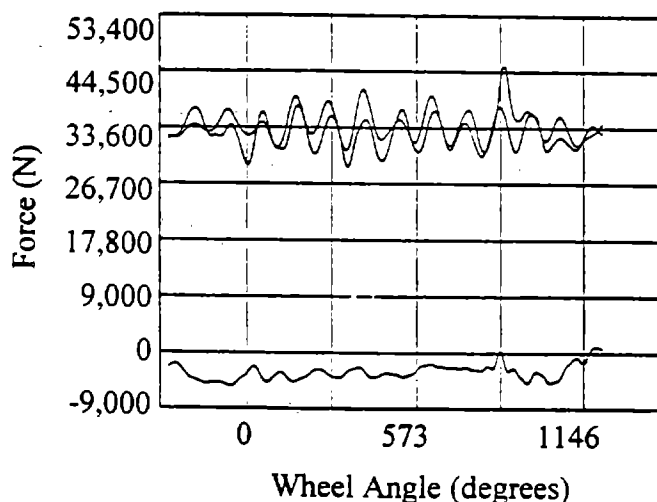
Figure 4-6. Comparison of WFT and axle-force measurements (static wheel load = 34,470 N [7,750 lbf], slow rolling).
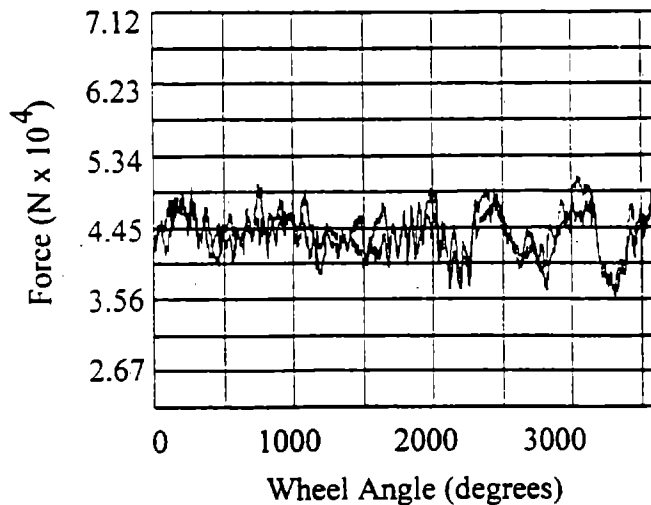
Figure 4-7. Comparison of WFT and axle-force measurements.

4.3.6 Effect of WFT Mass on Dynamic Load Coefficients (DLC's)

Three tests were used to evaluate the inertial effects of the WFT on the test vehicle. Two tests were conducted without the WFT. The third test was performed with the WFT assembly attached to the vehicle. Two different data sets without the WFT were used to demonstrate the variations between identical test setups. All of the tests used the following parameters:

- Air suspension.
- Penn5a profile (IRI of right track: 2.67 mm/m [169 in/mi], IRI of left track: 2.87 mm/m [182 in/mi]).
- Speed: 72.45 km/h (45 mi/h).
- Payload: Empty.
- Tire Type: Wide-base tires on rear, standard duals on front.

The following statistics in table 4-2 were obtained from the three tests:

81

Table 4-2. Dynamic force statistics.

Configuration	Left-rear DLC	Right-rear DLC	Left-rear mean force (N)	Right-rear mean force (N)	Left-rear maximum force (N)	Right-rear maximum force (N)
No WFT - A	0.1768	0.1258	17,220	19,231	29,888	28,780
No WFT - B	0.1699	0.1019	17,528	23,262	29,768	33,515
With WFT on left-rear hub	0.1721	0.1157	17,601	23,644	30,368	33,853

Left-rear DLC's varied 4 percent for repeated tests with identical test configurations. Adding the WFT resulted in 2.7 percent and 1.3 percent variation from tests A and B, respectively. Similar effects were observed on the right-rear DLC, even though no WFT was installed on that wheel. Further comparison was provided by the power spectral density of the left-rear scale force for the three tests, as shown in figure 4-8.
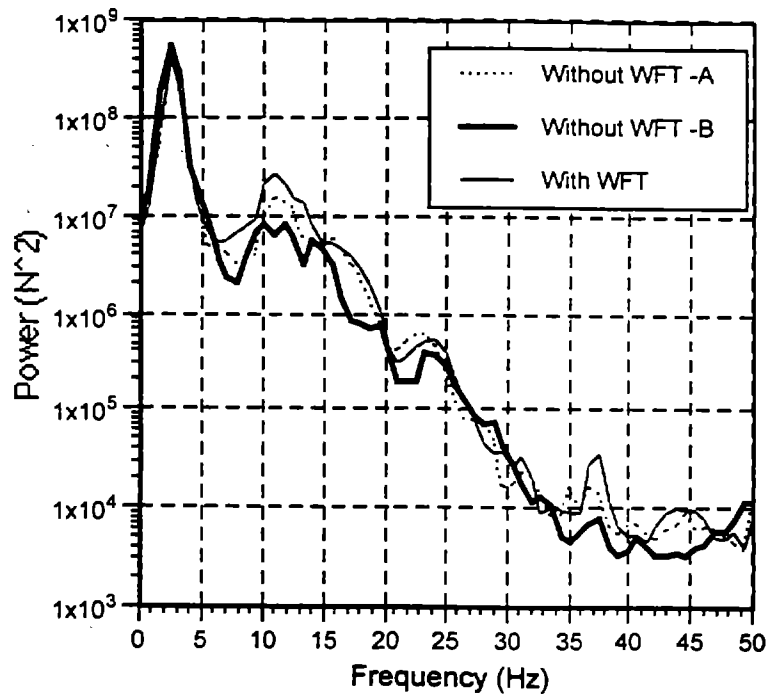
Figure 4-8. PSD of left-rear scale forces.

Further comparison of WFT mass on dynamic pavement loads is visualized for the left-rear wheel in the long time plot of figure 4-9 and in the expanded plot of figure 4-10.
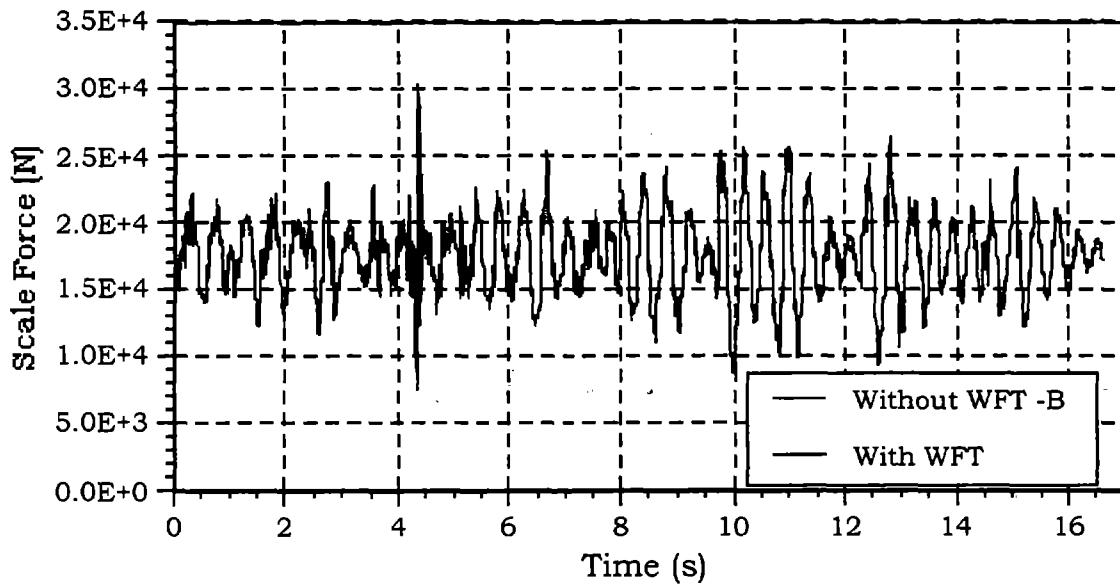
Figure 4-9. Left-rear scale force (Penn5a, 72 km/h [45 mi/h], empty truck).
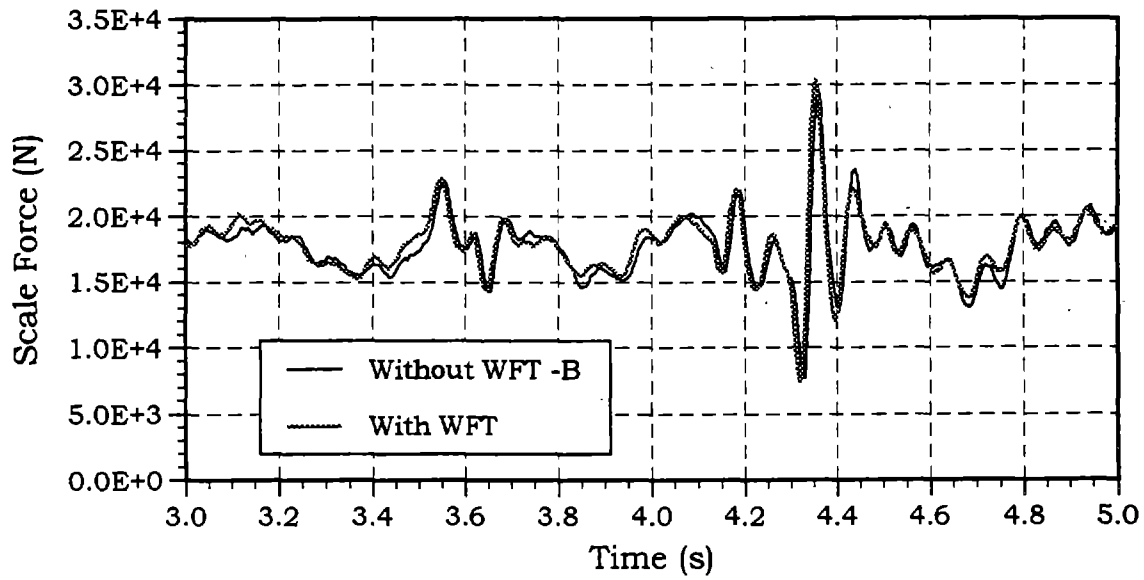
Figure 4-10. Closeup of left-rear scale force (figure 4-9).

Figure 4-11 and figure 4-12 are plots of right-rear scale force for the same tests.
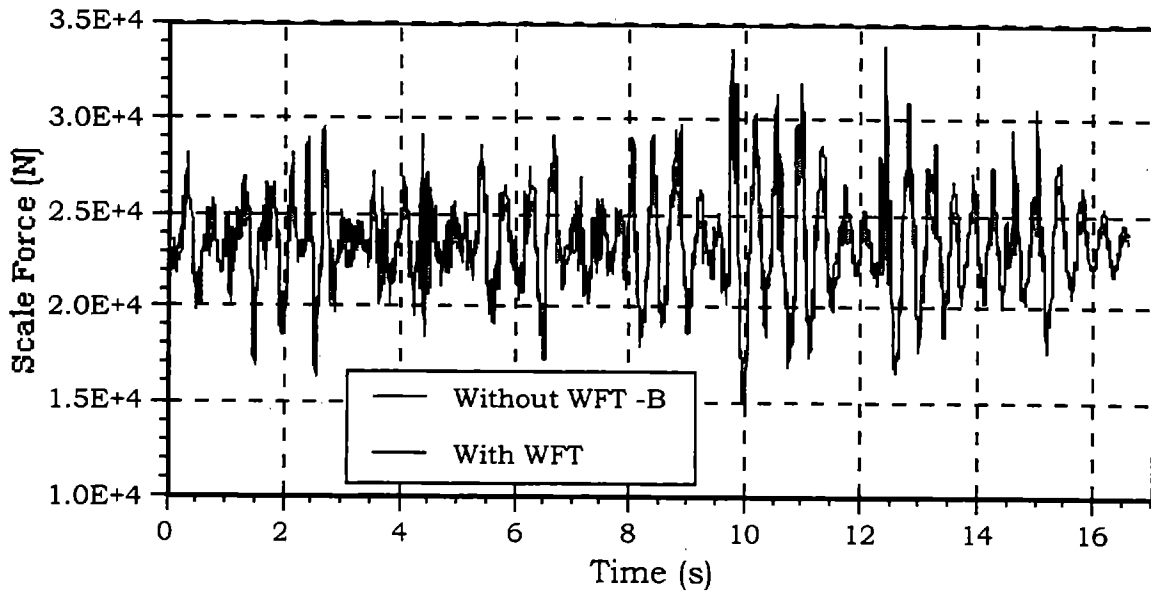
Figure 4-11. Right-rear scale force (Penn5a, 72 km/h [45 mi/h], empty truck).
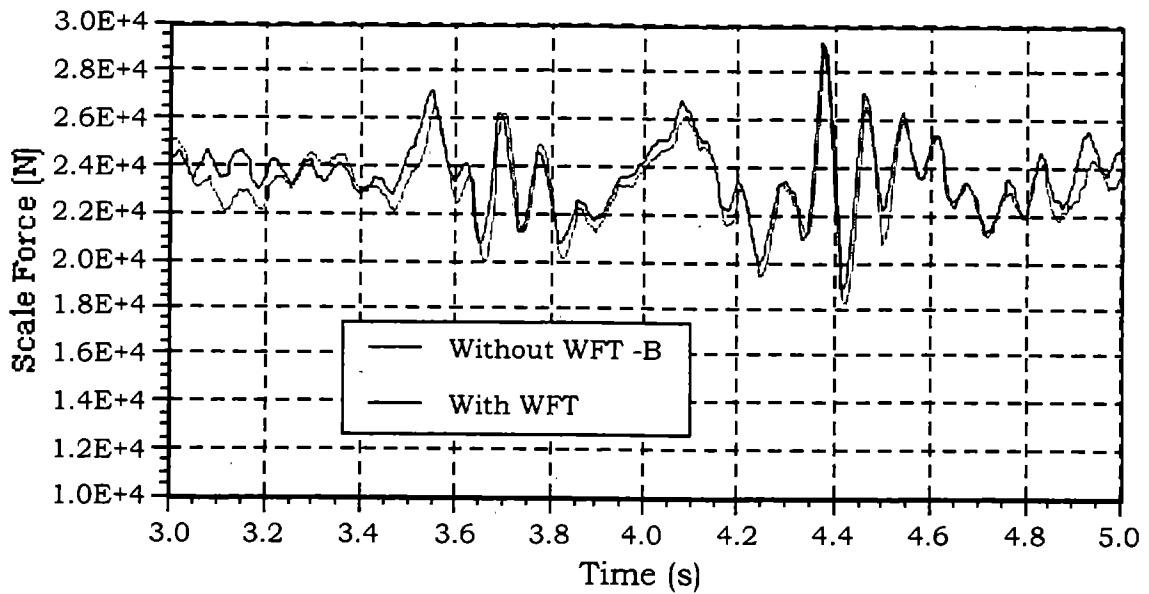
Figure 4-12. Closeup of right-rear scale force (figure 4-11).

4.4 CONCLUSIONS

A new wheel-force transducer was designed, fabricated, and tested. Unique error-correction algorithms were derived and applied to accommodate the periodic irregularities that appeared in the WFT strain-gauge bridge signals. The WFT response

84

was shown to correlate well with axle-strain data. The new FHWA WFT provided a valuable research tool for studying both the effects of various vehicle configurations on pavement and the effects of various road profiles and pavement types on vehicles.

A few additional observations regarding the WFT can be made. It was assumed that the original WFT, as received from FHWA, had been designed such that bridge gauges responded to shear forces and not to bending moments. The DYNTRAC tests in figure 4-6 through figure 4-8 were conducted using flat-wheel pans and therefore did not cause any significant change in lateral position of the resultant vertical wheel-pan force on tires. The effect of changes in bending moment was not observed in these tests. Recently, Parikh clearly showed that the WFT strain-gauge bridge "a" and "b" voltage outputs are affected by bending moments as well as by shear forces.[15] This was likely because of the original design, in which the cylindrical section on which the gauges were mounted was short relative to the cylinder diameter. Lateral pavement variations can result in a large change in the bending moment that is applied to the WFT for a given vertical wheel force. Such a change in bending moment affects WFT response. When a single wheel (rather than duals) is used, then large changes in the lateral position of vertical wheel force do not occur and, in this case, Parikh's results demonstrate that the WFT performs quite well. Wollyung et al. further discuss WFT performance.[4] They demonstrate that WFT data provide for reasonable calculations of DLC's, even when the WFT is used with dual tires.

85

CHAPTER 5. DETERMINATION OF TRUCK PARAMETERS FOR USE IN COMPUTER SIMULATION

5.1 OBJECTIVES

The main objective of the efforts described in this chapter was to determine values of parameters of the FHWA two-axle truck for use in computer simulation of dynamic interaction between the truck and the road surface.

The set of model parameters needed for computer simulation is determined by the form of the mathematical model used to represent the simulated system and by the particular simulation program. Specialized programs for computer simulation of truck dynamics are available for full-truck, half-truck, and quarter-truck models. The most comprehensive truck-simulation programs, such as Phase 4 or VSIM2d, use nonlinear full-truck models.[16,17] Other programs use a variety of mathematical models ranging in complexity from linear quarter-truck models to nonlinear half-truck models.[17,18] A brief review of the most common truck-simulation programs is given in section 5.2.

In general, the most accurate method for determining values of model parameters is by direct measurement. However, some parameters of truck dynamics such as suspension damping or Coulomb friction are difficult to measure accurately. Therefore, the approach taken in this study was to measure directly all those parameters that could be measured accurately and then use the experimental truck response data collected on DYNTRAC in combination with system identification methods to estimate the remaining parameters.[19] The results of the direct measurements of truck parameters are presented in section 5.3. The techniques employed in the measurements of truck parameters have been described in detail by Casciani.[20] The system identification methods used to estimate the values of the parameters that were difficult to measure directly are outlined in section 5.4. Several linear and nonlinear mathematical models of truck dynamics, including quarter-truck, half-truck, and full-truck models, are derived in section 5.5. Also included in section 5.5 are the sets of values of the parameters for the different models of truck dynamics.

Preceding page blank

5.2 COMPUTER SIMULATION OF TRUCK DYNAMICS

Each computer program for simulation of a dynamic system consists of two major parts: a mathematical model of the system, which includes a set of differential equations describing the relationships that exist among the system variables, and a computer code for a numerical solution of the model equations. As was pointed out in the previous section, a variety of mathematical models have been used in computer simulation of truck dynamics, ranging from the simplest quarter-truck (bounce mode only) models to half-truck (bounce and pitch modes) models to three-dimensional, full-truck (bounce, pitch, and roll modes) models. Selecting a mathematical model and a level of the model's complexity that is most appropriate for the simulation of the dynamic system often proves to be more difficult than commonly expected. On the one hand, excessive simplification of an actual system may result in leaving out a significant feature of the system performance. On the other hand, including minor features and/or parasitic effects leads to excessive complexity, wastes time and money, and may tend to obscure the most significant aspects being sought. Furthermore, more complex models involve more parameters, whose numerical values must be known in order to simulate the system. Determining the values of the model parameters can only be done with limited accuracy and, therefore, each additional parameter introduces an additional error and an associated uncertainty to the results of simulation. The more complex the model, the greater the number of parameter values to be determined, and the greater the uncertainty of the model. It is generally considered that *the simplest useful model is the best model.*[21]

When developing a mathematical model for a truck, one has to decide what structure of the model to use (quarter-truck, half-truck, or full-truck) and whether all truck components may be assumed to be linear or if nonlinear characteristics of certain system components have to be included.

Let us consider the structure of the truck model first. The quarter-truck is the simplest but also the least accurate model of truck dynamics because it ignores the effects of pitch and roll modes. Nevertheless, the quarter-truck model is frequently

used in studies of dynamic wheel forces, especially in the preliminary stages of the system analysis. Cebon pointed out that a linear quarter-truck model has dynamic characteristics that are broadly representative of the majority of single-axle trucks currently in use.[22] In the half-truck model, the effects of vehicle roll are assumed to be negligible. In the 1992 Organisation for Economic Co-operation and Development (OECD) report, it was concluded that the effects of roll dynamics of heavy trucks on pavement loading can be ignored except on very rough roads.[23] Cole and Cebon concluded from the results of validation of their three-dimensional truck model that the truck roll mode is not sufficiently excited at highway speeds to contribute significantly to dynamic pavement loading.[24] Karamihas et al. investigated the effect of axle roll (tramp) vibration on dynamic loading and pavement wear and found that on typical roads, axle roll mode may significantly increase dynamic loading and pavement wear if it is not well damped.[25] They also found that this effect is considerably stronger on asphalt concrete (AC) pavements than on Portland cement concrete (PCC) pavements because of the higher power spectral density content of the AC pavements in the frequency range where the natural frequency of the axle roll mode of a typical heavy truck lies (usually around 14 Hz).

In this study, the effect of truck roll on dynamic tire forces was investigated on DYNTRAC. Forty tests, in which different road profiles in the right- and left-wheel tracks were used, were then repeated with the same (right and/or left) road profile in both wheel tracks, thus minimizing the vehicle's roll motion. For each test run, values of the dynamic load coefficient (DLC) were calculated as the standard deviation of the dynamic wheel load, σ, divided by the mean wheel load, $\bar{F}$:

$$DLC = \frac{\sigma}{\bar{F}} \qquad (5\text{-}1)$$

The corresponding values of DLC for roll (different profiles in right- and left-wheel tracks) and no-roll (identical profiles in both wheel tracks) tests are shown graphically in figures 5-1 and 5-2 for the front- and rear-axle data, respectively. The coefficients of correlation, R^2, between the corresponding "roll" and "no-roll" data are 0.97 and 0.99 for

the front and rear axles, respectively. It can be seen from the graphs that the effect of the roll motion on dynamic loading is rather small.
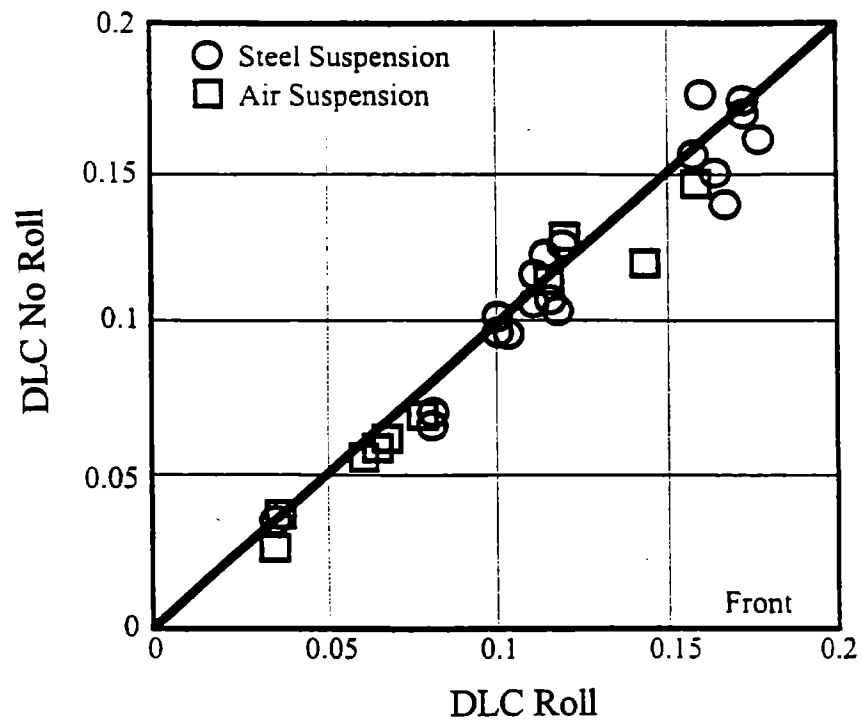
Figure 5-1. Values of DLC with (DLC$_R$) and without (DLC$_{NR}$) roll motion for front axle.
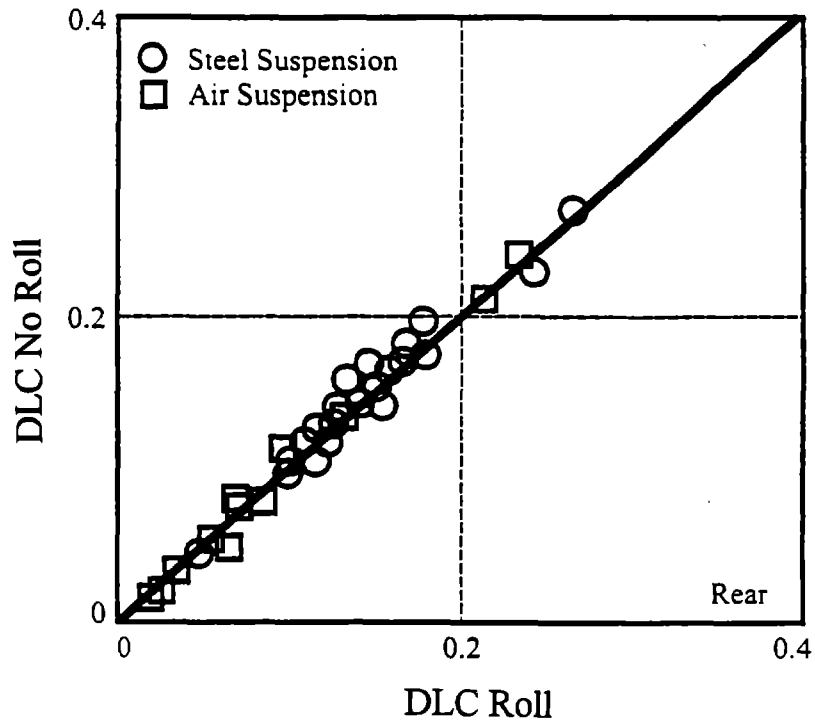
Figure 5-2. Values of DLC with (DLC_R) and without (DLC_{NR}) roll motion for rear axle.

It is interesting to note that the rear-axle DLC values obtained in no-roll tests are, on average, slightly greater than the DLC values obtained in tests with the roll motion. This may seem strange, as one would expect the dynamic forces to increase when an additional mode of vibration, in this case roll, is excited. However, it should be kept in mind that the excitation input is the same in both roll and no-roll tests, but the vehicle response to that input is either a combination of bounce and pitch motions in no-roll tests or a combination of bounce, pitch, and roll motions in roll tests; additionally, the vehicle roll motion is considerably less sensitive to the road input than bounce and pitch motions for typical vehicle and road characteristics. Karamihas et al. obtained similar results with use of computer simulation of a tractor-trailer combination.[25] It can thus be concluded from this study that the influence of the roll motion on dynamic wheel forces is very small and, therefore, a two-dimensional model provides, in most cases, a sufficiently accurate description of truck dynamics in studies of dynamic tire forces. Three-dimensional models may be necessary if road roughness is very high and/or if

91

other special conditions exist that require unusually high accuracy in the results of computer simulation.

In addition to selecting the structure of the mathematical model, one also has to decide in what form the mathematical equations should be derived and, in particular, whether the mathematical model should be linear or nonlinear to adequately represent the actual system. Strictly speaking, all existing systems exhibit characteristics that require nonlinear partial differential equations with time-varying coefficients to describe the system's dynamics accurately over a wide range of operating conditions. However, solving nonlinear partial differential equations with time-varying coefficients usually requires extraordinary computational resources to perform complex iterative solution procedures, an effort that can rarely be justified by the purpose of the simulation. Naturally, therefore, simplified mathematical descriptions in the form of linear, ordinary differential equations with constant coefficients are employed whenever possible. The mathematical models used in heavy-vehicle simulation are usually lumped, time invariant, and linear or nonlinear. The main source of nonlinearity relevant to dynamic tire forces is Coulomb friction in steel-leaf suspensions. This particular nonlinearity, and in fact any nonlinearity, manifests its presence strongly when the system deviates significantly from its normal operating condition.[21] More specifically, the effect of Coulomb friction in the truck's suspension is expected to have a stronger influence on dynamic tire forces when the truck is traveling over rough pavements, especially at high speeds. In general, linear truck models should only be used if they have been validated using experimental data or if they have been shown to compare well with nonlinear truck models over the range of operating conditions under consideration.

Computer programs that are available for simulation of heavy trucks can be divided into two groups: (1) specialized programs developed specifically for simulation of trucks and (2) general programs developed for simulation of a variety of dynamic systems. Examples of programs in the first group are Phase 4, VESYM, and VSIM2d. Examples of programs in the second group are commercially available software packages such as DADS, AUTOSIM, or MATLAB™ with the SIMULINK toolbox. The specialized programs are usually better suited to incorporate more complex vehicle-

92

specific features such as nonlinear characteristics of leaf-spring or walking-beam suspensions, conventional and antilock brakes, and various nonlinear models of tires. The main disadvantages of the specialized programs are that they are usually more difficult to modify and their postprocessing capabilities are not as powerful as the capabilities of the advanced general software packages such as MATLAB™.

A comprehensive comparison of the three specialized programs just mentioned was conducted by Kenis and Hammouda.[17] The main characteristics of these programs are summarized as follows.

Phase 4 is a heavy-truck simulation program written in Fortran at the Highway Safety Research Institute of the University of Michigan in 1980. The program numerically integrates differential equations of motion derived from Newtonian mechanics for three-dimensional models of trucks or tractors with up to three trailers with any desired loading. Four-spring and walking-beam tandem suspension models are included, and either linear or nonlinear tire models may be used. Braking can be simulated using conventional or antilock brakes, and either a known steering-wheel position input or a path-following driver model may be used. Look-up tables may be used to define nonlinear tire, spring, and brake characteristics. A desired road geometry may be defined in a user-written subroutine. The program has very limited postprocessing capabilities, and its numerical integration algorithm is out of date. It operates with a fixed integration time step, which is very inefficient and may lead to numerical instability if the integration time is not selected properly.

The VESYM program was developed at MIT and University of California, Berkeley, specifically for investigation of effects of dynamic loading applied by vehicles to pavements.[26] The program uses a two-dimensional model (bounce and pitch modes) and may be used to simulate trucks and tractors with multiple trailers with linear or nonlinear, passive or semi-active, single, tandem, and tridem suspensions, including four-spring, walking-beam, and air-bag suspensions. Three models are available to represent the tire-pavement interaction: point contact, fixed footprint, and adaptive footprint. A pre- and postprocessing program, MAKE-VIN, is available with VESYM.

93

The VSIM2d is a modification of VESYM developed at the FHWA.[17] It possesses all the capabilities of VESYM, except the semiactive suspension model and, additionally, it incorporates the roll dynamics of the truck.

Among the general programs, the two programs that are most attractive for simulation of truck dynamics are AUTOSIM and MATLAB™. The AUTOSIM program uses generic descriptions of mechanical systems composed of rigid bodies, elastic and viscous elements to automatically generate a simulation source code in a high-level language (Fortran or C) for the simulated system.[27,28] AUTOSIM has been used extensively in studies of vehicle dynamics and in investigations of dynamic wheel forces applied by heavy vehicles to pavements.[25]

MATLAB™ is a general simulation package that takes advantage of recent advances in the development of graphical user interfaces, which have greatly simplified the construction of computer simulation of dynamic systems.[21] In MATLAB™ with the SIMULINK toolbox, the simulation is built by developing a simulation block diagram with use of a library of linear and nonlinear blocks such as summers, integrators, constant gain blocks, and an extensive set of blocks representing common nonlinearities and multivariable functions, as well as user-defined functions. The most appropriate algorithm for numerical integration of the system differential equations can be chosen from a specified list. Easily implemented graphical routines are available to display time histories of the system variables. Finally, very powerful and user-friendly routines can be used for further processing of the simulation results, including frequency analysis and system identification, which were used extensively in this study.

The initial statement of work for this study called for the program VESYM to be used as the computer simulation tool for predicting dynamic wheel forces. As the work in the study progressed, it was decided that the main focus should be placed on DYNTRAC and field testing and that further work on computer simulation with VESYM would be conducted at FHWA. The role of the computer simulation in this study was thus considerably reduced. Because of that and because the only vehicle to be used in the testing program was a two-axle truck, which is a relatively simple dynamic system, it was determined that one of the general software packages would be quite appropriate

for the objectives of the study. MATLAB™ was selected primarily because of its superior frequency analysis and system identification capabilities. Additional reasons for selecting MATLAB™ were that it is very user-friendly and that it was available to the research team at no additional cost.

5.3 MEASUREMENT OF TRUCK PARAMETERS

The following truck parameters, of which some or all can be used in computer simulation of the different mathematical models of truck dynamics, were measured: wheel base, base (unladen) vehicle curb mass on front and rear axle, front and rear unsprung masses, sprung mass center of gravity (c.g.) position, sprung mass roll moment of inertia, sprung mass pitch moment of inertia, front and rear suspension spring constants, front and rear unsprung mass roll moments of inertia, front- and rear-axle roll center height, front and rear distances between suspension springs, front and rear track widths, distance between sprung mass center and rear axle, separation between dual tires, and tire spring constants. The results of the measurements are listed in table 5-1.

Table 5-1. Results of measurements of truck parameters.

Parameter	Value
Wheel base (distance from front axle to center of rear suspension)	6.45 m (254 in)
Base vehicle curb mass on front axle	3,370 kg (7,420 lb)
Base vehicle curb mass on rear axle	3,845 kg (8,460 lb)
Front-axle unsprung mass	670 kg (1,475 lb)
Rear-axle unsprung mass	900 kg (1,975 lb)
Sprung mass c.g. height	1.47 m (58 in)
Distance between sprung mass c.g. and front axle	3.36 m (132 in)
Distance between sprung mass c.g. and rear axle	3.09 m (122 in)
Sprung mass roll moment of inertia	4,520 N-m-s^2 (40,000 lb-in-s^2)
Sprung mass pitch moment of inertia	11,860 N-m-s^2 (105,000 lb-in-s^2)
Front suspension spring constant	270 kN/m (1,530 lb/in)

Rear suspension spring constant	
steel leaf	660 kN/m (3,760 lb/in)
air	560 kN/m (3,200 lb/in)
Front-axle roll moment of inertia	550 N-m-s^2 (4,880 lb-in-s^2)
Rear-axle roll moment of inertia	500 N-m-s^2 (4,470 lb-in-s^2)
Front unsprung mass roll center height	0.74 m (29.0 in)
Rear unsprung mass roll center height	0.86 m (34.0 in)
Distance between front springs	0.89 m (35.0 in)
Distance between rear springs	1.03 m (40.5 in)
Front-track width	2.04 m (80.5 in)
Rear-track width	1.83 m (72.0 in)
Separation between dual tires	0.34 m (13.5 in)
Tire spring constant	
standard radial (at 587 kPa [85 psi])	760 kN/m (4,330 lb/in)
low profile (at 587 kPa [85 psi])	770 kN/m (4,400 lb/in)
wide-base (at 724 kPa [105 psi])	1,060 kN/m (6,050 lb/in)

The measurements of some of the parameters such as wheel base, vehicle mass, unsprung mass, distance between suspension springs, track width, and separation between dual tires were straightforward. Determining values of other parameters was more involved and, in some cases, required additional processing of the results of measurements. The measuring techniques and the calculations associated with these measurements are briefly described as follows.

5.3.1 Sprung Mass C.G. Position

The truck's c.g. coordinates in the x-axis (passing through the vehicle longitudinally) and in the y axis (passing through the vehicle laterally) were found by moment calculations using the reaction forces measured under the wheels.

The c.g. height (in the z axis) was measured using a tilt table (shown in figure 5-3). Figure 5-4 shows a line drawing of a complete measuring setup. The measuring procedure followed the International Organization for Standardization's (ISO) standard

10392: 1992(E) titled, "Road vehicles with two axles - Determination of center of gravity."
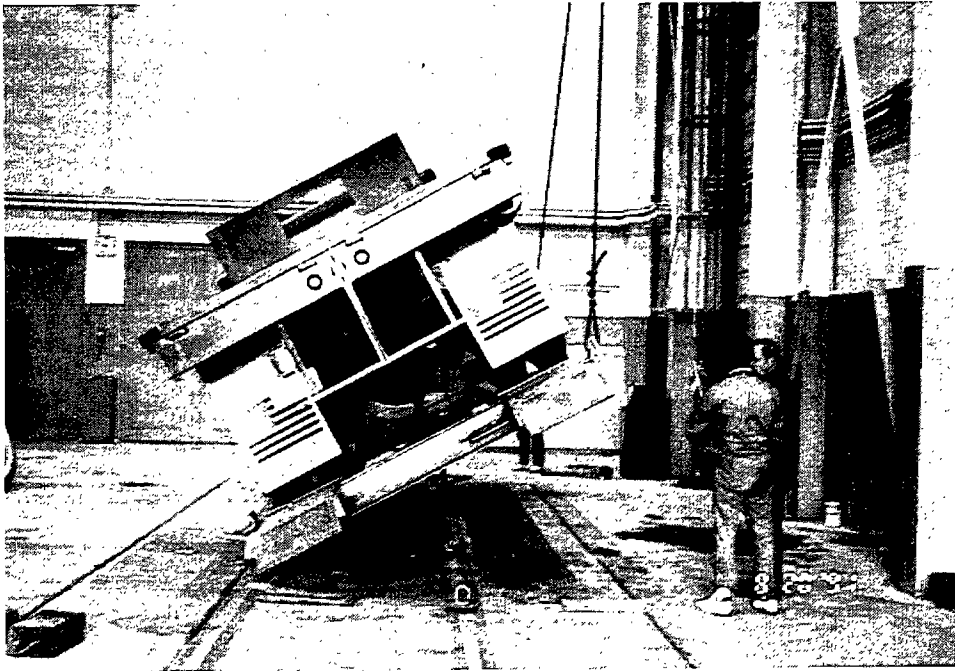
Figure 5-3. Truck on tilt table.
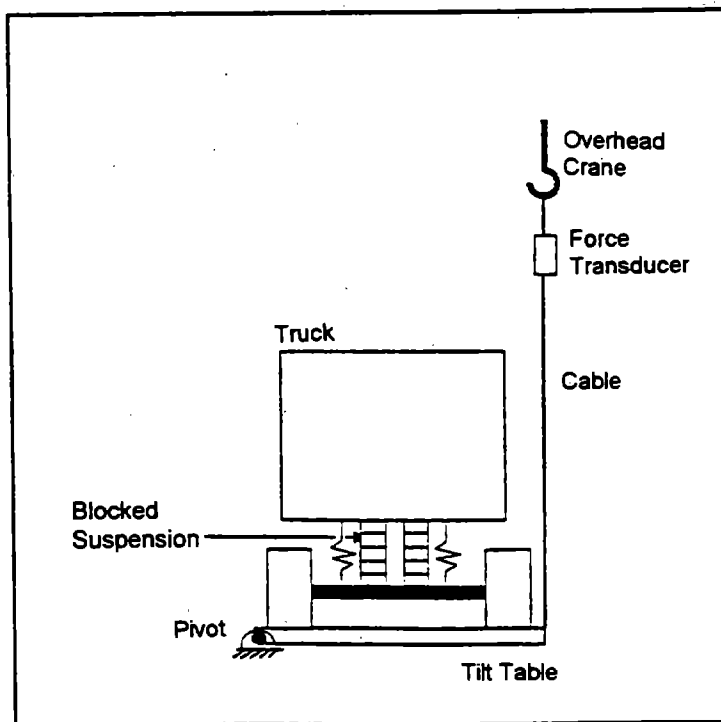
Figure 5-4. Line drawing of truck on tilt table.

The procedure starts with the truck being driven onto the tilt table. The truck suspension is then blocked to ensure that the entire vehicle acts as a rigid body. The table is gradually tilted using a cable attached to an overhead crane. A force transducer is attached to the cable. As the tilt angle is increased, the respective readings of the force in the cable are recorded. The recorded data are next used to calculate the location of the c.g. of the vehicle from equations provided in the ISO standard. To find the c.g. position of the sprung mass, the c.g. position of the vehicle is corrected to eliminate the effect of the unsprung mass. The unsprung mass (axle and wheel assemblies) had been disassembled, and its mass and the c.g. height were predetermined.

5.3.2 Sprung Mass Pitch Moment of Inertia

To find the sprung mass roll moment of inertia, an inertia table was used. The inertia table is a type of swing that acts as a compound pendulum (figure 5-5).
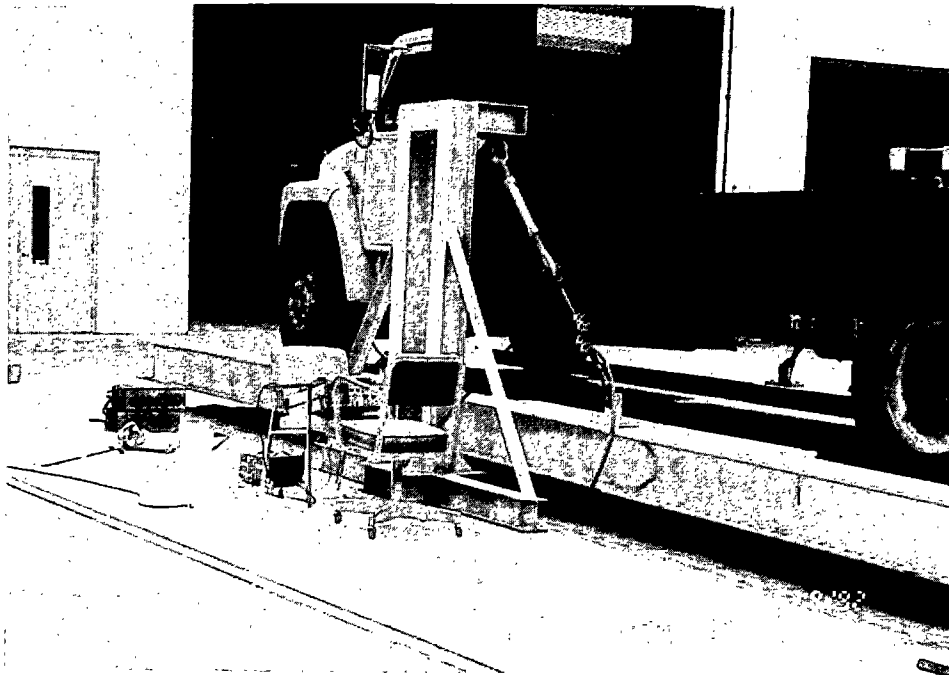
Figure 5-5. Inertia table for measuring sprung mass pitch moment of inertia.

The pivot of the swing is on the lateral axis of the vehicle. After the truck was driven onto the inertia table, small oscillations were induced. The period of oscillations of the

98

truck/table setup was measured using an oscilloscope, which received a signal from a rotational potentiometer installed at the pivot of the swing. The period of the table alone was also measured. Several measurements of the period of oscillations were conducted, and average values were calculated. The pitch moment of inertia was then calculated using the compound pendulum formula and parallel axis theorem:

$$J_{cg} = \frac{WdT^2}{4\pi^2} \tag{5-2}$$

$$J_o = J_{cg} + mx^2 \tag{5-3}$$

where
- W = weight of the vehicle.
- d = distance from the fulcrum to the c.g.
- T = period of oscillations.
- m = mass of the vehicle.
- x = distance by which the axis is translated.

It should be noted here that the yaw moment of inertia was assumed to be the same as the pitch moment of inertia.

5.3.3 Sprung Mass Roll Moment of Inertia

In measuring the pitch moment of inertia of the sprung mass, the inertia table was used again, but now it was arranged so that the pivot was in the longitudinal axis of the vehicle. Except for this difference, the measuring procedure was the same as that described in section 5.3.2. Figure 5-6 shows the measuring system prepared for the measurement of the roll moment of inertia of a transit bus.
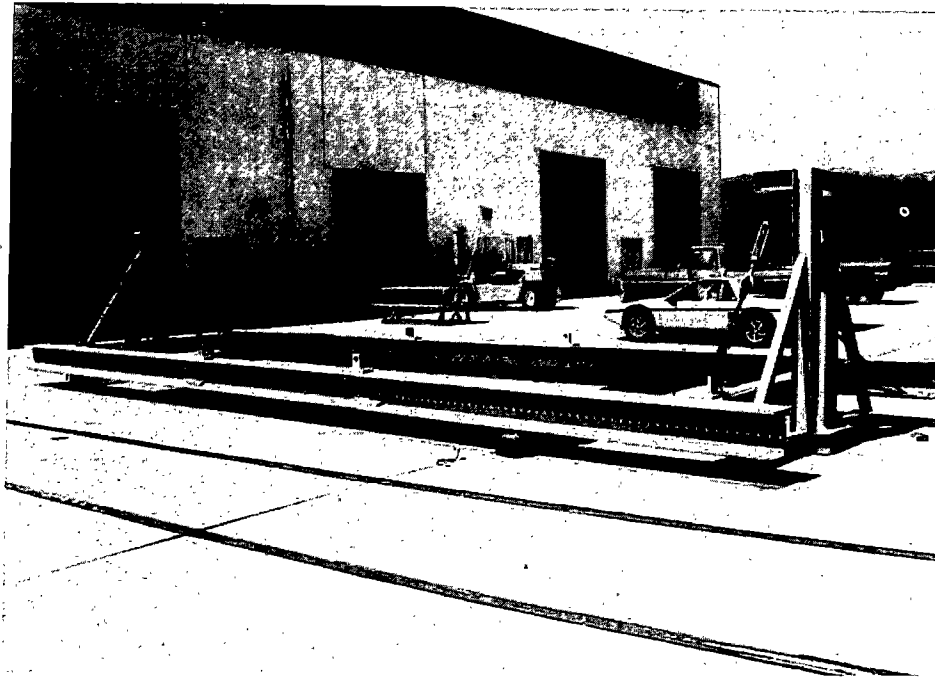
Figure 5-6. Inertia table for measuring sprung mass roll moment of inertia.

5.3.4 Suspension Spring Constants

Suspension spring constant is defined as the ratio of force applied to the suspension over the resulting deflection of the suspension. In defining a suspension spring constant, it is assumed that the force versus deflection characteristic is linear.

To find the spring constants of the steel-leaf suspension in the FHWA truck, it was therefore necessary to obtain the force versus deflection curves for the front and rear suspensions. The measuring procedure started with lifting the vehicle off the ground to eliminate the effects of the tires. A jack was then placed under the leaf spring of interest and a scale was placed horizontally under the jack to measure the vertical force acting on the leaf spring. Starting from a normal operating point (NOP), the suspension was gradually compressed, then relaxed, and then compressed again to return to the NOP, and the measurements of the force and deflection were taken. To compress the leaf spring, a turnbuckle mechanism was used. One end of the turnbuckle was attached to the ground and the other end was attached to the sprung mass. The compressing force was increased from its initial value until the suspension bump stops were reached. After the limit was reached, the force was decreased to

100

relax the spring to its initial state again. An overhead crane was then used to further relax the spring to a point where the force acting on the spring was approximately zero. The recorded force and deflection data collected for the front and rear leaf springs are shown in figures 3-1 and 3-2, respectively. Both characteristics are clearly nonlinear. The spring constants are estimated as slopes of the linearized force versus deflection characteristics in the vicinity of the normal operating points. The value of the spring constant for the air suspension was obtained from Navistar.

5.3.5 Unsprung Mass Roll Moment of Inertia

To determine the unsprung mass roll moment of inertia, the c.g. height of the unsprung mass had to be measured first. A swing shown in figure 5-7 was constructed for both measurements. The base of the swing was triangular in shape and its corners were connected to a common pivot point. The pivot point was on a rigid beam about which the swing could oscillate. The swing in this arrangement was considered to act as a compound pendulum.
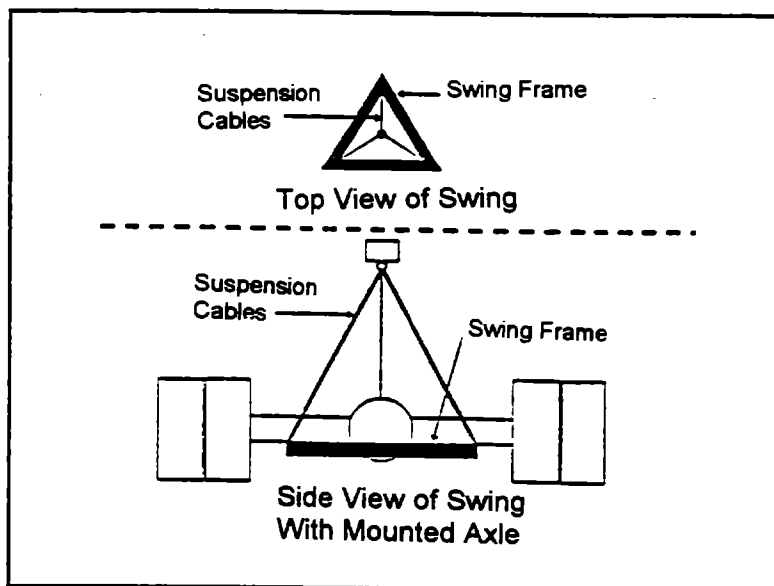
Figure 5-7. Axle assembly mounted in the swing apparatus.

101

To measure the c.g. position, the swing was first balanced so that its three sides were all parallel to the ground. Next, the axle (removed from the truck) was mounted on the swing, as shown in figure 5-7. Once the axle was mounted, the swing deviated from its initial horizontal position. To find the c.g. position, the axle's position on the swing was changed until the position in which the swing remained horizontal was found. Repeating this procedure in three different planes and using the geometric center of the axle as the reference point, the spatial location of the c.g. of the unsprung mass was determined.

With the c.g. position known, the unsprung mass was mounted on the swing at its c.g. position. Next, small oscillations were induced in the roll plane, and the period of oscillation was measured. Many trials were performed to obtain an average period of oscillation. The roll moment of inertia was then calculated using the compound pendulum formula and the parallel axis theorem given in section 5.3.2.

5.3.6 Roll Center Height

The measuring setup is shown in figure 5-8. The center of the spring track was marked, as can be seen in figure 5-8, using a tape that extends from approximately the middle of the bed to the ground. With the truck unloaded, an observer stood at a distance and aligned a rod with the tape line's initial position. The truck was then loaded with weight by an overhead crane. The weight was moved to different positions and, at each new position, the point at which the angled tape line intersected the rod line was observed. The roll center height was measured as the distance from that point to the ground.

Figure 5-8. Measuring roll center height of the truck.

5.3.7 Tire Spring Constants

Tire spring constant or tire stiffness, k_t, is defined as the slope of the linearized relationship between a vertical force applied to the tire, F_t, and the resulting tire deflection, x_t, i.e.,

$$k_t = \frac{\Delta F_t}{\Delta x_t} \tag{5-4}$$

If the slope of the force versus deflection curve changes significantly when the force changes, a nonlinear tire model has to be employed. In this study, the relationship between the force applied to a tire and tire deflection was assumed to be linear, and the tire was represented in the vehicle model as a linear spring. The following regression models were derived for spring constants of the three test tires as functions of inflation pressure using the tire testing data presented in chapter 6:

$$k_{tSR} = 0.71\ P_t + 345 \tag{5-5}$$

$$k_{tLP} = 0.84\ P_t + 281 \tag{5-6}$$

$$k_{tWB} = 1.03\ P_t + 313 \tag{5-7}$$

103

where k_t is in kN/m, P_t is in kPa, and SR, LP, and WB refer to standard radial tire, low-profile tire, and wide-base tire, respectively.

5.4 SYSTEM IDENTIFICATION

As indicated earlier, the strategy followed in determining the parameters of the truck models was to measure directly all those parameters that could be measured accurately and then use the statistical identification methods to obtain estimates of the remaining parameters. A general block diagram of the system identification is shown in figure 5-9. A computer simulation of a truck model is performed using actual road profile data as input signal. The tire force obtained from the computer simulation is compared with the tire force measured in field experiments involving the truck traveling over the same road profile. A system identification algorithm is employed to adjust the values of the estimated model parameters until the difference between the actual and simulated tire forces reaches a minimum. The difference between the actual and simulated tire forces is represented by the identification error, defined as

$$\varepsilon_F = \frac{1}{N} \sum_{i=1}^{N} [F_i - \hat{F}_i]^2 \qquad (5\text{-}8)$$

where F_i is a sequence of measured tire forces and $\hat{F}_i$ is a sequence of simulated tire forces, with $i=1, 2, ..., N$.

In estimating parameters of linear truck models, the MATLAB™ System Identification toolbox was used. The MATLAB™ algorithm can only be applied to linear models, so a different approach had to be used in estimating parameters of nonlinear models of truck dynamics. Two algorithms were used with the nonlinear models: an analytical least-squares method and the Gauss-Seidel method. The analytical least-squares method determines values of the model parameters for which the derivatives of a selected "identification cost function" with respect to the model parameters are all zero. The identification cost function for a quarter-truck model involves suspension deflection and velocity, sprung and unsprung mass accelerations, and tire force data.

104
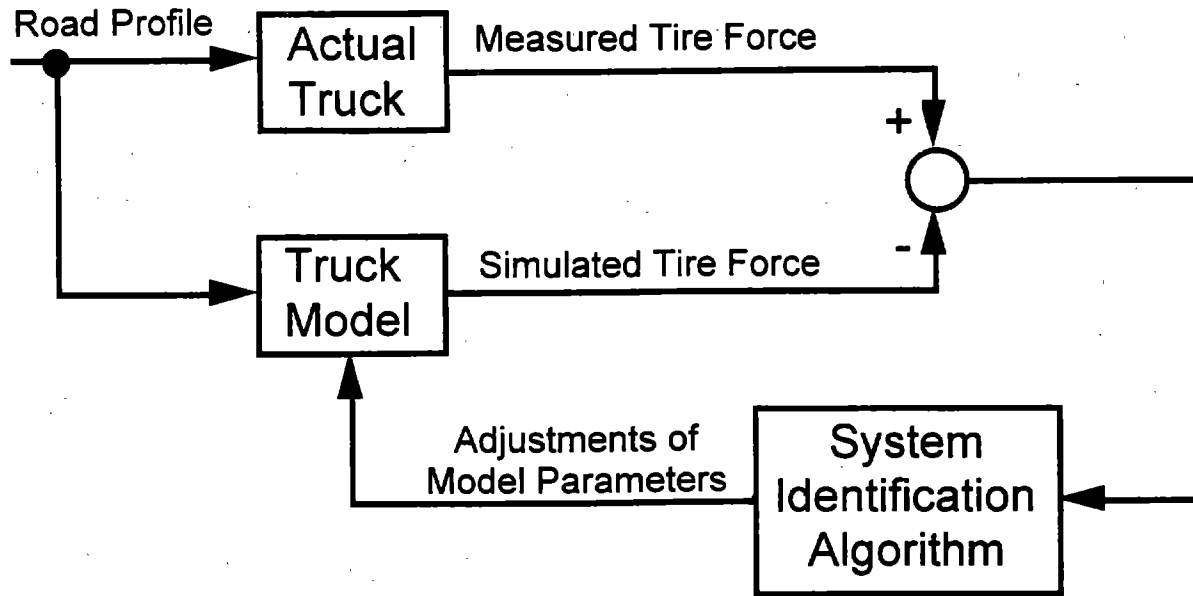
Figure 5-9. Block diagram of system identification approach.

Because not all of these signals were directly measured, the identification cost function could not be computed with sufficient accuracy and, as a result, the least-squares estimates of the nonlinear model parameters were unacceptable.[19] The problem of unavailability of measurements of all state variables necessary for identification of model parameters can be resolved using the state observer.[29]

Although system identification methods have been used extensively in estimation of model parameters, it has to be recognized that physical significance of the results of system identification is limited. It should be kept in mind that the estimates of model parameters obtained from system identification represent a set of values of the model parameters for which the difference between the output of the model and the particular experimental data used in the computation is minimal. However, since that difference is influenced not only by the values of the model parameters but also by other factors, such as the structure of the model, and by the measuring error involved in the experimental data, the estimates found in the system identification are affected by those other factors as well. There are some important general implications of this fact for estimating parameters of truck dynamics. First, it should be expected that the

estimates of the same parameter obtained with quarter-truck, half-truck, or full truck models may be different. Second, the estimates of the truck parameters are expected to be different for different sets of profile data, although this effect should be very small if the experimental data used in system identification provide a representative sample of all possible road profiles.

The results of estimation of truck parameters presented in the next section were obtained using MATLAB™; however, they can also be used in computer simulations with other truck simulation packages, such as Phase 4 (full-truck model parameters) or VESYM (half-truck model parameters).

5.5 MATHEMATICAL MODELS OF TRUCK DYNAMICS

Four models were developed in this study: linear quarter-truck, linear half-truck, linear full-truck, and nonlinear quarter-truck.

5.5.1 Linear Quarter-Truck Model

A schematic of the linear quarter-truck model is shown in figure 5-10. The basic equations of motion for this model are

$$\ddot{x}_s = (-c_s \dot{x}_s - k_s x_s + c_s \dot{x}_u + k_s x_u)/m_s \qquad \text{(5-9)}$$

$$\ddot{x}_u = (-c_s \dot{x}_u - (k_s + k_t)x_u + c_s \dot{x}_s + k_s x_s + k_t u)/m_u \qquad \text{(5-10)}$$

Most computer simulation programs, including MATLAB™, require mathematical models of simulated systems to be formulated in the form of state equations. The general matrix-vector form of the state model for a linear dynamic system is

$$\dot{q} = Aq + Bu \qquad \text{(5-11)}$$

$$y = Cq + Du \qquad \text{(5-12)}$$

where A is a state matrix, B is an input matrix, C is an output matrix, D is a direct transmission matrix, q is a state vector, u is an input vector, and y is an output vector.

In state models of truck dynamics, u is a vector of road profiles, $u = (u_1, u_2, \ldots , u_l)$, where l is the number of wheels, and y is a vector of tire forces, $y = (F_{t1}, F_{t2}, \ldots , F_{tl})$.
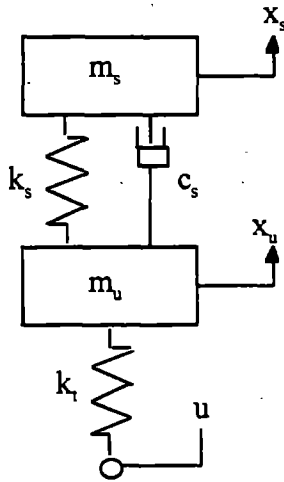
Figure 5-10. Linear quarter-truck model.

The state variables selected for the quarter-truck model are: $q_1 = x_s$, $q_2 = \dot{x}_s$, $q_3 = x_u$, and $q_4 = \dot{x}_u$. Matrices B and C become vectors and matrix D becomes a scalar for the quarter-truck model. The specific forms of the model matrices are

$$A = \begin{bmatrix} 0 & 1 & 0 & 0 \\ \dfrac{-k_s}{m_s} & \dfrac{-c_s}{m_s} & \dfrac{k_s}{m_s} & \dfrac{c_s}{m_s} \\ 0 & 0 & 0 & 1 \\ \dfrac{k_s}{m_u} & \dfrac{c_s}{m_u} & \dfrac{-(k_s+k_t)}{m_u} & \dfrac{-c_s}{m_u} \end{bmatrix}; \quad B = \begin{bmatrix} 0 \\ 0 \\ 0 \\ \dfrac{k_t}{m_u} \end{bmatrix};$$

$$C = \begin{bmatrix} 0 & 0 & k_t & 0 \end{bmatrix}; \quad D = \begin{bmatrix} -k_t \end{bmatrix};$$

The values of the model parameters, m_s, m_u, k_s, and c_s, are listed in table 5-2. The value of the tire spring constant, k_t, should be selected from table 5-1 depending on the particular tire type used in the simulation. All values of the quarter-truck model parameters were obtained from direct measurements, except for the suspension viscous damping constant, c_s, which was estimated using system identification.

Table 5-2. Parameters of the quarter-truck model.

Parameter	Value
m_s	1,350 kg (2,970 lb) front 1,470 kg (3,240 lb) rear
m_u	335 kg (740 lb) front 450 kg (990 lb) rear
k_s	270 kN/m (1,530 lb/in) front 660 kN/m (3,760 lb/in) rear (steel) 560 kN/m (3,200 lb/in) rear (air)
c_s	16.8 kN-s/m (96 lb-s/in) front [*] 89.0 kN-s/m (508 lb-s/in) rear [*]

[*] estimated values

The tire force simulated using the linear quarter-truck model with steel-leaf suspension was compared with the experimental tire force measured on DYNTRAC. The time histories and power spectral densities of the corresponding tire forces for the left-front and left-rear tires are shown in figures 5-11 through 5-14. The coefficient of correlation between the simulated and experimental tire forces was 0.78 and 0.88 for front and rear quarter-trucks, respectively. The agreement is fair, and it can be seen from the plots that the simulated model has clearly more damping than the actual truck, especially in the rear suspension. The body bounce natural frequency for the rear suspension is just under 4 Hz, which is considerably higher than expected. The wheel hop natural frequency is between 10 and 12 Hz for the front quarter-truck, but it is not visible in the rear quarter-truck frequency characteristic.
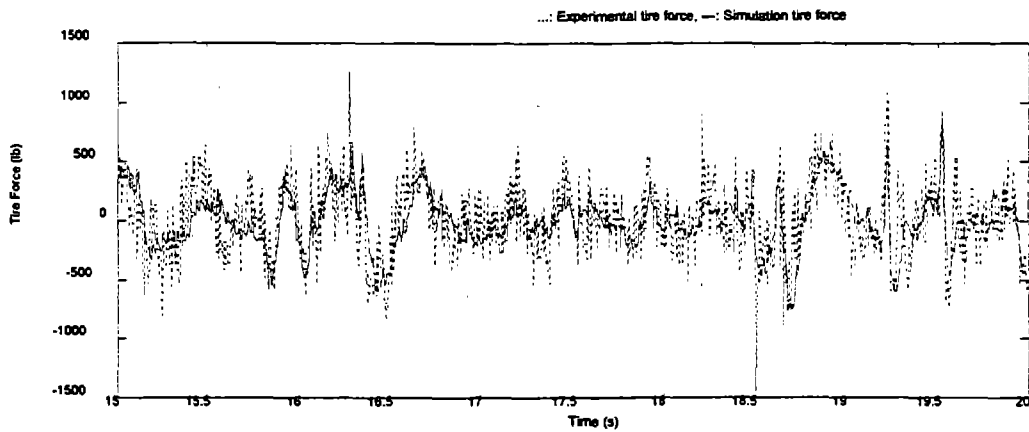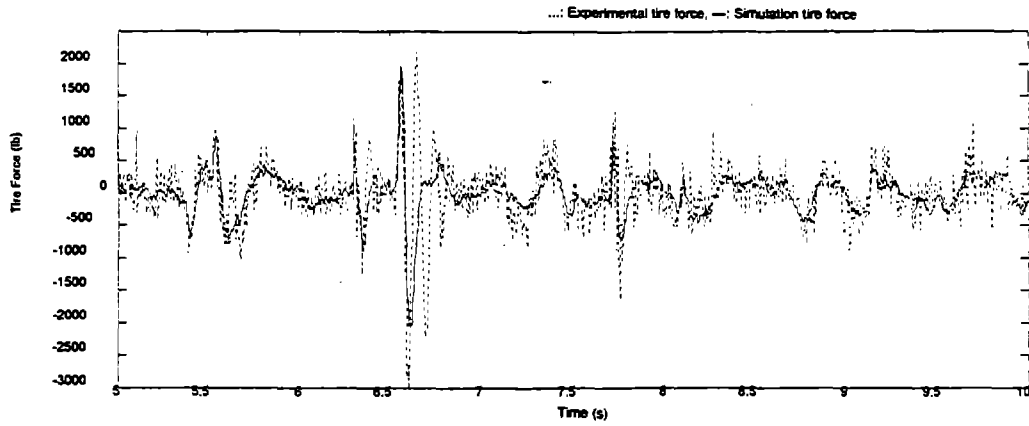
1 lb = 0.454 kg

Figure 5-11. Experimental and simulated left-front tire forces in time domain (quarter-truck model).
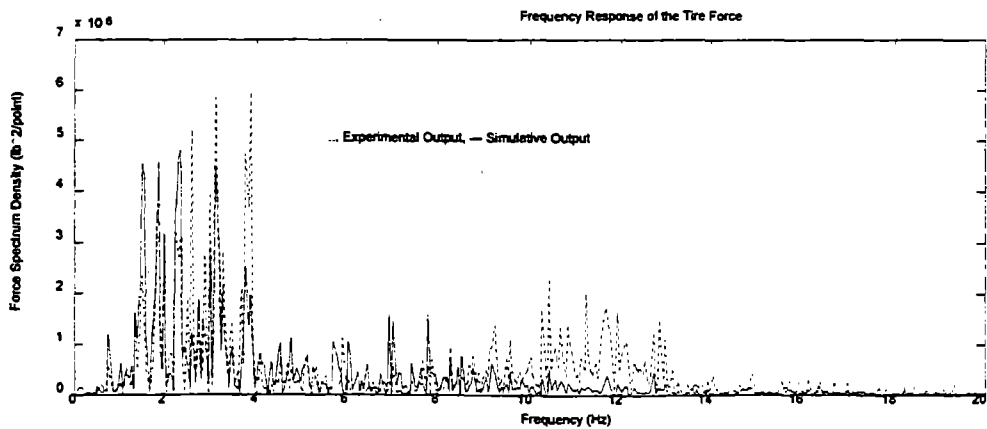
1 lb = 0.454 kg

Figure 5-12. Experimental and simulated left-front tire forces in frequency domain (quarter-truck model).

109

1 lb = 0.454 kg

Figure 5-13. Experimental and simulated left-rear tire forces in time domain (quarter-truck model).

1 lb = 0.454 kg

Figure 5-14. Experimental and simulated left-rear tire forces in frequency domain (quarter-truck model).

110

Additional insight into system dynamics may be gained from analysis of the system eigenvalues. In general, a linear fourth-order system, such as the quarter-truck, has four eigenvalues. For the front quarter-truck model with the parameters values as given in table 5-2, the following eigenvalues are obtained:

$$p_1 = -3.47 - j12.43$$
$$p_2 = -3.47 + j12.43$$
$$p_3 = -27.73 - j44.21$$
$$p_4 = -27.73 + j44.21$$

Each of the two pairs of complex conjugate numbers (p_1, p_2 and p_3, p_4) represents a mode of vibration, which can be characterized by a natural frequency and a damping ratio.[21] The values of the natural frequencies, f_n, and damping ratios, ζ, obtained from the front quarter-truck eigenvalues are

$$f_{n\,1,2} = 2.0 \text{ Hz} \qquad \zeta_{1,2} = 0.27$$

$$f_{n\,3,4} = 8.3 \text{ Hz} \qquad \zeta_{3,4} = 0.53$$

These frequencies and damping ratios represent the two fundamental modes of vibration of a quarter-truck: body bounce and wheel hop modes.

For the rear quarter-truck model, one pair of complex conjugate eigenvalues and two real eigenvalues were found:

$$p_1 = -2.29 - j18.97$$
$$p_2 = -2.29 + j18.97$$
$$p_3 = -8.47$$
$$p_4 = -245.5$$

The presence of only one pair of complex conjugate eigenvalues indicates that there is only one dominant mode of vibration for the rear quarter-truck model: the body bounce mode. The values of the natural frequency and damping ratio for this mode calculated using the values of p_1 and p_2 are

111

$$f_{n\,1,2} = 3.0\ Hz \qquad\qquad \zeta = 0.12$$

The other two eigenvalues, p_3 and p_4, represent time constants, τ_3 and τ_4, of an overdamped mode:[21]

$$\tau_3 = 0.12\ s$$
$$\tau_4 = 0.004\ s$$

The smaller time constant, τ_4, is negligible in the frequency range that is of interest in analysis of dynamic tire forces. The other time constant, τ_3, indicates the presence of additional damping in the model, so one can expect that the overall damping will be greater than what could be expected from the damping ratio of 0.12.

The analysis of eigenvalues can further be used to demonstrate the effect of payload on dynamic characteristics of the truck. The quarter-truck model considered so far represented the truck with no payload. For comparison, with a 3,636-kg (8,000-lb) payload, the eigenvalues of the rear quarter-truck become

$$p_1 = 2.42 - j12.71$$
$$p_2 = 2.42 + j12.71$$
$$p_3 = -10.09$$
$$p_4 = -211.07$$

The corresponding values of the natural frequency, damping ratio, and time constants are

$$f_{n\,1,2} = 2.0\ Hz \qquad\qquad \zeta = 0.19$$

$$\tau_3 = 0.10\ s \qquad\qquad \tau_4 = 0.005\ s$$

The most visible effect of adding payload is the decrease of the natural frequency from 3.0 Hz (without payload) to 2.0 Hz (with payload). There is also a slight increase in the damping ratio, but it would be difficult to evaluate the overall effect on damping, because it is also influenced by the two time constants. In general, decreasing the natural frequency and increasing damping ratio will reduce the

magnitude of dynamic tire forces. On the other hand, adding payload will obviously increase static loads applied by the vehicle to pavement.

Higher-order systems with more eigenvalues are more difficult to analyze using the approach employed above and, moreover, the results do not have the same clear physical significance as the results obtained with lower-order systems. In fact, higher-order dynamic systems are sometimes approximated by low-order models for which the analysis of eigenvalues reveals valuable, even if only approximate, information about the dominant traits of system dynamics. Therefore, this analysis will not be repeated for half-truck and full-truck models.

5.5.2 Linear Half-Truck Model

The longitudinal half-truck model incorporates the vehicle's bounce and pitch modes, but it does not include the roll mode vibration. A schematic of the four-degrees-of-freedom model of a half-truck with linear suspension is shown in figure 5-15.
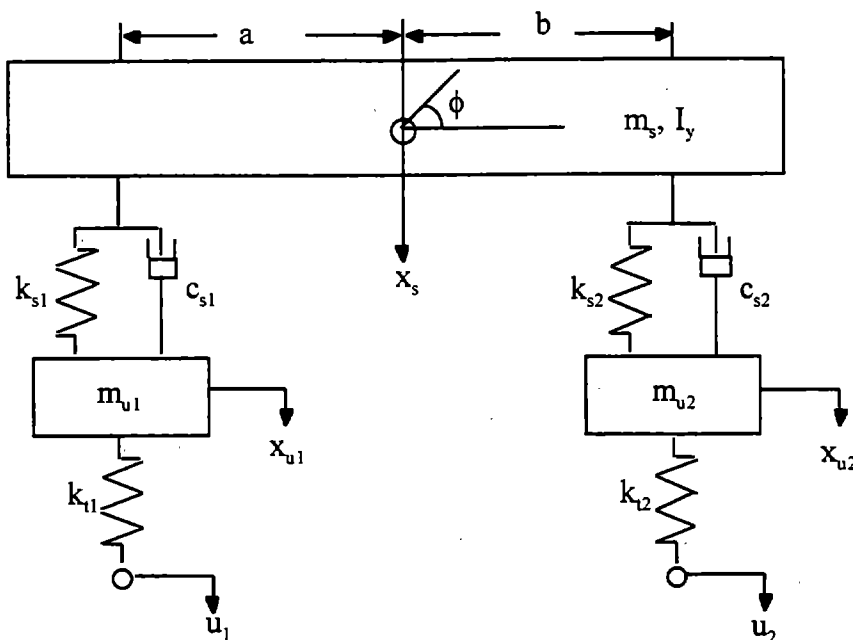
Figure 5-15. Linear half-truck model.

The following eight state variables are selected: $q_1 = x_s$, $q_2 = \phi$, $q_3 = x_{u1}$, $q_4 = x_{u2}$,

$q_5 = \dot{x}_s$, $q_6 = \dot{\phi}$, $q_7 = \dot{x}_{u1}$, $q_8 = \dot{x}_{u2}$. The input and output vectors, u and y, are two-dimensional, with their two components representing road profiles and tire forces for the front and rear wheels of the half-truck model. The system matrices, A, B, C, and D are

$A =$

$$
\begin{bmatrix}
0 & 0 & 0 & 0 & 1 & 0 & 0 & 0 \\
0 & 0 & 0 & 0 & 0 & 1 & 0 & 0 \\
0 & 0 & 0 & 0 & 0 & 0 & 1 & 0 \\
0 & 0 & 0 & 0 & 0 & 0 & 0 & 1 \\
\dfrac{-(k_{s1}+k_{s2})}{m_s} & \dfrac{k_{s2}b-k_{s1}a}{m_s} & \dfrac{k_{s1}}{m_s} & \dfrac{k_{s2}}{m_s} & \dfrac{-(c_{s1}+c_{s2})}{m_s} & \dfrac{c_{s2}b-c_{s1}a}{m_s} & \dfrac{c_{s1}}{m_s} & \dfrac{c_{s2}}{m_s} \\
\dfrac{k_{s2}b-k_{s1}a}{I_y} & \dfrac{-(k_{s2}b^2+k_{s1}a^2)}{I_y} & \dfrac{k_{s1}a}{I_y} & \dfrac{-k_{s2}b}{I_y} & \dfrac{c_{s2}b-c_{s1}a}{I_y} & \dfrac{-(c_{s2}b^2+c_{s1}a^2)}{I_y} & \dfrac{c_{s1}a}{I_y} & \dfrac{-c_{s2}b}{I_y} \\
\dfrac{k_{s1}}{m_{u1}} & \dfrac{k_{s1}a}{m_{u1}} & \dfrac{-(k_{s1}+k_{t1})}{m_{u1}} & 0 & \dfrac{c_{s1}}{m_{u1}} & \dfrac{c_{s1}a}{m_{u1}} & \dfrac{-c_{s1}}{m_{u1}} & 0 \\
\dfrac{k_{s2}}{m_{u2}} & \dfrac{-k_{s2}b}{m_{u2}} & 0 & \dfrac{-(k_{s2}+k_{t2})}{m_{u2}} & \dfrac{c_{s2}}{m_{u2}} & \dfrac{-c_{s2}b}{m_{u2}} & 0 & \dfrac{-c_{s2}}{m_{u2}}
\end{bmatrix}
$$

$$
B = \begin{bmatrix} 0 & 0 \\ 0 & 0 \\ 0 & 0 \\ 0 & 0 \\ 0 & 0 \\ 0 & 0 \\ \dfrac{k_{t1}}{m_{u1}} & 0 \\ 0 & \dfrac{k_{t2}}{m_{u2}} \end{bmatrix} ; \quad C = \begin{bmatrix} 0 & 0 & k_{t1} & 0 & 0 & 0 & 0 & 0 \\ 0 & 0 & 0 & k_{t2} & 0 & 0 & 0 & 0 \end{bmatrix} ; \quad D = \begin{bmatrix} -k_{t1} & 0 \\ 0 & -k_{t2} \end{bmatrix}
$$

The measured and estimated values of the model parameters are compiled in table 5-3. The appropriate values of the tire spring constants should be selected from table 5-1.

114

Table 5-3. Parameters of the linear half-truck model.

Parameter	Value
m_s	2,820 kg (6,210 lb)
m_{u1}	335 kg (740 lb)
m_{u2}	450 kg (990 lb)
I_y	5,930 N-m-s^2 (52,500 lb-in-s^2) 43,300 N-m-sec^2 (383,200 lb-in-s^2)*
k_{s1}	270 kN/m (1,530 lb/in)
k_{s2}	660 kN/m (3,760 lb/in) (steel) 560 kN/m (3,200 lb/in) (air)
c_{s1}	15.2 kN-s/m (87 lb-s/in)*
c_{s2}	84.9 kN-s/m (485 lb-s/in)*
a	3.36 m (132 in)
b	3.09 m (122 in)

* estimated values.

Sample plots of the time histories and power spectral densities of the simulated and experimental tire forces for the left half-truck with steel-leaf suspension are shown in figures 5-16 through 5-19. In general, the agreement between the simulated and measured forces is much better than it was for the quarter-truck model, as indicated by the values of the coefficient of correlation of 0.80 and 0.91 for front and rear tire forces, respectively. The combined body bounce and pitch modes dominate the frequency characteristic of the rear-tire forces with the natural frequency just under 4 Hz, the same as for the quarter-truck model.
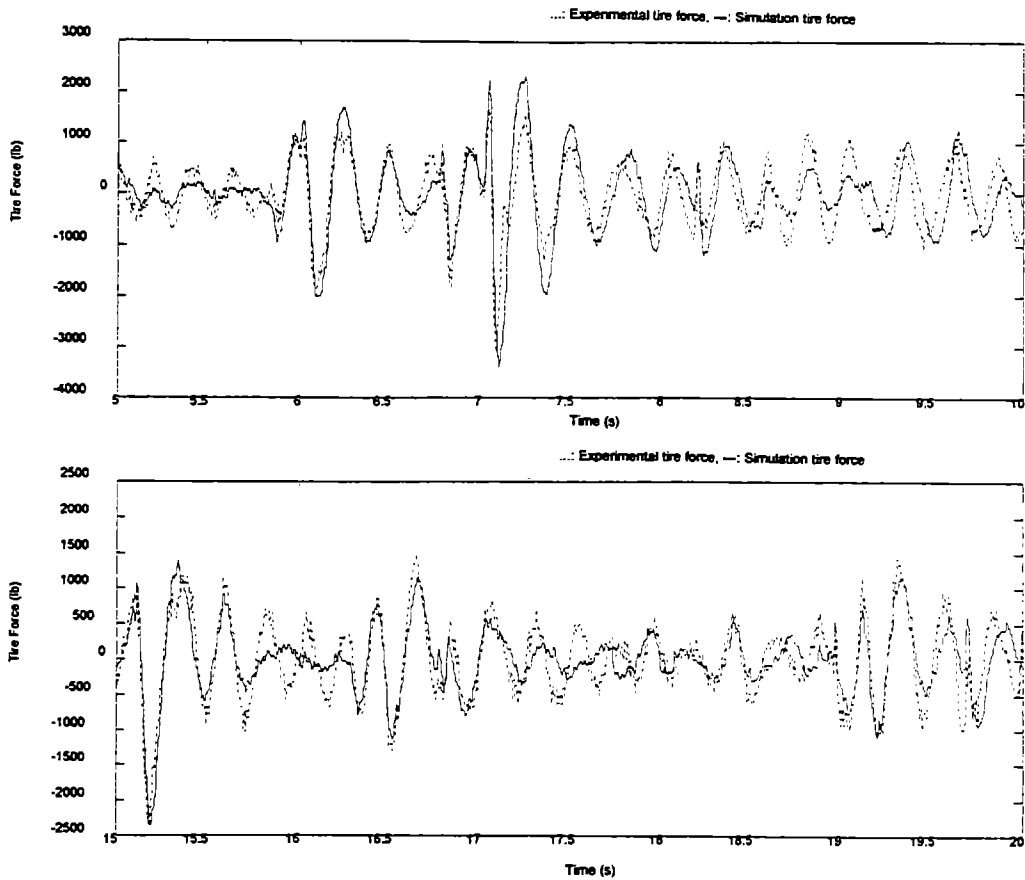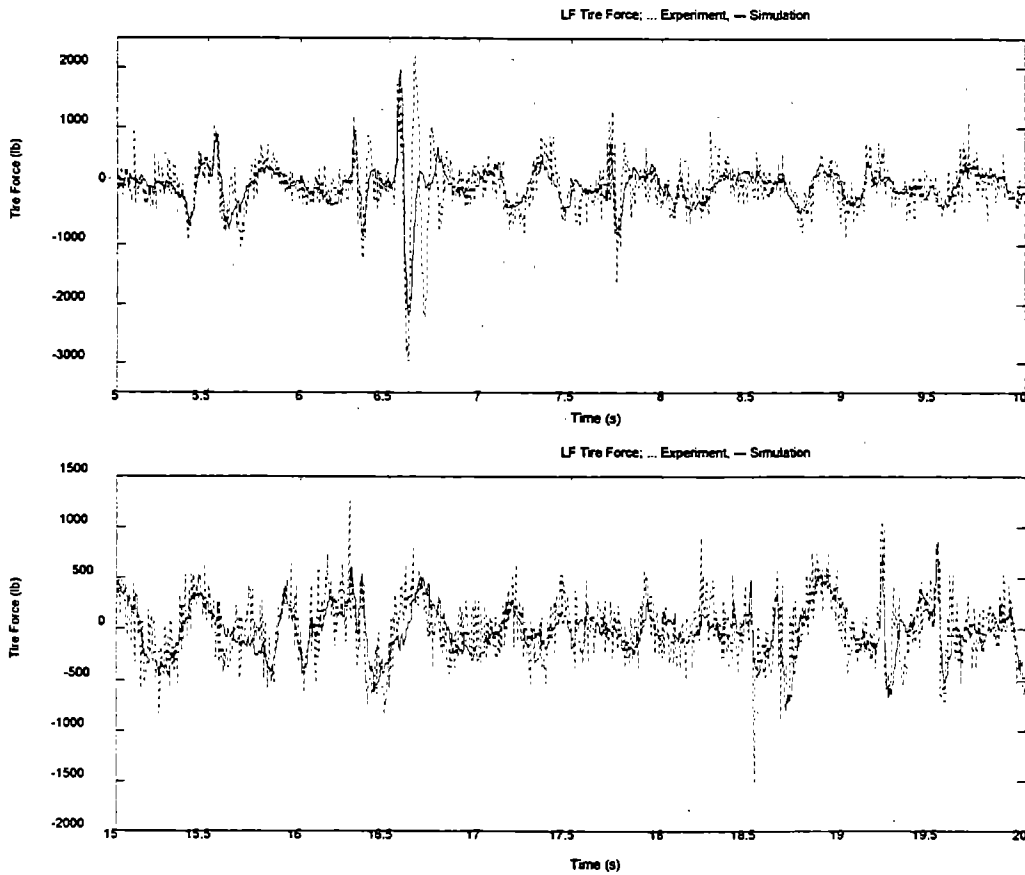
1 lb = 0.454 kg

Figure 5-16. Experimental and simulated left-front tire forces in time domain (half-truck model).
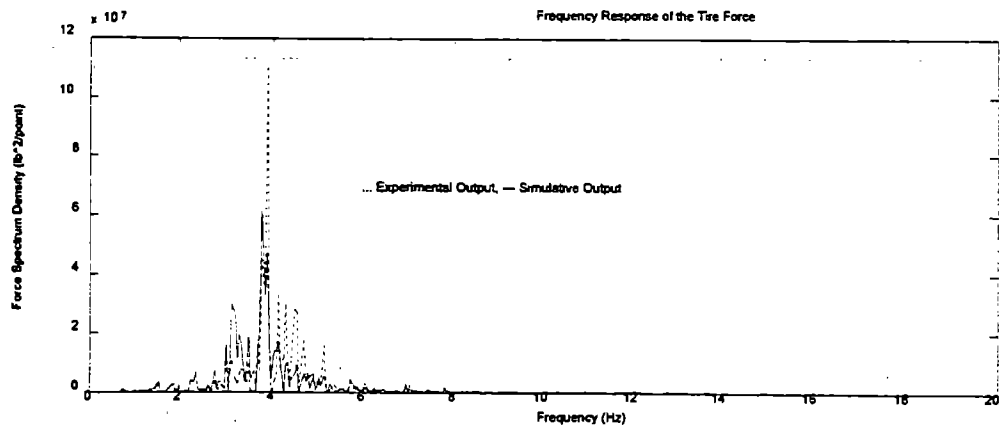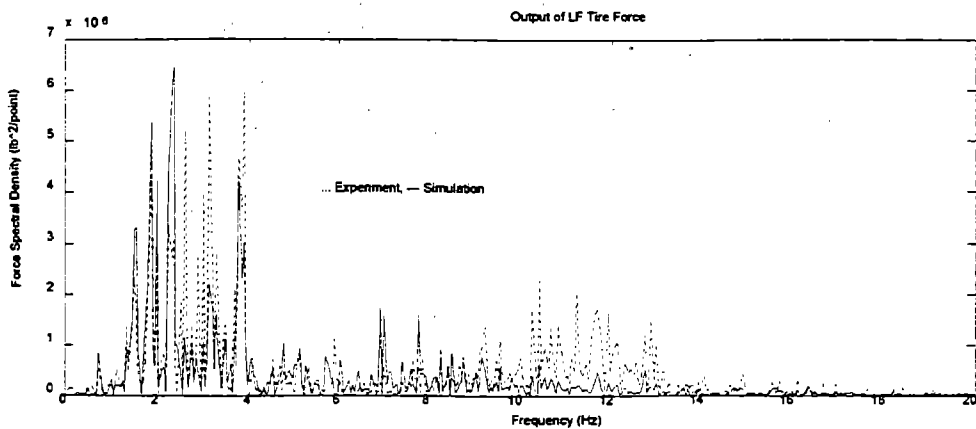

1 lb = 0.454 kg

Figure 5-17. Experimental and simulated left-front tire forces in frequency domain (half-truck model).

116

1 lb = 0.454 kg

Figure 5-18. Experimental and simulated left-rear tire forces in time domain (half-truck model).

1 lb = 0.454 kg

Figure 5-19. Experimental and simulated left-rear tire forces in frequency domain (half-truck model).

117

5.5.3 Linear Full-Truck Model

A seven-degree-of-freedom linear full-truck model is shown in figures 5-20 (side-view schematic) and 5-21 (front-view schematic). The system is represented by 14 state variables, and the following state variables are used here: $q_1 = x_{u1}$, $q_2 = \dot{x}_{u1}$,

$q_3 = x_{u2}$, $q_4 = \dot{x}_{u2}$, $q_5 = \phi_{a1}$, $q_6 = \dot{\phi}_{a1}$, $q_7 = \phi_{a2}$, $q_8 = \dot{\phi}_{a2}$, $q_9 = x_s$, $q_{10} = \dot{x}_s$, $q_{11} = \phi_b$,

$q_{12} = \dot{\phi}_b$, $q_{13} = \phi$, $q_{14} = \dot{\phi}$. The input and output vectors, u and y, are four-dimensional, each of their components representing road profiles and tire forces under each of the four wheels of the truck.
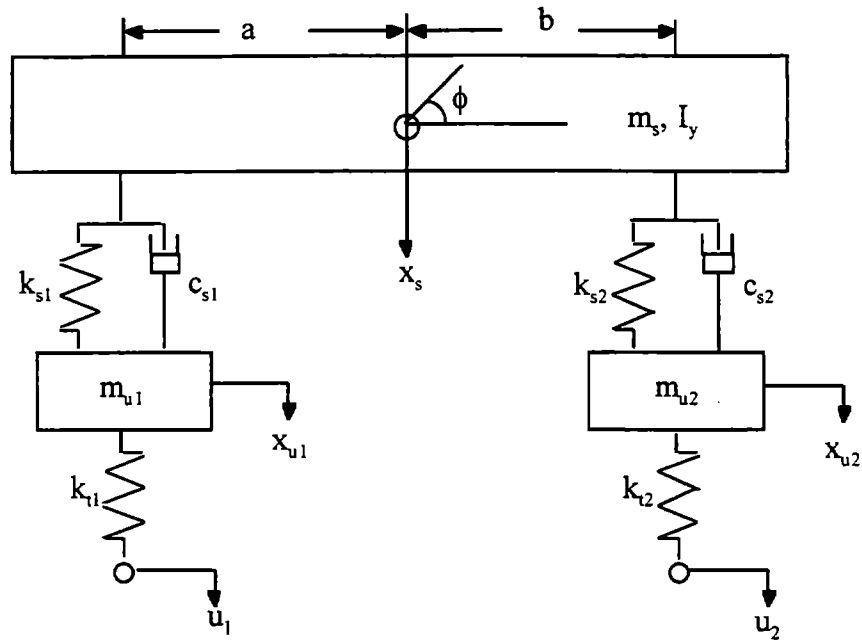
Figure 5-20. Linear full-truck model: Side-view schematic.
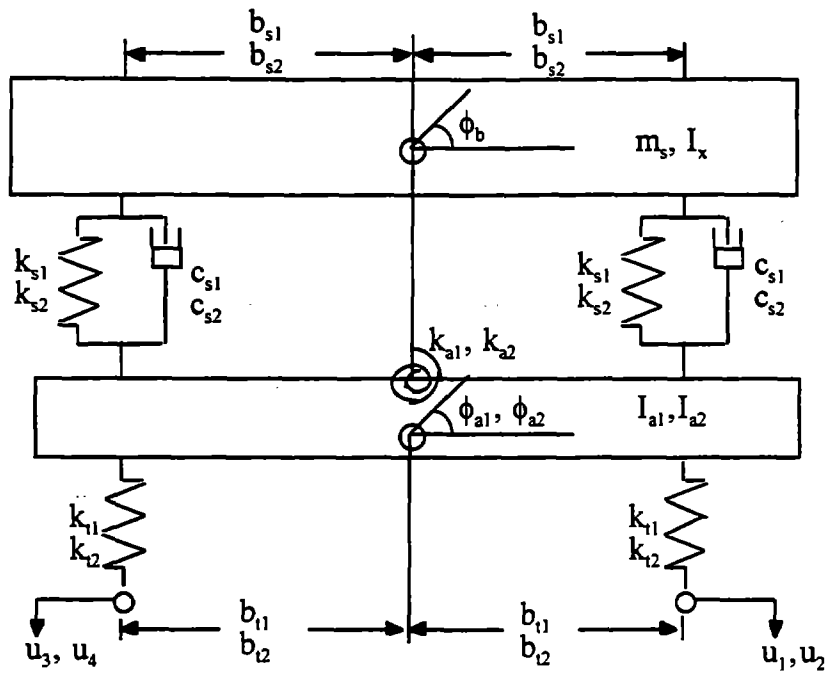
Figure 5-21. Linear full-truck model: Front-view schematic.

The system matrices, A, B, C, and D, are

$$A =$$

$$
\begin{bmatrix}
0 & 1 & 0 & 0 & 0 & 0 & 0 \\[4pt]
\dfrac{-2k_{t1}-2k_{s1}}{m_{u1}} & \dfrac{-2c_{s1}}{m_{u1}} & 0 & 0 & 0 & 0 & 0 \\[8pt]
0 & 0 & 0 & 1 & 0 & 0 & 0 \\[4pt]
0 & 0 & \dfrac{-2k_{t2}-2k_{s2}}{m_{u2}} & \dfrac{-2c_{s2}}{m_{u2}} & 0 & 0 & 0 \\[8pt]
0 & 0 & 0 & 0 & 0 & 1 & 0 \\[4pt]
0 & 0 & 0 & 0 & \dfrac{-2k_{s1}b_{s1}^2-2k_{t1}b_{t1}^2-k_{a1}}{I_{a1}} & \dfrac{-2c_{s1}b_{s1}^2}{I_{a1}} & 0 \\[10pt]
0 & 0 & 0 & 0 & 0 & 0 & 0 \\[4pt]
0 & 0 & 0 & 0 & 0 & 0 & \dfrac{-2k_{s2}b_{s2}^2-2k_{t2}b_{t2}^2-k_{a2}}{I_{a2}} \\[10pt]
0 & 0 & 0 & 0 & 0 & 0 & 0 \\[4pt]
\dfrac{2k_{s1}}{m_s} & \dfrac{2c_{s1}}{m_s} & \dfrac{2k_{s2}}{m_s} & \dfrac{2c_{s2}}{m_s} & 0 & 0 & 0 \\[8pt]
0 & 0 & 0 & 0 & 0 & 0 & 0 \\[4pt]
0 & 0 & 0 & 0 & \dfrac{2k_{s1}b_{s1}^2+k_{a1}}{I_x} & \dfrac{2c_{s1}b_{s1}^2}{I_x} & \dfrac{2k_{s2}b_{s2}^2+k_{a2}}{I_x} \\[10pt]
0 & 0 & 0 & 0 & 0 & 0 & 0 \\[4pt]
\dfrac{2k_{s1}a}{I_y} & \dfrac{2c_{s1}a}{I_y} & \dfrac{-2k_{s2}b}{I_y} & \dfrac{-2c_{s2}b}{I_y} & 0 & 0 & 0
\end{bmatrix}
$$

$$
\begin{bmatrix}
0 & 0 & 0 & 0 & 0 & 0 & 0 \\
0 & \dfrac{2k_{s1}}{m_{u1}} & \dfrac{2c_{s1}}{m_{u1}} & 0 & 0 & \dfrac{2k_{s1}a}{m_{u1}} & \dfrac{2c_{s1}a}{m_{u1}} \\
0 & 0 & 0 & 0 & 0 & 0 & 0 \\
0 & \dfrac{2k_{s2}}{m_{u2}} & \dfrac{2c_{s2}}{m_{u2}} & 0 & 0 & \dfrac{2k_{s2}b}{m_{u2}} & \dfrac{-2c_{s2}b}{m_{u2}} \\
0 & 0 & 0 & 0 & 0 & 0 & 0 \\
0 & 0 & 0 & \dfrac{2k_{s1}b_{s1}^2+k_{a1}}{I_{a1}} & \dfrac{2c_{s1}b_{s1}}{I_{a1}} & 0 & 0 \\
1 & 0 & 0 & 0 & 0 & 0 & 0 \\
\dfrac{-2c_{s2}b_{s2}^2}{I_{a2}} & 0 & 0 & \dfrac{2k_{s2}b_{s2}^2+k_{a2}}{I_{a2}} & \dfrac{2c_{s2}b_{s2}^2}{I_{a2}} & 0 & 0 \\
0 & 0 & 1 & 0 & 0 & 0 & 0 \\
0 & \dfrac{-2k_{s1}-2k_{s2}}{m_s} & \dfrac{-2c_{s1}-2c_{s2}}{m_s} & 0 & 0 & \dfrac{2k_{s2}b-2k_{s1}a}{m_s} & \dfrac{2c_{s2}b-2c_{s1}a}{m_s} \\
0 & 0 & 0 & 0 & 1 & 0 & 0 \\
\dfrac{2c_{s2}b_{s2}^2}{I_x} & 0 & 0 & \dfrac{-2k_{s1}b_{s1}^2-2k_{s2}b_{s2}^2-k_{a1}-k_{a2}}{I_x} & \dfrac{-2c_{s1}b_{s1}^2-2c_{s2}b_{s2}^2}{I_x} & 0 & 0 \\
0 & 0 & 0 & 0 & 0 & 0 & 1 \\
0 & \dfrac{2k_{s2}b-2k_{s1}a}{I_y} & \dfrac{2c_{s2}b-2c_{s1}a}{I_y} & 0 & 0 & \dfrac{-2k_{s1}a^2-2k_{s2}b^2}{I_y} & \dfrac{-2c_{s1}a^2-2c_{s2}b^2}{I_y}
\end{bmatrix}
$$

$$
B =
\begin{bmatrix}
0 & 0 & 0 & 0 \\
\dfrac{k_{t1}}{m_{u1}} & 0 & \dfrac{k_{t1}}{m_{u1}} & 0 \\
0 & 0 & 0 & 0 \\
0 & \dfrac{k_{t2}}{m_{u2}} & 0 & \dfrac{k_{t2}}{m_{u2}} \\
0 & 0 & 0 & 0 \\
\dfrac{-k_{t1}b_{t1}}{I_{a1}} & 0 & \dfrac{k_{t1}b_{t1}}{I_{a1}} & 0 \\
0 & 0 & 0 & 0 \\
0 & \dfrac{-k_{t2}b_{t2}}{I_{a2}} & 0 & \dfrac{k_{t2}b_{t2}}{I_{a2}} \\
0 & 0 & 0 & 0 \\
0 & 0 & 0 & 0 \\
0 & 0 & 0 & 0 \\
0 & 0 & 0 & 0 \\
0 & 0 & 0 & 0 \\
0 & 0 & 0 & 0
\end{bmatrix}
; \quad
C =
\begin{bmatrix}
k_{t1} & 0 & 0 & 0 & -k_{t1}b_{t1} & 0 & 0 & 0 & 0 & 0 & 0 & 0 & 0 & 0 \\
0 & 0 & k_{t2} & 0 & 0 & 0 & -k_{t2}b_{t2} & 0 & 0 & 0 & 0 & 0 & 0 & 0 \\
k_{t1} & 0 & 0 & 0 & k_{t1}b_{t1} & 0 & 0 & 0 & 0 & 0 & 0 & 0 & 0 & 0 \\
0 & 0 & k_{t2} & 0 & 0 & 0 & k_{t2}b_{t2} & 0 & 0 & 0 & 0 & 0 & 0 & 0
\end{bmatrix}
;
$$

$$
D =
\begin{bmatrix}
-k_{t1} & 0 & 0 & 0 \\
0 & -k_{t2} & 0 & 0 \\
0 & 0 & -k_{t1} & 0 \\
0 & 0 & 0 & -k_{t2}
\end{bmatrix}
$$

The measured and estimated values of the model parameters are compiled in table 5-4, except the values of tire spring constants, which can be found in table 5-1.

120

Table 5-4. Parameters of the linear full-truck model.

| Parameter	Value
m_s	5,640 kg (12,420 lb)
m_{u1}	670 kg (1,480 lb)
m_{u2}	900 kg (1,980 lb)
I_x	4,520 N-m-s² (40,000 lb-in-s²) 5,825 N-m-s² (51,550 lb-in-s²)*
I_y	11,860 N-m-s² (105,000 lb-in-s²) 63,300 N-m-s² (560,200 lb-in-s²)*
I_{a1}	550 N-m-s² (4,880 lb-in-s²) 414 N-m-s² (3,660 lb-in-s²)*
I_{a2}	500 N-m-s² (4,470 lb-in-s²) 401 N-m-s² (3,550 lb-in-s²)*
k_{s1}	270 kN/m (1,530 lb/in)
k_{s2}	660 kN/m (3,760 lb/in) (steel) 560 kN/m (3,200 lb/in) (air)
c_{s1}	12.1 kN-s/m (69 lb-s/in)*
c_{s2}	34.1 kN-s/m (195 lb-s/in)*
a	3.36 m (132 in)
b	3.09 m (122 in)
b_{s1}	0.39 m (15 in)
b_{s2}	0.50 m (20 in)
b_{t1}	1.02 m (40 in)
b_{t2}	0.92 m (36 in)

* estimated values.

121

Sample plots of time histories and power spectral densities of the simulated and experimental tire forces for the full-truck model with steel-leaf suspension are shown in figures 5-22 through 5-29. The coefficients of correlation between the simulated and experimental tire forces are 0.94, 0.91, 0.97, and 0.95 for left-front, right-front, left-rear, and right-rear tires, respectively. These values are very high, and the agreement between the simulated and experimental tire forces is very good. It should also be noted that the agreement for the full-truck model is considerably better than it was for the quarter-truck and half-truck models.
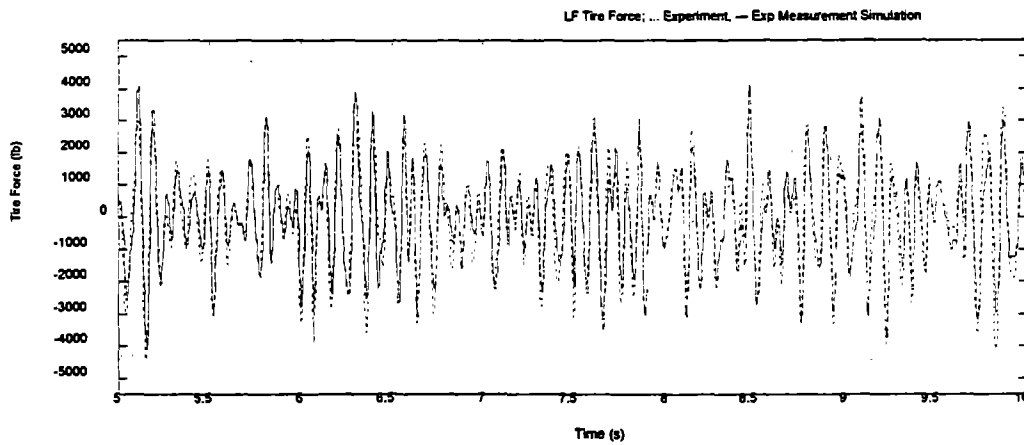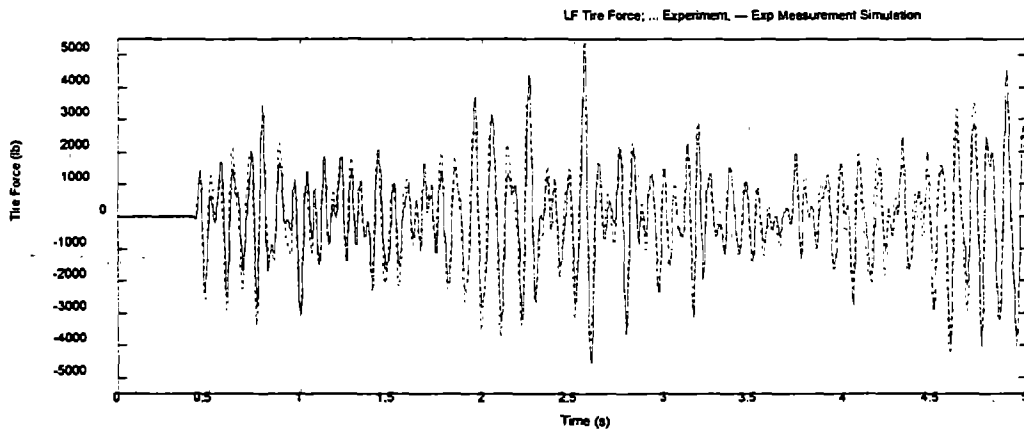
Figure 5-22. Experimental and simulated left-front tire forces in time domain (full-truck model).
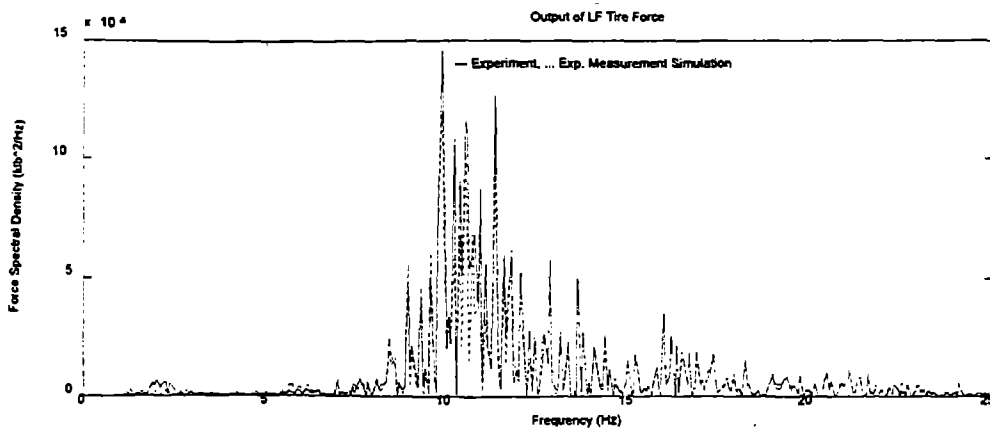
1 lb = 0.454 kg

Figure 5-23. Experimental and simulated left-front tire forces in frequency domain (full-truck model).
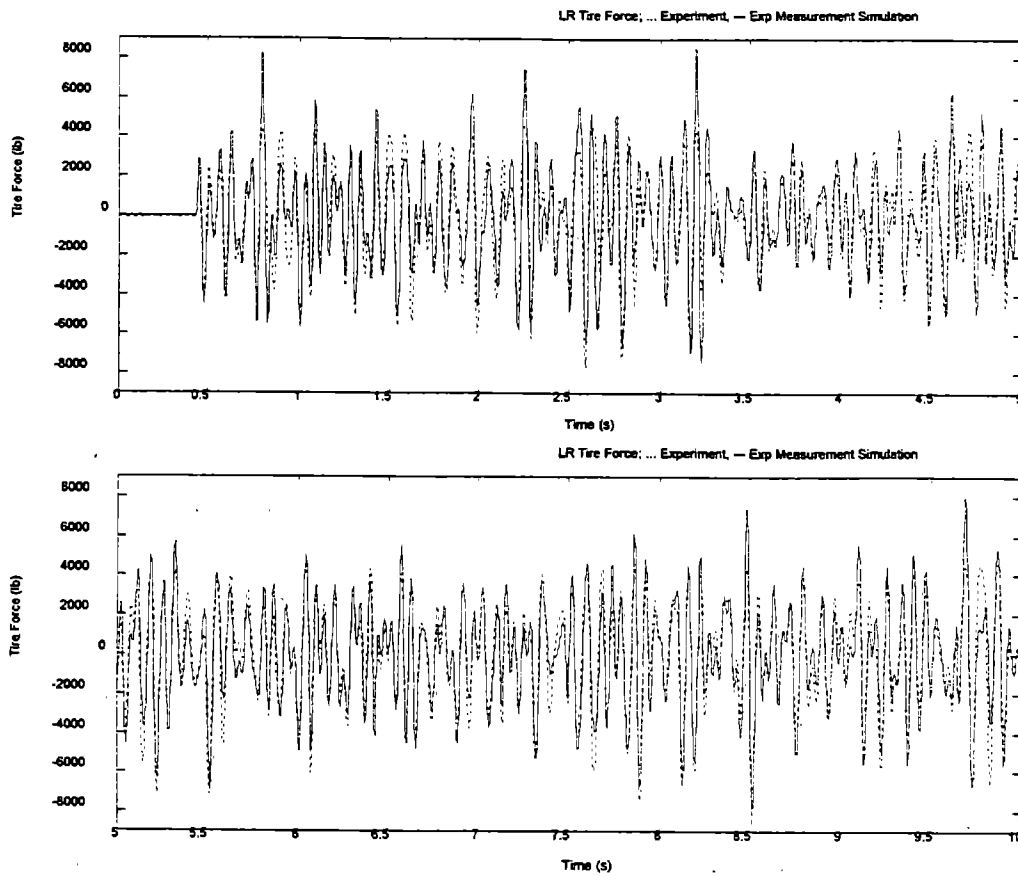
1 lb = 0.454 kg

1 lb = 0.454 kg

Figure 5-24. Experimental and simulated left-rear tire forces in time domain (full-truck model).
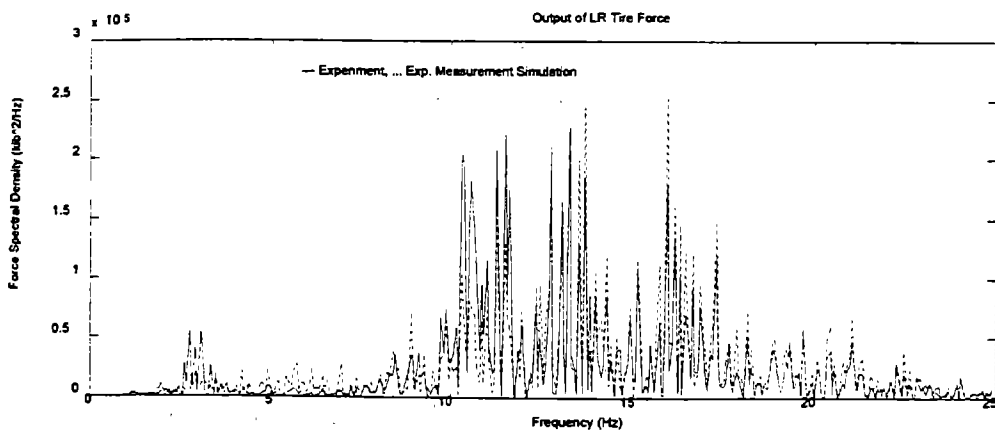
1 lb = 0.454 kg

Figure 5-25. Experimental and simulated left-rear tire forces in frequency domain (full-truck model).

124

RF Tire Force: ... Experiment, — Exp Measurement Simulation
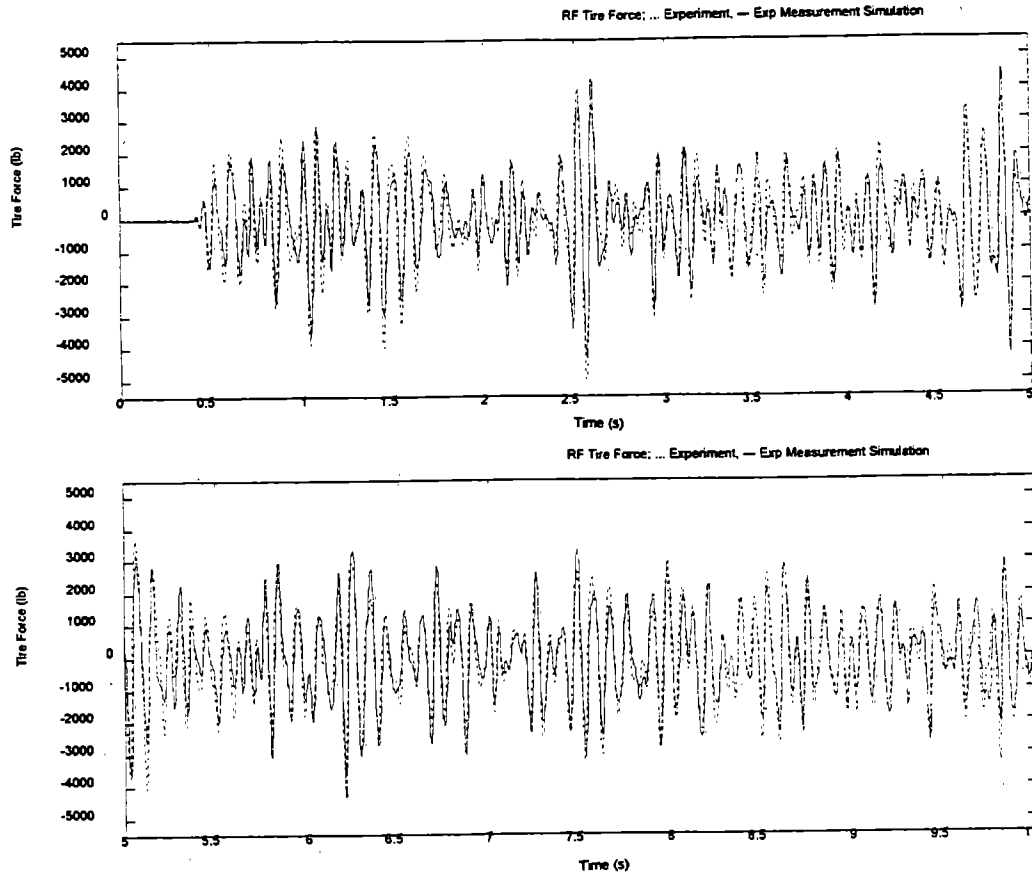
1 lb = 0.454 kg

Figure 5-26. Experimental and simulated right-front tire forces in time domain (full-truck model).

Output of RF Tire Force
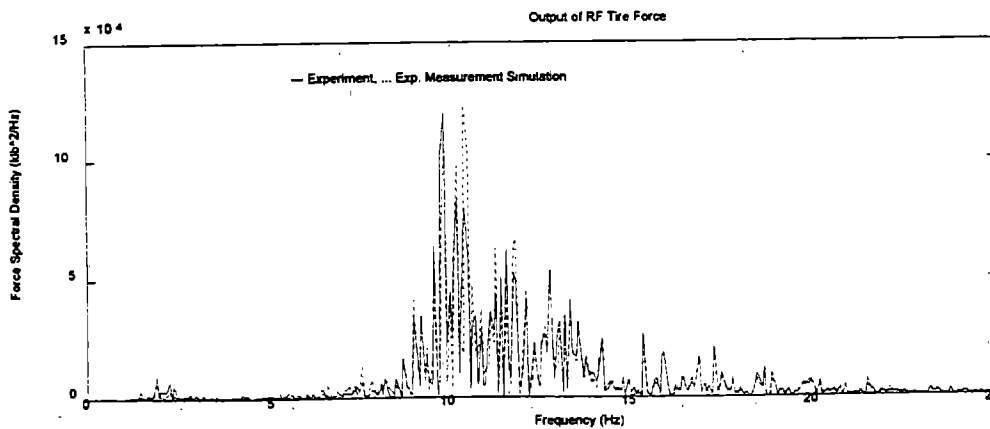
1 lb = 0.454 kg

Figure 5-27. Experimental and simulated right-front tire forces in frequency domain (full-truck model).
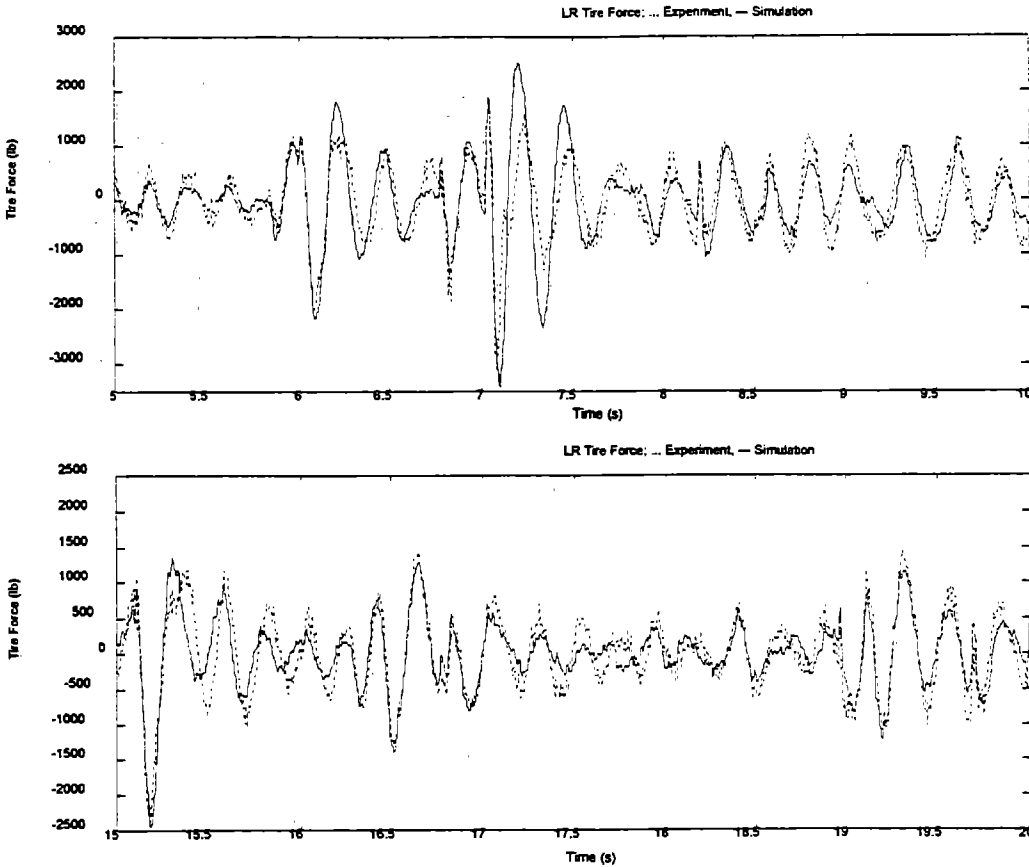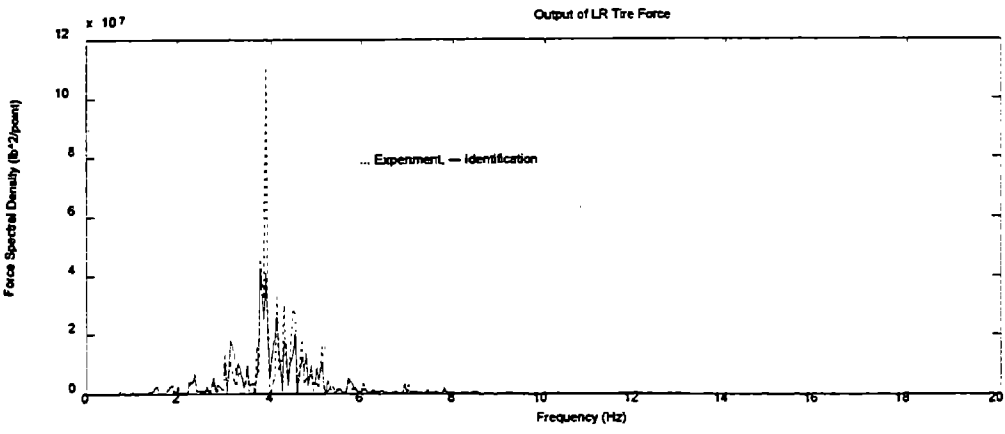
125
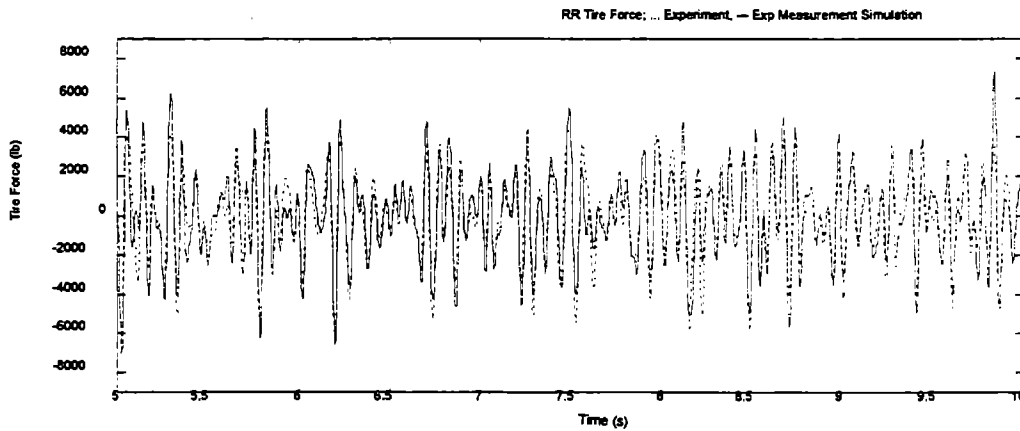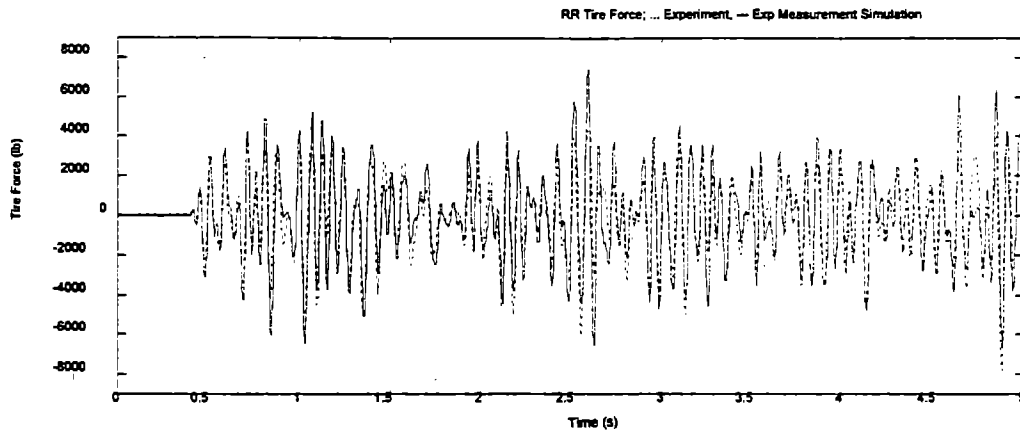
1 lb = 0.454 kg

Figure 5-28. Experimental and simulated right-rear tire forces in time domain (full-truck model).
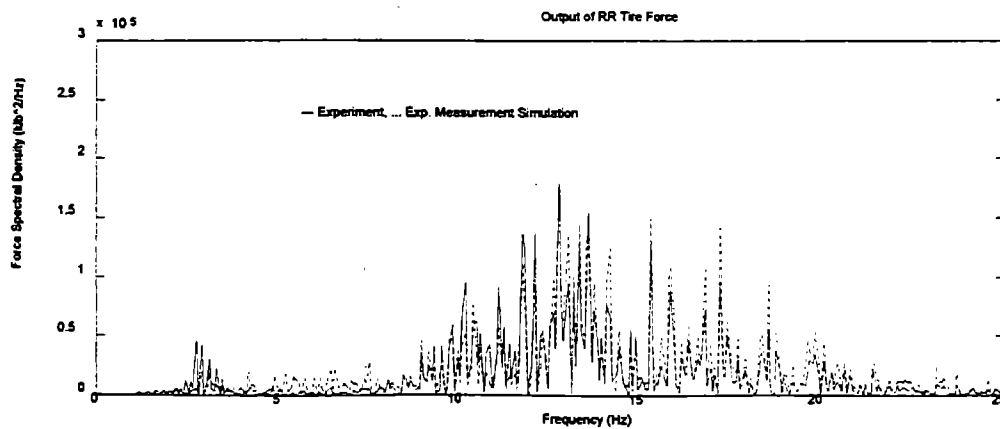
1 lb = 0.454 kg

Figure 5-29. Experimental and simulated right-rear tire forces in frequency domain (full-truck model).

5.5.4 Nonlinear Quarter-Truck Model

The main source of nonlinearity in truck dynamics is the Coulomb (dry) friction force generated by steel-leaf suspension. The effect of the Coulomb friction on tire forces becomes more pronounced on rougher roads. A schematic of the nonlinear quarter-truck model is shown in figure 5-30.
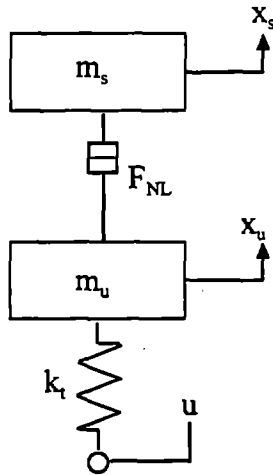
Figure 5-30. Nonlinear quarter-truck model.

Selecting the same state variables as for the linear quarter-truck model, the state-variable equations can be written in the following form:

$$\dot{x}_s = v_s$$

$$\dot{v}_s = \frac{1}{m_s} F_{NL}$$

$$\dot{x}_u = v_u$$

$$\dot{v}_u = -\frac{k_t}{m_u} x_u - \frac{1}{m_u} F_{NL} + \frac{1}{m_u} u$$

where F_{NL} is the nonlinear suspension force, which consists of three components: linear spring force, linear viscous damping force, and nonlinear Coulomb friction force. The mathematical expression for the nonlinear suspension force is

$$F_{NL} = -k_s(x_s - x_u) - c_s(\dot{x}_s - \dot{x}_u) - c_f \; SGN\{(\dot{x}_s - \dot{x}_u)\} \qquad \text{(5-13)}$$

where *SGN* is the sign function and c_f is the magnitude of the Coulomb friction force.

The measured and estimated values of the nonlinear quarter-truck model are listed in table 5-5. The values of the tire spring constant for the three test tire types can be found in table 5-1.

Table 5-5. Parameters of the nonlinear quarter-truck model.

Parameter	Value
m_s	1,350 kg (2,970 lb) front
	1,470 kg (3,240 lb) rear
m_u	335 kg (740 lb) front
	450 kg (990 lb) rear
k_s	270 kN/m (1,530 lb/in) front
	660 kN/m (3,760 lb/in) rear
c_s	10.5 kN-s/m (58 lb-s/in) front*
	20.1 kN-s/m (115 lb-s/in) rear*
c_f	0.48 N (108 lb) front*
	2.9 kN (652 lb) rear*

* estimated values.

Sample plots of time histories and power spectral densities of the simulated and experimental tire forces for the nonlinear quarter-truck model with steel-leaf suspension are shown in figures 5-31 through 5-34. The values of the coefficient of correlation between the simulated and experimental tire forces were 0.81 and 0.93 for front and rear tire forces, respectively. The agreement in this case is clearly better than it was for the linear quarter-truck model.

128
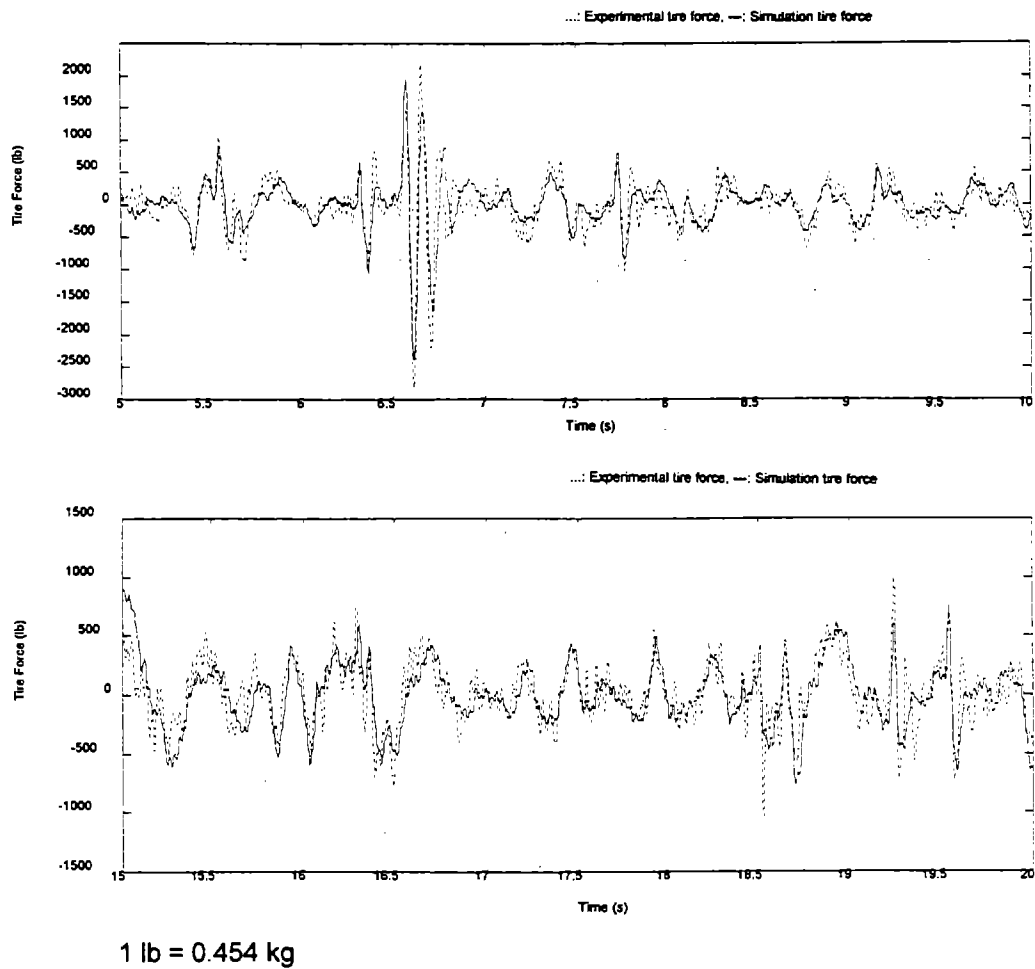
1 lb = 0.454 kg

Figure 5-31. Experimental and simulated left-front tire forces in time domain (nonlinear quarter-truck model).
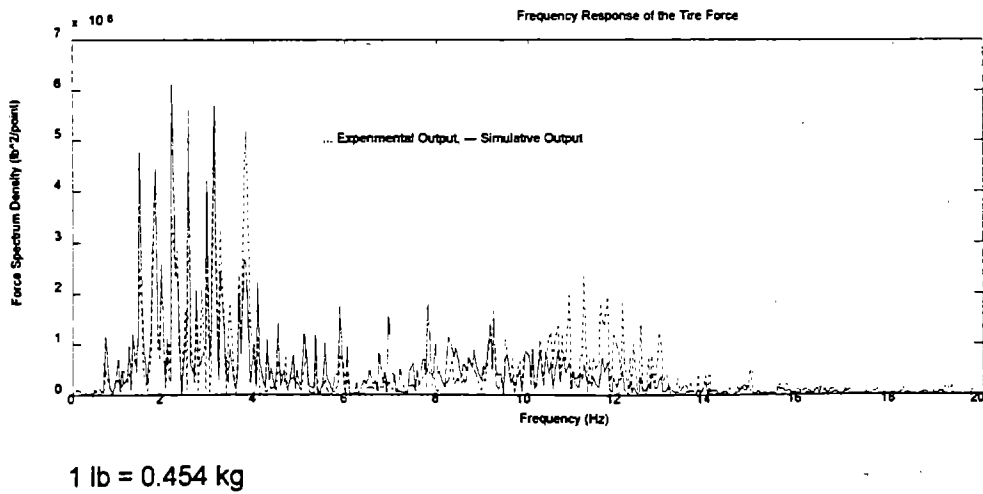
1 lb = 0.454 kg

Figure 5-32. Experimental and simulated left-front tire forces in frequency domain (nonlinear quarter-truck model).

129
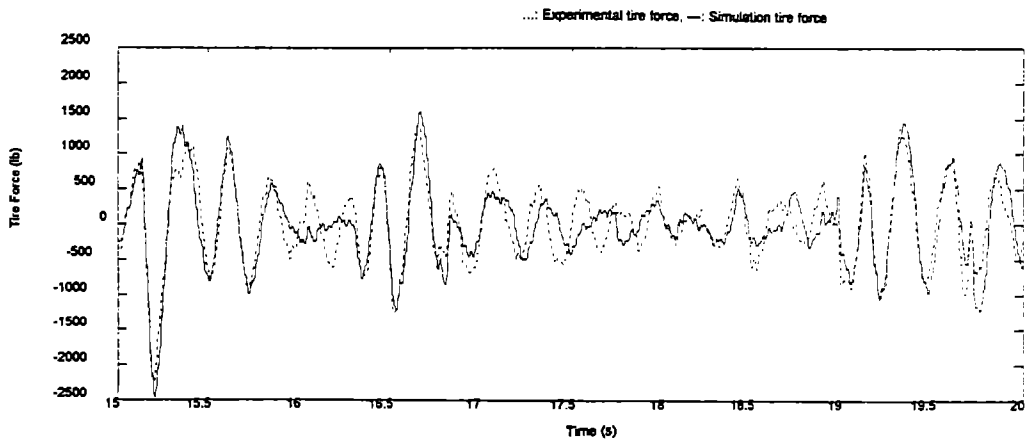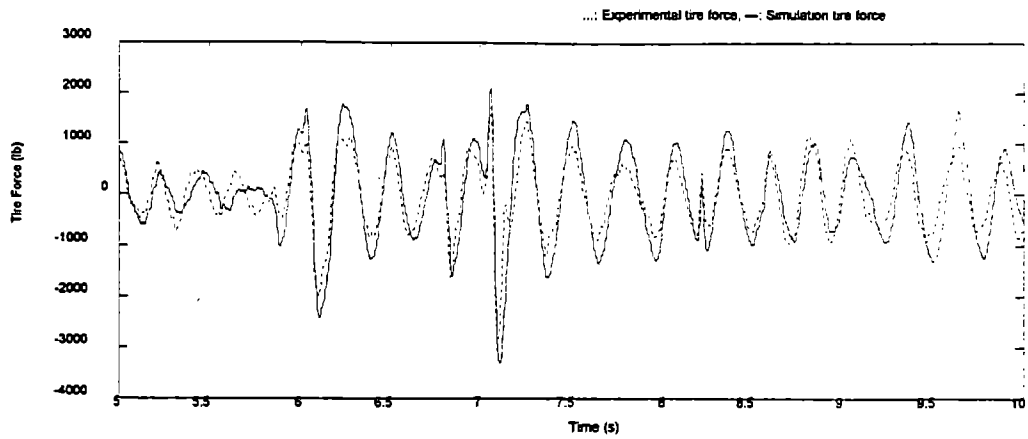
1 lb = 0.454 kg

Figure 5-33. Experimental and simulated left-rear tire forces in time domain (nonlinear quarter-truck model).
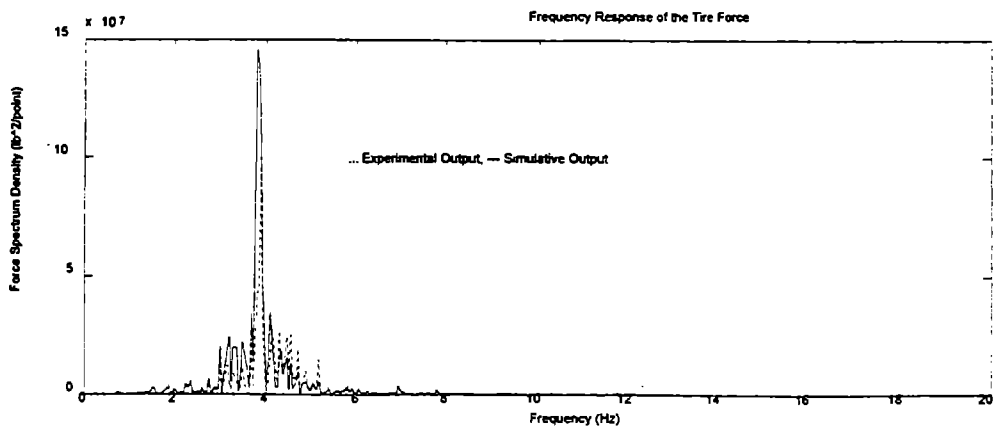
1 lb = 0.454 kg

Figure 5-34. Experimental and simulated left-rear tire forces in frequency domain (nonlinear quarter-truck model).

130

CHAPTER 6. TIRE TESTING

As explained in chapter 3, three tire types were selected for the test program: the 11R22.5 standard radial tire, 295/75R22.5 low-profile radial tire, and 425/65R22.5 wide-base (super single) tire. The following properties of the tires were considered relevant for the dynamic tire forces:

- Gross contact area.
- Net contact area.
- Tire deflection versus vertical load characteristic.
- Contact pressure distribution.

In addition to tire type, two other test variables were tire inflation pressure and vertical load. The tire inflation pressure was varied at three levels over the range of the manufacturer's recommended pressure ±25 percent. The tire vertical load was changed at four levels in the contact area and contact pressure measurements and at six levels in deflection versus load tests.

The methodology selected for measuring these characteristics and the results of the measurements are presented in the following sections of this chapter.

6.1 METHODOLOGY FOR MEASURING TIRE PROPERTIES

The following three methods were identified as capable of measuring the four tire-response characteristics relevant to dynamic tire forces:

- Force-pin method.
- Fuji-sensitive film method.
- Dynamic-pressure cells method.

Each of these methods was evaluated in terms of its ability to conduct the four necessary measurements and sensitivity to small changes in the inflation pressure (35 kPa [5 psi]) and vertical load (0.45 kN [100 lb]).

6.1.1 Force-Pin Method

The force-pin method uses a flat bed instrumented with a strain gauge.[30] The bed is capable of moving with the tire as the tire rotates at a very slow speed, less than 1 mi/h. Because the speed is so low, the method is practically considered static. Numerous points across the tire tread are tracked as they move through the length of the contact area to obtain the overall contact pressure profile. By moving the tire in the transverse direction relative to the flat bed, the two-dimensional stress distribution over the tire contact area can be measured. Since the strain-gauge sensor is smaller than the rib area of the tire tread, the pressure distribution under each rib can be measured.

The tire deflection versus load characteristic is measured in a similar manner. The tire is subjected to different load levels, and its vertical deflection is measured simultaneously.

Tire footprints are obtained by inking the tread area of the inflated tire while it is mounted on the same machine and subjected to preset loads. An imprint is left on a piece of paper placed between the tire and the machine's loading plate. The gross and net contact areas are measured from these imprints. The areas are calculated by a computer using signals from digitized boundary points of the imprints.

6.1.2 Fuji-Sensitive Film Method

This method involves applying a specified vertical load to a tire while the tire rests on a special type of pressure-sensitive film. The darkness of the tire imprint is directly proportional to the contact pressure. The investigation conducted in this study identified one major problem with this method—namely, the tendency of the pressure-sensitive film to respond to the compound stresses as a result of the interaction between the vertical and horizontal components at the tire-film interface. As a result,

132

the measured stresses appear larger than their actual values. This problem may be resolved by placing a debonding material at the tire-film interface to eliminate the shearing effect. However, an effective debonding agent is not known at this time. In addition, current calibration techniques for a pressure-sensitive film would not provide the required sensitivity to tire inflation pressure.

Furthermore, there is no provision in this method to measure the gross and net contact areas of the tire imprint. However, the contact areas could be measured in a manner similar to the one used in the force-pin method.

6.1.3 Dynamic-Pressure Cell Methods

This method was developed at the Technical Research Center in Finland to measure tire-stress distribution at highway speeds.[31] The measuring apparatus consists of a series of miniature dynamic pressure cells sandwiched between two steel plates. When the truck travels over the strip, the forces applied by the tire to the pressure cells are captured with use of a computer DAQ system. The plates can measure the stress at up to 16 points, 2 cm (0.79 in) apart in the transverse direction, thus covering a total width of 30 cm (11.8 in). One problem with this method is that it is impossible to indicate the position of the individual pressure cells relative to the tire ribs. This results in replicate measurements showing different pressure distributions depending on the locations of the pressure cells relative to the tire ribs.

Researchers at the Technical University of Denmark have developed a system to measure stress distribution under rolling tires. In this method, pressure cells are installed in the AC layer under the Danish Road Testing Machine (RTM).[32] The active faces of the pressure cells are flush with the pavement surface so that the pressures at the faces of the cells are equal to the tire contact stresses. The full pressure distribution across the tire imprints is measured by changing the transverse position of the tire relative to the pressure cells. The lateral position of the tire in the RTM can be controlled in 10-cm (4-in) increments. The RTM travels at a speed of 20 km/h (12.5 mi/h), which is considerably less than highway speeds.

The dynamic pressure-cell method have the advantage of providing dynamic stress distribution at highway speeds. However, their benefits to this study would be rather limited since they do not provide the measurements of tire deflection or tire gross and net contact areas. The measurement of these parameters would still have to be conducted statically, which would be inconsistent with the measured dynamic stresses. The findings from the evaluation of the three methods are summarized in table 6-1.

Table 6-1. Evaluation of the tire-testing methods.

Required Measurement	Method		
	Force Pin	Sensitive Film	Pressure Cells
Two-Dimensional Stress Distribution	Yes	Yes	Yes
Tire Deflection	Yes	No	No
Net Contact Area	Yes	Yes	No
Gross Contact Area	Yes	Yes	No
Sensitivity to Small Pressure Changes	Yes	No	No
Sensitivity to Small Load Changes	Yes	No	No

On the basis of the results of the evaluation, the force-pin method was selected for tire testing in this study.

6.2 TEST RESULTS

The tire tests were conducted by the Goodyear Tire and Rubber Company with use of the force-pin method. The results of the measurements of the gross and net contact areas, load versus deflection characteristics, and contact pressure distributions for the three test tires are presented in the following sections.

134

6.2.1 Gross and Net Contact Areas

The gross contact area is the entire area of contact between the tire and the surface, including both the ribs and the spacing between the ribs. The net contact area is the area of the ribs in contact with the pavement surface under the given load and inflation pressure. The length and the width data refer to the gross contact area. Tables 6-2, 6-3, and 6-4 show the results of the footprint measurements for the three test tires over the range of vertical loads and inflation pressures.

Table 6-2. Footprint data for the standard radial tire, 11R22.5.

Load (lb)	Tire Pressure (psi)	Length (in)	Width (in)	Gross Area (in^2)	Net Area (in^2)
1,750	70	6.30	6.65	32.9	23.8
	85	6.10	6.35	30.2	22.1
	100	5.90	6.15	28.0	20.1
2,500	70	7.50	7.70	45.9	35.1
	85	7.10	7.35	41.0	30.9
	100	6.80	7.05	37.8	28.3
4,250	80	9.10	7.85	63.7	49.9
	95	8.55	7.80	58.3	45.7
	110	8.20	7.80	54.4	42.6
5,500	90	9.90	7.85	71.7	57.1
	105	9.40	7.85	66.7	52.6
	120	8.85	7.85	62.1	49.3

1 lb = 0.454 kg
1 in = 2.54 cm
1 in^2 = 6.452 cm^2
1 psi = 6.9 kPa

135

Table 6-3. Footprint data for the low-profile tire, 295/75R22.5.

Load (lb)	Tire Press. (psi)	Length (in)	Width (in)	Gross Area (in^2)	Net Area (in^2)
1,750	70	6.55	6.65	33.9	24.5
	85	6.15	6.35	31.0	21.8
	100	5.85	6.05	28.5	20.0
2,500	70	7.55	7.70	46.5	35.1
	85	6.95	7.00	39.0	29.0
	100	6.85	6.95	38.2	27.9
4,250	80	9.25	7.80	65.1	50.6
	95	8.70	7.80	60.0	46.9
	110	8.35	7.75	55.7	43.2
5,500	90	10.25	7.80	74.9	59.2
	105	9.60	7.80	69.0	53.8
	120	9.10	7.80	64.1	50.1

1 lb = 0.454 kg
1 in = 2.54 cm
1 in^2 = 6.452 cm^2
1 psi = 6.9 kPa

Table 6-4. Footprint data for the wide-base tire, 425/65R22.5.

Load (lb)	Tire Press. (psi)	Length (in)	Width (in)	Gross Area (in^2)	Net Area (in^2)
1,750	90	7.30	11.05	71.1	48.0
	105	7.05	10.90	67.7	46.6
	120	6.65	10.70	62.9	42.0
2,500	90	9.00	12.65	102.2	74.0
	105	8.60	12.40	92.2	65.2
	120	8.30	11.95	87.6	60.9
4,250	100	9.60	12.65	111.3	80.8
	115	9.25	12.70	103.5	75.7
	130	8.85	12.60	97.3	69.5
5,500	115	10.60	12.80	124.5	93.9
	130	10.10	12.70	116.9	87.1
	145	9.60	12.60	109.8	78.5

1 lb = 0.454 kg
1 in = 2.54 cm
1 in^2 = 6.452 cm^2
1 psi = 6.9 kPa

A very important parameter for the pavement wear induced by tire forces is the net average contact pressure, P_c, calculated as the ratio of vertical load over net contact area. Multilinear regression of the data from tables 6-2, 6-3, and 6-4, gave the following equations for the net contact pressure as a function of load and inflation pressure for the three test tires:

$$P_{cSR} = 193 + 6.01\,L + 0.52\,P_t \qquad (6\text{-}1)$$
$$P_{cLP} = 195 + 4.18\,L + 0.55\,P_t \qquad (6\text{-}2)$$
$$P_{cWB} = 186 + 3.16\,L + 0.60\,P_t \qquad (6\text{-}3)$$

where

P_c = average contact pressure, kPa.
L = tire vertical load, kN.
P_t = tire inflation pressure, kPa.

The coefficient of correlation for the previous equations, R^2, is 0.99.

6.2.2 Load-Deflection Characteristics

The load-deflection measurements were conducted for the three test tires for several levels of inflation pressure and over a broad range of vertical loads. The results of the measurements are presented in tables 6-5, 6-6, and 6-7 and in figures 6-1 through 6-6.

Table 6-5. Load-deflection data for the standard radial tire, 11R22.5.

Load/Tire (lb)	Tire Pressure (psi)								
	70	80	85	90	95	100	105	110	120
	Tire Deflection (in)								
1,000	0.41	0.37	0.36	0.34	0.33	0.33	0.33	0.30	0.28
2,000	0.73	0.66	0.65	0.63	0.60	0.58	0.58	0.54	0.52
3,000	1.02	0.92	0.89	0.87	0.82	0.81	0.80	0.76	0.72
4,000	1.25	1.15	1.11	1.07	1.03	1.01	0.98	0.94	0.90
5,000	1.48	1.36	1.32	1.28	1.22	1.20	1.18	1.13	1.08
6,000	1.72	1.57	1.52	1.47	1.40	1.38	1.35	1.30	1.24

1 lb = 0.454 kg
1 in = 2.54 cm
1 psi = 6.9 kPa

138

Table 6-6. Load-deflection data for the low-profile tire, 295/75R22.5.

Load/Tire	Tire Pressure (psi)						
(lb)	70	80	85	95	100	110	115
	Tire Deflection (in)						
1,000	0.38	0.35	0.33	0.30	0.30	0.28	0.27
2,000	0.70	0.63	0.62	0.56	0.55	0.52	0.50
3,000	0.95	0.87	0.85	0.78	0.77	0.72	0.70
4,000	1.21	1.10	1.07	0.97	0.95	0.88	0.87
5,000	1.44	1.33	1.28	1.18	1.14	1.08	1.04
6,000	1.68	1.53	1.48	1.36	1.33	1.24	1.22

1 lb = 0.454 kg
1 in = 2.54 cm
1 psi = 6.9 kPa

Table 6-7. Load-deflection data for the wide-base tire, 425/65R22.5.

Load/Tire (lb)	Tire Pressure (psi)						
	70	80	85	95	100	110	115
	Tire Deflection (in)						
1,000	0.27	0.24	0.25	0.24	0.23	0.22	0.21
2,000	0.49	0.45	0.45	0.44	0.42	0.40	0.37
3,000	0.72	0.65	0.65	0.62	0.59	0.56	0.52
4,000	0.92	0.85	0.84	0.79	0.76	0.73	0.67
5,000	1.11	1.03	1.02	0.96	0.92	0.87	0.81
6,000	1.29	1.19	1.17	1.11	1.07	1.02	0.95
7,000	1.46	1.35	1.33	1.25	1.21	1.15	1.08
8,000	1.63	1.51	1.47	1.38	1.35	1.28	1.20
9,000	1.80	1.67	1.63	1.53	1.48	1.41	1.32
10,000	1.96	1.82	1.78	1.67	1.62	1.53	1.43
11,000	2.10	1.96	1.91	1.80	1.74	1.65	1.53

1 lb = 0.454 kg
1 in = 2.54 cm
1 psi = 6.9 kPa
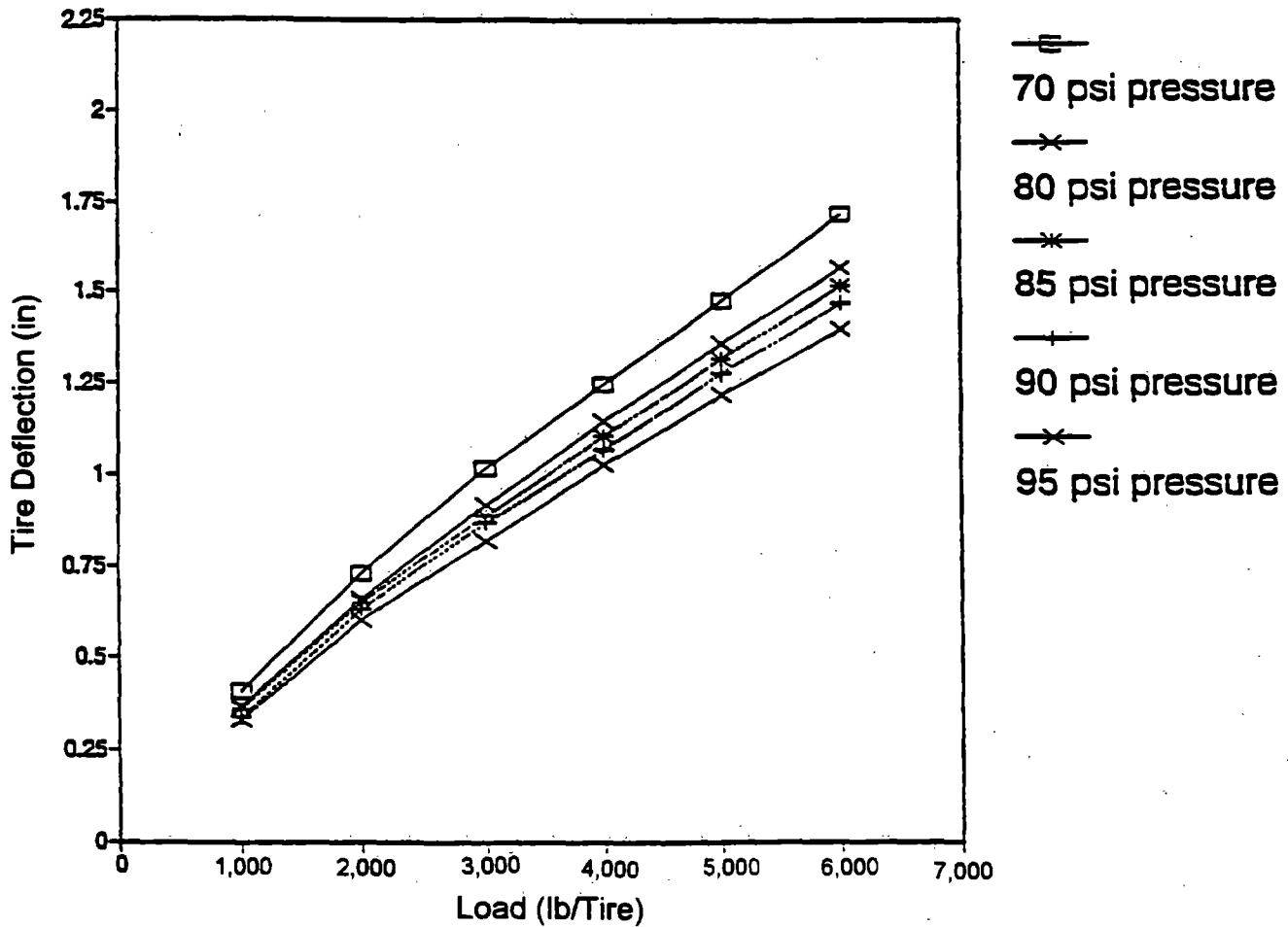
Figure 6-1. Load-deflection characteristics of the standard radial tire, 11R22.5, for inflation pressures of 483, 552, 586, 621, and 655 kPa (70, 80, 85, 90, and 95 psi).
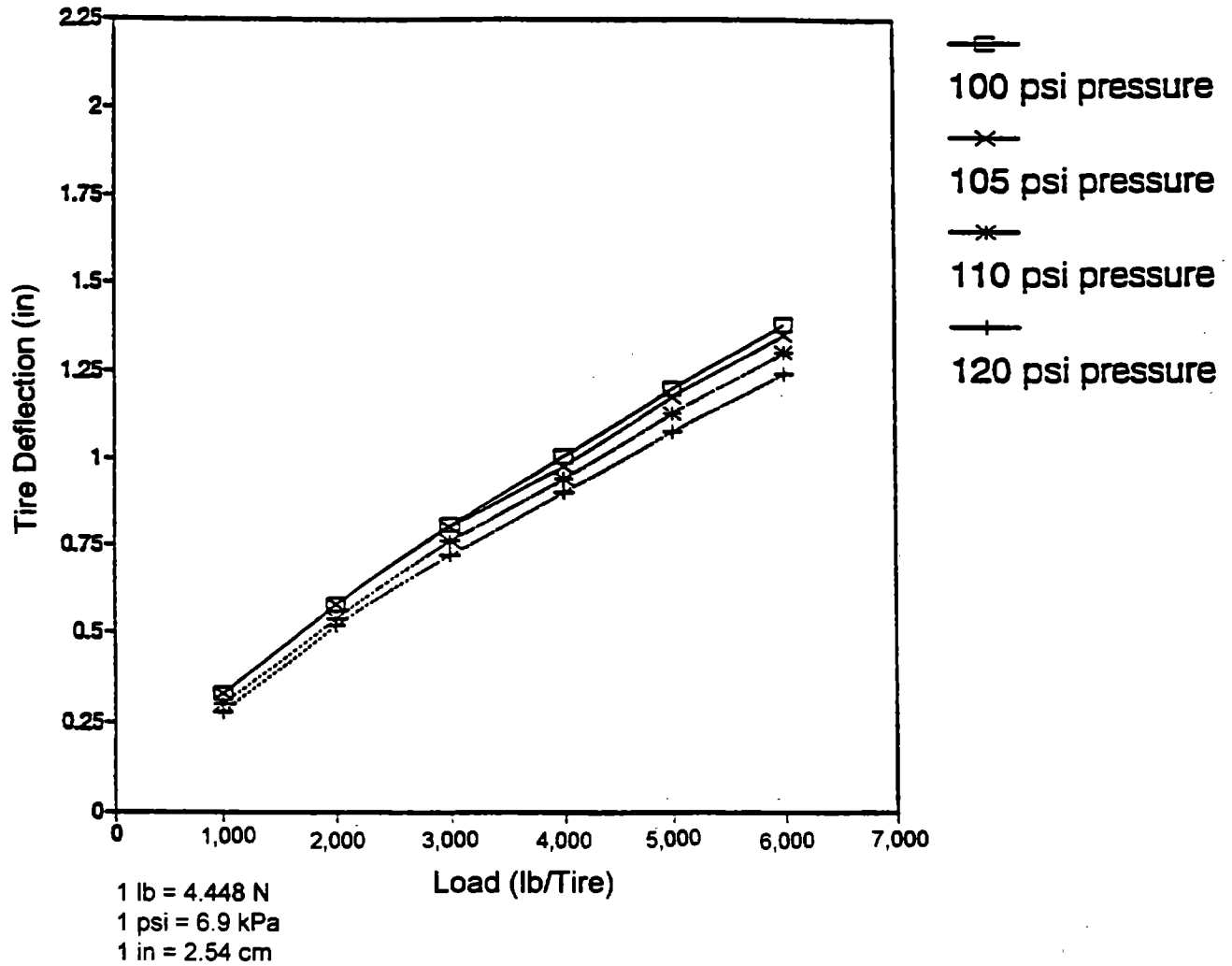
Figure 6-2. Load-deflection characteristics of the standard radial tire, 11R22.5, for inflation pressures of 690, 724, 758, and 827 kPa (100, 105, 110, and 120 psi).
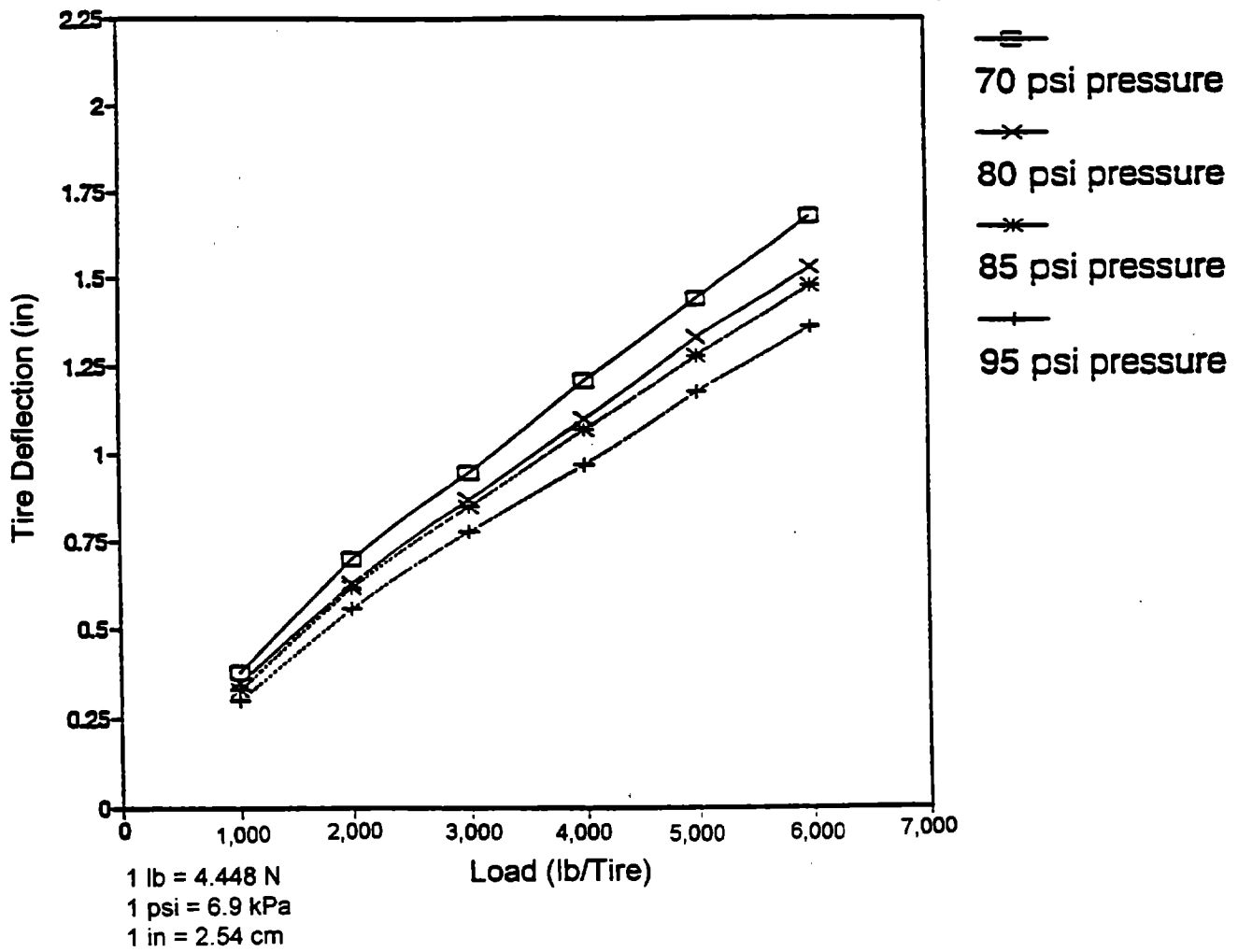
Figure 6-3. Load-deflection characteristics of the low-profile tire, 295/75R22.5, for inflation pressures of 483, 552, 586, and 655 kPa (70, 80, 85, 95 psi).
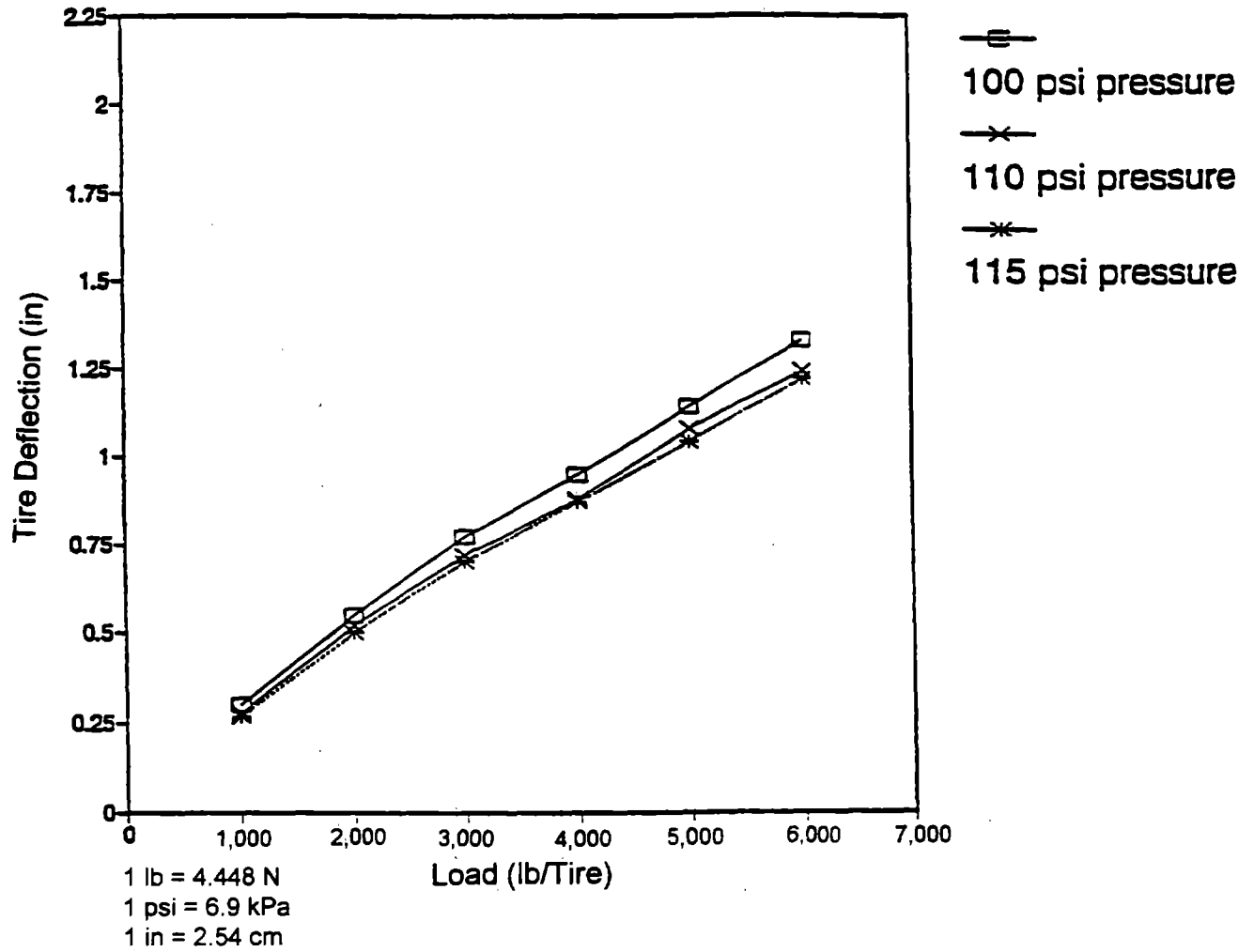
Figure 6-4. Load-deflection characteristics of the low-profile tire, 295/75R22.5, for inflation pressures of 690, 758, and 793 kPa (100, 110, and 115 psi).

144
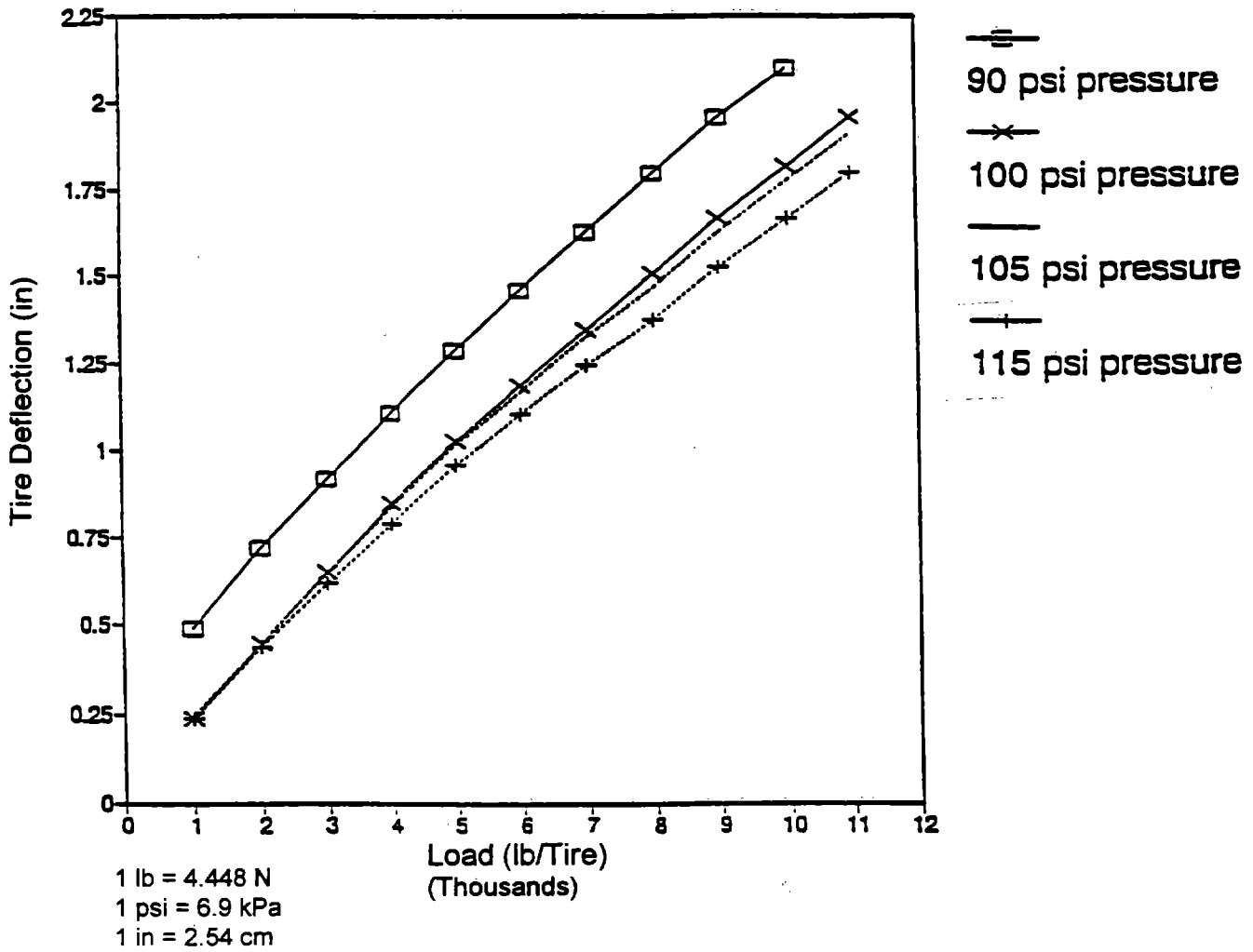
Figure 6-5. Load-deflection characteristics of the wide-base tire, 425/65R22.5, for inflation pressures of 621, 690, 724, and 793 kPa (90, 100, 105, and 115 psi).
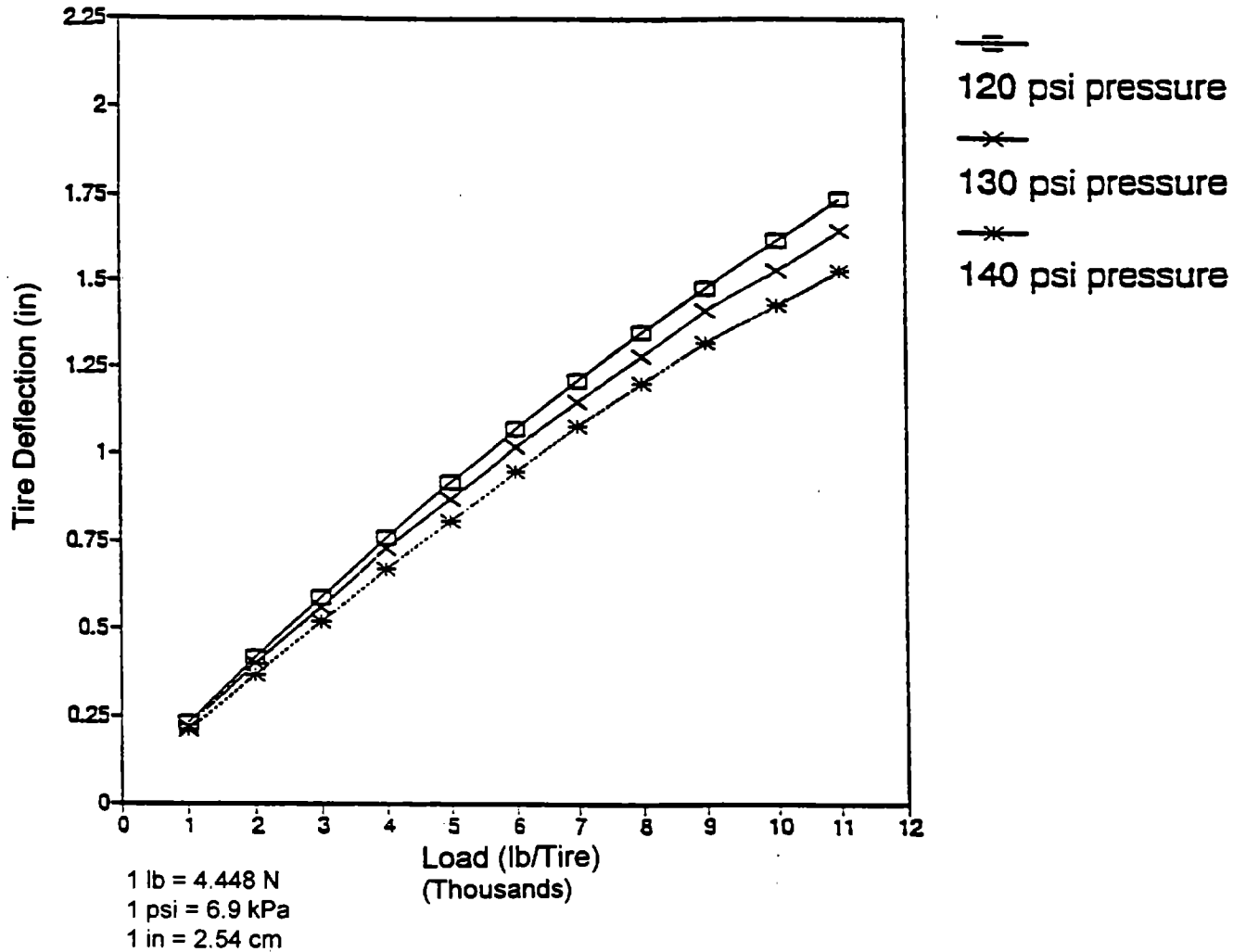
Figure 6-6. Load-deflection characteristics of the wide-base tire, 425/65R22.5, for inflation pressures of 827, 896, and 965 kPa (120, 130, and 140 psi).

Tire load-deflection characteristics determine tire stiffness (or tire spring constant), defined as the derivative of load with respect to deflection, which has a strong effect on the level of dynamic tire forces. Using linear regression, the following equations were derived for the spring constants of the three test tires as functions of inflation pressure:

$$k_{t\,SR} = 0.71\ P_t + 345 \tag{6-4}$$
$$k_{t\,LP} = 0.84\ P_t + 281 \tag{6-5}$$
$$k_{t\,WB} = 1.03\ P_t + 313 \tag{6-6}$$

where k_t is in kN/m.

146

6.2.3 Contact Pressure Distribution

The stress distribution at the tire-pavement interface was measured. The force-pin method measures the stress distribution across the tire width and registers the average stress at each individual rib. Dual tires have five ribs, while wide-base tires have six ribs. The results of the measurements are listed in tables 6-8, 6-9, and 6-10. The plots of the data are shown in figures 6-7 through 6-12.

Table 6-8. Stress-distribution data for the standard radial tire, 11R22.5.

Load (lb)	Tire Pressure (psi)	Tire Rib				
		1	2	3	4	5
		Contact Stress (psi)				
1,750	70	29	116	134	118	33
	85	22	124	148	129	21
	100	18	135	163	142	21
2,500	70	63	115	129	111	65
	85	57	141	157	140	67
	100	46	140	163	144	55
4,250	80	100	120	139	121	106
	95	99	133	153	134	105
	110	98	152	173	151	102
5,500	80	121	129	148	129	136
	95	121	143	163	143	133
	110	117	161	184	162	135

1 lb = 0.454 kg
1 psi = 6.9 kPa

147

Table 6-9. Stress-distribution data for the low-profile tire, 295/75R22.5.

Load (lb)	Tire Pressure (psi)	Tire Rib				
		1	2	3	4	5
		Contact Stress (psi)				
1,750	70	32	127	140	125	37
	85	22	139	155	139	26
	100	20	150	170	151	21
2,500	70	60	126	142	125	71
	85	57	141	157	140	67
	100	53	154	172	155	62
4,250	80	104	134	152	131	110
	95	98	150	169	147	107
	110	98	167	188	165	104
5,500	80	124	130	150	128	127
	95	123	145	168	143	129
	110	123	168	191	166	129

1 lb = 0.454 kg
1 psi = 6.9 kPa

148

Table 6-10. Stress-distribution data for the wide-base tire, 425/65R22.5.

Load (lb)	Tire Pressure (psi)	Tire Rib					
		1	2	3	4		5
		Contact Stress (psi)					
1,750	70	66	111	162	137	167	54
	85	105	59	142	176	165	183
	100	51	164	191	184	194	44
2,500	70	104	149	170	159	169	95
	85	101	127	185	155	181	99
	100	97	181	202	189	203	88
4,250	80	117	132	185	161	176	115
	95	120	174	199	185	195	113
	110	119	10	217	205	214	105
5,500	80	134	153	210	185	199	128
	95	132	189	219	205	210	128
	110	133	141	243	177	229	126
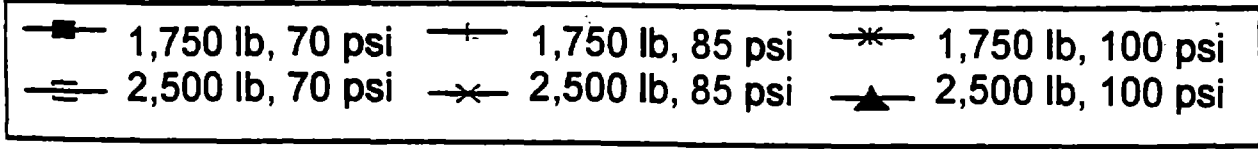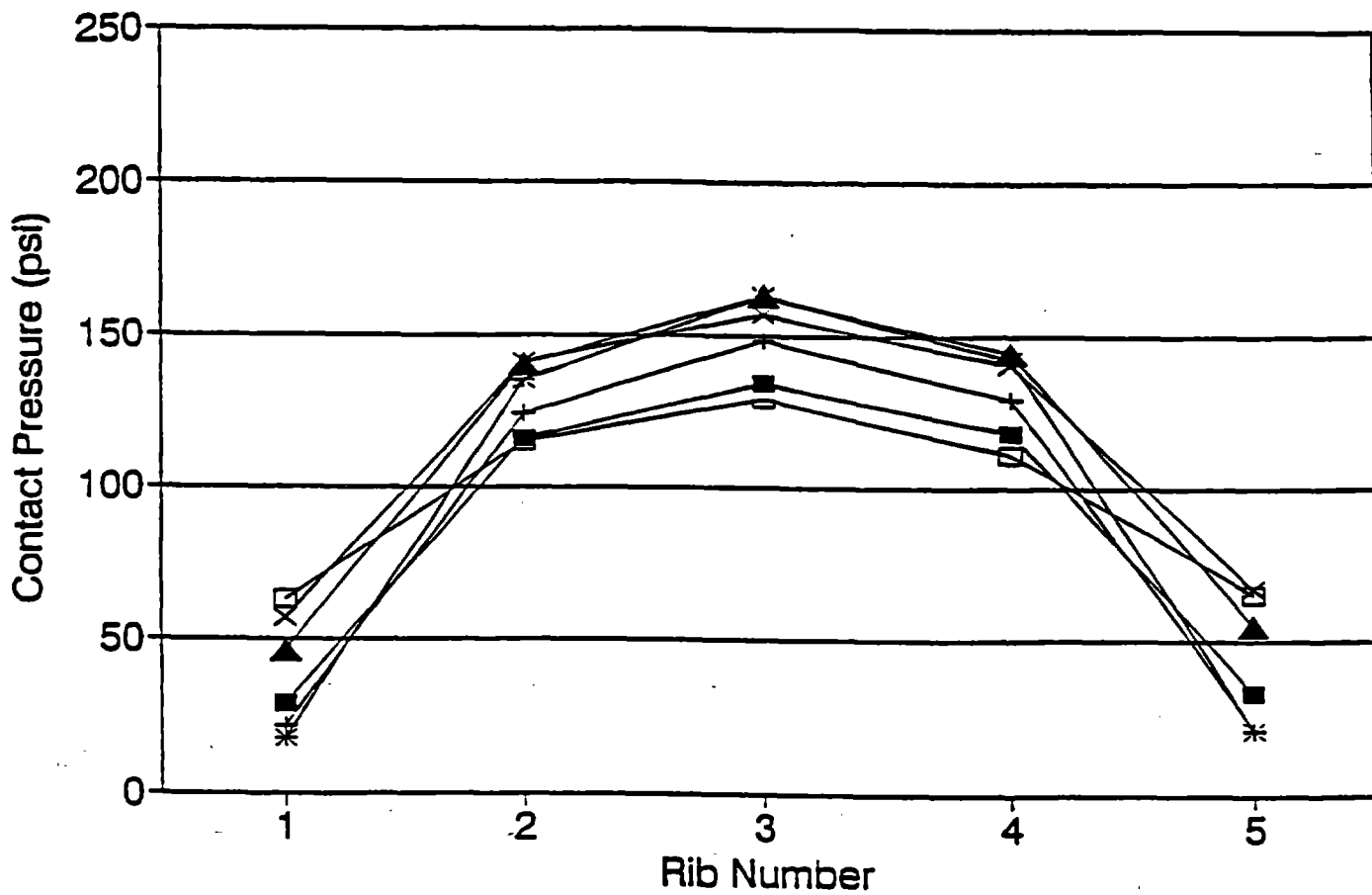
1 lb = 0.454 kg
1 psi = 6.9 kPa

Figure 6-7. Contact stress distribution for the standard radial tire, 11R22.5, under
7.79- and 11.1-kN (1,750- and 2,500-lb) tire loads.
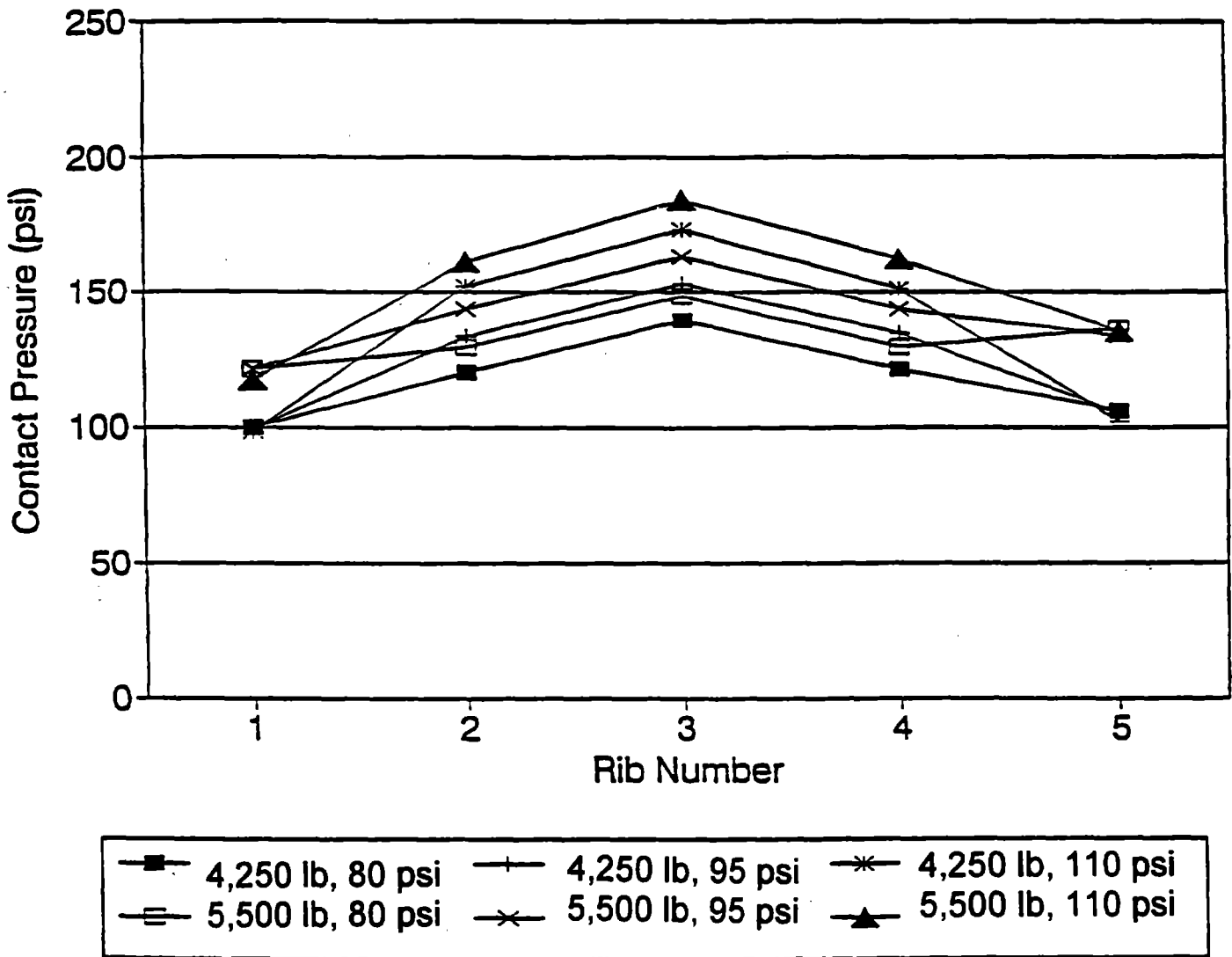
1 lb = 4.448 N
1 psi = 6.9 kPa

Figure 6-8. Contact stress distribution for the standard radial tire, 11R22.5, under 18.9- and 24.5-kN (4,250- and 5,500-lb) tire loads.
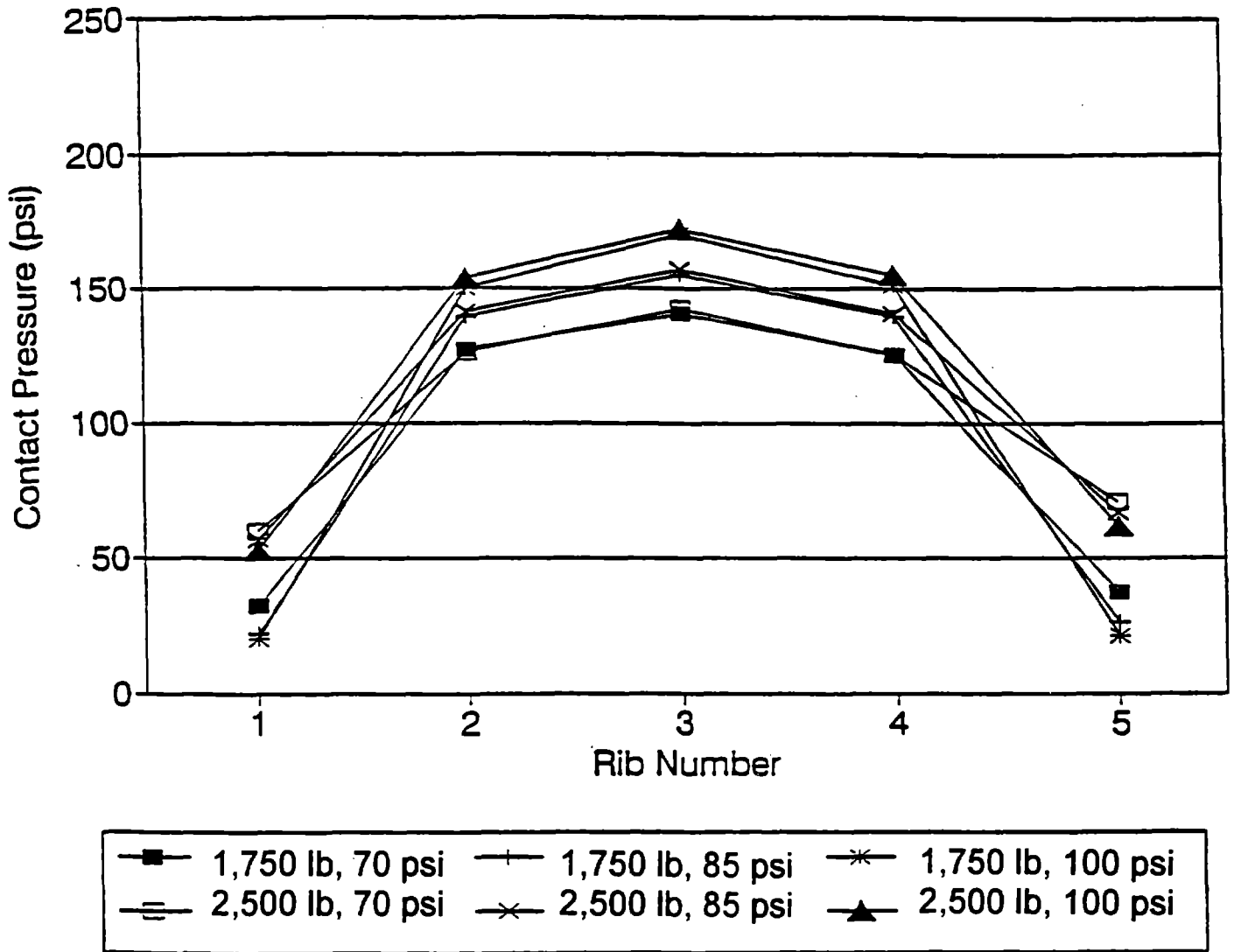
1 lb = 4.448 N
1 psi = 6.9 kPa

Figure 6-9. Contact stress distribution for the low-profile tire, 295/75R22.5, under
7.79- and 11.1-kN (1,750- and 2,500-lb) tire loads.
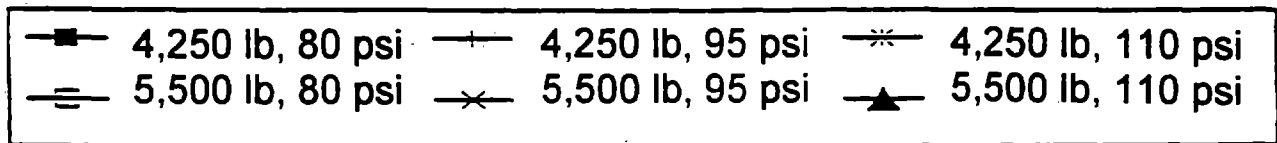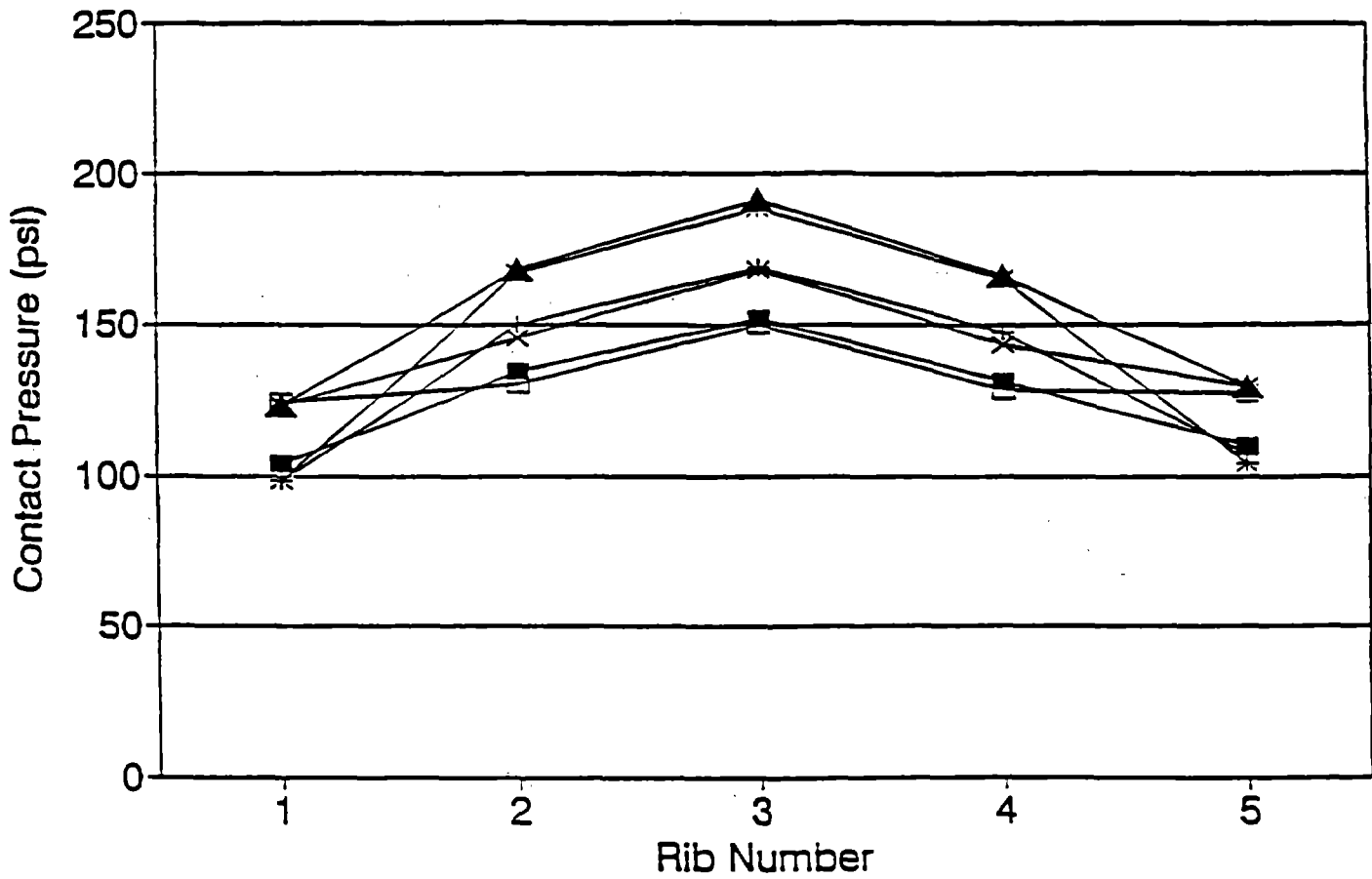
1 lb = 4.448 N
1 psi = 6.9 kPa

Figure 6-10. Contact stress distribution for the low-profile tire, 295/75R22.5, under 18.9- and 24.5-kN (4,250- and 5,500-lb) tire loads.

153
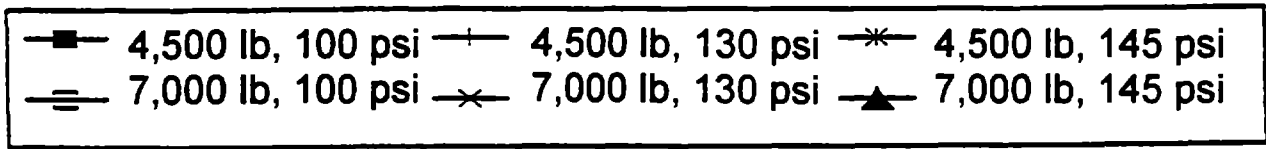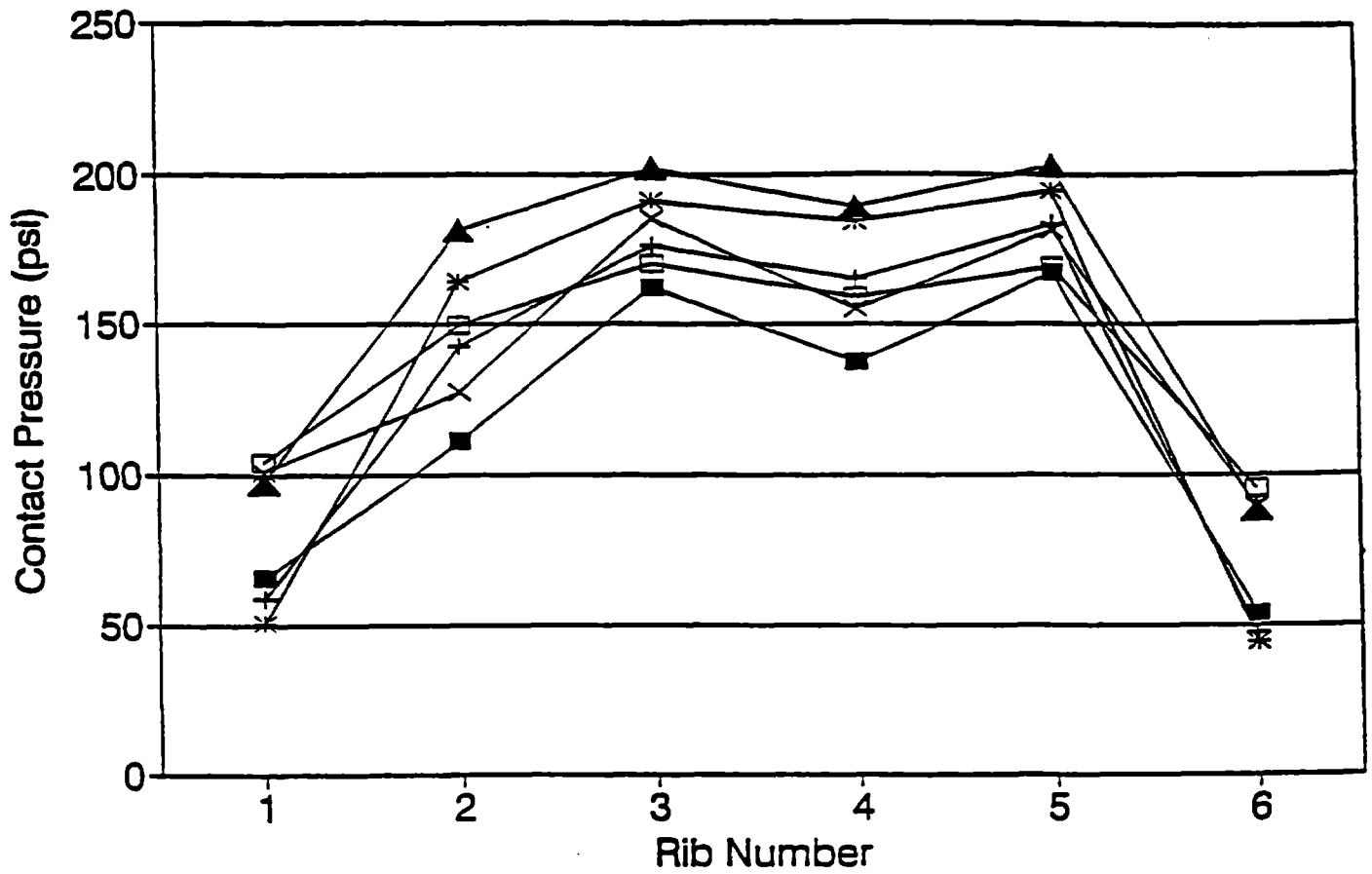
Figure 6-11. Contact stress distribution for the wide-base tire, 425/65R22.5, under 20.0- and 31.2-kN (4,500- and 7,000-lb) tire loads.

	8,500 lb, 100 psi	8,500 lb, 130 psi	8,500 lb, 145 psi
	9,750 lb, 115 psi	9,750 lb, 130 psi	9,750 lb, 145 psi
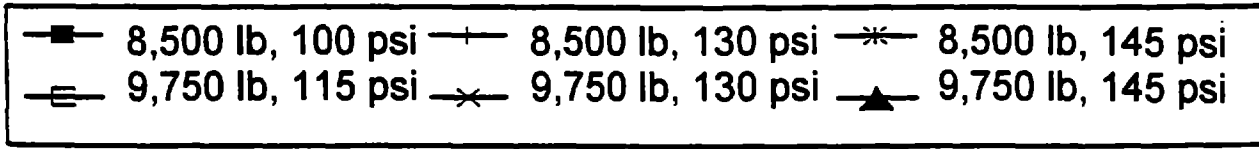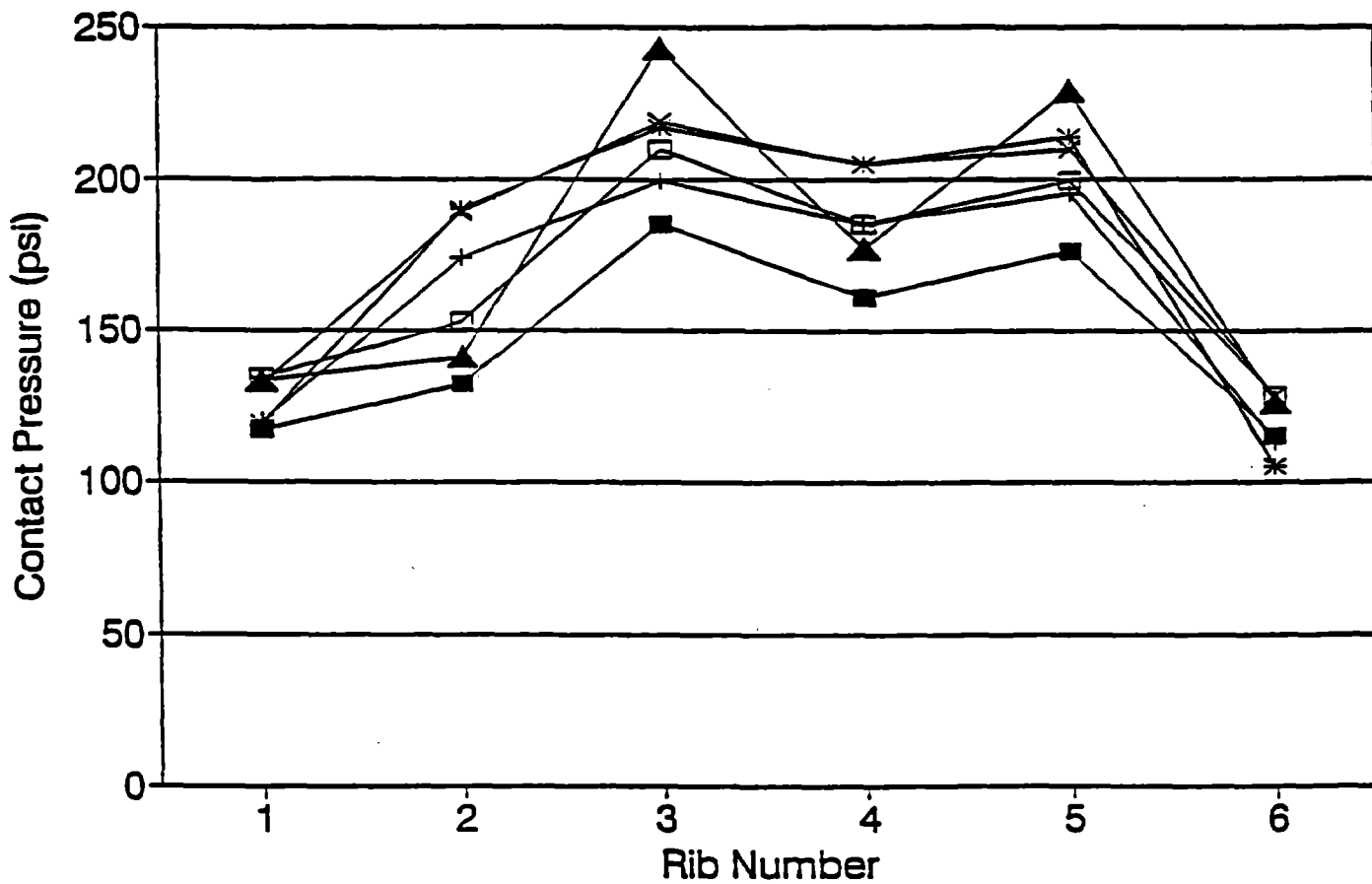
1 lb = 4.448 N
1 psi = 6.9 kPa

Figure 6-12. Contact stress distribution for the wide-base tire, 425/65R22.5, under 37.8- and 43.4-kN (8,500- and 9,750-lb) tire loads.

It can be seen from the plots that the maximum contact stress for both dual tires occurred at the center of the contact area. The maximum contact stress is about 60 to 70 percent higher than the inflation pressure. It can also be seen that the contact stress at the edges of the tires increases as the tire load increases. In the case of the wide-base tire, the maximum contact stress is also 60 to 70 percent higher than the inflation pressure; however, it covers a wider portion of the contact area (see figures 6-11 and 6-12). The edge contact stresses under the wide-base tire also increase when the tire load increases.

For comparison, figures 6-13, 6-14, and 6-15 show the contact stress data obtained from the Danish RTM, described in section 6.1.3, for a 12R22.5 dual tire, which is similar to the 11R22.5 tire tested in this study. The major difference between these plots and the plots shown in figures 6-7 and 6-8 is that the stresses are measured by the RTM at 11 points within the contact area, some of which are located near the edges of individual ribs, where the stress is considerably lower. These low-pressure points are not measured in the force-pin method. The magnitudes of the contact stresses measured by the force-pin method and the RTM method are very similar, except for the low-stress points.
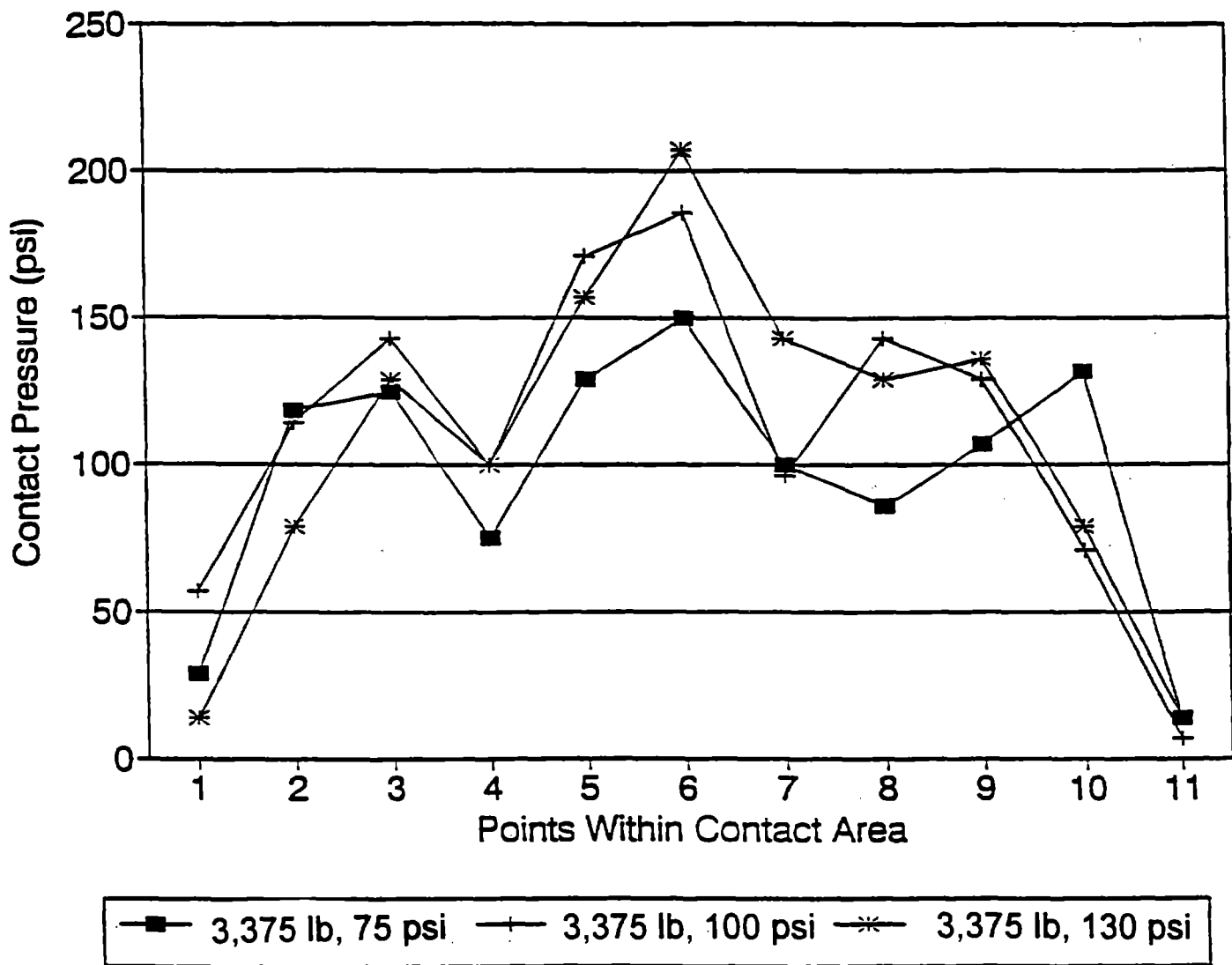
Figure 6-13. Contact stress distribution for a 12R22.5 tire measured by the RTM at 20 km/h (12.5 mi/h) under a vertical load of 15.0 kN (3,375 lb).

1 lb = 4.448 N
1 psi = 6.9 kPa
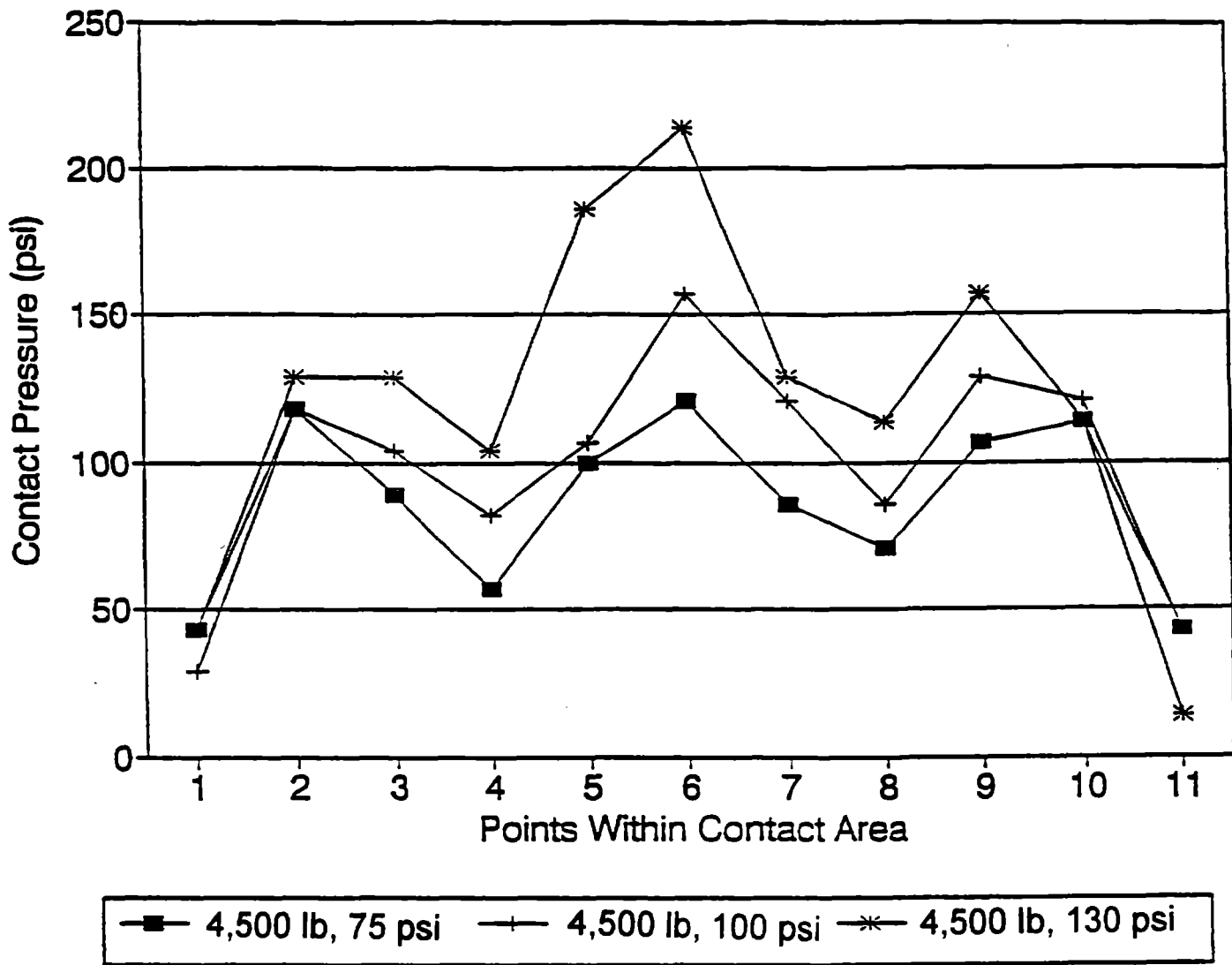
1 lb = 4.448 N
1 psi = 6.9 kPa

Figure 6-14. Contact stress distribution for a 12R22.5 tire measured by the RTM
at 20 km/h (12.5 mi/h) under a vertical load of 20.0 kN (4,500 lb).
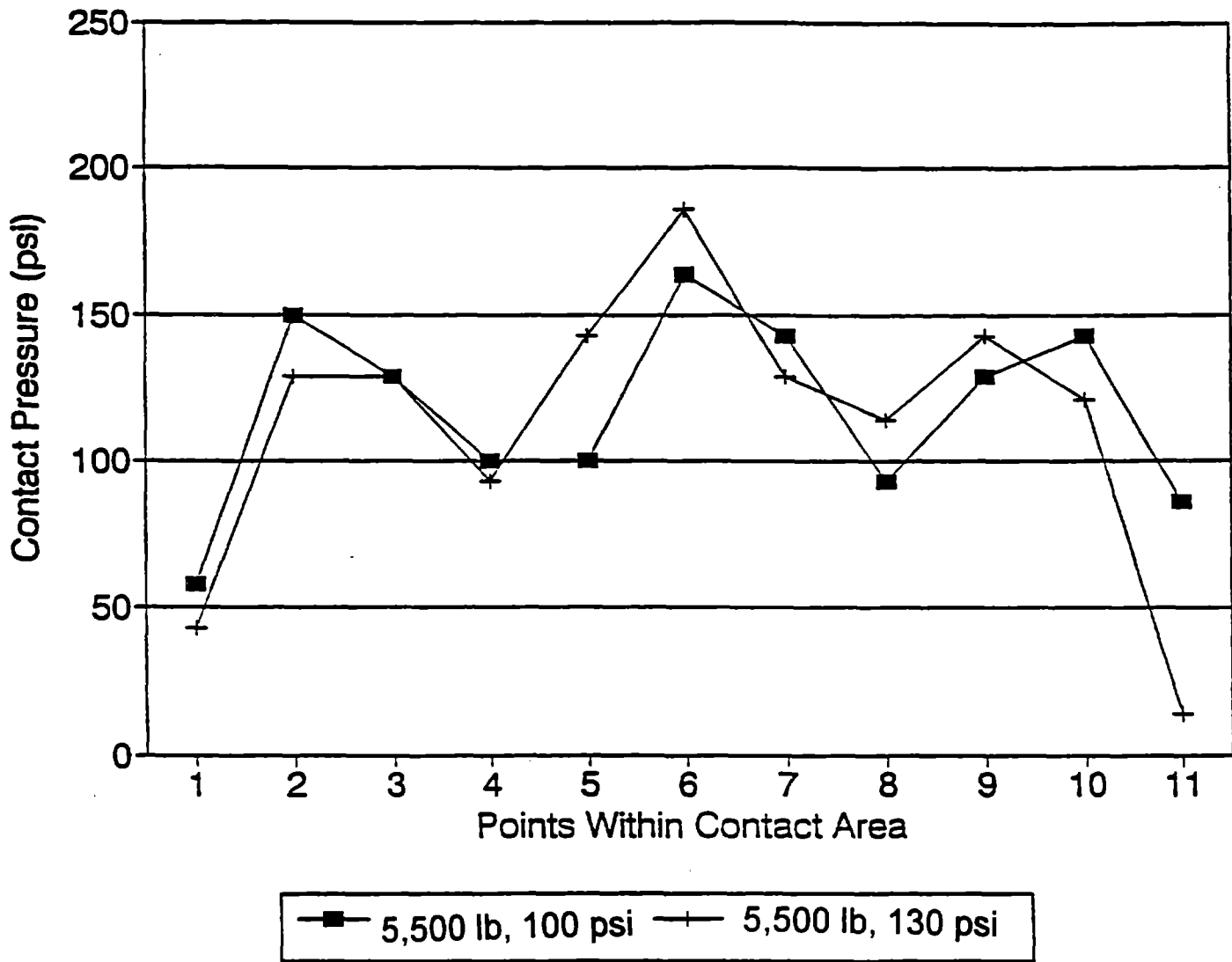
Figure 6-15. Contact stress distribution for a 12R22.5 tire measured by the RTM at 20 km/h (12.5 mi/h) under a vertical load of 24.5 kN (5,500 lb).

The contact stresses measured with the force-pin method for the wide-base tire were compared with the results of measurements obtained with the Finnish pressure-cells strip described in section 6.1.3. Figures 6-16, 6-17, and 6-18 present the data from the Finnish study collected with a wide-base tire at speeds of 5, 48, and 80 km/h (3, 30, and 50 mi/h), respectively. It can be seen from these plots that the effect of speed on contact stresses is very small. The distributions of the contact stresses across the tire width have similar shapes as those obtained with the force-pin method,

although the force-pin method measured higher maximum contact stresses than the pressure-cells strip.
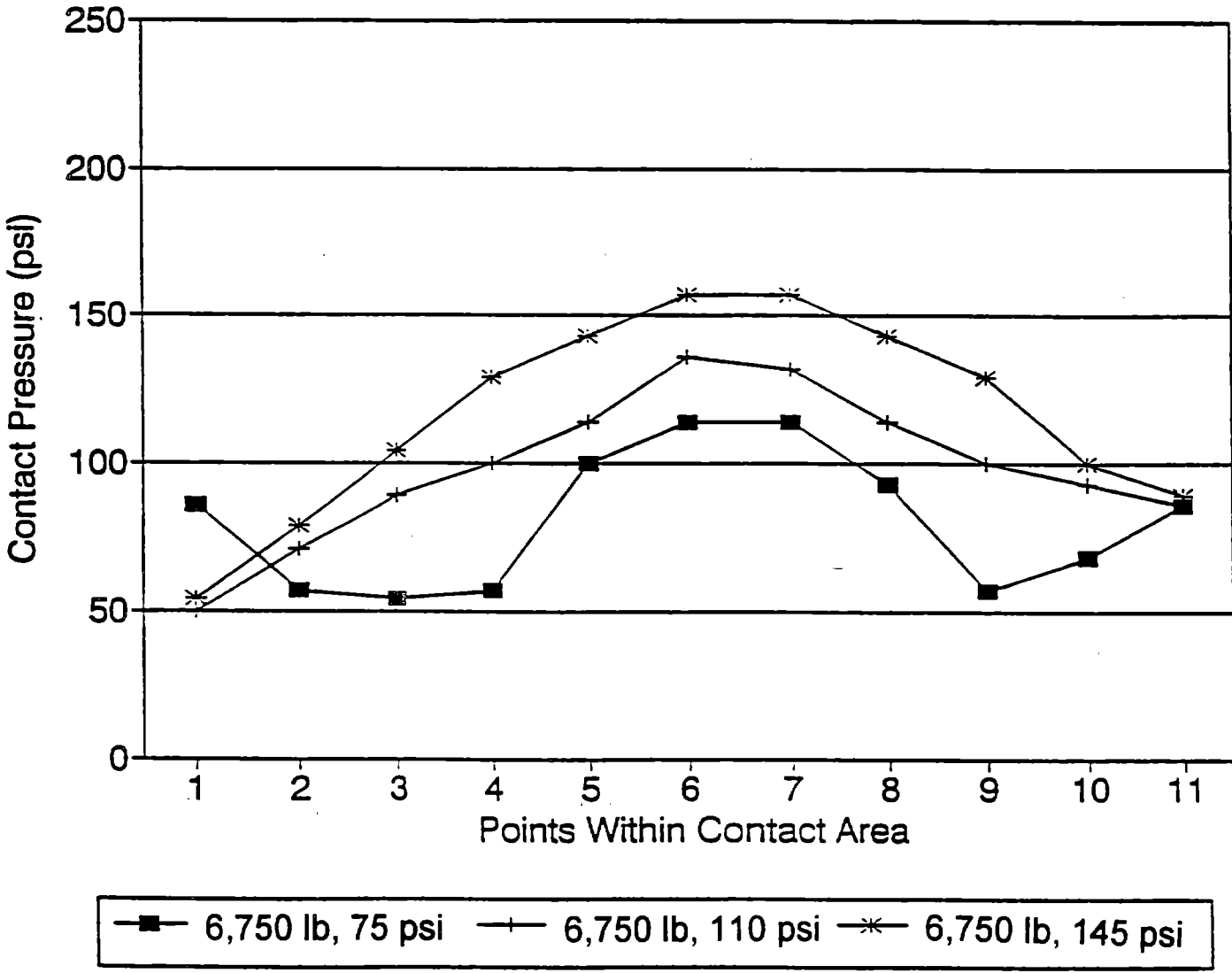
1 lb = 4.448 N
1 psi = 6.9 kPa

Figure 6-16. Contact stress distribution for a wide-base tire measured by the pressure-cells strip at 5 km/h (3 mi/h) under a vertical load of 30.0 kN (6,750 lb).
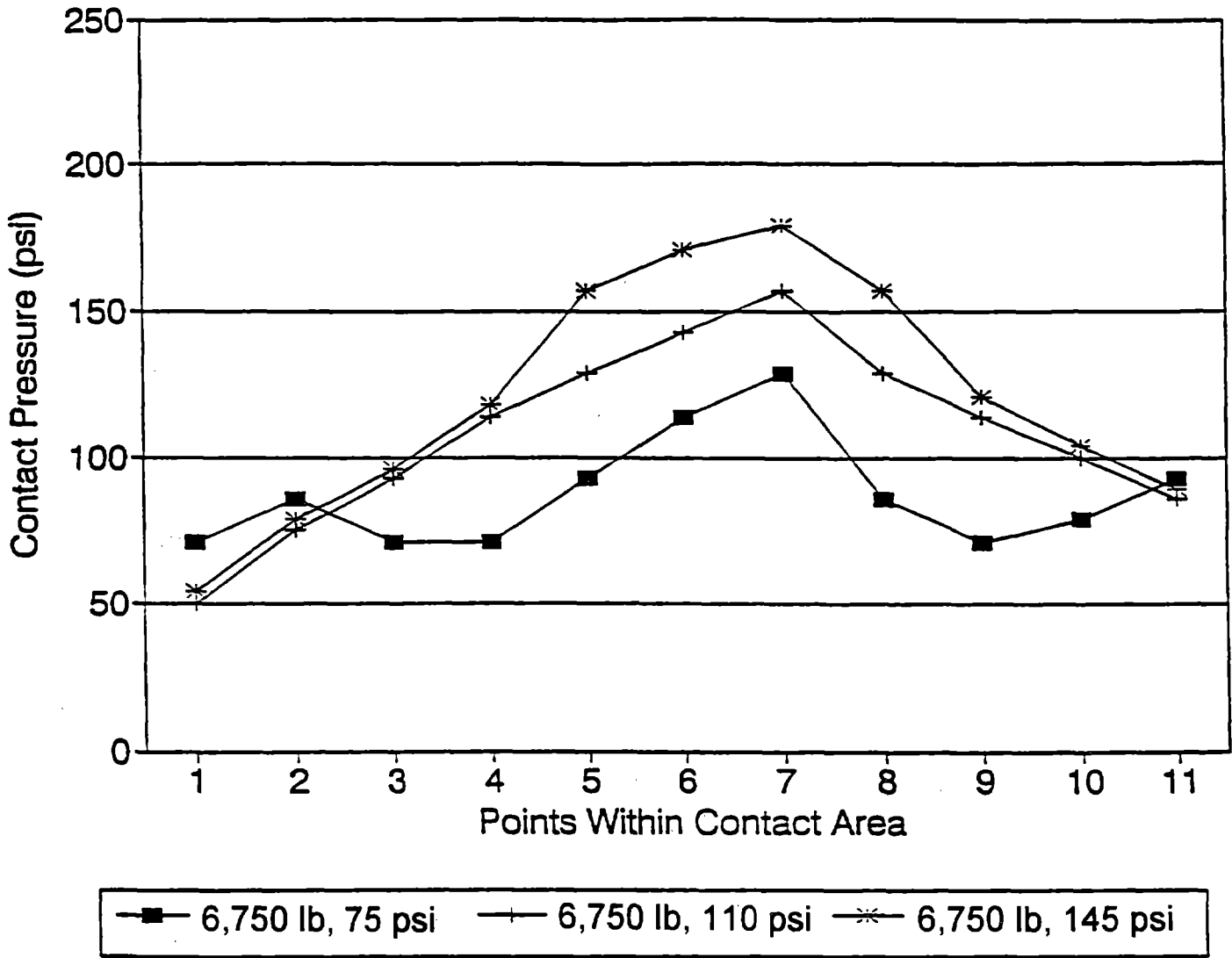
Figure 6-17. Contact stress distribution for a wide-base tire measured by the pressure-cells strip at 48 km/h (30 mi/h) under a vertical load of 30.0 kN (6,750 lb).
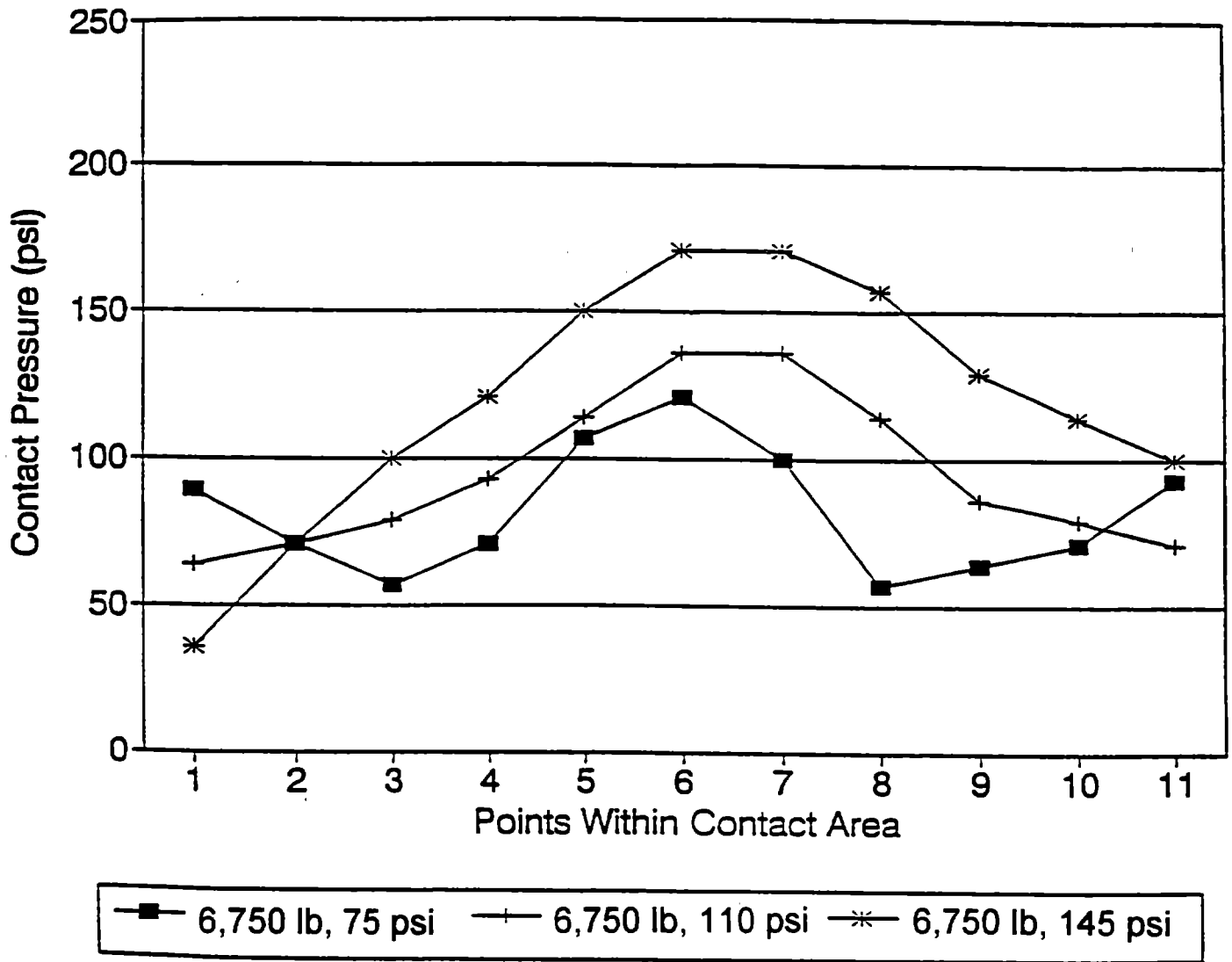
Figure 6-18. Contact stress distribution for a wide-base tire measured by the pressure-cells strip at 80 km/h (50 mi/h) under a vertical load of 30.0 kN (6,750 lb).

CHAPTER 7. TEST RESULTS

A complete listing or graphing of the test results is not possible because of the large number of tests and sensor measurements. This chapter will present plots of typical sensor measurements; compare the effects of load, speed, and roughness parameters; and briefly discuss the data processing required to summarize the test results.

7.1 DYNTRAC TESTS

There were several sets of tests performed with DYNTRAC, including changing load, tire pressure, tire type, vehicle speed, and road roughness. Both leaf-spring and air suspensions were tested with the same test vehicle.

7.1.1 Typical Sensor Measurements

The sensors used to measure the performance of the test vehicle are described in detail in chapter 2. Figures 7-1 through 7-5 are typical sensor measurements. These plots are for a high-roughness (IRI = 6.47 mm/m [410.4 in/mi]) Virginia road profile simulation. The speed of the simulation is 72 km/h (45 mi/h), and the payload on the vehicle is 35.2 kN. The sensors in the following figures are those associated with the left-rear actuator and left-rear axle of the test vehicle.

Figure 7-1 is the actuator displacement during the simulation. The high-roughness profile has displacements as high as 65 mm (2.56 in) occurring in less than 1 s. The actuator displacement shown from 26 to 29 s was artificially added during preprocessing of the road profile to ensure that the actuator returned to its original position. This type of preprocessing was done for all simulations.
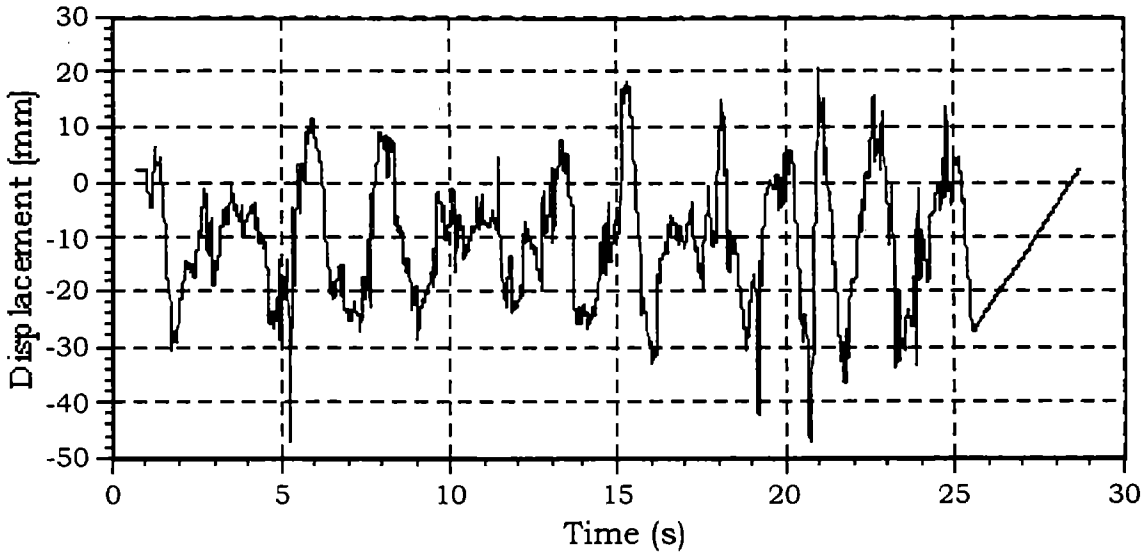
Figure 7-1. Left-rear actuator displacement.

Dynamic wheel forces exceed 70 kN in figure 7-2. It should be noted that a static measurement of the left-rear wheel force was 33.73 kN.
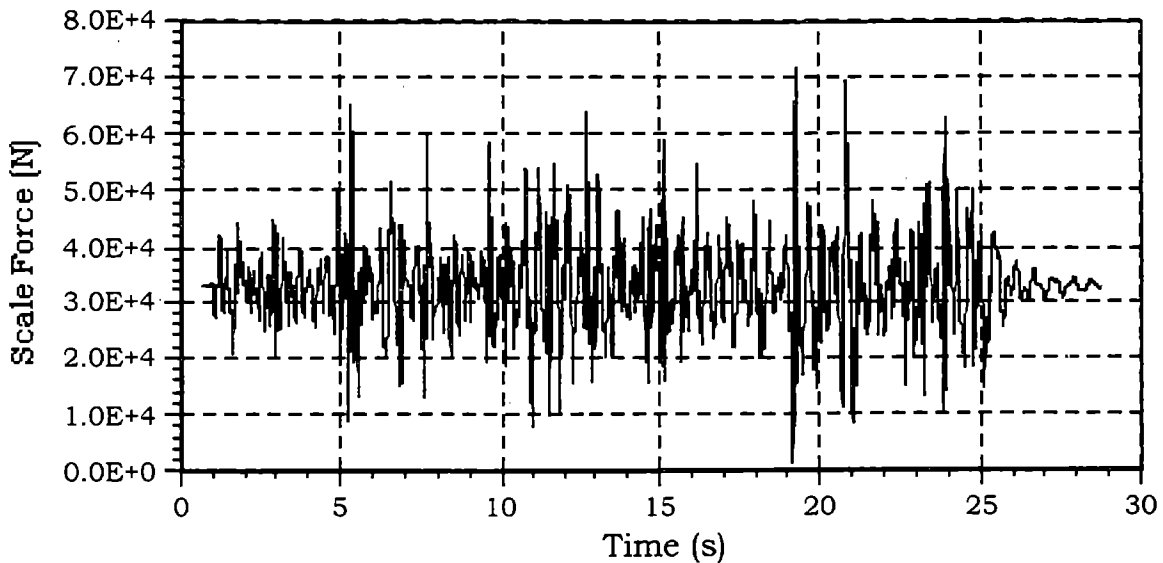
Figure 7-2. Left-rear scale force.

The change in distance between the vehicle axle and frame is shown in figure 7-3. The large deflection just after the 5-s mark corresponds to the large actuator displacement shown in figure 7-1, and also to one of the peak dynamic wheel forces

shown in figure 7-2. Suspension deflection was not measured during air suspension tests because of equipment malfunction.
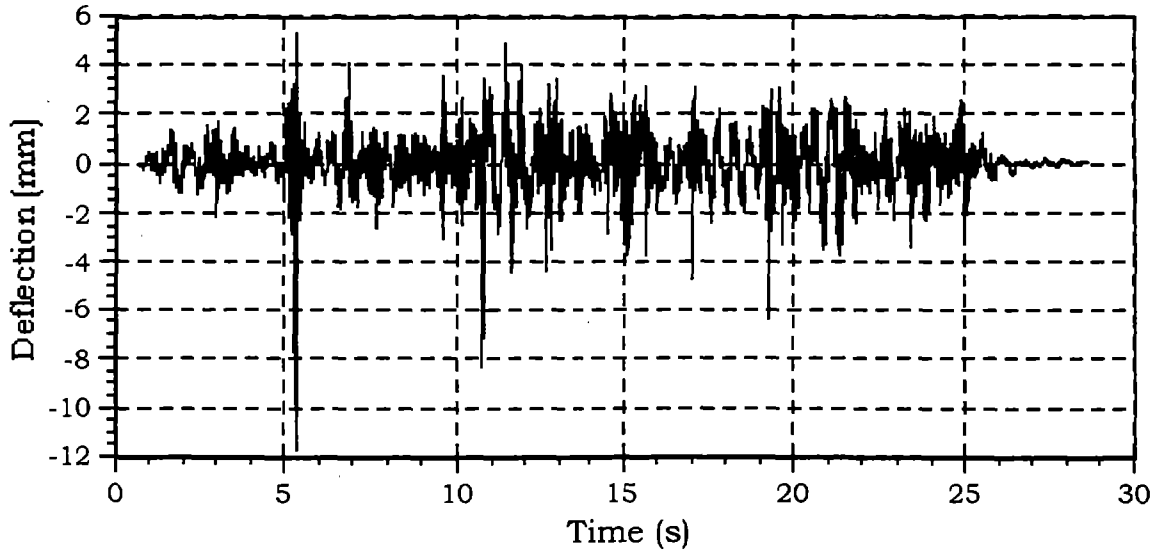
Figure 7-3. Left-rear suspension deflection.

Figures 7-4 and 7-5 show peak accelerations well above four times the gravitational acceleration. The axle accelerometer is mounted to the axle approximately 400 mm (15.76 in) from the center of the dual tires. The chassis accelerometer is located underneath the left-rear corner of the truck bed. Figure 7-4 shows axle acceleration peaks as large as 10 g. Figure 7-5 shows chassis acceleration peaks greater than 2 g.
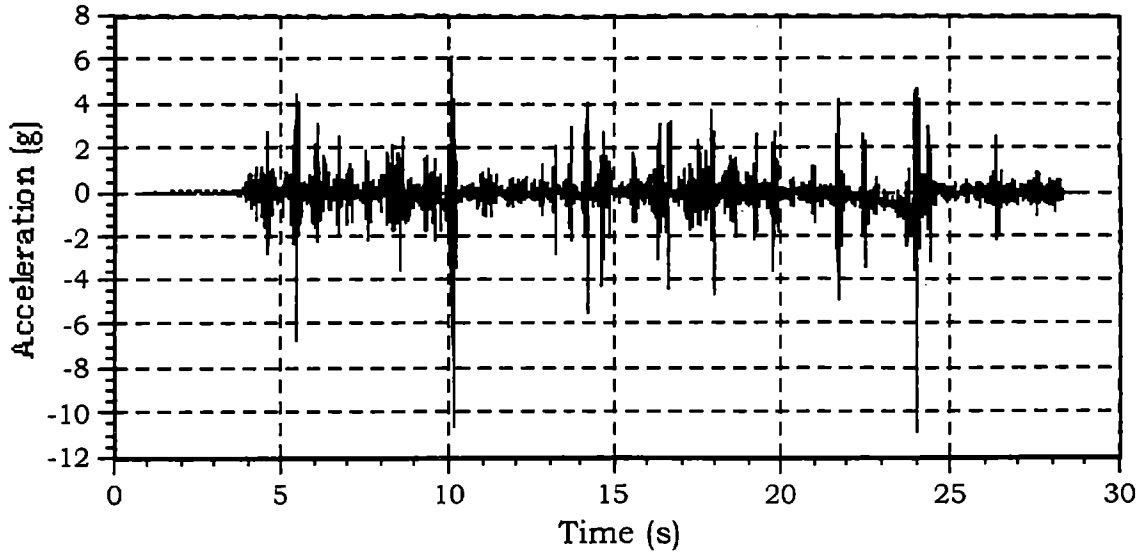
Figure 7-4. Left-rear axle acceleration.
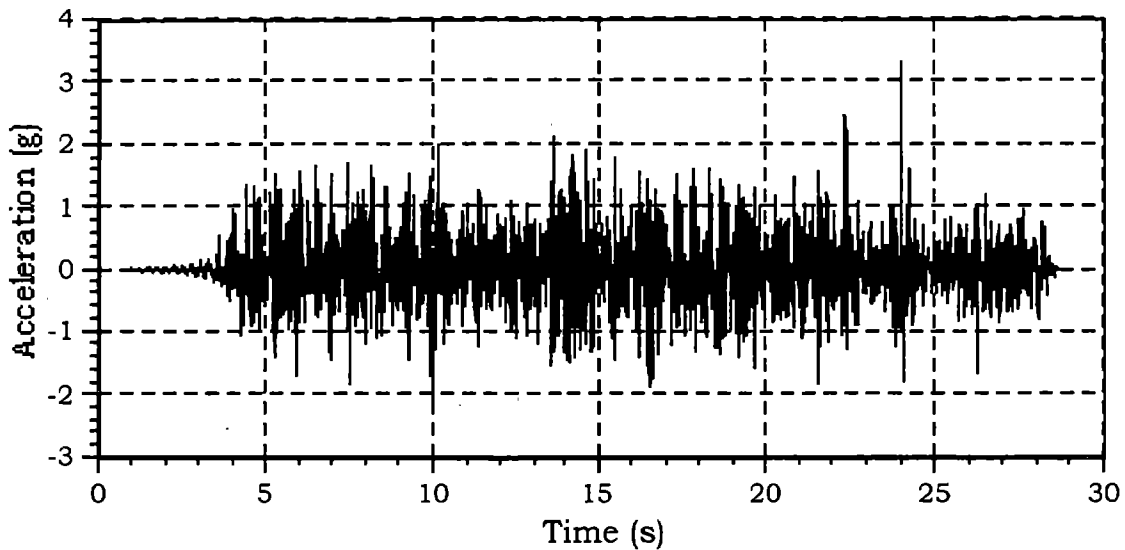
Figure 7-5. Left-rear chassis acceleration.

7.1.2 Processing

Acceleration data are digitally filtered using a 5th-order Butterworth filter with a corner frequency of 50 Hz. Digital filtering was applied both forwards and backwards to eliminate phase effects. Acceleration is determined by multiplying the accelerometer voltage by the factory-specified calibration factor. Data from the actuator displacement transducers and vehicle suspension displacement transducers are also processed using factory-specified calibration factors. Slopes and offsets obtained from static and

166

dynamic calibrations are used to process wheel scale and axle-strain gauge signals, in order to obtain force measurements.

Anti-aliasing filters were added to the DAQ system before the DYNTRAC tests on the steel suspension with Virginia profiles. This system filtered all channels at 50 Hz with analog Cauer filters that have a 70-dB rejection at 1.5 times the cutoff frequency.

7.1.3 Dynamic Wheel Forces Compared

Figures 7-6 through 7-14 present left-rear dynamic wheel forces in both the time and frequency domain. Variations of road roughness, vehicle speed, vehicle payload, and suspension type are individually examined while holding other variables constant.

7.1.3.1 High and Low Roughness Profiles

Figures 7-6 and 7-7 present vehicle response during simulations of low- and high-roughness Virginia road profiles. The low-roughness profile IRI is 1.1 mm/m (69.7 in/m), while the high-roughness profile IRI is 5.3 mm/m (336.0 in/m). Vehicle speed is 72 km/h (45 mi/h), and vehicle load is 35.2 kN. In the time domain, it is obvious that the high-roughness road results in higher magnitude dynamic wheel forces. This is also evident in the frequency domain.
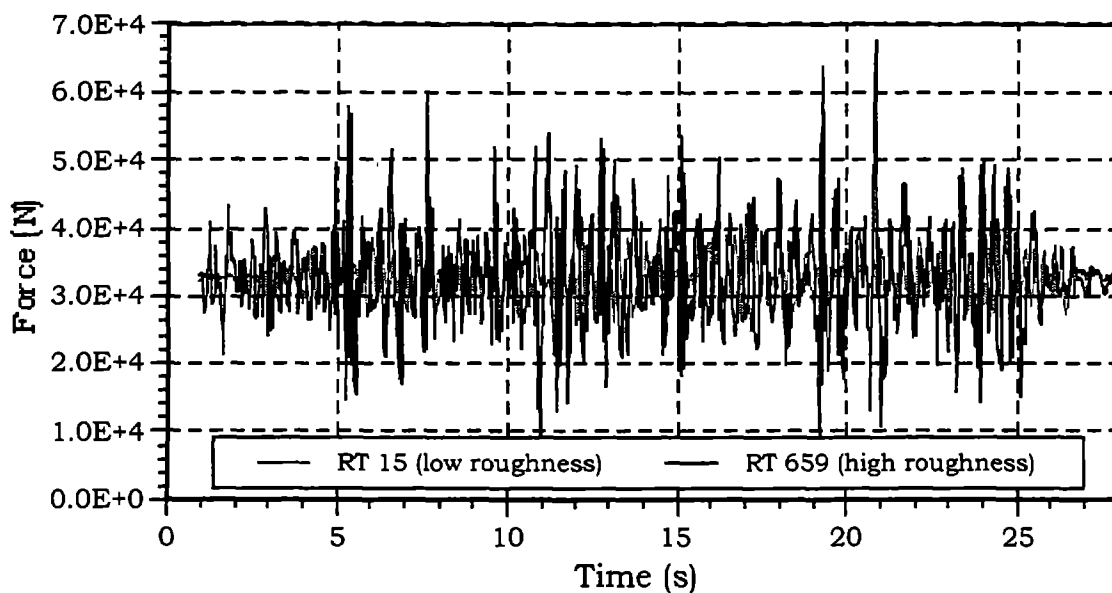
Figure 7-6. Left-rear wheel force during high- and low-roughness tests.
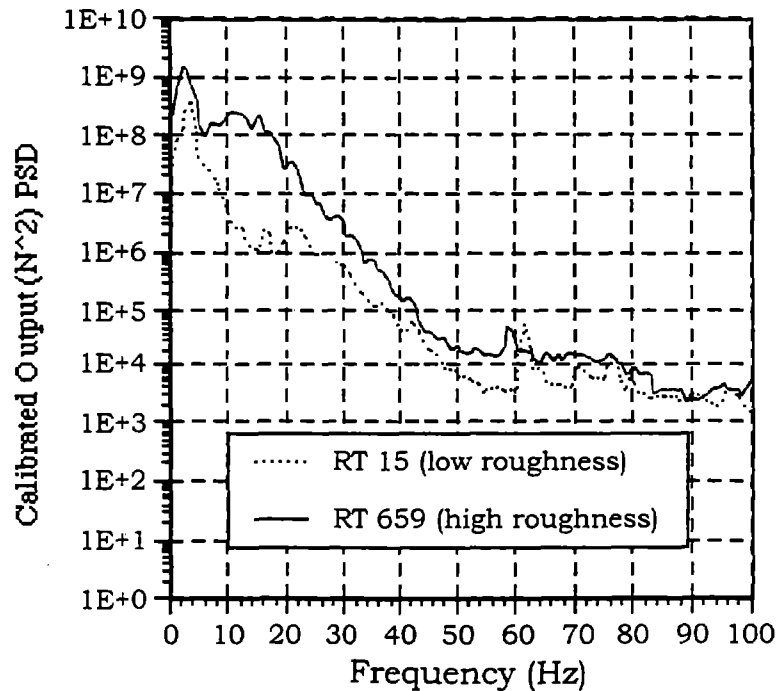
Figure 7-7. Power spectrum of left-rear wheel forces from low- and high-roughness tests.

7.1.3.2 Low and High Speeds

The high-roughness Virginia road profile with a vehicle load of 35.2 kN is used in figures 7-8 and 7-9 to demonstrate the effects of speed. The x axis of the plot is distance instead of time, so that the dynamic forces will match similar profile features. Note that figure 7-1 is a plot of the same profile at 72 km/h (45 mi/h). The peak forces in figure 7-8 correspond to the large changes in elevation shown in figure 7-1. Amplitude of low-frequency forces are similar for these two speeds, as shown in figure 7-9. The power spectrum of the wheel forces shows an increase in the 7- to 22-Hz range for the 88-km/h (55-mi/h) test.

168
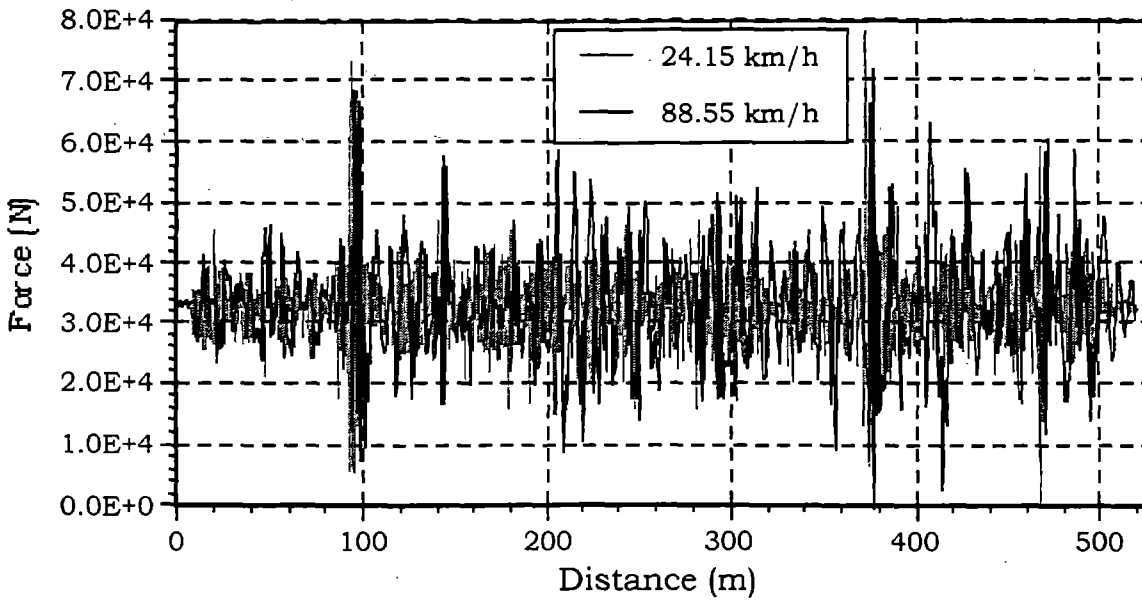
Figure 7-8. Left-rear wheel force from 24- and 48-km/h tests.
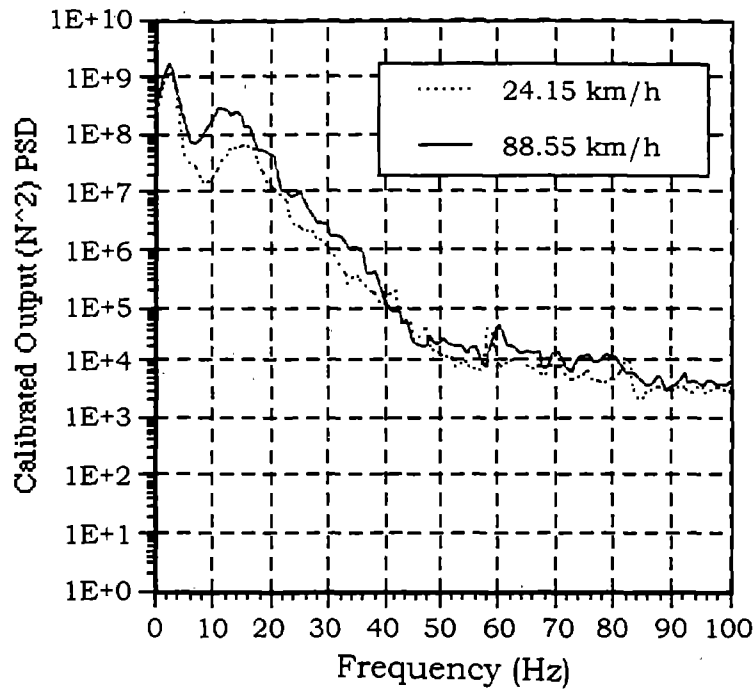
**Figure 7-9. Power spectrum of left-rear wheel force at
24 and 48 km/h.**

7.1.3.3 Empty and Fully Loaded

The previous plots presented data for the leaf-spring or steel suspension

configuration. Figures 7-10 and 7-11 present data for the air-suspension configuration.

169

The high-roughness Pennsylvania road profile at 88 km/h (55 mi/h) was used as the simulation input. The two payload configurations were empty and full (61.6 kN). The forces shown in figure 7-10 are offset, so their mean forces coincide. In several instances, the dynamic forces of the fully loaded simulation were more than 10 kN larger than those from the empty vehicle simulation. The figure 7-11 power spectrums of these data reveal that the 61.6-kN payload shifts the chassis heave frequency downward from about 3 Hz to about 2 Hz.
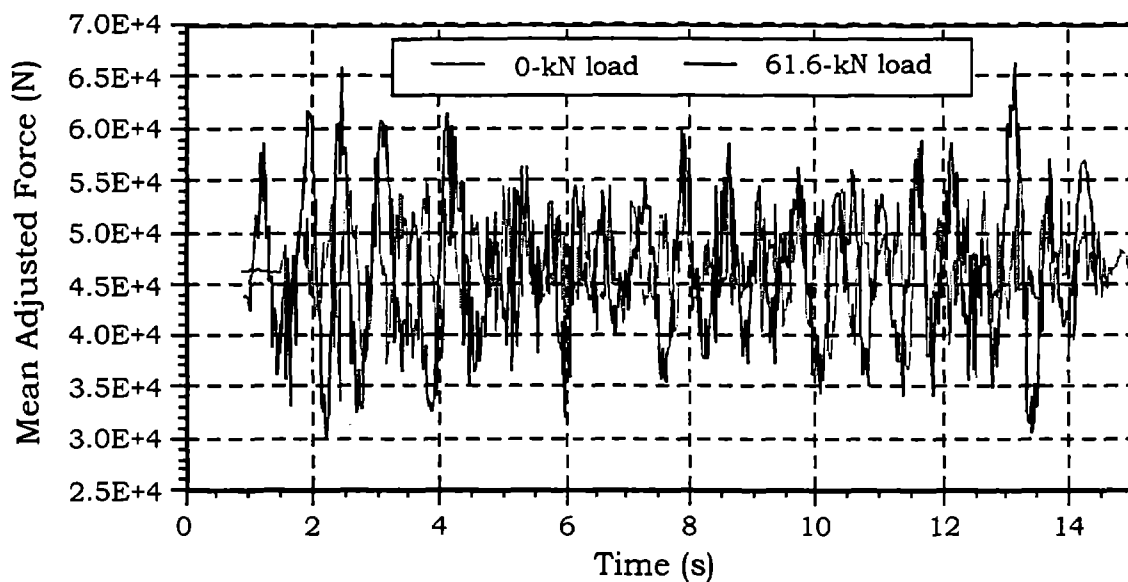
Figure 7-10. Mean adjusted left-rear wheel force at empty and fully loaded configurations.
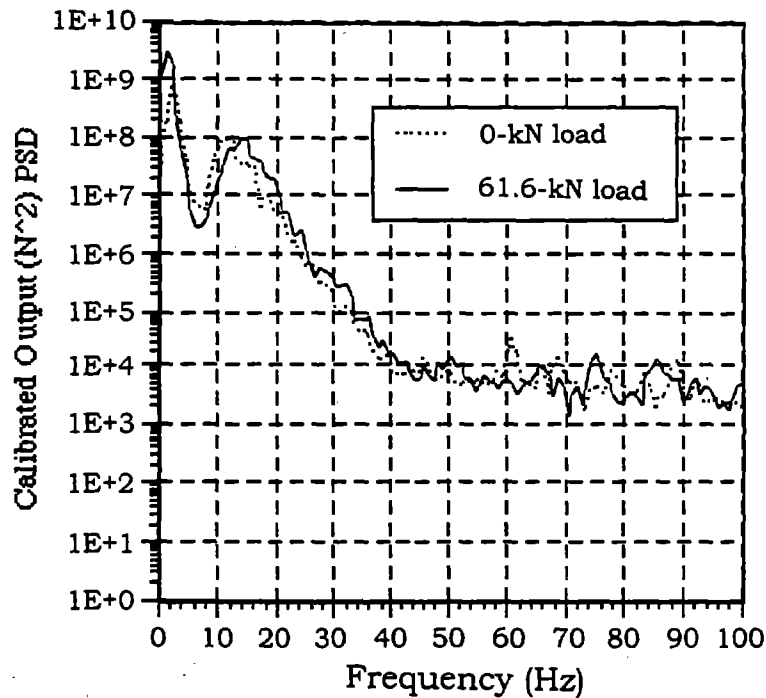
Figure 7-11. Power spectrum of left-rear wheel forces (empty and fully loaded)

7.1.3.4 Leaf Spring and Air Suspension

The effects of air and steel suspensions on dynamic wheel forces are demonstrated in simulations using the high-roughness Virginia road profile at 72 km/h (45 mi/h) with a payload of 35.2 kN. Peak forces in figure 7-12 are higher for steel suspension than for air suspension. In the 5-s snapshot of dynamic forces in figure 7-13, the two suspensions have different responses in both magnitude and phase. In figure 7-14, the air suspension has a slightly higher frequency response in the low frequencies (0 to 3 Hz), then drops below the steel suspension's response.

Figures 7-12 and 7-14 demonstrate that:

- Air suspension did not significantly reduce the highest peaks (amplitude of the 2-Hz frequency response).

- Air suspension significantly reduced wheel forces in the 4- to 10-Hz frequency range.

- Air suspension shifted the chassis heave frequency slightly downward, from about 2.5 Hz to about 2 Hz.

- Air suspension did not significantly reduce force amplitudes in the neighborhood of the wheel heave frequency (10 to 14 Hz).
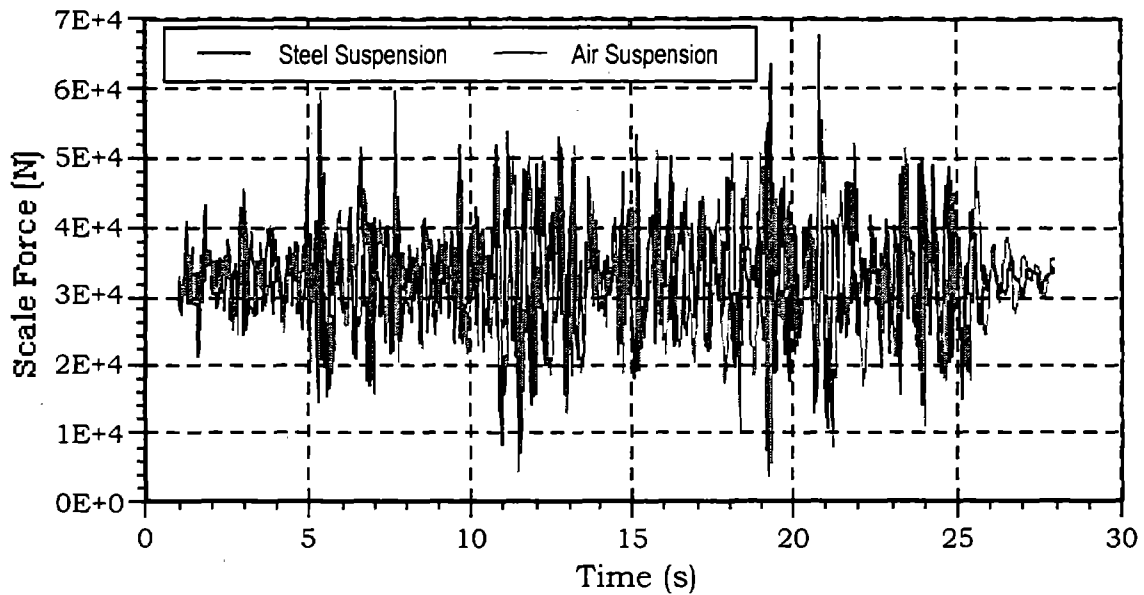
Figure 7-12. Left-rear wheel force for air and steel suspensions.
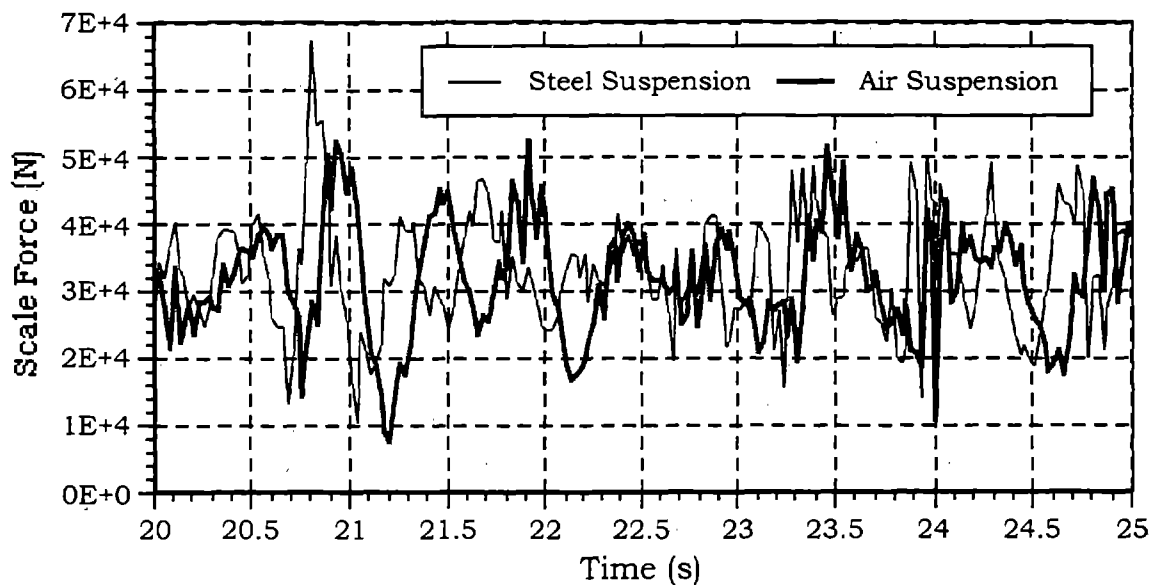
Figure 7-13. Five-second zoom of left-rear wheel force for air and steel suspensions.
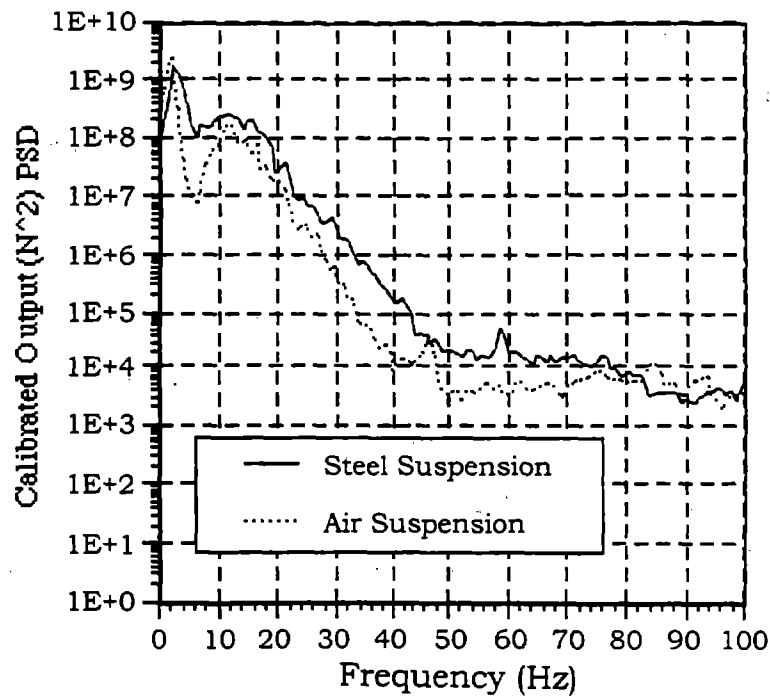
Figure 7-14. Power spectrum of left-rear wheel force for air and steel suspensions.

7.1.4 Graphical Summary of Test Results

Figures 7-15 through 7-22 present DLC's that were calculated from DYNTRAC tests. A DLC is plotted as a function of the variations in load, speed, and roughness. Five data points are missing from the plots because the test was aborted because of equipment or safety concerns or because the data file became corrupted before archiving was accomplished. The missing data points were:

- Figure 7-16, 35.2-kN payload, Pennsylvania medium roughness, 48 km/h (30 mi/h).

- Figure 7-17, 61.6-kN payload, Pennsylvania high roughness, 48 km/h (30 mi/h).

- Figures 7-19 and 7-20, 17.6-kN payload, Virginia high roughness, 88 km/h (55 mi/h).

- Figures 7-19 and 7-20, 35.2-kN payload, Virginia high roughness, 48 km/h (30 mi/h).

- Figures 7-19 and 7-20, 35.2-kN payload, Virginia high roughness, 88 km/h (55 mi/h).

These graphs show that the DLC's increase with speed and road roughness. Also, in some of the figures, the DLC's appear to be inversely proportional to payload. Since a DLC is equal to the standard deviation of the dynamic wheel force divided by the mean wheel force, the DLC is not sensitive to the change in magnitude of forces due to different payloads. Figure 7-23 is a plot of DLC force, which is derived from both DLC and mean force.

$$DLC\,Force = \overline{F} \cdot (1 + DLC) \tag{7-1}$$

where $\overline{F}$ is the meandynamic wheel force.

The trends with respect to speed and road roughness are still present but are not as profound because of the introduction of the mean force. The effects of test variables on DLC and pavement damage are discussed in detail in the next chapter.
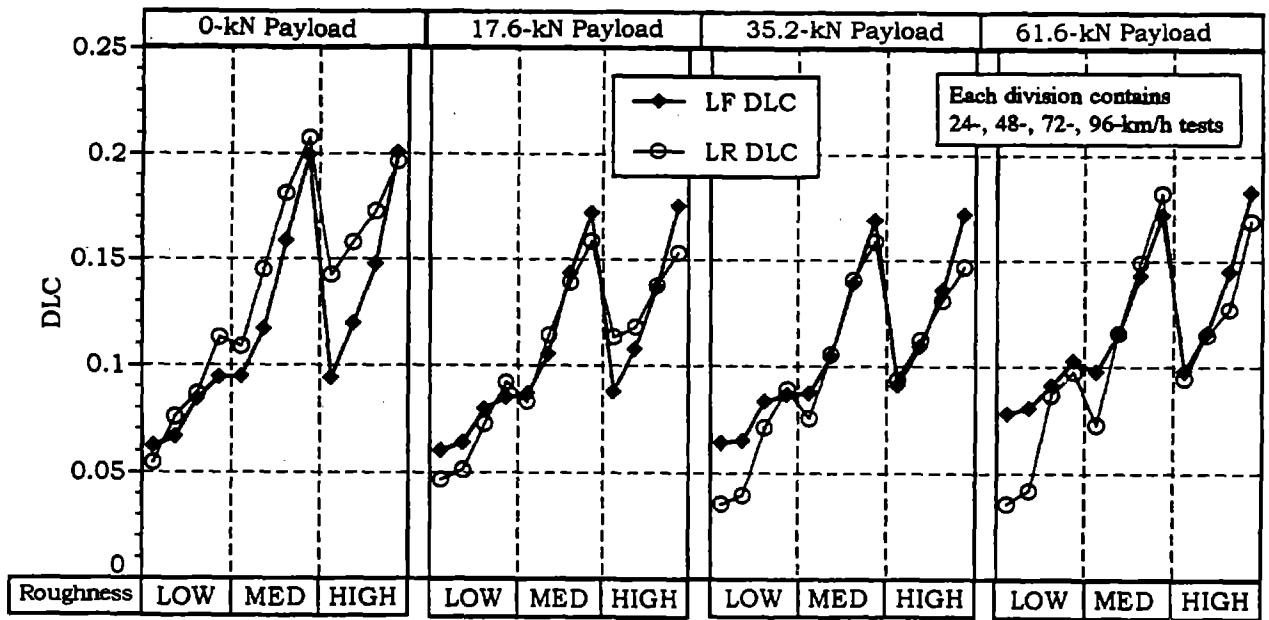
Figure 7-15. DLC from DYNTRAC tests for steel suspension, standard tires, and Pennsylvania profiles.
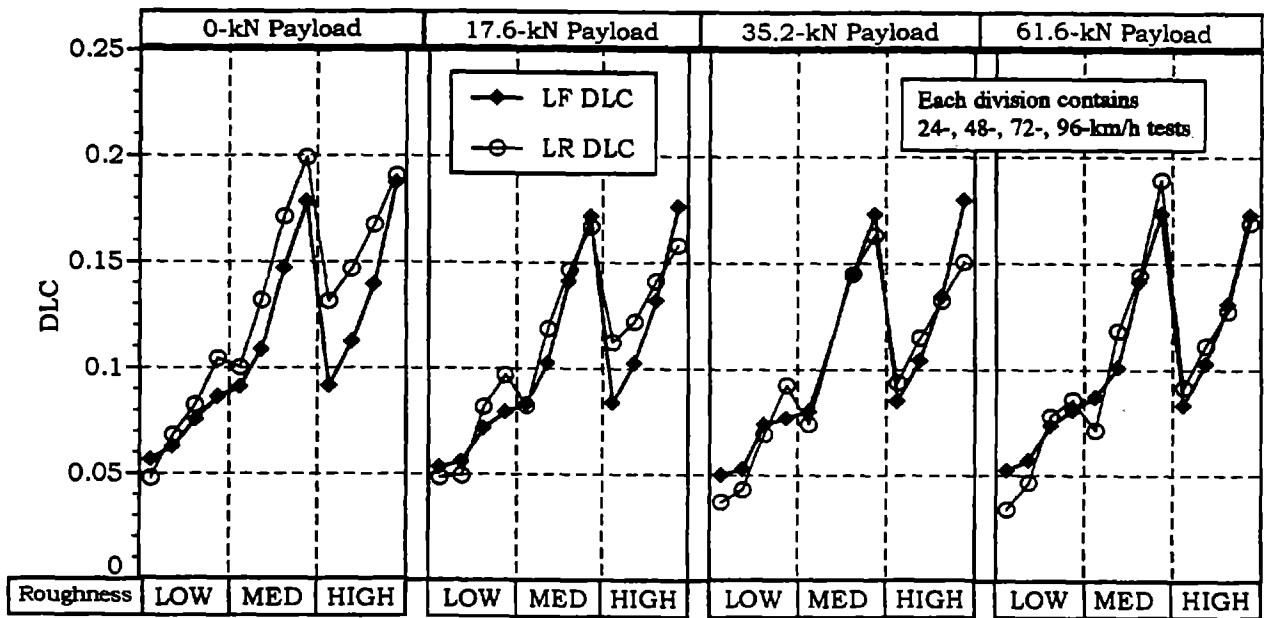
Figure 7-16. DLC from DYNTRAC tests for steel suspension, low-profile tires, Pennsylvania profiles.

175
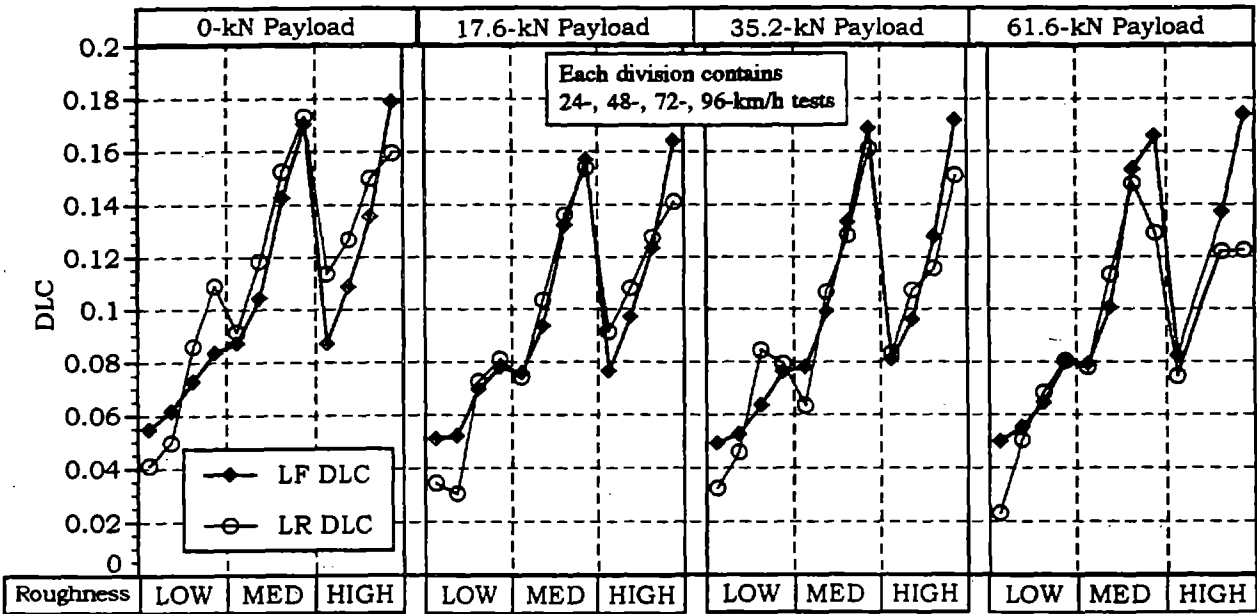
Figure 7-17. DLC from DYNTRAC tests for steel suspension, wide-base tires, Pennsylvania profiles.
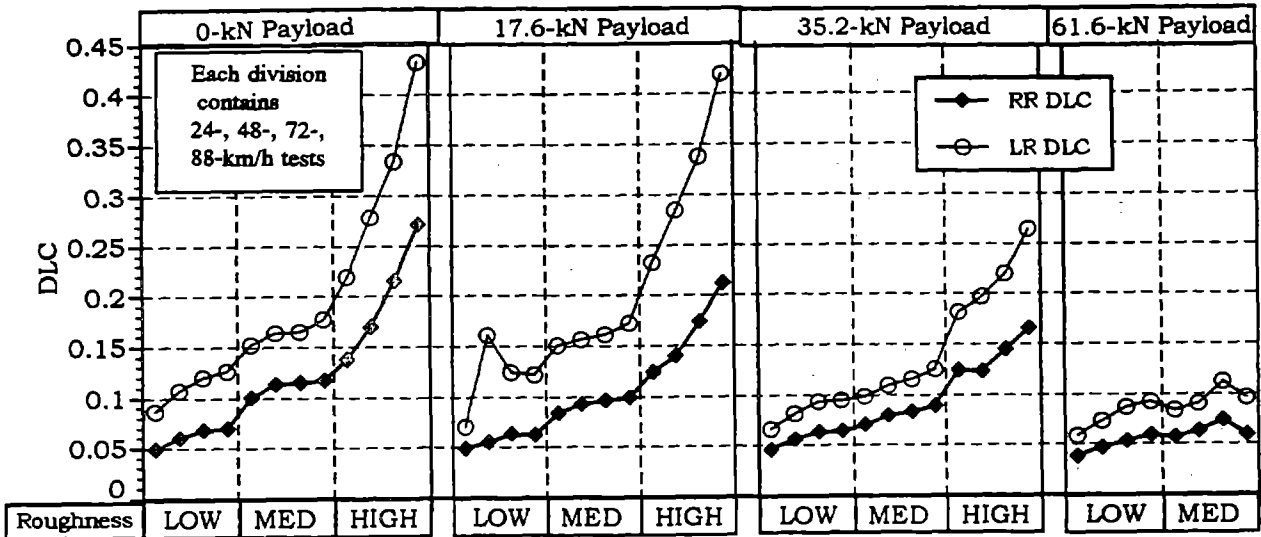
Figure 7-18. DLC from DYNTRAC tests for steel suspension, standard tires, Virginia profiles.

176
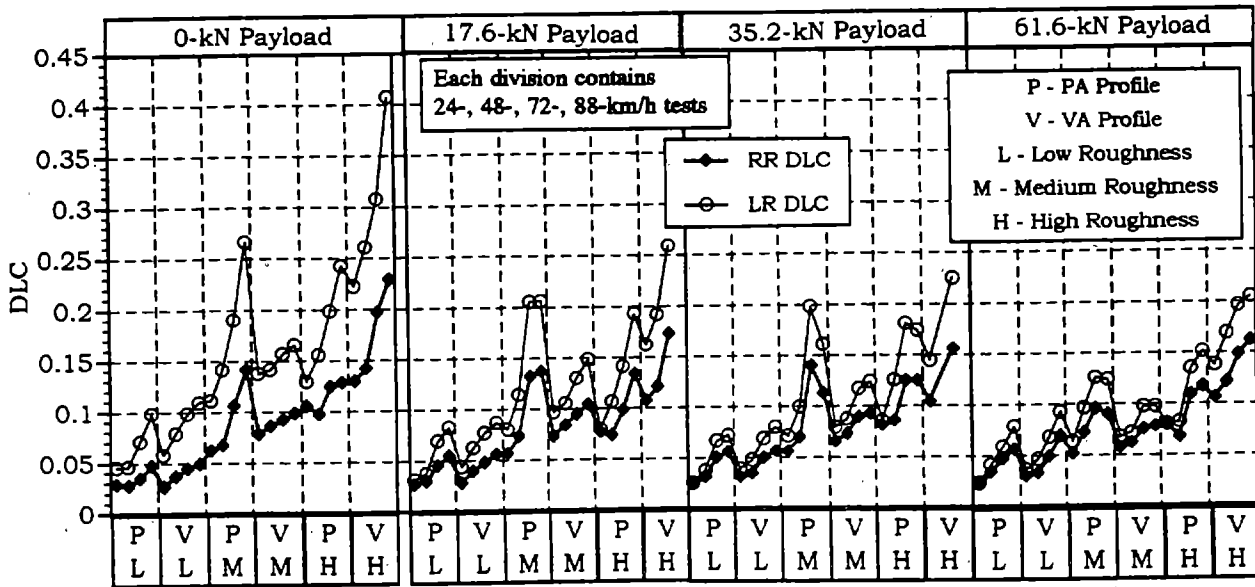
Figure 7-19. DLC from DYNTRAC tests for air suspension, standard tires, rear wheels.
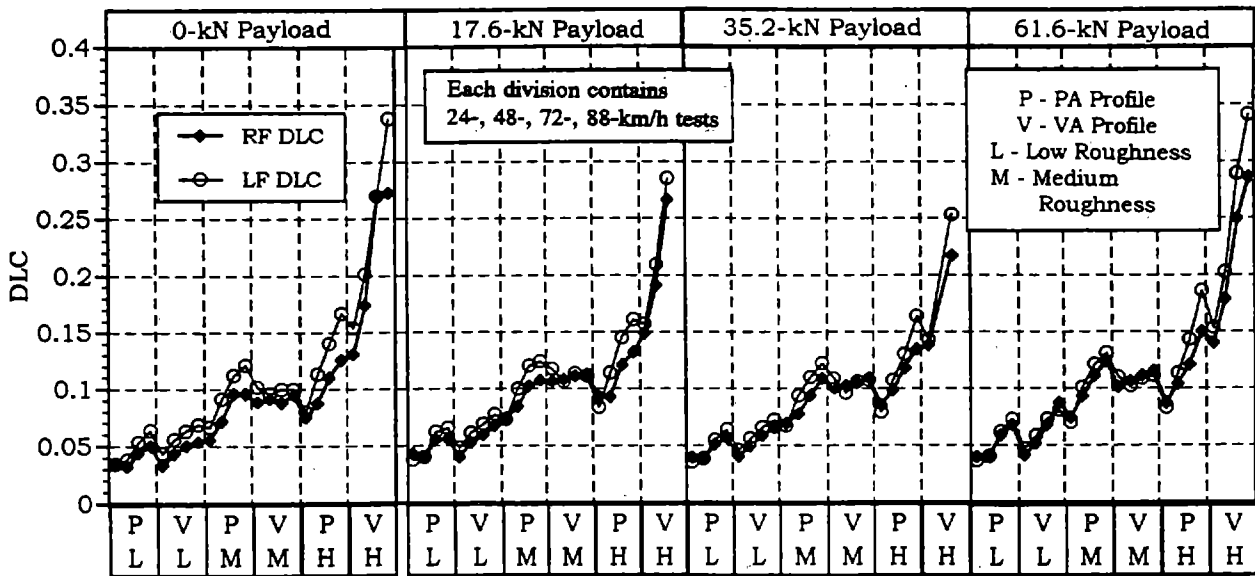
Figure 7-20. DLC from DYNTRAC tests for air suspension, standard tires, front wheels.
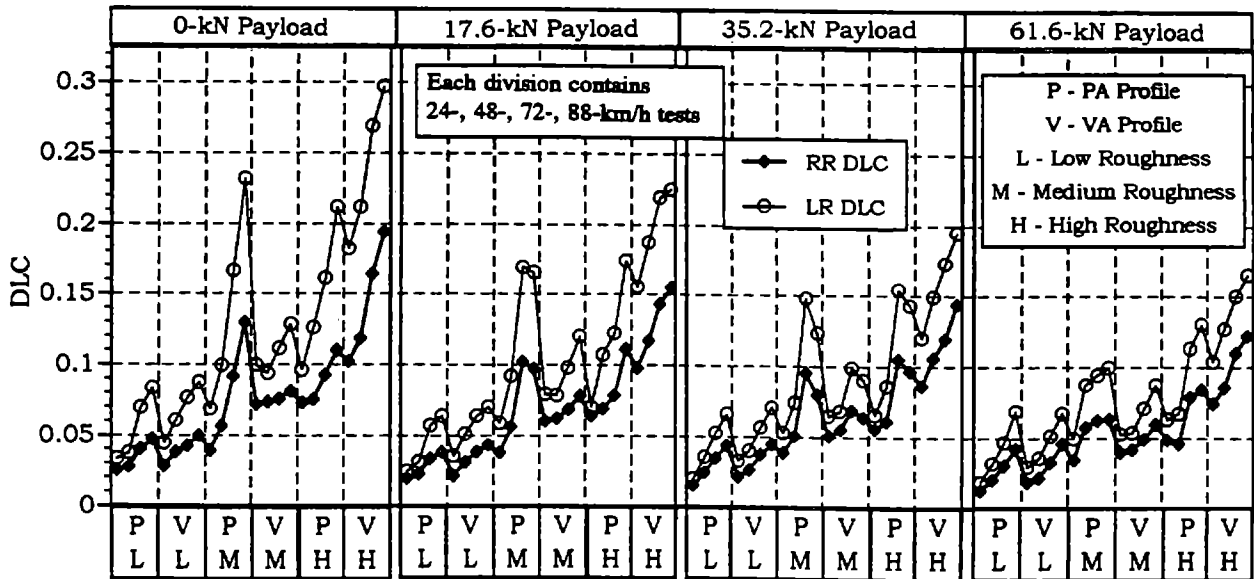
Figure 7-21. DLC from DYNTRAC tests for air suspension, wide-base tires, rear wheels.
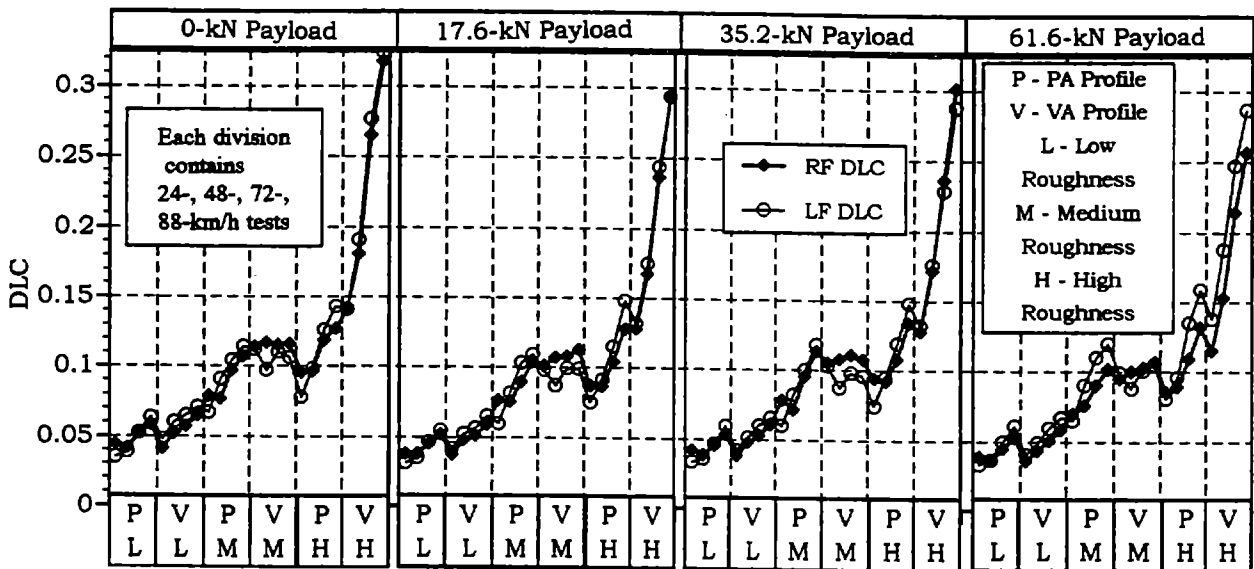
Figure 7-22. DLC from DYNTRAC tests for air suspension, wide-base tires, front wheels.

178
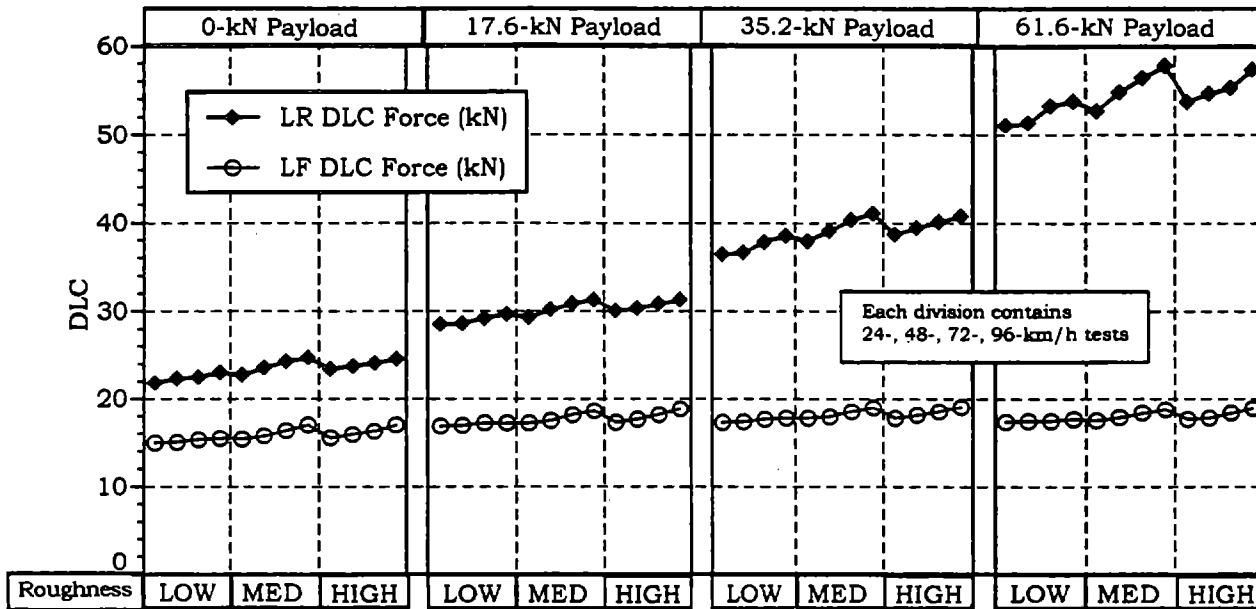
Figure 7-23. DLC forces from DYNTRAC tests for steel suspension, standard tires, Virginia profiles.

7.2 FIELD TESTS

7.2.1 Typical Sensor Measurements

Dynamic wheel forces from field tests are measured using axle-strain gauges and accelerometers mounted to the axles. Calibration and calculation of wheel forces are described in detail in chapter 2. The following figures are typical wheel force, suspension deflection, and accelerations from the left-rear axle of the test vehicle. The field test data shown in figures 7-24 through 7-27 are for the high-roughness road at 72 km/h (45 mi/h) with a payload of 35.2 kN. The static weight of the left-rear wheel was 35.4 kN.
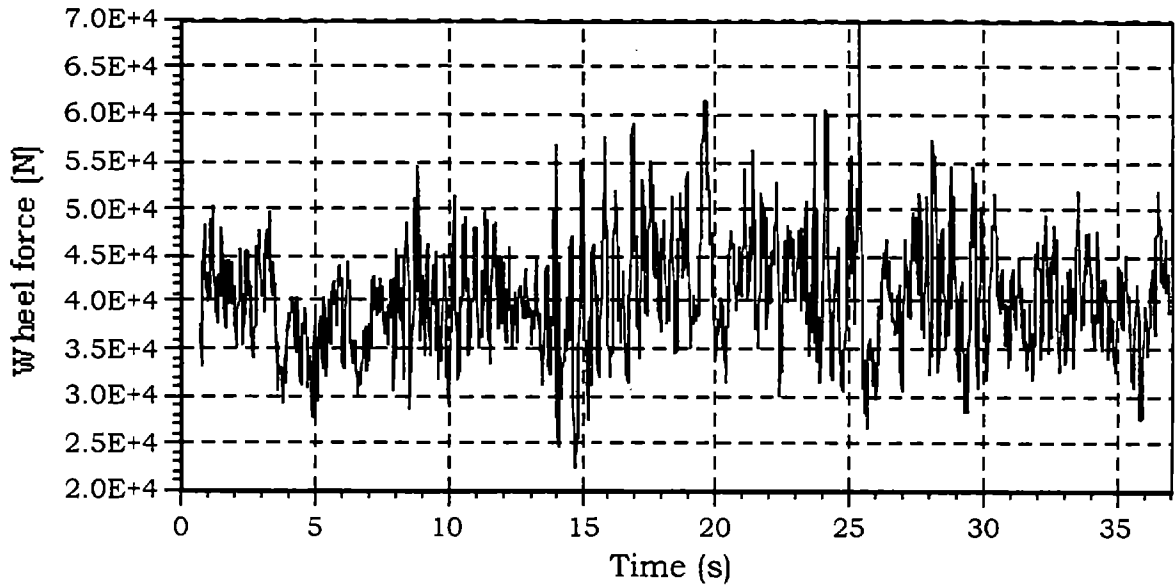
Figure 7-24. Left-rear wheel force.
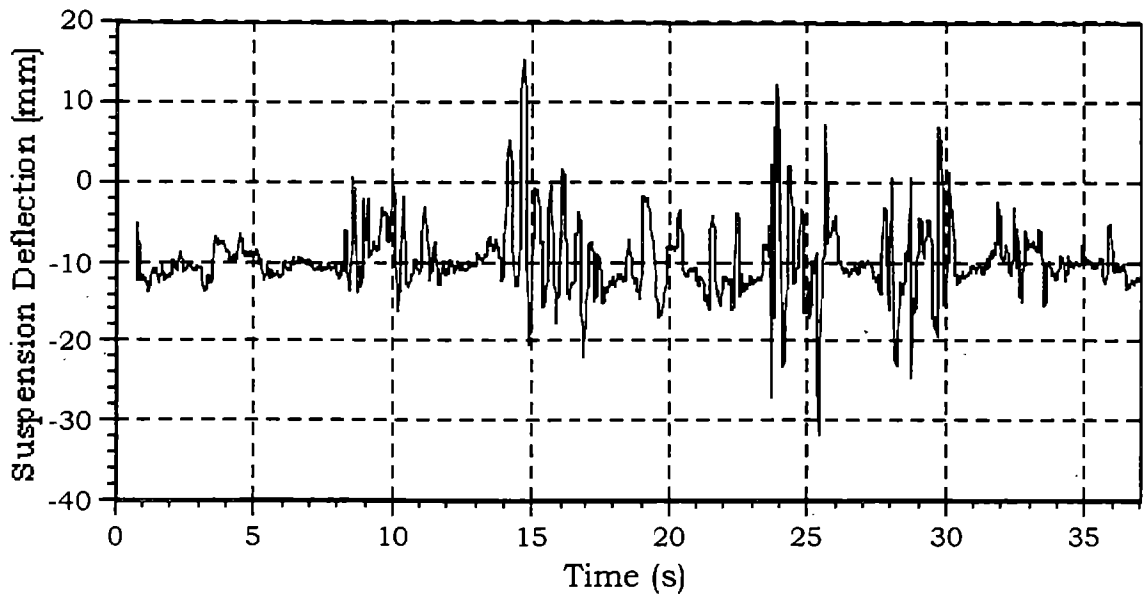
Figure 7-25. Left-rear suspension deflection.

Axle accelerations are used to determine the inertial loads generated by the mass of the axle and wheel assembly that is distal to the axle-strain gauges. Inertial force is added to axle force to obtain wheel force.

180
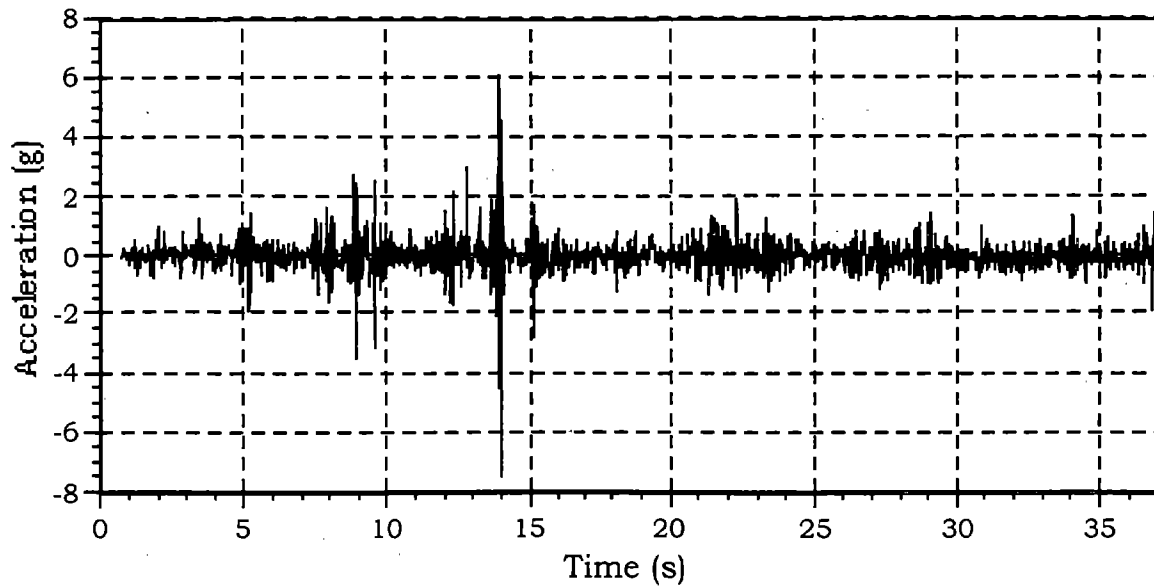
Figure 7-26. Left-rear axle acceleration.
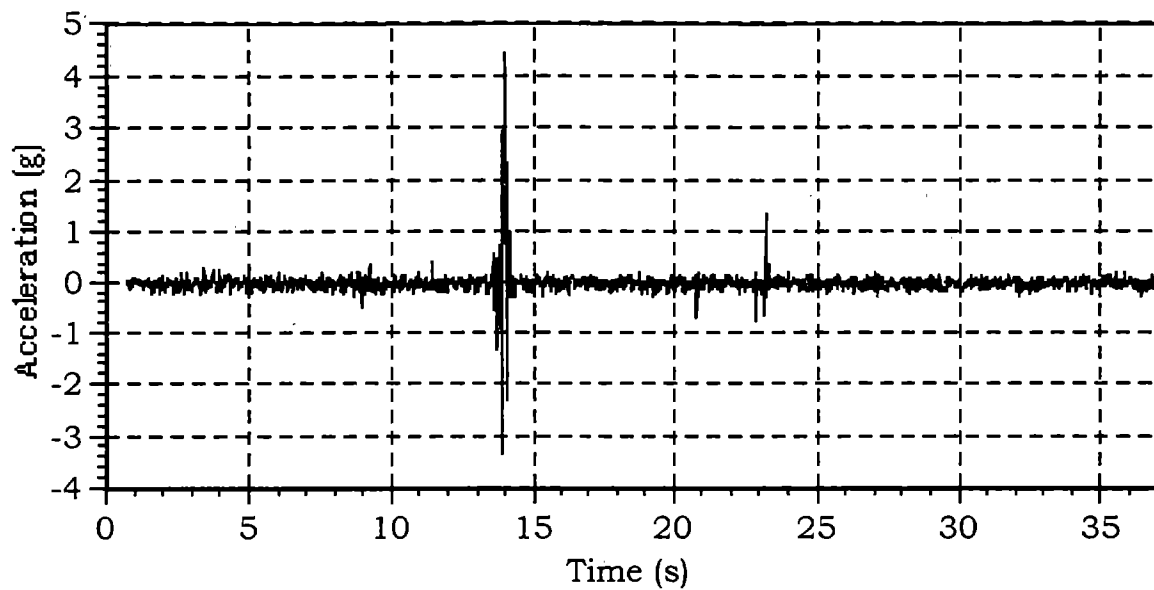
Figure 7-27. Left-rear chassis acceleration.

7.2.2 Processing

Data acquisition was started manually. An optical sensor indicated the start of the test section and also indicated position along the test section every 100 m (109 yd).

181

7.2.3 Graphical Summary of Test Results

DLC's are calculated from field test data. Figures 7-28 and 7-29 show that DLC generally increases with speed and roughness. Higher DLC's are seen in the lighter load configurations. These observations are consistent with those made from DYNTRAC results.
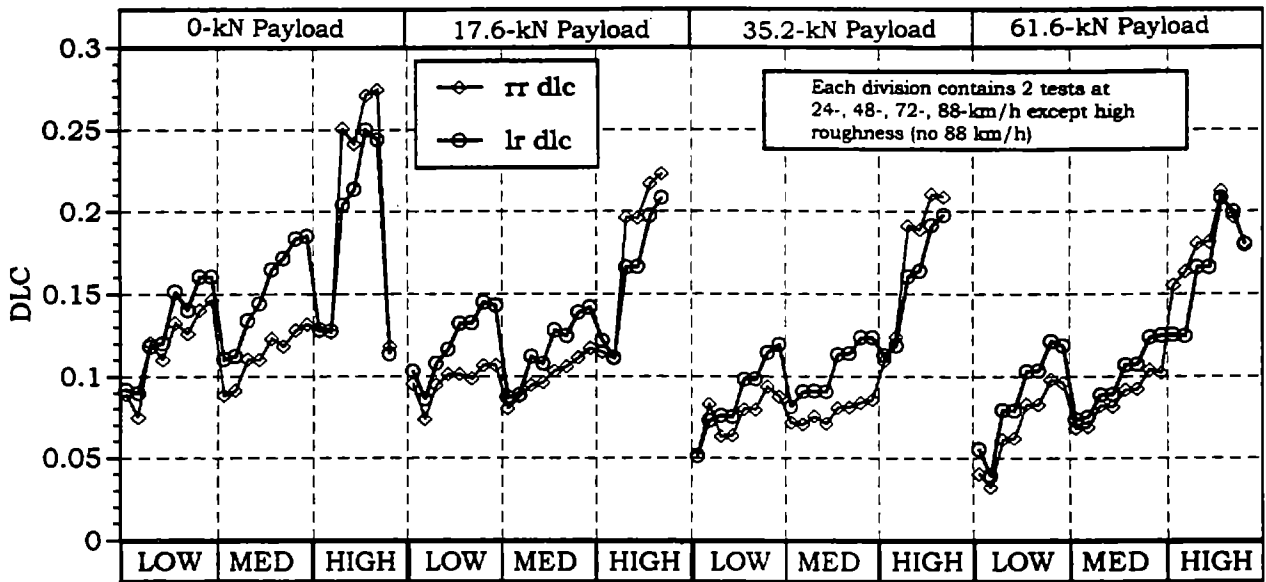
Figure 7-28. DLC from field tests for steel suspension, standard tires, rear wheels.
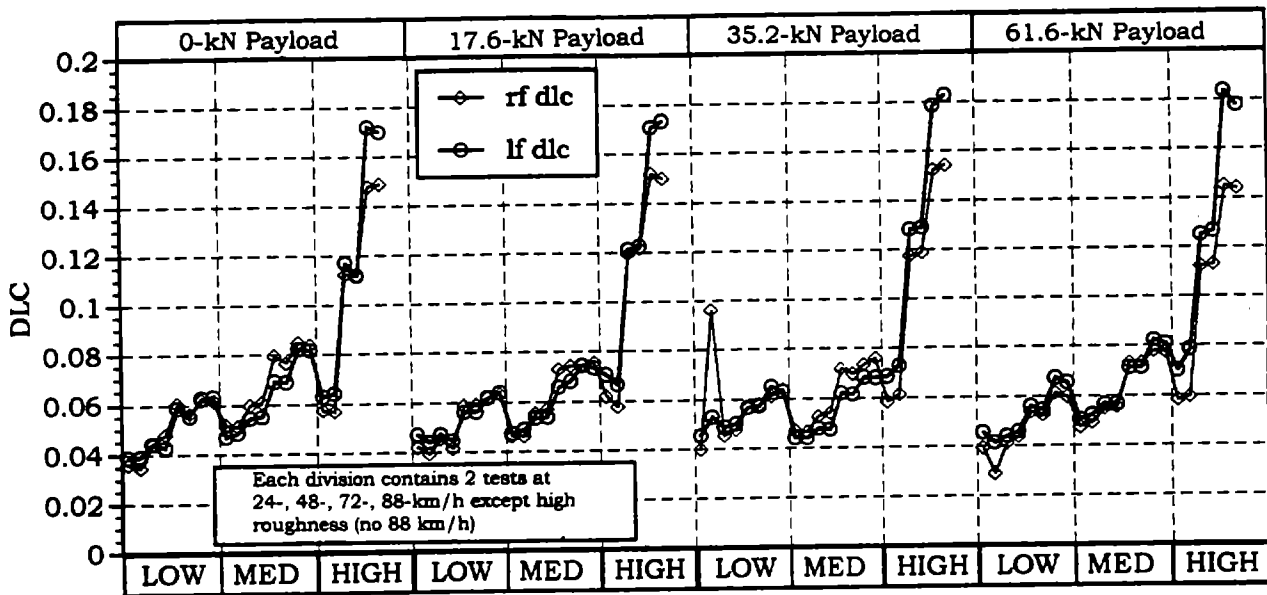
Figure 7-29. DLC from field tests for steel suspension, standard tires, front wheels.

DLC's calculated from DYNTRAC and field tests are examined in detail in the following chapter. Relationships between DLC and the test parameters are determined through graphic and statistical analyses.

The actual profile experienced by the vehicle varied according to the exact position of the vehicle on the test road. Speed is not constant in the field tests. Pavement markings every 100 m (109 yd) allow for more precise velocity measurement than the vehicle's speedometer; however, speed throughout the test road is not constant when compared with DYNTRAC tests.

CHAPTER 8. ANALYSIS OF DATA

This chapter presents the results of analysis of data collected in experiments conducted on DYNTRAC and in field tests. The data were presented in chapter 6. The data analysis was performed to accomplish three main objectives: (1) to evaluate the effects of test variables, including tire type, suspension type, road roughness, vehicle speed, axle load, and tire inflation pressure on the magnitude of dynamic tire forces; (2) to assess vehicle damaging power to pavements for various combinations of test variables; and (3) to compare data obtained from field tests, DYNTRAC tests, and computer simulation.

8.1 EFFECTS OF TEST VARIABLES ON DYNAMIC TIRE FORCES

The magnitude of the dynamic tire forces is commonly evaluated in terms of the DLC defined as the ratio of standard deviation over mean load.[10] DLC has been used as a measure of dynamic tire forces in this study.

8.1.1 Regression Models of DLC

The experimental data were used to derive regression models of DLC as a linear function of road roughness, vehicle speed, mean wheel load, and tire inflation pressure for various combinations of suspension and tire types. The general form of the regression models was

$$DLC = a_0 + a_1 r + a_2 v + a_3 L + a_4 P_t \qquad (8\text{-}1)$$

A total of 52 models were derived. The values of the parameters, coefficients of correlation, and standard deviations of the DLC models are listed in table 8-1. Several general observations will be made at this point, based on the results presented in table 8-1, leaving a more detailed discussion to the following sections of this chapter.

Table 8-1. Regression models of DLC.

	Source of Data	Site	Suspen-sion	Wheel	Tire Type	Model Parameters					R²	Standard Deviation
						Constant	Speed	Road Roughness	Load	Tire Pressure		
1	DYNTRAC	PA	Steel	LF	SR	0.04490	0.00109	0.02500	-0.00301	-	0.894	0.0166
2	DYNTRAC	PA	Steel	LF	SR	0.03160	0.00109	0.02500	-0.00268	1.20E-05	0.893	0.0166
3	DYNTRAC	PA	Steel	LR	SR	-0.00181	0.00118	0.03380	-0.00088	-	0.808	0.0196
4	DYNTRAC	PA	Steel	LR	SR	-0.02990	0.00118	0.03380	-0.00088	4.20E-05	0.822	0.0188
5	DYNTRAC	PA	Steel	LF	LP	0.03580	0.00119	0.02810	-0.00369	-	0.812	0.0185
6	DYNTRAC	PA	Steel	LF	LP	0.03110	0.00119	0.02800	-0.00396	1.50E-05	0.813	0.0184
8	DYNTRAC	PA	Steel	LR	LP	-0.01460	0.00122	0.03380	-0.00068	-	0.852	0.0169
8	DYNTRAC	PA	Steel	LR	LP	-0.02690	0.00122	0.03380	-0.00068	1.80E-05	0.854	0.0168
9	DYNTRAC	PA	Steel	LF	WB	0.05380	0.00114	0.02690	-0.00463	-	0.898	0.0185
10	DYNTRAC	PA	Steel	LF	WB	0.03300	0.00114	0.02680	-0.00459	3.00E-05	0.808	0.0180
11	DYNTRAC	PA	Steel	LR	WB	-0.00950	0.00109	0.02840	-0.00055	-	0.808	0.0182
12	DYNTRAC	PA	Steel	LR	WB	-0.02580	0.00110	0.02830	-0.00055	2.50E-05	0.814	0.0169
13	DYNTRAC	VA	Steel	LF	SR	0.25400	0.00142	0.04310	-0.01988	-	0.682	0.0540
14	DYNTRAC	VA	Steel	LR	SR	0.06590	0.00124	0.04090	-0.00281	-	0.865	0.0456
15	DYNTRAC	VA	Steel	RF	SR	-0.01800	0.00109	0.03050	0.00885	-	0.652	0.0481
16	DYNTRAC	VA	Steel	RR	SR	0.03910	0.00063	0.02150	-0.00138	-	0.899	0.0348
18	DYNTRAC	PA & VA	Steel	LF	SR	0.03580	0.00116	0.03240	-0.00355	-	0.838	0.0249
18	DYNTRAC	PA & VA	Steel	LR	SR	0.00143	0.00120	0.03850	-0.00118	-	0.888	0.0265
19	Road	VA	Steel	LF1	SR	-0.00880	0.00055	0.01660	0.00004	-	0.828	0.0122
20	Road	VA	Steel	LF2	SR	-0.00490	0.00055	0.01860	-0.00025	-	0.852	0.0122
21	Road	VA	Steel	LF12	SR	-0.02660	0.00059	0.01500	0.00118	-	0.882	0.0140
22	Road	VA	Steel	LR1	SR	0.08520	0.00096	0.01490	-0.00140	-	0.864	0.0132
23	Road	VA	Steel	LR2	SR	0.08530	0.00096	0.01620	-0.00149	-	0.888	0.0136
24	Road	VA	Steel	LR12	SR	0.08240	0.00101	0.01400	-0.00134	-	0.842	0.0146
25	Road	VA	Steel	RF1	SR	0.01090	0.00055	0.01210	-0.00085	-	0.844	0.0098
26	Road	VA	Steel	RF2	SR	0.00820	0.00053	0.01240	-0.00045	-	0.889	0.0125
28	Road	VA	Steel	RF12	SR	0.00490	0.00058	0.01060	-0.00028	-	0.844	0.0128
28	Road	VA	Steel	RR1	SR	0.05030	0.00059	0.02050	-0.00122	-	0.842	0.0158
29	Road	VA	Steel	RR2	SR	0.04690	0.00060	0.02180	-0.00126	-	0.883	0.0154
30	Road	VA	Steel	RR12	SR	0.04490	0.00068	0.01900	-0.00110	-	0.806	0.0181
31	DYNTRAC	PA	Air	LF	SR	-0.08820	0.00118	0.03330	0.00182	-	0.880	0.0139
32	DYNTRAC	PA	Air	LR	SR	-0.04460	0.00185	0.04120	-0.00108	-	0.856	0.0308
33	DYNTRAC	PA	Air	RF	SR	-0.09310	0.00084	0.03030	0.00360	-	0.885	0.0114
34	DYNTRAC	PA	Air	RR	SR	-0.03180	0.00100	0.03100	-0.00040	-	0.819	0.0158
35	DYNTRAC	PA	Air	LF	WB	-0.04140	0.00106	0.03030	-0.00013	-	0.883	0.0125
36	DYNTRAC	PA	Air	LR	WB	-0.02380	0.00158	0.03450	-0.00151	-	0.883	0.0255
38	DYNTRAC	PA	Air	RF	WB	-0.01310	0.00083	0.02980	-0.00083	-	0.889	0.0100
38	DYNTRAC	PA	Air	RR	WB	-0.01910	0.00086	0.02390	-0.00068	-	0.809	0.0136
39	DYNTRAC	VA	Air	LF	SR	-0.10600	0.00108	0.03820	0.00396	-	0.812	0.0310
40	DYNTRAC	VA	Air	LR	SR	0.00190	0.00111	0.03330	-0.00106	-	0.848	0.0249
41	DYNTRAC	VA	Air	RF	SR	-0.06430	0.00091	0.03080	0.00188	-	0.854	0.0246
42	DYNTRAC	VA	Air	RR	SR	-0.00253	0.00068	0.01980	-0.00038	-	0.898	0.0133
43	DYNTRAC	VA	Air	LF	WB	-0.01300	0.00119	0.03620	-0.00223	-	0.824	0.0302
44	DYNTRAC	VA	Air	LR	WB	0.01680	0.00101	0.02920	-0.00160	-	0.918	0.0168
45	DYNTRAC	VA	Air	RF	WB	-0.04300	0.00108	0.02960	0.00016	-	0.823	0.0294
46	DYNTRAC	VA	Air	RR	WB	0.00810	0.00058	0.01680	-0.00080	-	0.928	0.0102
48	DYNTRAC	PA & VA	Air	LF	SR	-0.10800	0.00116	0.03860	0.00346	-	0.830	0.0234
48	DYNTRAC	PA & VA	Air	LR	SR	-0.02040	0.00148	0.03580	-0.00109	-	0.889	0.0294
49	DYNTRAC	PA & VA	Air	RF	SR	-0.08130	0.00086	0.03020	0.00290	-	0.883	0.0186
50	DYNTRAC	PA & VA	Air	RR	SR	-0.00604	0.00083	0.02080	-0.00041	-	0.890	0.0188
51	DYNTRAC	PA & VA	Air	LF	WB	-0.05390	0.00114	0.03590	0.00002	-	0.836	0.0243
52	DYNTRAC	PA & VA	Air	LR	WB	-0.00220	0.00132	0.03010	-0.00154	-	0.830	0.0233
53	DYNTRAC	PA & VA	Air	RF	WB	-0.02910	0.00088	0.03020	-0.00022	-	0.852	0.0211
54	DYNTRAC	PA & VA	Air	RR	WB	0.00165	0.00082	0.01690	-0.00081	-	0.838	0.0139

LF = left-front wheel RF = right-front wheel SR = standard radial tire
LR = left-rear wheel RR = right-rear wheel LP = low-profile tire WB = wide-base tire

186

The significance of statistical models depends very strongly on the number of observations used in the derivation of the models. The number of observations in the regression models presented in this chapter of the report varied between 50 and 200, which is considered sufficiently large for models in the form given by equation 8-1. All models except four have a coefficient of correlation with experimental data, R^2, that is greater than 0.8, and the majority of the models have a coefficient of correlation greater than 0.85. The standard deviations between the DLC models and the experimental data are less than 0.03 for all but five models.

In general, the models demonstrate that road roughness and vehicle speed have the strongest effect on dynamic wheel loads. Wheel static load has a relatively lesser effect, and tire inflation pressure has no significant impact on DLC.

8.1.2 Effect of Tire Type

Three tire types were tested, including two dual tires (standard radial and low-profile tires) and a wide-base tire. Three sets of data were collected in DYNTRAC experiments, one for each tire type, for the same test conditions (steel leaf-spring suspension and Pennsylvania road profiles). The following regression models were derived relating DLC's for different tire types:

$$DLC_{WB} = 0.903 \; DLC_{LP} \qquad\qquad \textbf{(8-2)}$$

$$DLC_{WB} = 0.881 \; DLC_{SR} \qquad\qquad \textbf{(8-3)}$$

$$DLC_{SR} = 1.02 \; DLC_{LP} \qquad\qquad \textbf{(8-4)}$$

where subscripts WB, LP, and SR denote wide-base, low-profile, and standard radial tires, respectively. The coefficients of correlation, R^2, for the models were 0.918, 0.921, and 0.984 for equations 8-2, 8-3, and 8-4, respectively. The experimental data and the regression lines are shown in figures 8-1, 8-2, and 8-3.
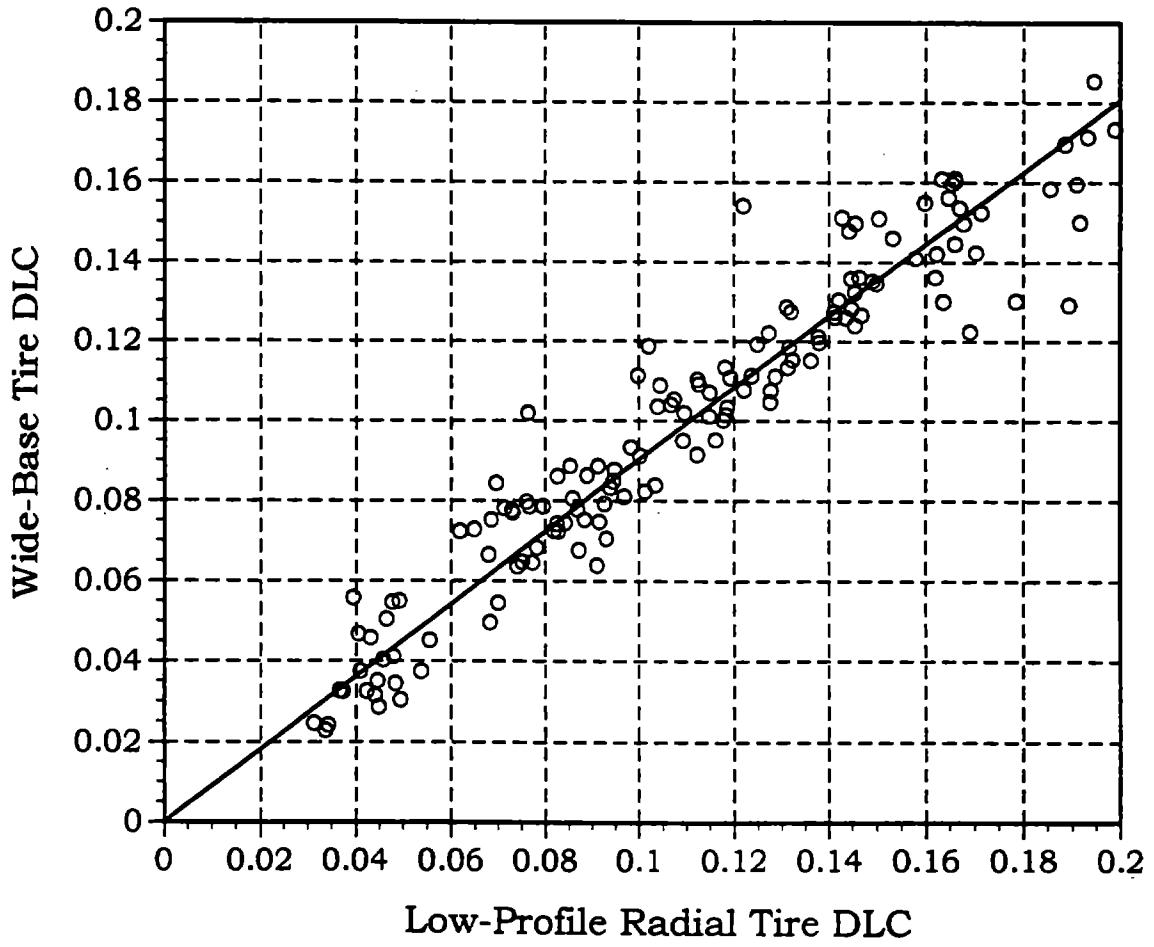
Figure 8-1. DLC's of wide-base tire versus low-profile tire.
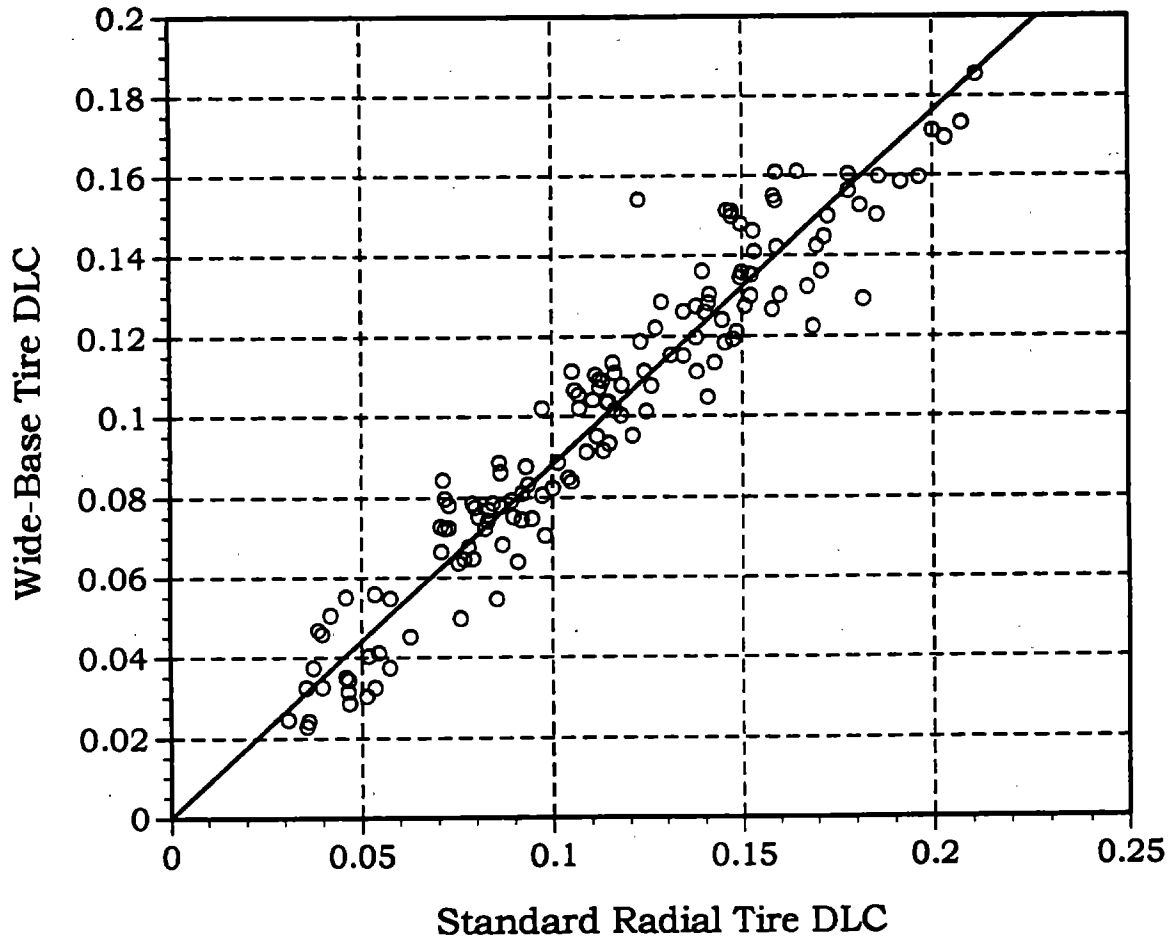
Figure 8-2. DLC's of wide-base tire versus standard radial tire.
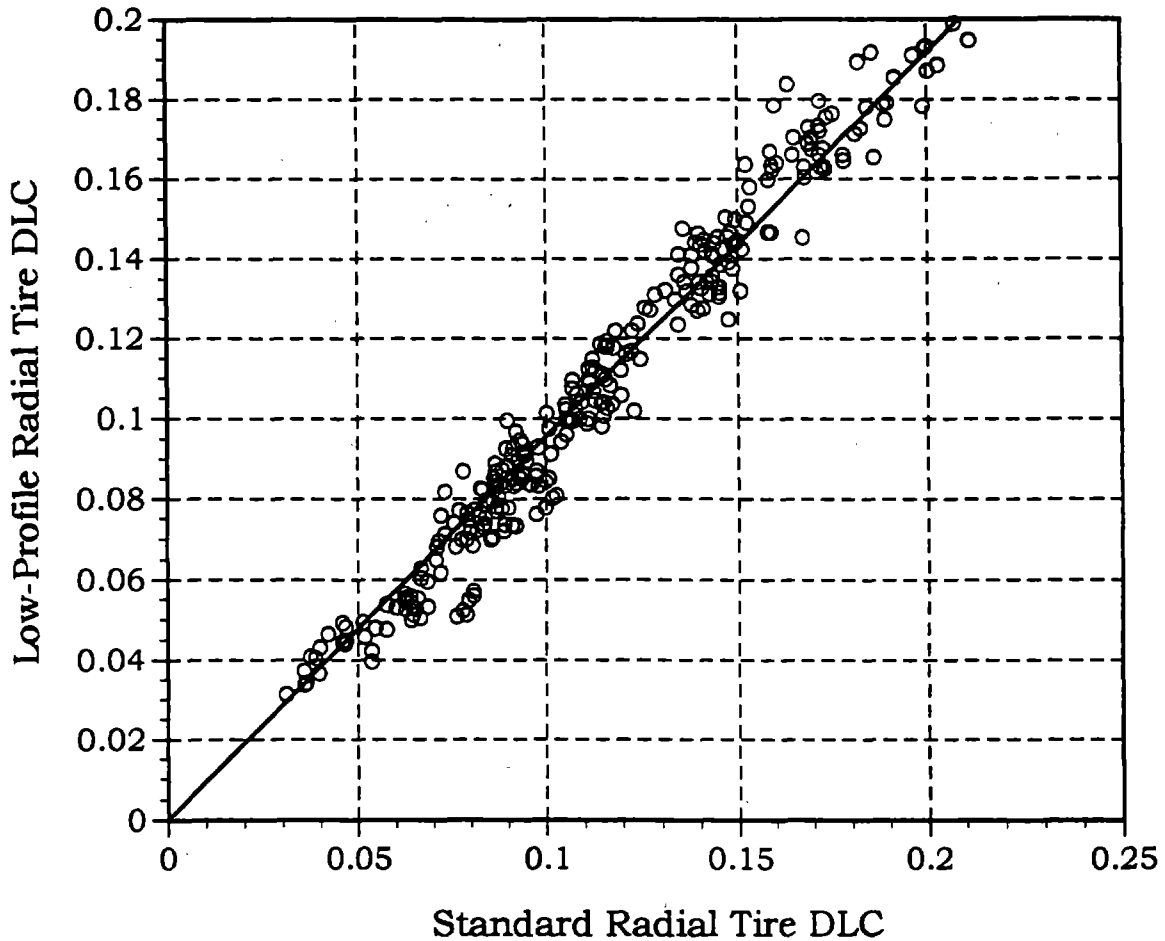
Figure 8-3. DLC's of standard radial tire versus low-profile tire.

The regression models just presented lead to two conclusions. First, the magnitudes of the dynamic wheel loads produced by the two dual tires are very similar. On the basis of equation 8-4, it can be expected that the standard radial tire will produce DLC values approximately 2 percent higher than the values obtained from the low-profile tire. Second, the wide-base tire produced DLC's 10 to 12 percent lower than those of the dual tires. The key to understanding the dynamic performance of the three tires is their stiffness. Table 8-2 shows values of the spring constants for the three tire types. The spring constants were calculated with use of the equations derived in section 6.3.2. It can be seen that the spring constants of the two dual tires are very close, whereas the spring constant of the wide-base tire is approximately 30 percent smaller than the spring constants of the dual tires at their respective manufacturer-recommended

190

inflation pressures. Overall, the differences between magnitudes of dynamic wheel loads generated by the three tire types were found to be quite small.

Table 8-2. Spring constants of test tires, kN/m (lb/in).

Tire Type	Tire Inflation Pressure, kPa (psi)		
	483 (70)	656 (95)	828 (120)
Standard Radial (2 tires)	1376 (7840)	1620 (9258)	1864 (10623)
Low-Profile (2 tires)	1373 (7826)	1662 (9472)	1951 (11119)
Wide-Base	N/A	988 (5628)	1165 (6637)

8.1.3 Effect of Suspension Type

To investigate the effect of suspension type on dynamic tire forces, the truck's rear-axle, progressive leaf-spring suspension was replaced by an air suspension. The truck with the air suspension was then subjected to the same series of tests on DYNTRAC as those conducted with the steel suspension. Details of the design of the two suspensions were presented in chapter 2.

First, to obtain an overall comparison of the performance of the two suspensions, a simple regression model was derived relating values of DLC obtained with the two suspensions and standard radial tires on both axles, and for all combinations of the remaining test variables. The following equation was obtained:

$$DLC_S = 1.04 \, DLC_A \qquad (8\text{-}5)$$

where subscripts S and A refer to steel and air suspensions, respectively. The tire force data measured under the left-rear tire was used in deriving equation 8-5. Figure 8-4 shows the distribution of the experimental data and the regression line given by equation 8-5. The model indicates that, on average, the magnitude of dynamic tire forces generated by the truck with steel suspension is approximately 4 percent larger than the magnitude of dynamic tire forces generated by the truck with air suspension. However, upon careful inspection of the data shown in figure 8-4, it can be observed

191

that in the lower range of DLC's, roughly less than 0.15, most data points lie above the regression line, whereas in the higher range of DLC's, roughly greater than 0.15, the data points are located mostly below the regression line. To verify this observation, the experimental data used in the derivation of equation 8-5 were divided into two subsets. The first subset included all data points with values of steel suspension DLC being smaller or equal to 0.15, and the second subset with steel suspension DLC's greater than 0.15. A linear regression was then performed on each of the two data subsets and the following models were obtained:

$$DLC_S = 1.18 \, DLC_A \qquad \text{for } DLC_S \leq 0.15 \qquad \qquad (8\text{-}6)$$

$$DLC_S = 0.93 \, DLC_A \qquad \text{for } DLC_S > 0.15 \qquad \qquad (8\text{-}7)$$
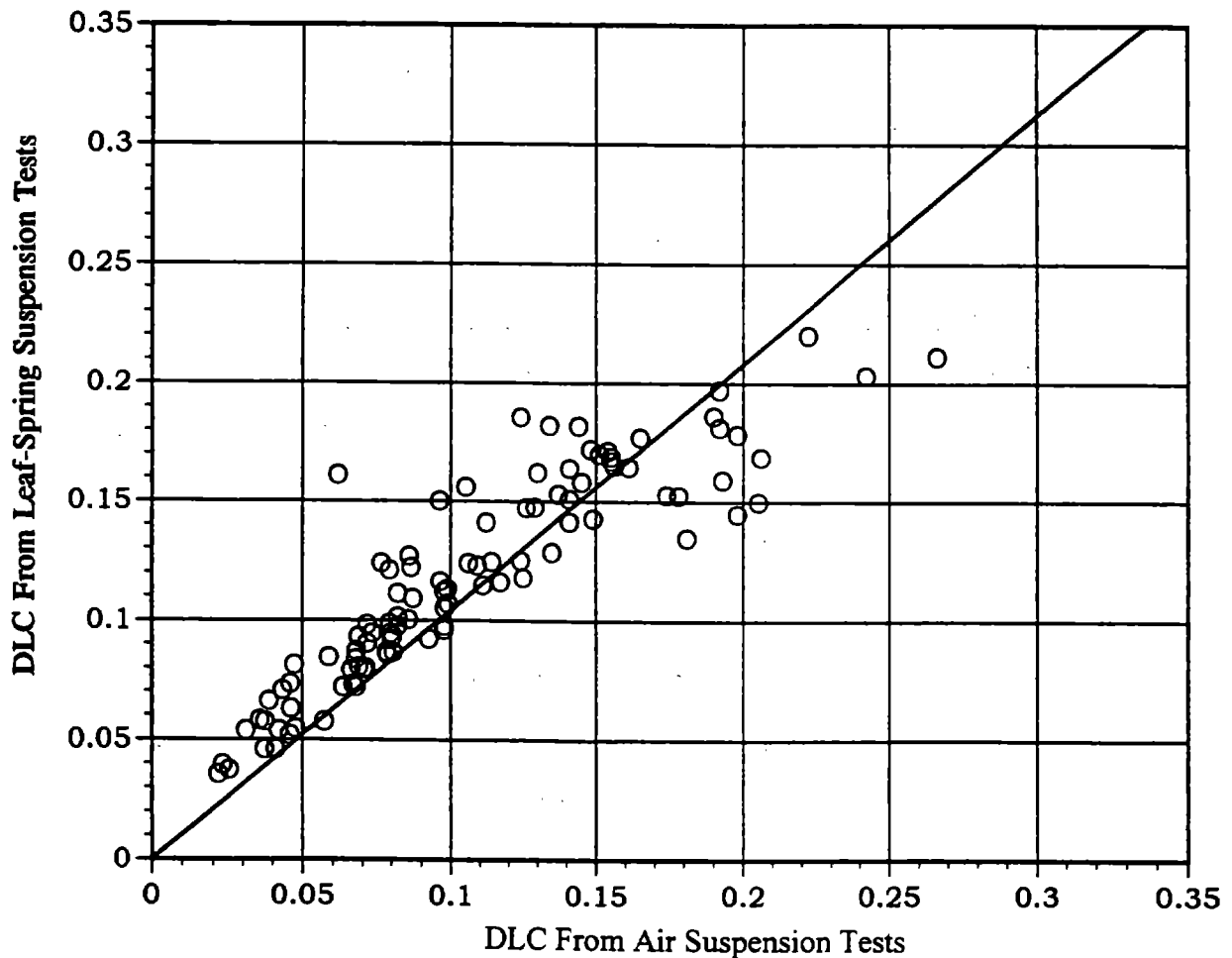
Figure 8-4. Correlation between steel and air suspension DLC's.

192

This finding, which is considered one of the major results of this study, clearly demonstrates that a simple statement that air suspension generates lower dynamic tire forces than steel suspension would be very misleading. For the particular type of vehicle tested in this study, air suspension proved indeed to be superior to steel suspension, but only for those combinations of road roughness, vehicle speed, and axle load for which the values of DLC with steel suspension are smaller than approximately 0.15. It can thus be concluded that the benefits of replacing steel suspension with air suspension in the particular model of truck tested in this study (in terms of the magnitude of dynamic tire forces) would, indeed, be very significant only if the truck traveled mostly over relatively smooth pavements and/or if it traveled at low speeds so that the average value of DLC was less than 0.15. On the other hand, the superiority of air suspension over steel suspension would be considerably smaller or none at all if the truck traveled mostly on rough pavements and at relatively high speeds, thus generating tire forces with DLC higher than 0.15.

In general, air suspensions are considered to generate lower dynamic tire forces than steel suspensions.[33] However, some researchers have reported test results similar to those obtained in this study, in which air suspension did not offer any benefits over steel suspension in terms of dynamic pavement loading.[34] To explain the results obtained in this study, it should first be noted that the superiority of one suspension type over another depends on the vehicle and road conditions measured in terms of the DLC, with the air suspension being clearly superior to steel suspension under conditions generating DLC's lower than 0.15, but the steel suspension being slightly better under conditions resulting in DLC's higher than 0.15. An important implication of this observation is that the system nonlinearities must play a key role in the performance of one or both suspension systems. If both suspensions were linear systems, one would always be performing better than the other, regardless of the operating conditions. The dominant nonlinearity in a truck's suspension system is the friction between the leafs of the steel suspension. This is illustrated by the force versus deflection characteristics shown in figures 3-1 and 3-2 for the truck's front and rear suspensions, respectively. To evaluate the effects of the steel suspension nonlinearity

on vehicle dynamics, consider the operation of the rear-axle suspension on relatively smooth (low DLC) and relatively rough (high DLC) roads in essentially the same manner as proposed by Cole and Cebon.[6]

On smooth roads, the suspension deflections are small, and the system trajectory follows a relatively narrow hysteretic loop, as shown in figure 8-5. Two parameters that determine the magnitude of dynamic tire forces under these conditions are suspension stiffness, k_s = tan α, and damping or, equivalently, the amount of energy dissipated in the suspension, represented in figure 8-5 by the shaded area enclosed by the hysteretic loop. On rough roads, suspension deflections are large, and the resulting hysteretic loop shown in figure 8-6 is much larger, which leads to lower stiffness (smaller α) and higher damping (larger shaded area) than the same parameters shown in figure 8-5. It can thus be concluded that when road roughness increases, the steel suspension stiffness decreases and the damping increases. Both processes lead to improved performance of the steel suspension in terms of dynamic tire forces on rougher roads, which explains the experimental results obtained in this study.
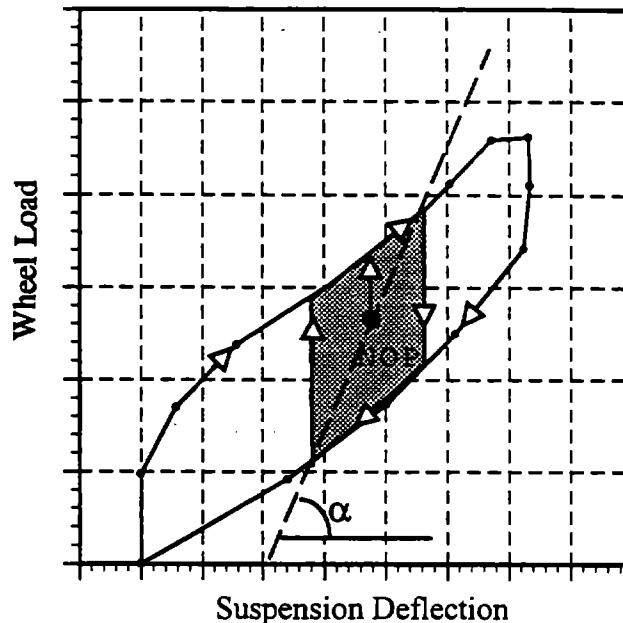
Figure 8-5. Suspension on smooth roads.

194
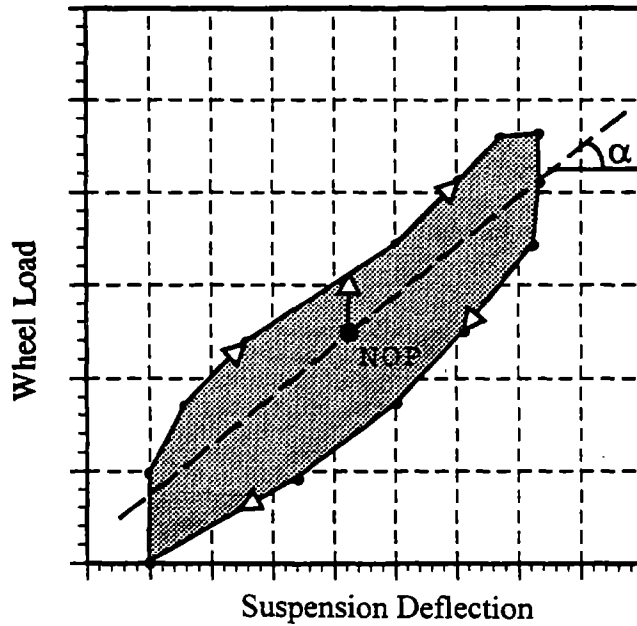
Figure 8-6. Suspension on rough roads.

The results presented above clearly demonstrate that the benefits of using air suspension instead of steel suspension must be evaluated with great care and that there is no basis for expecting either suspension type to be superior for all vehicle designs and under all operating conditions.

8.1.4 Effects of Road Roughness, Speed, Load, and Tire Inflation Pressure

To evaluate the effects of road roughness, vehicle speed, wheel static load, and tire inflation pressure on dynamic pavement loading, linear regression models of DLC as a function of the test variables for three tire types for the truck equipped with steel suspension were derived. The model equations for the left-front-axle wheel with standard radial and low-profile tires are

$$DLC_{SR} = 0.0316 + 0.025 \, r + 0.0011 \, v - 0.0028 \, L + 0.012*10^{-3} \, P_t \qquad \text{(8-8)}$$

$$DLC_{LP} = 0.0311 + 0.028 \, r + 0.0012 \, v - 0.0040 \, L + 0.014*10^{-3} \, P_t \qquad \text{(8-9)}$$

where

r = international roughness index, mm/m.

v = vehicle speed, km/h.

L = mean wheel load, kN.

P_t = tire inflation pressure, kPa.

The following equations were derived for the left-rear-axle wheel:

$$DLC_{SR} = -0.0299 + 0.034\ r + 0.0012\ v - 0.0009\ L + 0.042*10^{-3}\ P_t \qquad (8\text{-}10)$$

$$DLC_{LP} = -0.0269 + 0.034\ r + 0.0012\ v - 0.0008\ L + 0.018*10^{-3}\ P_t \qquad (8\text{-}11)$$

$$DLC_{WB} = -0.0258 + 0.028\ r + 0.0011\ v - 0.0006\ L + 0.025*10^{-3}\ P_t \qquad (8\text{-}12)$$

It can be seen that there are profound similarities among the three models in each of the front- and rear-axle wheel sets. This is particularly true for the coefficients relating to road roughness and vehicle speed. To evaluate the effects of the test variables on DLC, two parameters will be introduced. The first parameter, sensitivity S_i, provides a measure of an impact of an i-th test variable on DLC. The sensitivity of DLC to a variable x_i is defined by

$$S_i = \frac{\partial DLC}{\partial x_i}\ \bar{x}_i \qquad (8\text{-}13)$$

where $\bar{x}_i$ is a baseline value of the test variable x_i. The second parameter used in the evaluation is the amount by which a test variable has to change to produce a change in DLC of 0.01, which can be expressed as

$$\Delta x_i = 0.01\frac{\bar{x}_i}{S_i} \qquad (8\text{-}14)$$

196

or as a percentage of the baseline value

$$\delta_i = \frac{\Delta x_i}{\bar{x}_i} 100\% = \frac{1}{S_i} \qquad (8\text{-}15)$$

As the latter equation demonstrates, the two parameters, S_i and δ_i, are directly related, but each parameter provides a different perspective on the effects of test variables on DLC. The DLC sensitivity parameters, S_i, for road roughness, vehicle speed, mean wheel load, and tire inflation pressure obtained from regression models 8-6 through 8-10 are shown in table 8-3. These results clearly demonstrate that road roughness and vehicle speed have a very strong effect on DLC. Static wheel load has a significant impact on front-axle tire forces, but its effect on rear-axle DLC's is much smaller. It can also be seen that the impact of tire inflation pressure on DLC is much smaller than the impact of the other test variables. The values of the other sensitivity parameter, δ_i, shown in table 8-4, indicate that a change in DLC of 0.01 can be caused by a change in vehicle speed of 11 to 13 percent, 8 to 10 km/h (5 to 6 mi/h), a change in road roughness of approximately 15 percent, 0.3 m/km (20 in/mi), a change in front-axle static wheel load of 15 to 22 percent or 2.5 to 3.6 kN (560 to 800 lb), a change in rear-axle static wheel load of 40 to 60 percent or 10 to 18 kN (2250 to 3800 lb), or a change in tire inflation pressure of 40 to 150 percent or 230 to 880 kPa (30 to 130 psi) for dual tires and approximately 55 percent or 400 kPa (60 psi) for wide-base tires.

Table 8-3. DLC-sensitivity parameters for a truck with steel suspension.

Tire Type	Wheel	S_V	S_r	S_L	S_{Pt}
Standard Radial	Left Front	0.0888	0.0524	-0.0451	0.0069
Low-Profile	Left Front	0.0860	0.0598	-0.0661	0.0085
Standard Radial	Left Rear	0.0846	0.0808	-0.0263	0.0248
Low-Profile	Left Rear	0.0888	0.0820	-0.0199	0.0108
Wide-Base	Left Rear	0.0898	0.0604	-0.0165	0.0180

Table 8-4. Percent changes of test variables necessary to change DLC by 0.01 (steel suspension).

Tire Type	Wheel	δ_v	δ_r	δ_L	δ_{Pt}
Standard Radial	Left Front	12.8	19.1	-22.2	145.2
Low-Profile	Left Front	11.6	16.8	-15.1	118.6
Standard Radial	Left Rear	11.8	14.1	-38.1	40.6
Low-Profile	Left Rear	11.3	13.9	-50.4	92.6
Wide-Base	Left Rear	12.6	16.6	-60.5	55.8

Although the regression models have been derived using large sets of data and have relatively high coefficients of correlation and small standard deviations, it must be kept in mind that they are only linear approximations of truly nonlinear relationships that exist between DLC and the test variables. Therefore, the engineering significance of these models is obviously limited and they should be interpreted with great care. Nevertheless, based on the models, it can be concluded that the magnitude of dynamic tire forces generated by the truck is strongly affected by speed and road roughness and moderately affected by wheel load. Tire inflation pressure has no significant effect on dynamic tire forces and, therefore, can be eliminated from further analysis.

The general trends discussed above are also illustrated in figures 8-7 through 8-18, showing DLC as a function of speed for three levels of roughness, four levels of static load, and three tire types. It is interesting to note that the DLC curves for medium- and high-roughness road profiles are very close. The reason for this is that the road roughness was classified as low, medium, and high on the basis of the road profile IRI value. It has been shown that IRI, which is calculated using a mathematical model of a passenger quarter-car,[35] is not always an appropriate indicator of dynamic tire forces generated by a heavy truck in response to road roughness.[12,14]
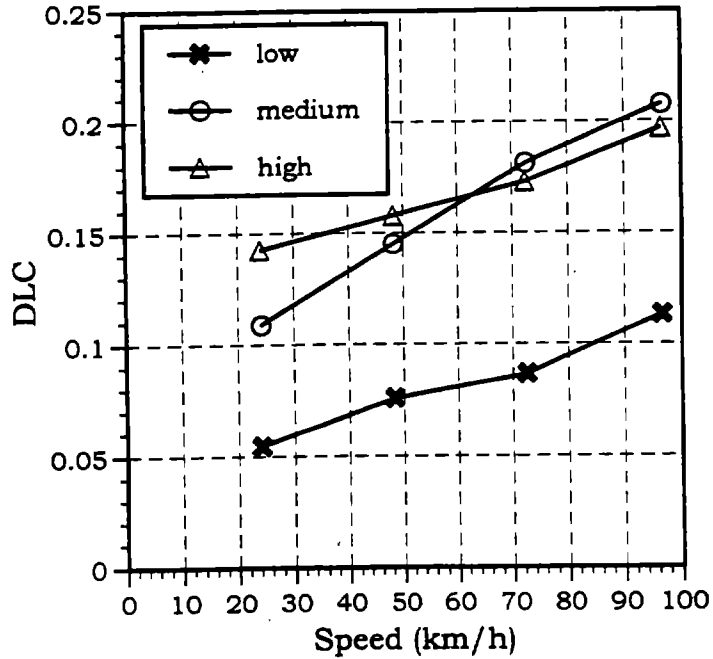
Figure 8-7. DLC versus speed for rear-axle standard radial tire (truck empty).
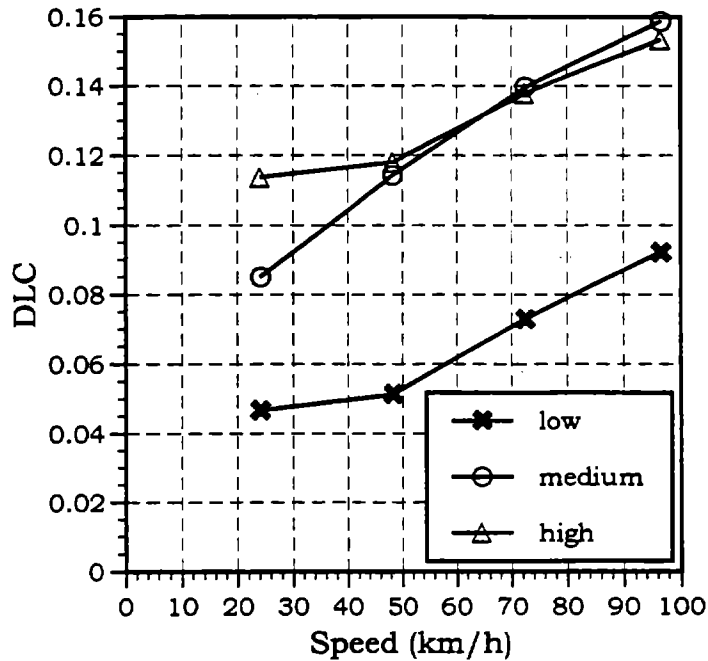
Figure 8-8. DLC versus speed for rear-axle standard radial tire (18.6-kN payload).

199
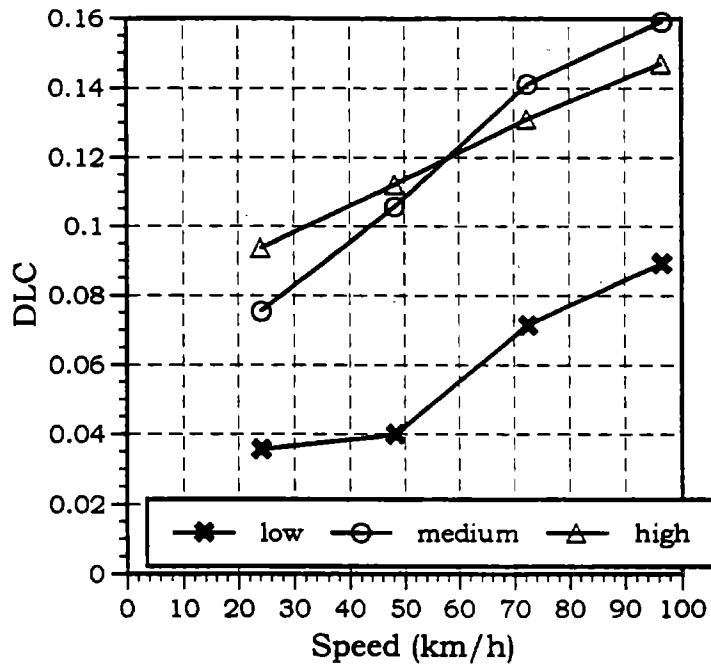
Figure 8-9. DLC versus speed for rear-axle standard radial tire (35.2-kN payload).
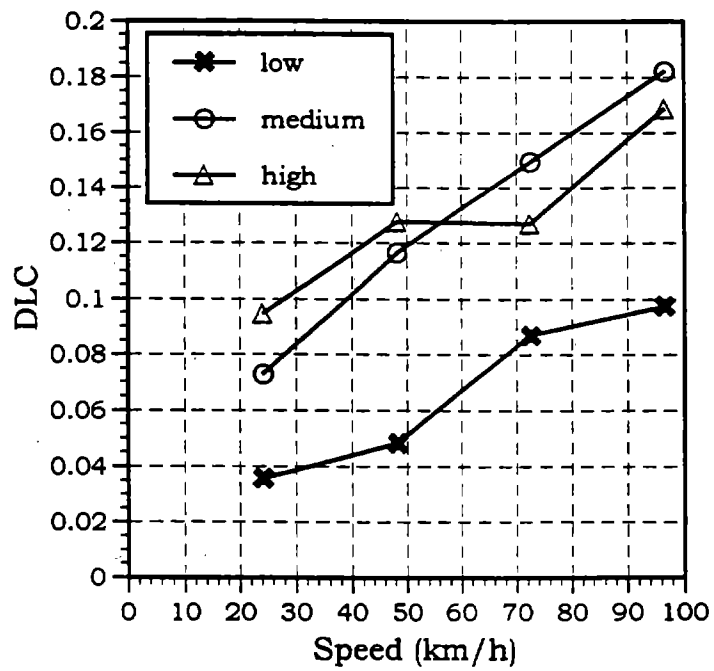
Figure 8-10. DLC versus speed for rear-axle standard radial tire (61.4-kN payload).

200
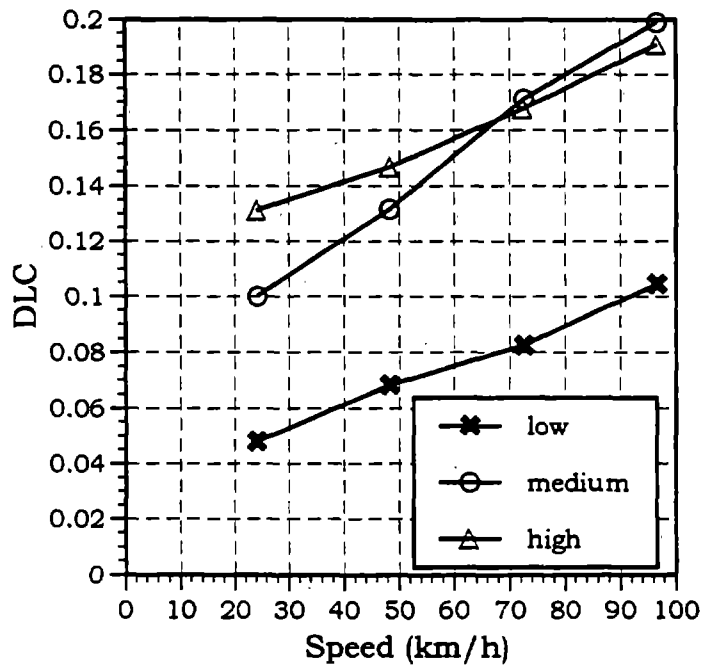
Figure 8-11. DLC versus speed for rear-axle low-profile tire (truck empty).
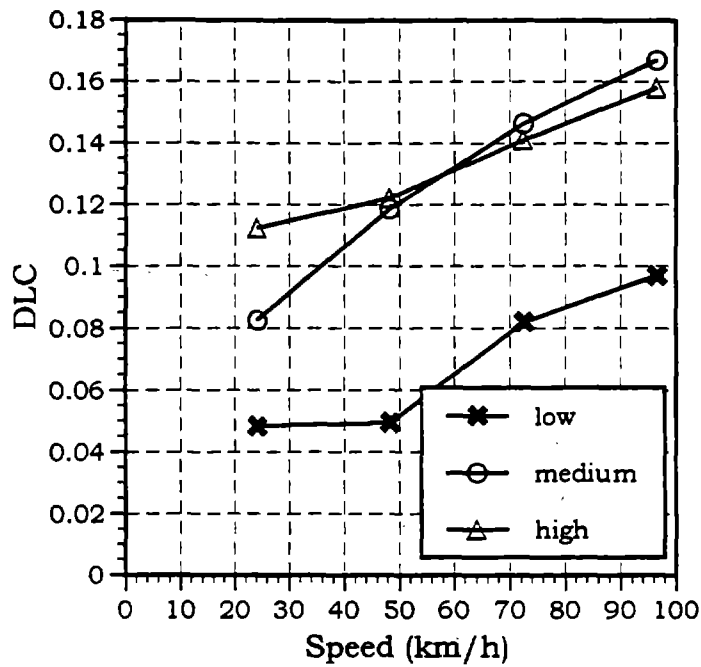
Figure 8-12. DLC versus speed for rear-axle low-profile (18.6-kN payload).

201
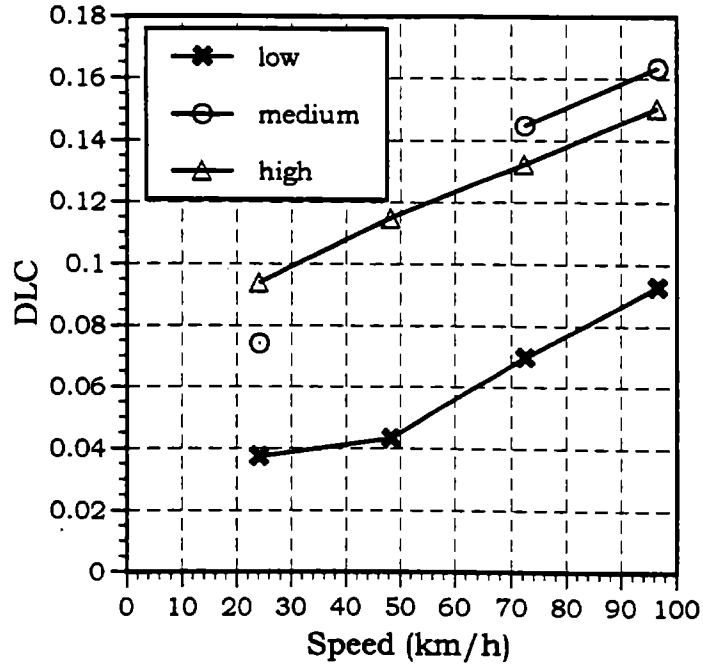
Figure 8-13. DLC versus speed for rear-axle low-profile (35.2-kN payload).
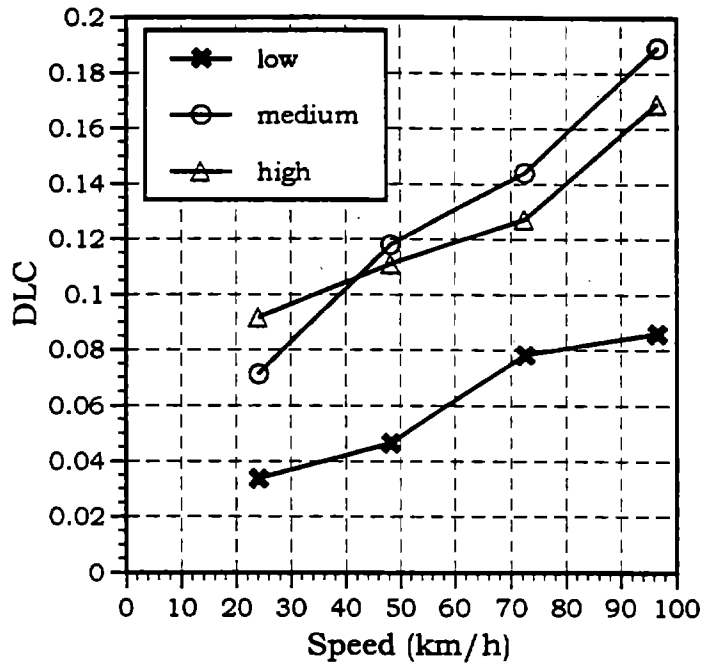
Figure 8-14. DLC versus speed for rear-axle low-profile (61.4-kN payload).

202
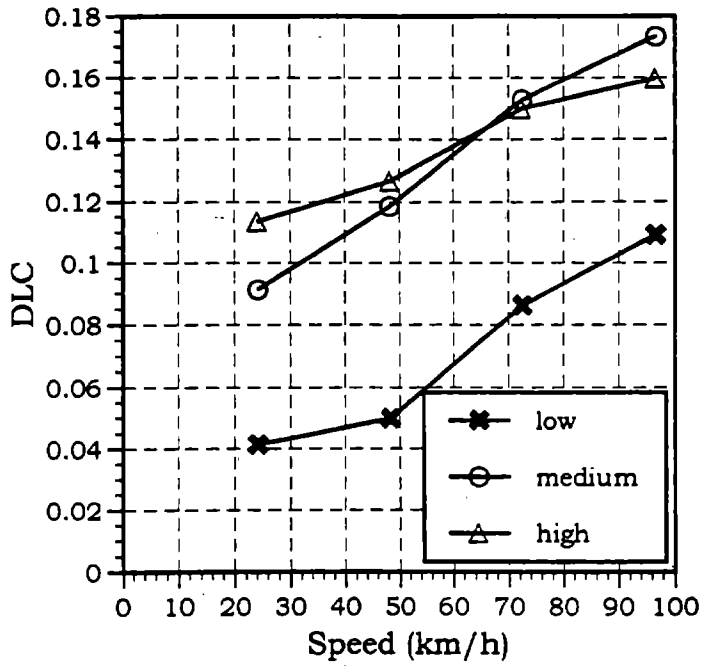
Figure 8-15. DLC versus speed for rear-axle wide-base tire (truck empty).
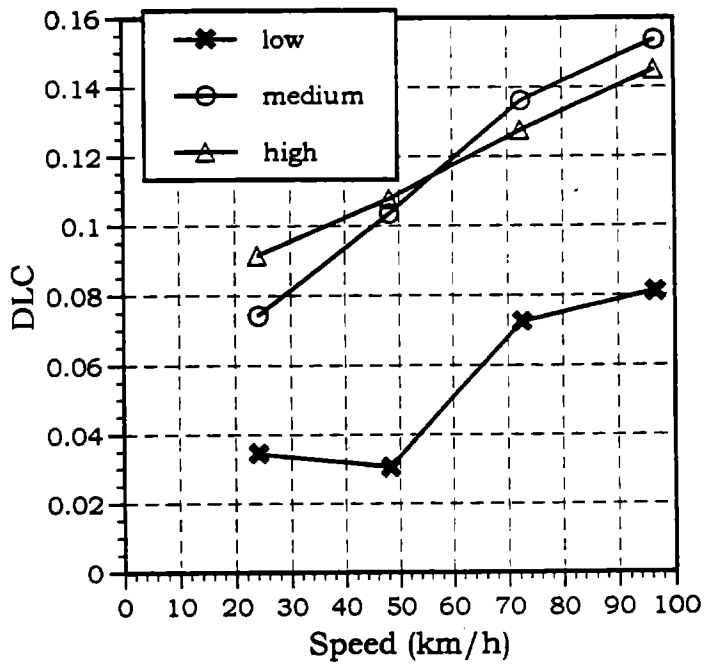
Figure 8-16. DLC versus speed for rear-axle wide-base tire (18.6-kN payload).
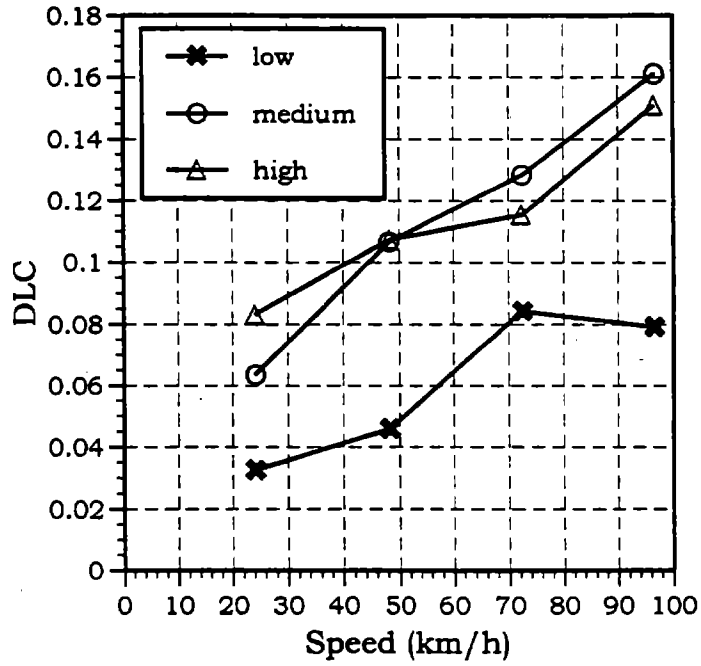
Figure 8-17. DLC versus speed for rear-axle wide-base tire (35.2-kN payload).
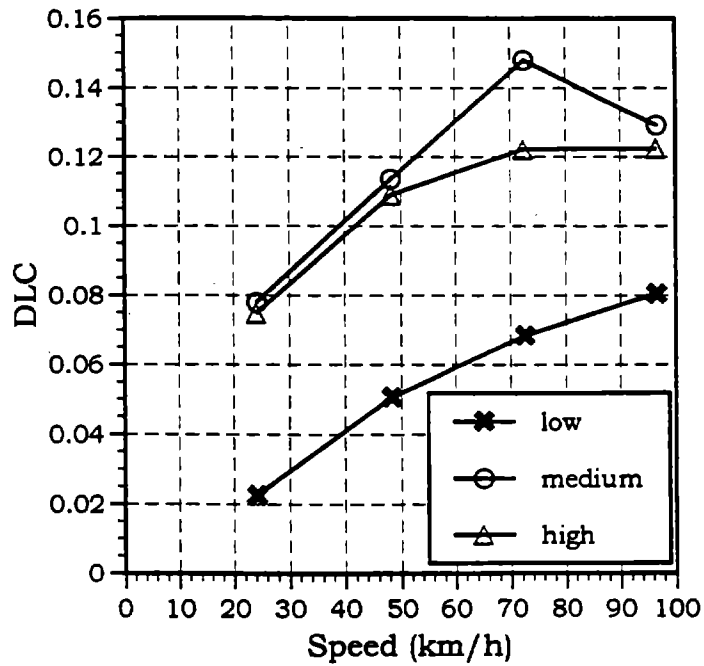
Figure 8-18. DLC versus speed for rear-axle wide-base tire (61.4-kN payload).

204

8.2 EFFECTS OF TEST VARIABLES ON PAVEMENT DAMAGE

The main reason for studying dynamic tire forces is their pavement-damaging potential. To assess a truck's pavement-damaging potential, Eisenmann et al. derived a road stress factor:[36]

$$\Phi = (\eta_1 \, \eta_2 \, L)^4 \, (1 + 6s^2 + 3s^4) \qquad \textbf{(8-16)}$$

where

η_1 = coefficient reflecting wheel configuration (1.0 for wheels with single tires, 0.9 for wheels with dual tires).

η_2 = coefficient reflecting tire-pavement contact pressure.

s = coefficient of variation of dynamic wheel load.

The coefficient η_2 is assumed to be a linear function of the tire-pavement contact pressure, P_c,

$$\eta_2 = 0.65 + 0.5 \, P_c \qquad \textbf{(8-17)}$$

where P_c is in N/mm^2. The coefficient of variation, s, is usually replaced by DLC. A dynamic road stress factor is defined as

$$\nu = 1 + 6s^2 + 3s^4 \qquad \textbf{(8-18)}$$

There is still a continued debate among researchers as to whether Eisenmann's road stress factor is an appropriate and accurate measure of a vehicle's pavement-damaging potential. Equation 8-16 was derived assuming that dynamic loads are randomly distributed along the road. In fact, since peak wheel loads are generated by heavy vehicles in response to road profiles and since dynamic characteristics of heavy vehicles traveling on a particular road tend to be similar, the dynamic wheel loads are expected to be spatially repeatable (i.e., peak loads are applied at specific locations along the road). Spatial repeatability of dynamic loads applied by heavy trucks to roads as well as loads applied by landing aircraft to runways has been recently confirmed.[5,37] Nevertheless, Eisenmann's road stress factor was

considered appropriate for comparison of the pavement-damaging potential of the same vehicle with different types of tires and different types of suspensions.

The following baseline values of the test variables were selected:

P_t = 587 kPa (85 psi) for dual tires and 724 kPa (105 psi) for wide base tires.

v = 89 km/h (55 mi/h).

R = 2.05 m/km (130 in/mi).

L = 29.7 kN (6,674 lb), (14.85 kN [3,337 lb] per dual tire).

The results of calculations are presented in table 8-5. As these results indicate, the pavement-damaging potential of the test truck is about the same for the two dual tires but increases by approximately 80 percent when single wide-base tires are used.

Table 8-5. Results of calculation of road stress factor for three tire types.

Tire Type	Standard	Low-Profile	Wide-Base
DLC	0.1413	0.1414	0.1310
v	1.1212	1.1212	1.1041
η_1	0.9	0.9	1.0
P_c, N/mm²	0.56	0.62	0.83
η_2	0.93	0.96	0.98
Φ, 10^{-16} kN⁴	42.82	43.36	89.24

To compare the pavement-damaging potential of the truck with steel and air suspensions, one may notice that

$$\frac{\Phi_S}{\Phi_A} = \frac{v_s}{v_A} \tag{8-19}$$

Using the same baseline values of the test variables, the following values of the dynamic road stress factor for the truck with air suspension were obtained:

206

$$v_A = 1.0812 \text{ for standard radial tires}$$

and

$$v_A = 1.0452 \text{ for wide-base tires}$$

The values above are 5 and 6 percent lower than the corresponding values for the truck with steel suspension.

As pointed out earlier, Eisenmann's road stress factor formula assumes randomness of dynamic wheel loads and, therefore, underestimates pavement-damaging potential. Sweatman suggested that the severity of the dynamic loads can be better evaluated by the 95th percentile impact factor, which can be estimated by

$$IF_{95th} = 1 + 1.645 \, DLC \qquad (8\text{-}20)$$

and the corresponding road stress factor:[10]

$$\Phi_{95th} = (IF_{95th})^4 \qquad (8\text{-}21)$$

The results of comparison of steel and air suspensions with standard radial and wide-base tires using the 95th percentile road stress factor are shown in table 8-6. It can be seen that the 95th percentile road stress factor values for the truck with air suspension are approximately 20 and 30 percent lower than the values obtained for the steel suspension with standard radial and wide-base tires, respectively.

Table 8-6. Values of 95th-percentile road stress factor for steel and air suspensions.

	Steel Standard Radial	Air Standard Radial	Steel Wide-Base	Air Wide-Base
DLC	0.1413	0.1084	0.1310	0.0848
IF_{95th}	1.2324	1.1883	1.2155	1.1395
Φ_{95th}	2.31	1.93	2.18	1.69

In general, the pavement-damaging potential of heavy vehicles increases when vehicle speed and road roughness increase. Furthermore, pavement damage is expected to be greater by up to 85 percent when wide-base single tires are used instead of dual tires. The type of dual tires and the tire inflation pressure have no significant effect on pavement damage. Air suspension is expected to cause less pavement damage than steel suspension. The estimate of the magnitude of improvement that can be contributed to air suspension varies widely depending on whether dynamic wheel loads are assumed to be spatially repeatable (20 to 30 percent improvement) or randomly distributed along the road (5 percent improvement).

8.3 COMPARISON OF DYNTRAC, FIELD, AND COMPUTER-SIMULATION RESULTS

8.3.1 Comparison of DYNTRAC and Field-Test Results

Road tests were conducted at three sites in Virginia. The field testing program followed a full factorial experimental design with three levels of road roughness, four levels of speed, four levels of load, one tire type (standard radial dual tire), and one suspension type (steel-leaf spring). Two runs were made for each combination of test variables.

As it was explained earlier, the tests on DYNTRAC were conducted without Remote Parameter Control compensation because DYNTRAC's frequency response characteristic showed fairly uniform gain over the frequency range responsible for generating truck tire forces (0 to 20 Hz). As a result, the characteristics of dynamic tire forces measured on DYNTRAC were expected to represent a consistent and accurate extrapolation of the dynamic tire force characteristics obtained from road tests, even though there were small differences between the DYNTRAC actuator displacements and the measured road profiles. It should also be emphasized here that the extent to which the DYNTRAC actuators were unable to follow the input road profile was independent of all vehicle test variables, i.e., tire type, tire inflation pressure, and, most importantly, static axle load, as illustrated in figure 3-18.

It appears that the most significant factor responsible for the differences between the results of tests on DYNTRAC and road tests was the truck's inability to follow closely the wheel paths of the profilometer in tests conducted on in-service roads. The values of the IRI for the left- and right-wheel tracks (shown in table 3-2) are significantly different on all three sites in Virginia, especially on the medium- and high-roughness roads, indicating that there was a considerable transverse roughness gradient on the test sections of the roads. Therefore, even a small difference between the lateral position of the truck wheels relative to the lateral position of the profilometer wheels would cause a significant difference between the road profile traveled over by the truck and the road profile measured by the profilometer, which was then used as input in experiments on DYNTRAC. Another factor contributing to the error was the time delay between measuring the profile and conducting the tests with the truck. It was possible that the profile changed due to environmental conditions and pavement loading. The only way to ensure that the measured road profile is the same as the profile the truck is traveling over, would be to install the profile measuring equipment (laser distance sensors and accelerometers) on-board the test truck. It should also be pointed out here that the agreement between the data collected in repeated tests was excellent, which leads to the conclusion that the truck followed the same wheel paths in the repeated tests but, at the same time, each of the truck wheel paths was different from the profilometer wheel paths.

It can be seen from table 8-1 that the coefficients of correlation for regression models of DLC derived from the tests on DYNTRAC versus DLC obtained in road tests are relatively low, especially for the front-axle DLC models. The DYNTRAC tests with Virginia site profiles were conducted immediately before the failure of the left-front actuator, which probably contributed considerably to the poor quality of the front-axle tire data in these tests. The highest value of R^2 (0.899) was obtained for the right-rear wheel model. This model took the following form:

$$DLC = 0.0391 + 0.022\ r + 0.0006\ v - 0.0014\ L \qquad (8\text{-}22)$$

The regression model obtained from road data is

$$DLC = 0.0449 + 0.019\ r + 0.0008\ v - 0.0011\ L \qquad \text{(8-23)}$$

These two models are very similar. The agreement between the DLC models derived from the left-rear-wheel data is not as good. The DYNTRAC model is

$$DLC = 0.0659 + 0.041\ r + 0.0012\ v - 0.0028\ L \qquad \text{(8-24)}$$

whereas the model obtained from the field data is

$$DLC = 0.0824 + 0.014\ r + 0.0010\ v - 0.0014\ L \qquad \text{(8-25)}$$

The distributions of the DLC data obtained from DYNTRAC tests versus DLC from field tests for both rear-axle wheels are shown in figures 8-17 and 8-18. As it was explained earlier, the magnitude of dynamic tire forces on DYNTRAC was somewhat lower than on corresponding road sites because of the inherent inertia of the DYNTRAC actuators. Figure 8-19 presents curves of DLC versus vehicle speed for four levels of static load obtained in road and in DYNTRAC tests for right-rear wheel at the speed of 82.5 km/h (51.3 mi/h). The distributions of the DLC data obtained from DYNTRAC and road tests versus road roughness are displayed in figures 8-20 through 8-22. Again, these plots show the DLC values obtained in DYNTRAC tests being slightly lower than the values obtained in road tests; however, both DYNTRAC and road DLC curves follow the same pattern.
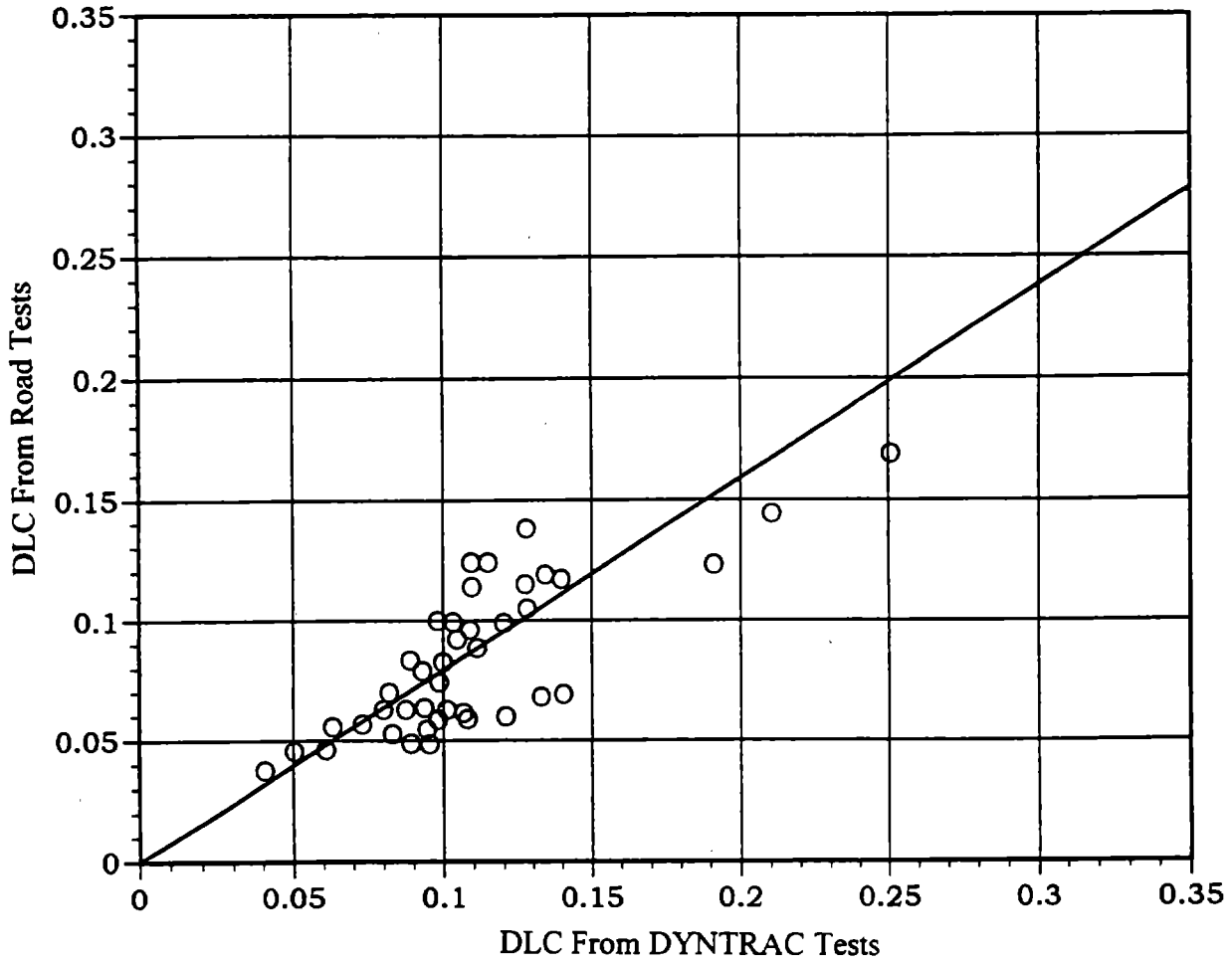
Figure 8-19. Correlation between DLC values obtained from DYNTRAC and field tests for right-rear wheel.
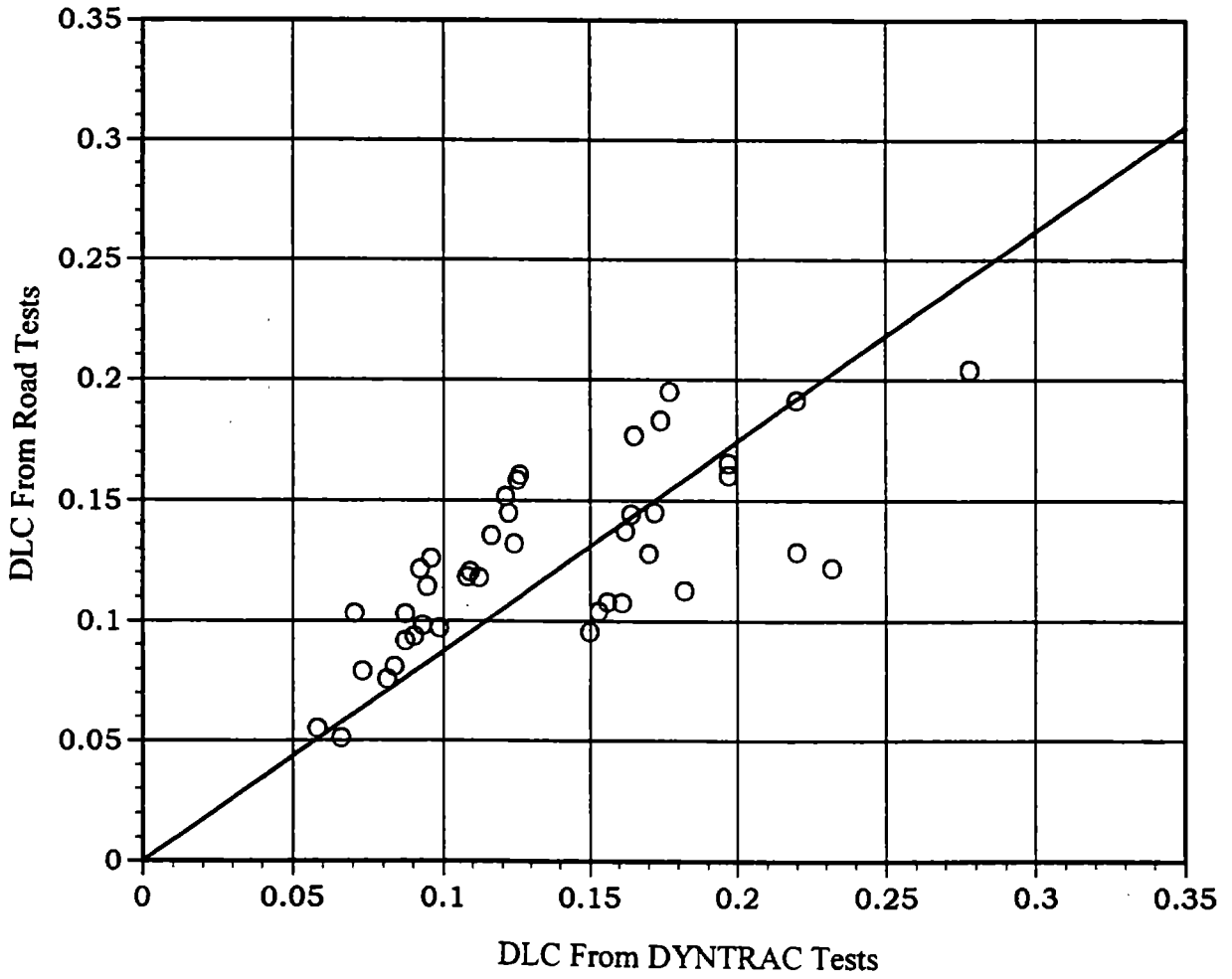
Figure 8-20. Correlation between DLC values obtained from DYNTRAC and field tests for left-rear wheel.
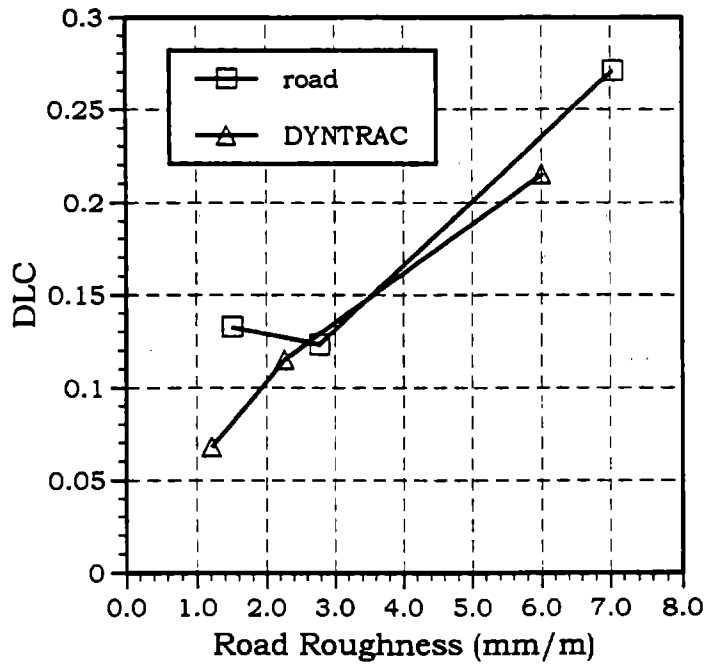
Figure 8-21. DLC's obtained from DYNTRAC and road tests versus road roughness (truck empty).
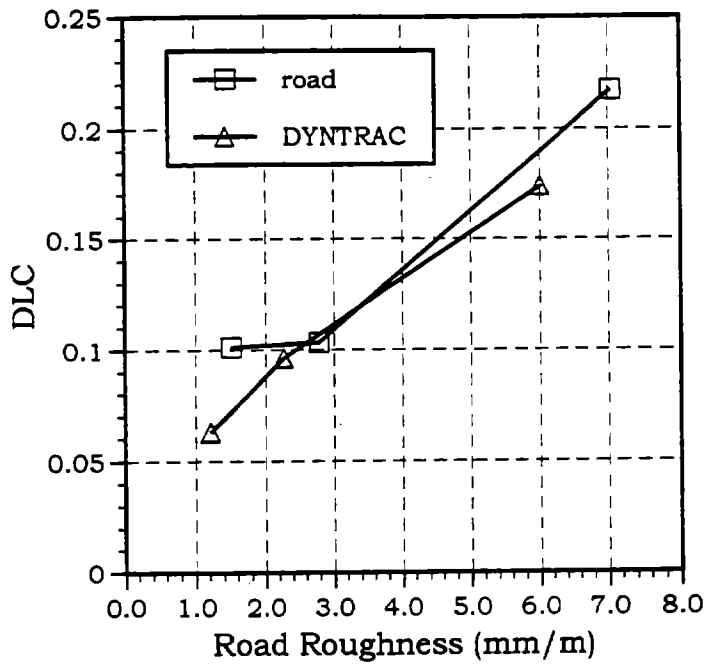
Figure 8-22. DLC's obtained from DYNTRAC and road tests versus road roughness (18.6-kN payload).

213
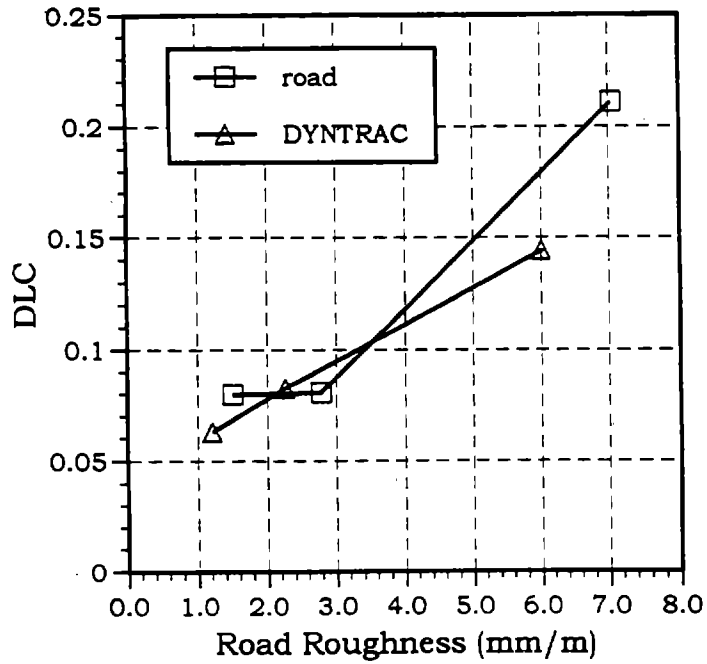
Figure 8-23. DLC's obtained from DYNTRAC and road tests versus road roughness (35.2-kN payload).
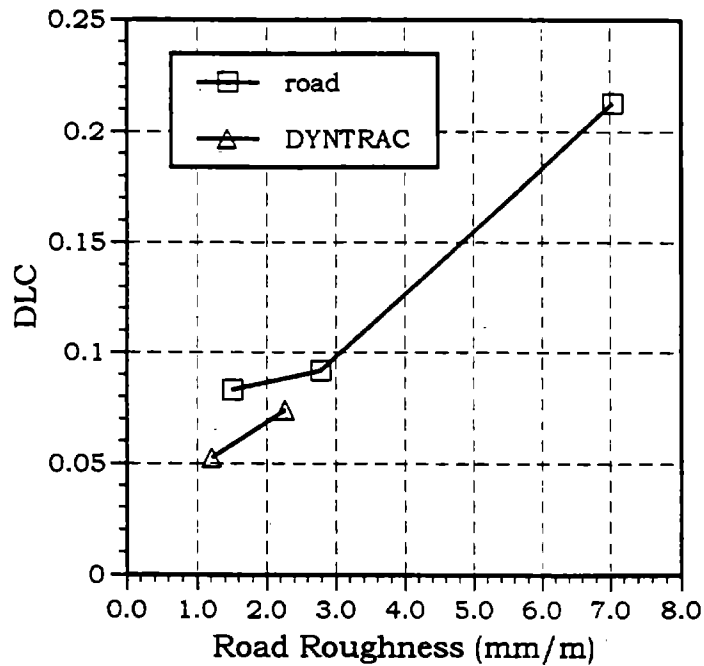
Figure 8-24. DLC's obtained from DYNTRAC and road tests versus road roughness (61.4-kN payload).

214

8.3.2 Computer-Simulation Results

The computer-simulation models used in this study were described in chapter 5. These models were used primarily to identify parameters of the test truck. The criterion employed in the identification of the truck parameters was the difference between simulated and experimental tire forces, measured in tests on DYNTRAC. In general, the results of identification presented in chapter 5 showed good agreement between the computer-simulated and measured tire forces.

The experimental results expressed mathematically in the form of equations 8-6 and 8-8 are considered to represent one of the major findings of this study, and clearly demonstrate that a simple statement that air suspension generates lower dynamic tire forces than steel suspension would be very misleading. For the particular type of vehicle tested in this study, air suspension proved indeed to be superior to steel suspension, but only for those combinations of road roughness, vehicle speed, and axle load for which the values of DLC with steel suspension are smaller than approximately 0.15. It can thus be concluded that the benefits of replacing steel suspension with air suspension in the particular model of truck tested in this study (in terms of the magnitude of dynamic tire forces) would, indeed, be very significant only if the truck traveled mostly over relatively smooth pavements and/or if it traveled at low speeds so that the average value of DLC was less than 0.15. On the other hand, the superiority of air suspension over steel suspension would be considerably smaller or none at all if the truck traveled mostly on rough pavements and at relatively high speeds, thus generating tire forces with DLC higher than 0.15.

To explain the results obtained in this study, it should first be noted that the superiority of one suspension type over another depends on the vehicle and road conditions measured in terms of the DLC, with the air suspension being clearly superior to steel suspension under conditions generating DLC's lower than 0.15 but then the steel suspension being slightly better under conditions resulting in DLC's higher than 0.15. An important implication of this observation is that the system nonlinearities must play a key role in the performance of one or both suspension systems. If both

215

suspensions were linear systems, one would always be performing better than the other, regardless of the operating conditions. The dominant nonlinearity in the truck's suspension system is the friction between the leafs of the steel suspension, illustrated by the force versus deflection characteristics shown in figures 3-2 and 3-4 for the truck's front and rear suspensions, respectively. To evaluate the effects of the steel suspension nonlinearity on vehicle dynamics, the operation of the rear-axle suspension on relatively smooth (low DLC) and relatively rough (high DLC) roads must be considered in essentially the same manner as proposed by Gillespie.[38]

On smooth roads, the suspension deflections are small and the system trajectory follows a relatively narrow hysteretic loop, as shown in figure 8-5. Two parameters that determine the magnitude of dynamic tire forces under these conditions are suspension stiffness, $k_s = \tan \alpha$, and damping or, equally, the amount of energy dissipated in the suspension, represented in figure 8-5 by the shaded area enclosed by the hysteretic loop. On rough roads, suspension deflections are large, and the resulting hysteretic loop shown in figure 8-6 is much larger, which leads to lower stiffness (smaller α) and higher damping (larger shaded area) than the same parameters shown in figure 8-5. It can thus be concluded that when road roughness increases, the steel suspension stiffness decreases and the damping increases, with both processes leading to improved performance of the steel suspension in terms of dynamic tire forces on rougher roads, which explains the experimental results obtained in this study.

The results presented above clearly demonstrate that the benefits of using air suspension instead of steel suspension must be evaluated with great care and that there is no basis for expecting either suspension type to be superior for all vehicle designs and under all operating conditions.

The model indicates that, on average, the magnitude of dynamic tire forces produced by the truck with steel suspension is approximately 4 percent larger than the magnitude of dynamic tire forces generated by the truck with air suspension. However, upon more careful inspection of figure 8-4, it can be observed that the ratio of air to steel suspension DLC's in the lower range of DLC, roughly less than 0.15, is significantly smaller than in the higher range of DLC values, roughly greater than 0.15.

To verify this observation, the experimental data used to derive model 8.5 were divided into two sets. The first set included all data that resulted in values of steel suspension DLC being smaller than or equal to 0.15 and the other set included data with steel suspension DLC's greater than 0.15. Linear regression performed on the two sets of data produced the following models:

$$DLC_S = 1.18 \, DLC_A \qquad \qquad \text{(8-26)}$$

for DLC_S less than or equal to 0.15 and

$$DLC_S = 0.93 \, DLC_A \qquad \qquad \text{(8-27)}$$

for DLC_S greater than 0.15. This observation, which is considered to be one of the major findings of this study, clearly demonstrates that a statement that air suspension is 4 percent better than steel suspension, as indicated by equation 8-5, or even that air suspension is simply better than steel suspension, can be misleading. The benefits of replacing steel suspension with air suspension (in terms of the magnitude of dynamic tire forces) in the particular model of truck tested in this study would be very significant if the truck traveled mostly over relatively smooth pavements and/or at lower speeds so that the average value of DLC was less than 0.15. On the other hand, the superiority of air suspension over steel suspension would be considerably smaller or none at all if the truck traveled mostly on rough pavements and at relatively high speeds, thus generating DLC's higher than 0.15. It should also be added that there is nothing "magic" about the value of DLC being equal to 0.15, which was selected somewhat arbitrarily. The important conclusion from these considerations is that the effect of changing the truck suspension from steel to air will depend on the truck dynamics as well as on the conditions under which the truck will operate.

217

CHAPTER 9. SUMMARY AND CONCLUSIONS

The work conducted under this contract can be divided into three major areas:
(1) development of equipment necessary for conducting the testing program, (2)
performing the tests and collecting data, and (3) analysis and evaluation of the test
results.

The main efforts in the first area were directed toward the development of
efficient, reliable, and user-friendly equipment necessary for completion of an extensive
testing program outlined in the contractual statement of work. The three main pieces of
equipment used in the study were the servo-hydraulic road simulator DYNTRAC, a two-
axle truck, and a wheel-force transducer.

The DYNTRAC simulator was not operational when the project began, and a
major effort was devoted to making DYNTRAC operational and then improving its
performance to the level necessary for the accomplishment of the research objectives
of this study. The work conducted on the DYNTRAC included numerous modifications
of the existing mechanical, electrical, and hydraulic system components; rewriting of
large portions of the control code; evaluation and installation of wheel scales; design of
the longitudinal and lateral restraints; development of the new DAQ system; and tuning
of the servovalve-control system parameters for optimal performance of the hydraulic
actuators. The modified road simulator provided an excellent tool to study dynamic tire
forces. In simulating road profile inputs, the displacements of the actuators did not
follow the input road profiles exactly because of their inherent inertia, but the frequency
response characteristics of the actuators showed a fairly uniform magnitude over the
frequency range of 0 to 20 Hz, which is the primary range of dynamic truck tire forces.
Because of the uniform frequency response characteristics, no attempt was made to
use a remote parameter control algorithm in tests conducted on DYNTRAC.

The two-axle truck was instrumented with axle-strain gauges, accelerometers,
LVDT's, and an on-board computer DAQ system. The truck instrumentation allowed for
measurement of vertical tire forces as well as the truck's response to road profile inputs.
Furthermore, the vehicle's wheels were changed from cast spokes to disk wheels. The

Preceding page blank

truck's suspension was changed from steel-leaf spring to air suspension and then back to steel-leaf spring. Several mathematical models of truck dynamics were derived, and the values of the model parameters were determined either from direct measurements and/or from system identification for those parameters that were difficult to measure directly.

A new wheel-force transducer was designed. Four transducers were fabricated, tested, and delivered to the sponsor. The results of the tests showed good correlation between results of measurements obtained using the wheel-force transducers and results obtained with the axle-strain gauges. It has been demonstrated that the new wheel-force transducers provide a reliable and accurate tool for measuring DLC's. The performance of the transducers can be further improved by reducing or eliminating the effects of the bending moments, especially in tests conducted on dual tires.

The tests involving the two-axle truck were conducted on the road simulator, on three road sites in Virginia, and on the instrumented road section at the FHWA research facility in McLean, Virginia. In addition, three tire types were tested at the Goodyear Tire and Rubber Company. The test variables in the DYNTRAC tests involved suspension type, tire type, vehicle speed, road roughness, axle static load, and tire inflation pressure. A total of 564 combinations of test variables were used in the tests. Hundreds of additional tests were performed using step, sinusoidal, and white-noise inputs to evaluate the performance of DYNTRAC and to identify the parameters of the mathematical models of truck dynamics. The field tests on in-service roads in Virginia were conducted with only one tire type (standard radial dual tire) and one tire inflation pressure, with the latter variable found to have an insignificant effect on dynamic tire forces. The road tests were conducted for 76 combinations of the test variables, and two runs were made for each combination. An excellent agreement was found between the results of the replicate tests. In tire tests, tire-pavement net contact area, tire-pavement gross contact area, tire deflection versus load characteristic, and tire-pavement contact pressure distribution were measured for each of the three test tires: 11R22.5 standard radial dual tire, 295/75R22.5 low-profile dual tire, and 425/65R22.5 wide-base single tire.

The scope of tests conducted on the instrumented road section was very limited because of poor performance of the strain gauges that were installed in the test pavement prior to the beginning of this study. The supporting equipment and procedures for the instrumented road tests were developed, including an effective and highly repeatable triggering system for the computer data acquisition, synchronization of the vehicle and pavement DAQ systems, and accurate measurement of the vehicle position with respect to the location of the pavement strain gauges. All data collected in these tests were delivered to the project Contracting Officer's Technical Representative.

The data collected in the testing program were analyzed to determine the effects of the test variables on the magnitude of dynamic tire forces and to evaluate the pavement-damaging potential of the vehicle under different operational and design conditions. The dynamic tire forces were characterized by the DLC.

The test results demonstrated that the two dual tires generate essentially the same dynamic loads, whereas the single wide-base tire generates approximately 10 percent lower DLC's than either dual tire. The difference between dynamic loads produced by dual and single tires is caused primarily by the differences between their respective stiffnesses (single tires are approximately 30 percent softer than two dual tires).

Analysis of the effects of suspension type on dynamic tire forces revealed very interesting results. Air suspensions are generally considered to be more "road friendly" and to generate lower dynamic loads than steel suspensions. In this study, air suspension proved indeed to be superior to steel suspension, but only for those combinations of road roughness, vehicle speed, and other test variables for which the values of DLC with steel suspension were lower than 0.15. However, there were no benefits in terms of dynamic tire forces under the conditions that resulted in the steel suspension's DLC being greater than 0.15, which usually occurred at higher vehicle speeds and/or on high-roughness roads. As it was explained in detail in chapter 8, the main reason for this observation was the nonlinear friction between the leafs of the steel suspension. Because of this nonlinearity, the steel suspension's damping increases and its stiffness decreases, leading to higher DLC's, which improves the

221

dynamic performance of the steel suspension. This finding demonstrates that evaluating road friendliness of a suspension based on suspension design is, in principle, wrong. It also provides a strong argument for performance-based standards that should be used in determining vehicle potential for generating dynamic pavement loads. Furthermore, these results indicate that great care must be exercised in developing the appropriate test procedures necessary to evaluate road friendliness of truck suspensions because of their nonlinear characteristics. For example, the significance of test procedures using single-amplitude input test signals, including step and sinusoidal signals, would be very limited.

The analysis of the effects of other test variables revealed that the magnitude of dynamic tire forces is strongly affected by vehicle speed and road roughness and moderately affected by static axle load. Changes of tire inflation pressure within 25 percent of the manufacturer-recommended pressure were found to have a negligible effect on dynamic loads. Linear regression models were derived, providing a quantitative relationship between the test-truck DLC and the test variables. New sensitivity parameters were introduced as objective measures of influence of the test variables on dynamic tire forces.

The focus of this study was on the magnitude of dynamic tire forces applied by heavy vehicles to pavements. It is quite clear, however, that the magnitude of dynamic forces measured by DLC does not provide an adequate measure of a vehicle's pavement-damaging potential. Research on the development and validation of an accurate methodology for determining the effects of dynamic wheel forces on pavement whole-life performance is still under way. A theoretical framework for such a methodology was developed by Collop and Cebon in 1994.[39] It can be expected that the proposed methodology will be validated in the near future with the use of the experimental pavement performance data collected at the CAPTIF facility in New Zealand as part of the OECD DIVINE project and/or the data from the FHWA's Long Term Pavement Performance program. Until the new methodology is fully developed and validated, alternative approximate methods must be used. In this study, the Eisenmann's road stress factor was used to assess the truck's pavement-damaging

potential. On the basis of this approach, the pavement-damaging potential of the test vehicle was estimated to be 85 percent greater when wide-base single tires are used instead of dual tires. It should be noted, however, that in arriving at this conclusion, it was assumed (as is commonly assumed in most published research) that the distribution of the tire-pavement contact pressure is uniform over the entire contact area under both dual tires. Although it seems possible that there may be significant variations in the distribution of the dynamic load between the two dual tires, especially when the truck is traveling over a rough pavement, there are no experimental data available to verify the extent to which the assumption of uniform pressure distribution is correct. Furthermore, in evaluating pavement-damaging potential, it was found that air suspension would be expected to cause less pavement damage than steel suspension, but the magnitude of the improvement that can be contributed to the type of suspension varies considerably depending on whether dynamic wheel loads are assumed to be spatially repeatable (more significant improvement) or randomly distributed along the road (less significant improvement).

As pointed out earlier, a validated whole-life pavement performance model will be necessary to assess the impact of dynamic tire forces on pavement damage. The results of tests conducted in this study demonstrated that the magnitude of dynamic loading is significant in comparison to static loads applied by heavy vehicles to pavements. The standard deviation of the dynamic forces was up to 20 percent of the static load under typical vehicle and road conditions and much higher than 20 percent when the test vehicle was traveling at high speed on very rough roads. Since it has been established that dynamic loads are spatially repeatable, it is also relevant that the peak dynamic loads, measured in experiments conducted on in-service roads, exceeded the static loads by over 200 percent. It can thus be concluded that the dynamic tire forces constitute a significant factor contributing to pavement wear. Further research is needed to develop and validate a methodology that will allow for a quantitative assessment of the effects of both static and dynamic tire forces on pavement whole-life performance.

APPENDIX: OPERATIONAL PROCEDURES AND GUIDELINES FOR DYNTRAC SYSTEM AND ON-ROAD TESTING

The following document is a general manual for conducting vehicle research with the dynamic truck actuator (DYNTRAC) system and in-service road testing. This manual is not a substitute for manufacturer and vendor manuals of equipment associated with the project, or for established procedures for safety and the fundamentals of good test engineering. Research of this nature involves the operation of potentially dangerous equipment, so considerable planning and system checking should be undertaken before beginning testing.

OPERATION OF DYNTRAC

SYSTEM DESCRIPTION

The road simulator system, designated the Dynamic Truck Actuation system or DYNTRAC, is located at the Turner-Fairbank Highway Research Center (TFHRC) in McLean, Virginia. The simulator consists of a four-post servo-hydraulic system; position, acceleration, and force sensors with data acquisition (DAQ) system; and a control computer capable of inputting road profiles to the servo-hydraulic controllers. A drawing of the servohydraulic system is shown in figure 2-6.
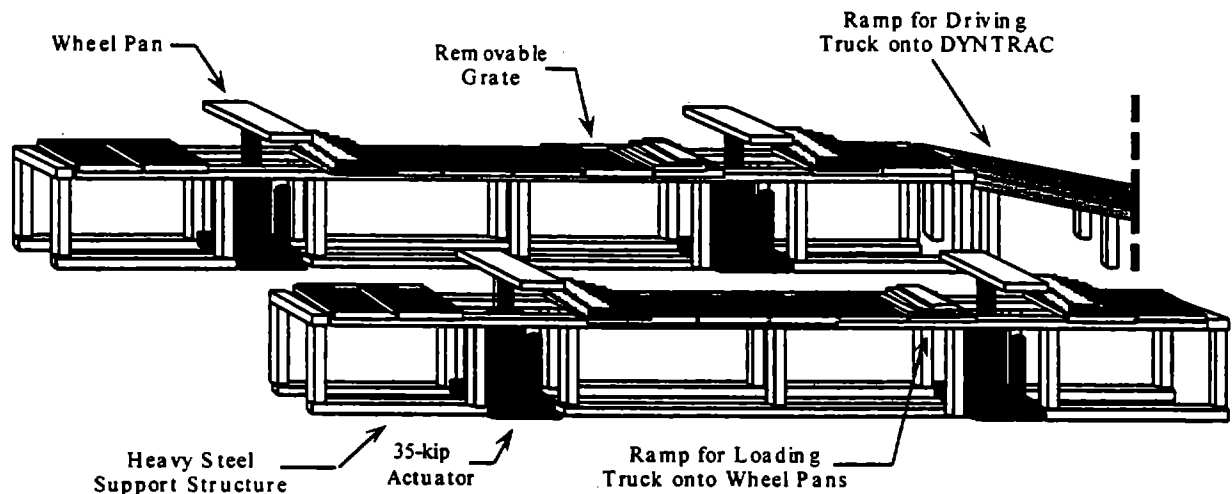
Figure 1. DYNTRAC system.

Mechanical And Servo-Hydraulic Systems

The mechanical systems include the steel frame and grate assembly that positions the truck over the actuators and supports the vehicle when not placed on the actuators. The frame is constructed in such a way that the actuators can be moved to accommodate several axle configurations. The frame was attached to the floor of the lab by rebar "bolts" that extended to the floor below the lab. Steel ramps are positioned in front of DYNTRAC by a forklift for placing and removing the vehicle. Wooden ramps

226

are also needed to step the vehicle up from the grates to the actuator wheel pans. The wheel pans, on which the wheels of the vehicle are positioned during testing, are connected to the pistons of the actuators. The wheel pans also serve as mounting points for the dynamic wheel scales and vehicle restraints.

Two different restraint systems were used to keep the vehicle properly positioned on the actuators. The original system's fore/aft restraint consisted of a heavy steel bracket bolted to the front of the front pans and to the rear of the rear pans. The bracket could then be adjusted to tire size and exact position of the wheel. The system's lateral restraint was a steel bracket bolted to the top surface of the wheel pan next to the vehicle's tire. This bracket interfered with the placement of dynamic-force scales on the pan. A new restraint system was implemented because of these problems as well as the need for force scales. Both systems work effectively in restraining a test vehicle.

The second system was designed and constructed, consisting of fore/aft restraints and lateral restraints. The fore/aft system was mainly made of aluminum and only required attachment to the rear pans. The restraint consisted of beams held in front and behind the rear wheels by a crossed linkage. The lateral restraint was a steel rod welded to a disk that was slid against the side of the tire. Two restraints were used for each wheel pan; the posts were held in place by brackets attached to the sides of the wheel pan.

The final restraint configuration was a combination of both systems. The second system's lateral restraint worked effectively and reduced the rotation of the pans. The mounting of the restraints also allowed the incorporation of a dynamic wheel scale into the wheel pan assembly. The fore/aft restraints from the second system occasionally struck the suspension/brake assembly of the vehicle during testing of the steel-suspension configuration. When the air suspension was introduced, it was not possible to use the new fore/aft restraint. The first system's fore/aft restraints were used to finish testing. The only remaining problem with the first system was that the heavy restraints often stripped out the threaded holes in the wheel pans.

The servo-hydraulic components of DYNTRAC were powered by hydraulic pumps located in the basement of the lab. The pumps supply hydraulic oil at 20,670 kPa to two hydraulic service manifolds, which filter and distribute fluid to the servovalves. The manifolds also help minimize pressure fluctuations in the fluid supply. Servovalves in each of the four actuators control the direction and amount of fluid to the actuators. Servovalves are controlled by electronic signals from the control console. The flow of oil into the actuator controls the movement of the piston in the actuator. The piston is attached to the wheel pan on which rests a wheel of the test vehicle.

The manifolds and actuators have nitrogen-filled accumulators that reduce pressure fluctuations and provide storage for pressurized fluid. The rear actuators also have a static support system that supports some of the weight of the vehicle during testing. The system uses a precharge of nitrogen gas to support the piston rod. All four actuators are 160-kN rated, with a 31.3-cm^2 piston area. The position of the piston rod is measured internally by a linear-variable displacement transducer (LVDT). The sensor signal is used in the control of the actuator and is recorded during testing as a measure of the actual profile input to the vehicle.

A road profile is simulated in this system through the control computer. The control computer sends an analog voltage signal representing the vertical profile of the road to the control console. The control console operates the servovalve on the basis of the computer input and operational settings from the console. The performance of each actuator is determined by a control loop that uses the piston's position and differential pressure as feedback signals to the controller. These settings can be used to tune the system's performance so that piston movement closely approximates profiles generated by the control computer. A flow chart of the operation of a single actuator is shown in figure 2-7. Figure 2-8 illustrates the performance of the left-rear actuator. The two signals shown in figure 2-8 are the road profile as generated by the control computer (actuator input) and the displacement of the actuator piston (actuator output). This test simulated a 48-km/h run over a medium-roughness road with an international road roughness index (IRI) of 2.6 mm/m. Ideally, the actuator output should be the same as the road profile.
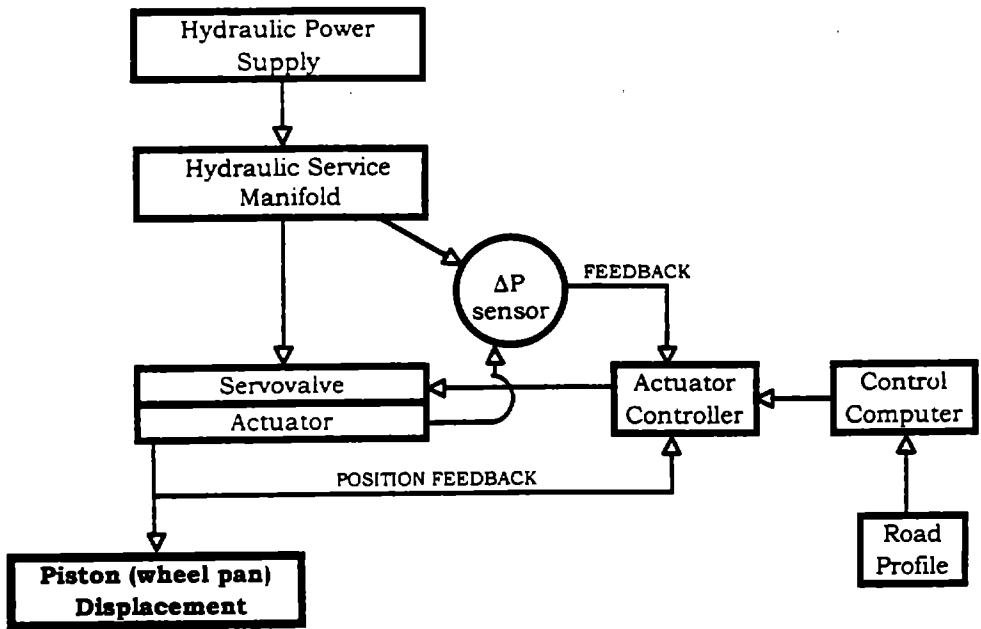
Figure 2. Flow chart of actuator control.
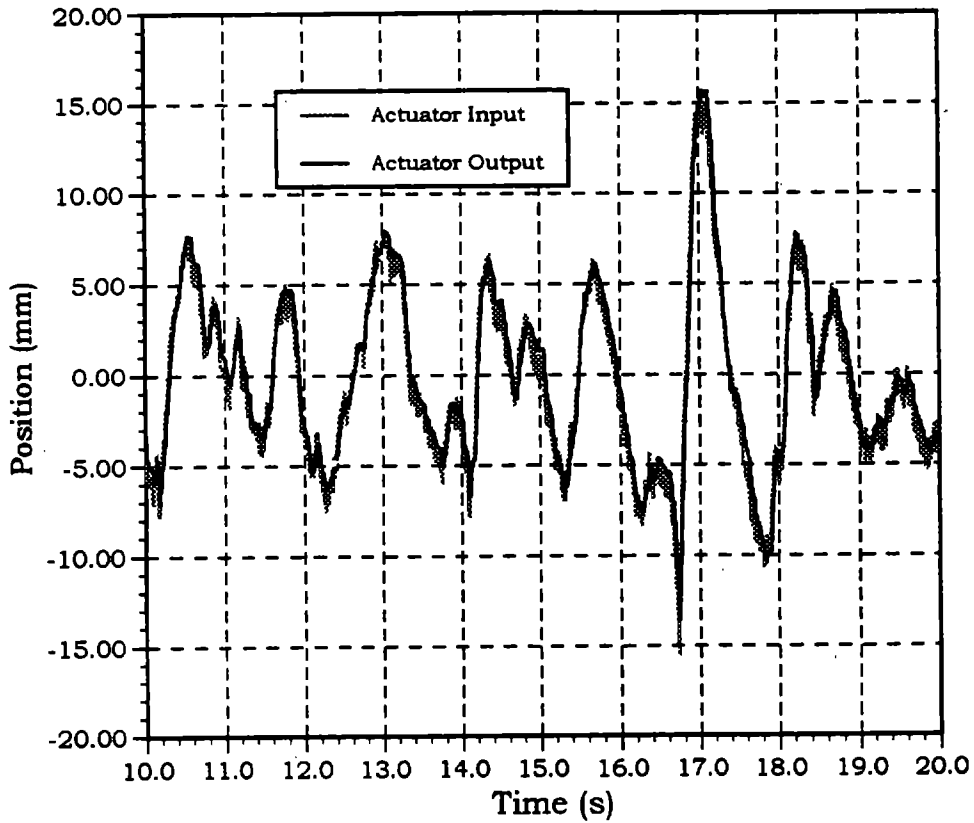
Figure 3. Actuator performance.

229

The control computer is a PC with a 386 processor; the computer's digital output is converted to analog voltages by a digital-to-analog output board installed in the computer's expansion slot. The analog signals then reach "sample and hold" circuit cards that make sure the signals for each actuator controller are synchronized. At this point, the actuator input signals are sampled by a DAQ system and are included with the test data.

SYSTEM PREPARATION

Check System Structure and Hydraulics

Check out the DYNTRAC structure and hydraulics. Check for the following:

- Hydraulic leaks around the actuators and hydraulic lines.

- Make sure at least 500 psi (3,450 kPa) of nitrogen pressure is available; check the tank gauge or the pressure in the control panel if the pressure valve is open.

- Rebar bolts that hold DYNTRAC to the floor are tight.

- Grates and ramps are properly positioned and secure.

- Wheel pans and wheel scales are securely fastened.

- Connections to actuator servovalves and LVDT's are tight.

- Cables to DYNTRAC and truck sensors are not being kinked or cut by surrounding machinery.

- Proper clearance for the movement of the wheel pans.

- Wheel pans are aligned properly.

- No equipment is stacked on DYNTRAC that may vibrate off.

Check Sensors and DAQ System

Check the sensors and DAQ system. A detailed description of the DAQ system and vehicle sensors is included in later sections of this document.

- Make sure scales are on, zeroed, and producing the proper output voltage.

- Check cable connections to sensors and DAQ system.

- Check the calibration values for the truck's axle-strain gauges. During loading and unloading of the test vehicle, monitor the output voltage of the axle-strain gauges. Use the axle-strain-gauge calibration values to calculate wheel force and compare with wheel-scale measurements. If these values deviate significantly, an equipment problem may exist, and new calibrations tests must be conducted for the axle-strain gauges.

- Make sure the channel designations in the computer match DYNTRAC and the truck's sensors.

- Make sure enough space is left on the computer's hard drive for test data.

Vehicle Checks and Preparations

- Make sure fuel tank is completely full.
- Determine whether the brakes should be on or off for testing.
- Make sure instrumentation in the cab is properly secured and the remote controls are working.
- Make sure any payload on the bed of the truck is secured.

Startup of Hydraulics and Warmup of the System

The hydraulic pump must be operational for testing to begin. The pump used was associated with the Structures Lab of TFHRC, and its operation is not part of the manual. It should be noted that the valves are easier to open with the pump off.

1. Open up nitrogen system and set pressure to 400 psi (2,760 kPa). This is accomplished by opening the valves to the actuators (channels 1 and 2) and from the tank, making sure the vent valve is closed (shut-off), and adjusting the control knob until 400 psi (2,760 kPa) is indicated on the regulated

pressure gauge. If a loud hissing sound is heard, the vent valves are still open and must be closed.

2. Open hydraulic lines to DYNTRAC (alert structure personnel).

3. Turn on the hydraulic pump.

4. Power up the MTS Systems Corp. control console by turning on the red toggle switch. The switch is located on the left side of the console underneath the control panels.

5. Verify that the truck is properly secured on DYNTRAC. The full footprint of the tires must be located on the wheel scales. Fore/aft restraints must be secured; make sure bolts are tight and are not stripped out. Lateral restraints must be secured in their brackets and located within 0.5 in (1.27 cm) of the tire. The use of nonpetroleum-based lubricant on the face of the restraint is recommended. Verify that the bolts in the lateral restraint brackets are tight and are not stripped.

6. Press RESET and then ENTER on the master control section of the MTS controller (see figure 4).

7. Press DISPLAY SELECT next to the right-front controller, below the master controls.

8. Bring the system up to pressure. Press the LOW PRESSURE button, pause five seconds, then press the HIGH PRESSURE button.

MTS Control Panel

Master Controls		Right Rear	Left Rear
	Master Span Master Set Pnt.	Right Front	Left Front

Figure 4. Layout of MTS Controller.

232

9. Power up the control computer and run the desired DYNTRAC control program. DYN7.EXE (located in the DYNTRAC directory) is used for road simulation testing. More instructions for the program are included in a later section of this document.

10. Bring the actuators up to their zero point. Press and hold the master set point control (up arrows) until the actuators reach their zero point, which is $z = 3$ in. Make sure all of the actuators are level and responded to the set point command. Also press and hold the up arrows for the master span setting.

11. Warm up the system. Select program source to INTERNAL on the MTS controller. Verify that the amplitude and frequency controls of the function generator on top of the console have been turned all the way down. Press the RUN button on the master controls, turn on the power to the generator, and select the sine function and a frequency between 0.5 and 1 Hz. Slowly turn up the amplitude until the actuators are traveling about 3-4 in (7.62-10.16 cm). The truck should be slowly rising and falling with no jerking or loud noises. Run the system under this input for at least 15 min.

12. Use this warmup test to check sensor and DAQ system performance, verify experimental setup, and to log the settings of the controller.

13. After the warmup period, turn down the amplitude of the signal generator and press the STOP button.

14. If testing is to be conducted using the DYNTRAC control computer, change the program source to EXTERNAL and remember to press the RUN button before beginning the actual test.

Data Recording and Experimental Setup

An accurate recording of the settings, sensor information, test conditions, actions, and problems encountered is essential to conducting repeatable simulations and collecting viable data. These are some of the items that should be recorded:

- Any new sensors, their location, serial number, and calibration factors.

- Any changes to the electrical systems of DYNTRAC or the instrumentation.

- All settings to the conditioners and power sources for the instrumentation.

- All settings on the MTS controller console.

- Special conditions of DYNTRAC such as pump status and nitrogen pressure.

- Version of DYNTRAC control program and names of profiles used or settings of function generator used (also note the model of generator).

- The instrumented truck's configuration including tire type and tire pressure.

- The static readings of the DYNTRAC scales and truck LVDT's.

- The loading configuration of the truck and the speed of the profile.

- The sampling rate of the DAQ system, the length of the test, and the signals sampled and which channel they are stored in.

- The file name of the recorded data and the information pertinent to that test.

- Any problems encountered or nonstandard actions.

OPERATION OF THE SIMULATOR

Notices

> This system has high voltage lines, 3,000 psi hydraulic lines, and heavy equipment moving at extremely high speeds.
> EXERCISE MAXIMUM CAUTION AT ALL TIMES!

Do not stand near DYNTRAC while it is operation.

Do not leave the MTS controller while RUN button is on.

Do not exit the DYNTRAC program while MTS controller is in RUN mode.

Any changes to the MTS controls during a simulation can possibly cause a dangerous response from the actuators.

Do not touch/adjust DYNTRAC's actuator control lines or attempt any other maintenance without lowering the wheel pans and turning the pressure from HIGH to LOW to OFF.

Use ladders/platforms to climb onto DYNTRAC and the vehicle, and proceed carefully. Thin layers of oil can be deposited on most surfaces making them extremely slippery.

Control

There are three source of control for the actuators of DYNTRAC: manual controls, control computer, and signal generator. The startup of the system has already been detailed in the preparation portion of the manual.

When changing settings of the signal generator or changing control programs on the computer, make sure the MTS controller mode has been changed to STOP.

Manual Controls

Refer to MTS Reference and Operational Manuals for a complete description of the hydraulic components and controllers. This section will only provide an overview of the use of the controls; operators of DYNTRAC should have access to these manuals and should have read at least the Operations Manual. Figure 5 shows the layout of the controls for DYNTRAC; more complete diagrams and pictures can be found in the MTS manuals.

MTS Control Panel

Master Controls		Right Rear	Left Rear
	Master Span Master Set Pnt.	Right Front	Left Front

Figure 5. Layout of DYNTRAC manual controls.

As mentioned in the startup procedure, after turning on power to the console, press the RESET and ENTER buttons on the MTS Microconsole. Complete the remaining steps in the startup procedure. Display and control options must be set for each actuator. Since the actuators' position is controlled through the actuator LVDT's, the AC controller is used. Activate the AC controllers by pressing and holding the CONTROL TRANSFER ENABLE button on the Microconsole and press the CONTROL button located on the top of each actuator's AC controller. The ACT light should be on for each AC controller. Also make sure DISPLAY is selected for each AC controller. If any problems are encountered, refer to the appropriate sections of the MTS manuals.

The control settings on each AC controller are listed in table 1. The only control that will move the actuator is SET POINT. This positions the zero point of the actuator. It is normally set at 5. The actuator moves ±76.2 mm (3 in) about this point. Use this control to level the vehicle or move an individual wheel pan without affecting the other three. Remember that the actuator moves about the set point; improper setting of this control could result in the actuator striking its limits during a simulation.

Table 1. Actuator controls.

Control	Description
Set Point	Controls the static, mean level offset to the actuator. It can also be used to manually raise & lower the actuators.
Span	Determines the amplitude of the actuator's output with respect to the dynamic input (0 - 100% scale).
Gain	Adjusts the forward gain of the servo control loop.
ΔP	Controls amount of control signal correction relative to the differential pressure in the actuator.
Rate	Adjusts the level of the first derivative of the feedback signal.
Controller Card	Contains potentiometers for gain, symmetry, and phase of transducer output (adjusted by manufacturer representative only).

The remaining controls deal with the dynamic performance of the actuators. These are used to "tune" the actuators for better response. This should be done periodically; the MTS manuals describe the process in detail.

Computer Control

A computer program is used to simulate road profiles. The input for the program is an ASCII file containing a header and a two-column matrix of road elevations. The header contains information such the distance between elevation measurements, measurement units, and the length of the matrix. The user specifies the following information:

- Road profile.
- Number of times the profile is to be run.
- Speed simulated.
- Gain setting for output.
- Vehicle wheelbase.
- Profile roll and step limits.

The computer will check the profile so that it does not exceed actuator capabilities and the roll and step limits specified. A step limit makes sure the

237

profile does not have a sudden change elevation over a certain tolerance. The roll limit ensures there are no significant differences between left- and right-track elevations at any given time. The computer will then convert the distance-based input into time-based input for the actuators on the basis of speed and wheelbase settings.

After booting up the control computer, change to the DYNTRAC directory. The current simulation control program is DYN7.EXE. Upon running, a warning will display to make sure the hydraulics have been initiated before beginning the program. Enter the filename for the profile to be simulated (usually ending with .PRO), number of times the profile is to be run, the speed simulated, gain, and wheelbase of the test vehicle. Press ENTER on the keyboard, and the profile will be read into memory and checked for any roll or step errors. At this point the simulation is ready to run. Perform the following steps:

1. Check to make sure the DYNTRAC area is clear of people and the startup procedures have been followed.

2. Verify that the DAQ system is ready to capture data. Current data acquisition setup uses a digital trigger line to start acquisition.

3. Check the following settings on the MTS controller: Hydraulic Pressure - HIGH, Program/Record - RUN, and Program Source - EXTERNAL.

4. VISUALLY CHECK AGAIN THAT THE AREA IS CLEAR.

5. Press ENTER on the keyboard again to start the simulation. Escape will abort the run.

The computer program will then send control commands to the MTS controller. Once the end of the profile is reached, the actuators will return to the set point. If more than one iteration of the profile was selected, the profile will now run again. This loop will continue as required, pausing between to reset the actuator position.

Input profiles are also in the DYNTRAC/PROFILE directory. DYNTRAC-ready profiles have filenames that end with ".PRO" and are text files. These files can be easily opened and altered using any DOS editor program. New profiles can be made

238

by observing the header information in the existing profiles and providing similar info for the new profile. Make sure the length of the profile and spacing of the data points is correctly indicated. A list of profiles used in this project is listed in chapter 3.

There are several other control programs in the DYNTRAC directory; their names and functions are listed in table 2.

Table 2. DYNTRAC computer control programs.

File name	Function
DYN7.EXE	Road simulation.
DYNSTEP.EXE	Sends a step signal to the actuators, user in-puts the size of the step.
STEPTRIG.EXE	Same as above plus a digital signal is sent to trigger a DAQ system.
SMOOTH.EXE	Program will slowly move the actuators to the desired position.
DYNWN.EXE	Similar to DYN7, except no delay is used between front and back actuators, this program is for random noise input profiles WN50.PRO and WN25.PRO

Signal Generator

The operation of the signal generator was detailed in the startup procedures.

System Checks and Shutdown

When testing involves hours of operation, perform periodic inspections of the system. The vibrations, movements of the vehicle, and large dynamic loads can be a potential source of failure for the vehicle, DYNTRAC, or the sensors. After a defined interval of testing, press the STOP button on the microcontroller and physically check the following:

- Inspect the vehicle restraints for any loosening, stripping, or other failures.

- Check that the payload restraints are secure.

- Make sure the wheel pans have not rotated underneath the wheels. A crane or axle-stand can be used to hold up the truck while the rotated pan is lowered with the SET POINT controller. The pan can then be righted and returned to its proper position.

239

- Vehicle DAQ system and sensor electrons are still secured and operating properly.

- Hydraulic lines and actuators show no signs of leaking or excessive wear.

- Verify sensor operation by viewing data recorded from a recent test.

- Check the nitrogen supply pressure.

This time is also a good opportunity to convert and backup test data.

When testing is finished for the day, DYNTRAC and supporting systems should be powered down and returned to a safe position. This includes lowering the actuators, shutting off the hydraulic pressure, closing the proper valves, and powering down the control and DAQ computers.

1. Press the STOP button on the MTS Microcontroller.

2. Press and briefly hold the down arrows on the master setpoint controller; the actuators should lower to their bottom position.

3. Press the LOW hydraulic pressure control, pause for 5 to 10 s, then press the OFF button.

4. Turn off the power toggle switch on the MTS cabinet.

5. Exit the DYNTRAC control program if used and turn off the control computer.

6. Exit the DAQ program and power down the DAQ computer. Perform data backups if necessary.

7. Close the valves that supply hydraulic fluid to DYNTRAC. They are located in the basement.

VEHICLE SENSORS AND DATA ACQUISITION

The following sections describe the equipment and procedures used to instrument and conduct tests with the FHWA two-axle truck. Since DYNTRAC does not necessarily require this truck for testing, and the instrumentation and configuration of the truck itself have changed, the information presented here should be considered a guide or an example of how to conduct similar research.

VEHICLE SENSORS

The test vehicle was instrumented with various sensors to measure dynamic wheel forces through sensing axle strain, axle acceleration, truck chassis acceleration, and suspension deflection. Sensor power supply, conditioning, and data acquisition equipment was placed in the cab of the truck. Data acquisition was accomplished with a portable computer with a 48-channel analog input board and data acquisition program by Intelligent Instrumentation.

The typical sensor configuration used during tests included the following sensors:

- Half-bridge strain-gauge circuits placed at the end of each axle.

- Accelerometers located at the end of each axle.

- LVDT's measuring the distance between the end of each axle and the body of the truck.

- Accelerometers mounted under each corner and the center of the truck bed.

- Thermally isolated accelerometer mounted on the right end of the rear axle.

The axle instrumentation is shown in figures 2-2 and 2-3. An infrared emitter-receiver sensor was also used during field tests for position and velocity measurement.

241
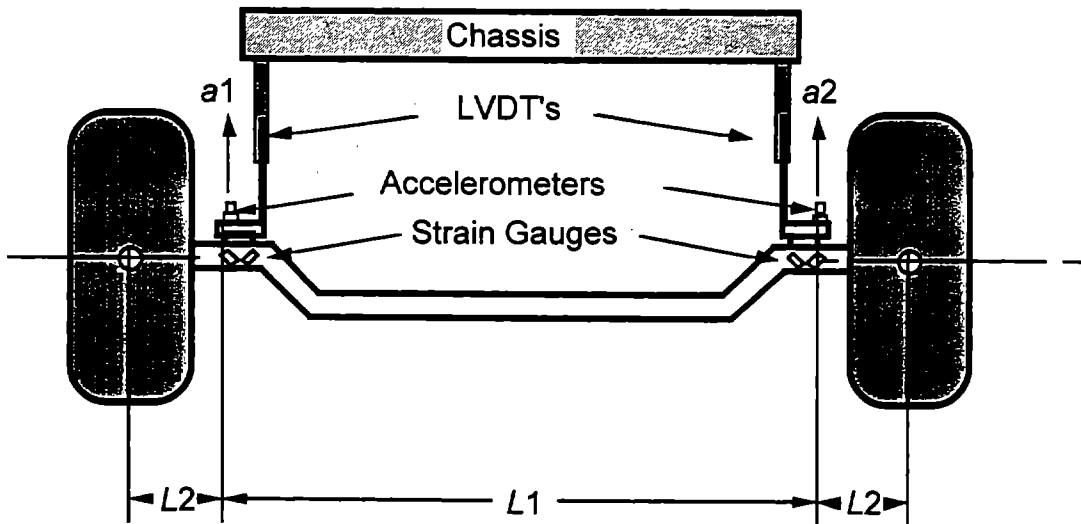
Figure 6. Front-axle instrumentation.
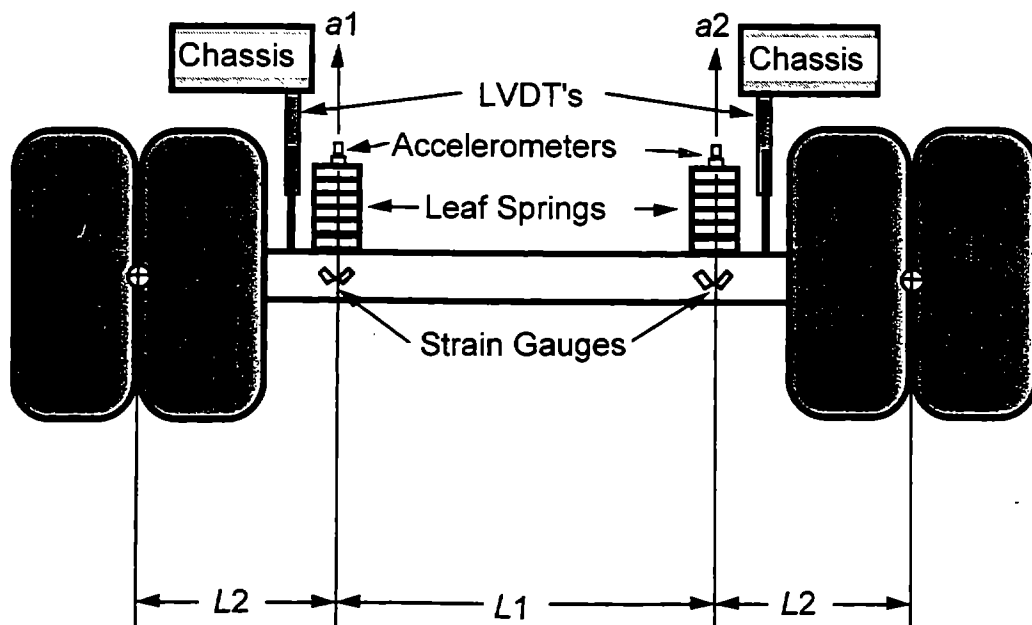
Figure 7. Rear-axle instrumentation.

Typical static strain-gauge calibrations are shown in figures 8 and 9. These calibrations changed throughout the testing program because of changes in strain-gauge conditioning equipment and the replacement of the rear-axle gauges after the suspension was changed. Calibration values for other vehicle sensors are shown in table 3.

Table 3. Vehicle-sensor calibrations.

Sensor Type	Calibration Value	Output Units	Notes
Piezo Crystal Accelerometer	90 mV/g	g's	1 g = 9.81 m/s²
Linear-Variable Differential Transducer (LVDT)	25.4 mm/V	Millimeters	Position measurement
Strain Gauges arranged to measure shear	see figures 2-5 and 2-6	Newtons	for wheel force, outboard mass inertia must be added
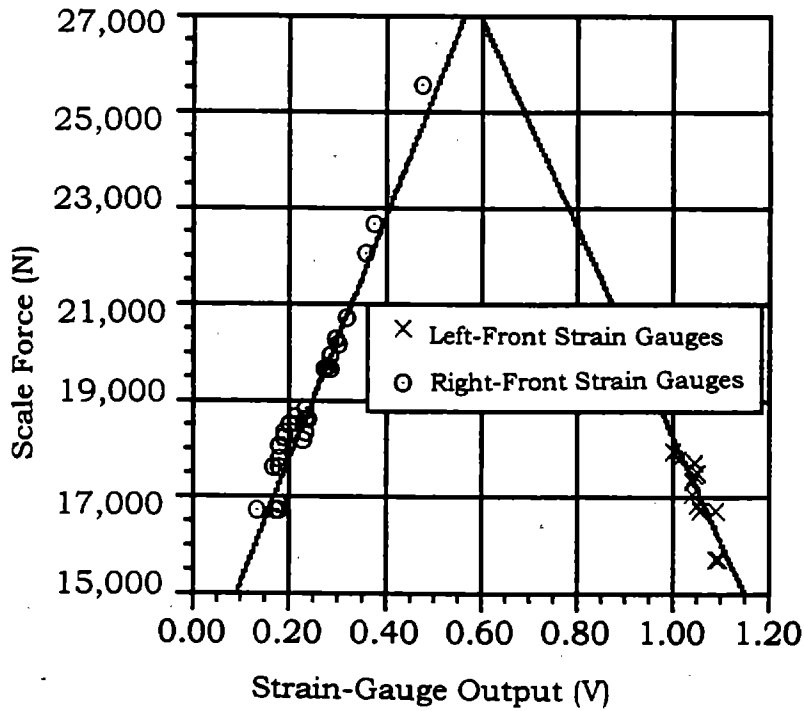
Figure 8. Front-axle strain-gauge calibration.
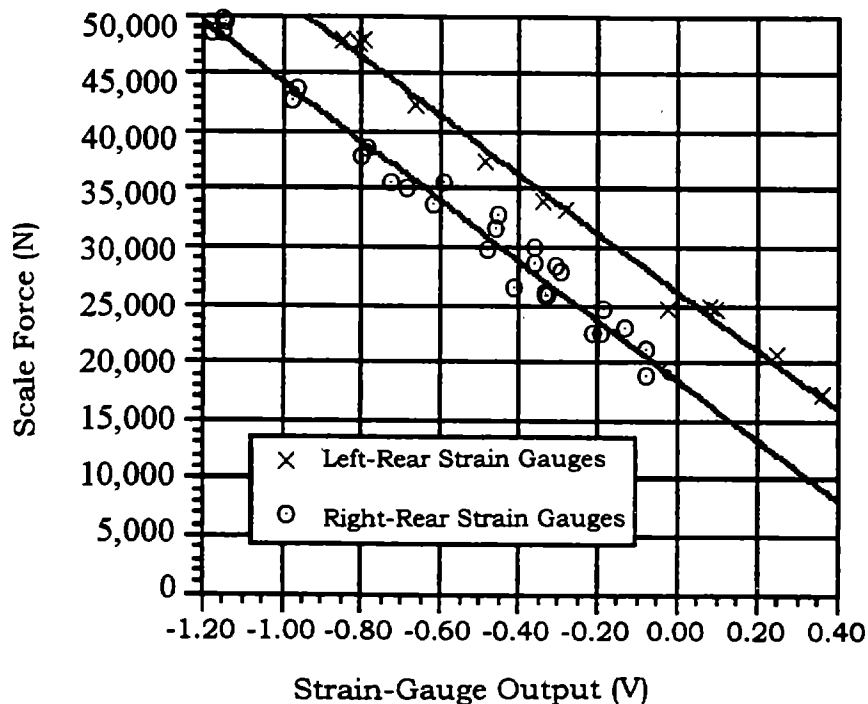
Figure 9. Rear-axle strain-gauge calibration.

Dynamic wheel forces were measured by combining the dynamic strain of the axle and the inertial load of the mass outboard of the axle. Strain gauges are bonded near the ends of the front and rear axles. The gauges are oriented to measure the shearing strain in the axle. These gauges only measure the axle strain at the gauge location; any force generated outside the gauges must be measured by other means. Since the vehicle weight is transferred to the suspension "before" the axle-strain gauge location, only the inertial effects of the outboard mass should be considered. This outboard mass consists of a portion of the axle, the brake drum, wheel assembly, and tires. These inertial forces can be calculated using the outboard mass and the acceleration of the outboard mass.

Outboard mass acceleration can be determined with axle accelerations measured by the two accelerometers combined with kinematic analysis of the rigid axle. To illustrate this process, consider the front-axle assembly in figure 2-2. Because of the assembly of the truck wheel, the center of gravity (c.g.) of the outboard mass can be considered the center of the tire. The distance between the tire c.g. and strain

244

gauge/accelerometer location is $L2$, and the distance between accelerometers is $L1$. The signal from the left accelerometer is $a1$ and the right is $a2$.

Two calculations must be performed to determine the left-outboard mass acceleration from the given data. The c.g. acceleration can be separated into the relative acceleration between the c.g. position and the right accelerometer, and the absolute acceleration of the axle based on the right accelerometer. The relative acceleration is determined by subtracting the two acceleration signals and projecting the acceleration to the c.g. position. The left-outboard mass or left-wheel acceleration is determined by the following equation:

$$a_{wheel} = a2 + \tfrac{L1+L2}{L1} \cdot (a1 - a2) \tag{2-1}$$

The force from the outboard mass is then simply the mass times the wheel acceleration. That force is then added to the force measured by the axle-strain gauges to get the total dynamic wheel force.

OPERATION OF VEHICLE DATA ACQUISITION SYSTEM

Introduction

It is hoped this guide will provide the basic information needed to use the Dolch and ChartStream for data acquisition. This guide is oriented toward data acquisition for vehicle dynamics, specifically DYNTRAC tests and on-road tests.

The guide will cover two configurations provided and a simple guide to creating customized configurations. The guide will also briefly describe the hardware needed for data acquisition. Help messages are available on-line for most ChartStream screens. To further understand ChartStream, see the ChartStream manual (a large, red Intelligent Instrumentation binder).

For detailed information or assistance, call Intelligent Instrumentation at 1-(800) 685-9911. The serial number for the program is 935S196. It was purchased by Robert

Wollyung through the Vehicle Forces Program at The Pennsylvania Transportation Institute.

Hardware Information

The Dolch computer is outfitted with an Intelligent Instrumentation 16-channel data acquisition (DA) board (PCI-20098C-2) with a 32-channel expander (PCI-20031M-1). This provides 48 channels of analog input. Input cards are provided with screw terminals and are connected to the Dolch via ribbon cables.

The ribbon connection for channels 0 through 15 is connected to the small external port connector on the left side of the Dolch. The ribbon for channels 16 through 31 should already be connected to internal connection on the Intelligent Instruments card in connector labeled P2 slot. The cable should be extending out of an open expansion slot. An additional cable can be internally connected to the P3 slot for channels 32 through 47. Connecting these cables internally should be done with great care. Damage can be done to the computer or the expansion cards during cable installation either through physical damage or electrical damage through static electricity. Internal connections should be made only once; the cables should be left attached to the DA board because frequent contact with the expansion cards will increase the chance of permanent damage.

Individual sets of analog channels can be selected by ChartStream for monitoring. Any channel monitored that do not carry a signal should be grounded to itself. Cross-talk can be seen between channels that carry a signal and empty channels. This cross-talk is eliminated when empty channels are grounded out or removed from the data acquisition program setup.

Software Introduction

The ChartStream program is separated into two main sections: Data Acquisition and Data Analysis. These two sections can be treated as independent programs.

The first step in using ChartStream for data acquisition is to configure a test setup. This test setup tells the computer and the DA board what channels are being

246

sampled, the gain and sampling rate settings, and other software-triggered options of the DA board. The setup determines how the real-time data are displayed and how data acquisition is triggered. The test setup can also create calculated values from the data or generate values from a look-up table. These values would be included in the stored raw data.

Acquiring the data is simply done by recalling the desired test setup, manually starting or triggering the data acquisition, and then ending the acquisition. You are then asked if you wish to keep the data and then if you wish to convert the direct-memory-access- (DMA-) saved data to ChartStream data now or at a later time.

The data can then be displayed in great detail using the data analysis section. Data can be plotted using strip charts or plots. Calculations can be done with the data and plotted. In this section, the ChartStream data can be exported in ASCII format.

The other sections of ChartStream include DOS utilities, calculation and table libraries, troubleshooting, and modifying other program settings.

The operation of the software is explained in this manual for three different conditions. The first section will deal with a setup already created for the sensors on the FHWA flat-bed truck. The second section will also be for a predetermined setup; the channels are configured for the FHWA truck on the DYNTRAC system. The last section will give a brief and simplified description of how to configure test setups.

Vehicle Setup Data Acquisition

The FHWA truck setup is already configured for the four-axle strain gauges, the axle LVDT's and accelerometers, the chassis accelerometers, and one wheel-force transducer. The gains are set at unity; the sampling frequency is set at 250 Hz. The data triggering is set for manual (keyboard). The channel assignments are as follows:

Channel No.	Card & Chn. No.	Sensor	Channel No.	Card & Chn. No.	Sensor
0	Card 1: 0	LF-Axle Strain Gauge	10	Card 1: 10	RF-Axle LVDT
1	Card 1: 1	LR-Axle Strain Gauge	11	Card 1: 11	RR-Axle LVDT
2	Card 1: 2	RF-Axle Strain Gauge	12	Card 1: 12	LF-Chassis Accel.
3	Card 1: 3	RR-Axle Strain Gauge	13	Card 1: 13	LR-Chassis Accel.
4	Card 1: 4	LF-Axle Accelerom.	14	Card 1: 14	RF-Chassis Accel.
5	Card 1: 5	LR-Axle Accelerom.	15	Card 1: 15	RR-Chassis Accel.
6	Card 1: 6	RF-Axle Accelerom.	16	Card 2: 0	Center-Chassis Acc
7	Card 1: 7	RR-Axle Accelerom.	17	Card 2: 1	WFT Bridge A
8	Card 1: 8	LF-Axle LVDT	18	Card 2: 2	WFT Bridge B
9	Card 1: 9	LR-Axle LVDT	19	Card 2: 3	WFT Accelerometer
			20	Card 2: 4	WFT Resolver

Procedure

1. Connect cables to computer, and cards to the cables.

2. Connect sensors to the cards according to the channel assignment table for the Truck Setup.

3. Connect the mouse to the Dolch.

4. Boot up the Dolch computer; if the magneto-optical drive is to be used, boot it up first.

5. Change to the ChartStream directory by typing: **cd CHRTSTRM** <return> at the C: prompt.

6. Start the ChartStream program by typing: **CSR** <return> at the prompt.

7. Select Acquire Data.

8. Select Test Setup: TRUCK.SET.

9. You may use the predefined Real-Time Display setup or modify it at this time.

10. The data collected will be saved as TRUCK.DAT; if this file already exists, the program will ask you to overwrite or rename the setup. Rename the setup to suit your needs. The setup will need to be renamed each time you collect data unless you rename the data file after data acquisition.

11. After taking care of how the data are to be saved, the real-time display graphs should begin. The graphs are displaying the signals, but they are not being saved to disk.

12. Check signals by looking at real-time graphs or tabular display and check to make sure the correct sampling frequency is active (see Real-Time Display Guide).

13. Data acquisition that is saved to disk is started by pressing **F4**.

14. Stop data acquisition by pressing **F10**.

15. You will be asked if you wish to save the data.

16. If you want the data saved, it will then ask if you want the DMA file converted to ChartStream format now or at a later date. It is usually best to convert it now; the process does not take long.

17. The data can now be loaded and displayed in the ChartStream Analyzer package. The data can also be converted to ASCII at this time using ChartStream Analyzer.

DYNTRAC Setup Data Acquisition

This setup is designed for use with the FHWA truck and the DYNTRAC system located at the Turner-Fairbank Highway Research Center. Data are collected from both the vehicle and the shaker system. The channel locations are the same as for the truck setup, with more channels added. The additional channels are for the Intercomp dynamic wheel scales and the actuator LVDT's. A digital 1 trigger will be used to start and stop data acquisition. The channel assignments are as follows:

Channel No.	Card & Chn. No.	Sensor	Channel No.	Card & Chn. No.	Sensor
0	Card 1: 0	LF-Axle Strain Gauge	15	Card 1: 15	RR-Chassis Accel
1	Card 1: 1	LR-Axle Strain Gauge	16	Card 2: 0	Center Chassis Acc
2	Card 1: 2	RF-Axle Strain Gauge	17	Card 2: 1	WFT Bridge A
3	Card 1: 3	RR-Axle Strain Gauge	18	Card 2: 2	WFT Bridge B
4	Card 1: 4	LF-Axle Accelerom.	19	Card 2: 3	WFT Accelerometer
5	Card 1: 5	LR-Axle Accelerom.	20	Card 2: 4	WFT Resolver
6	Card 1: 6	RF-Axle Accelerom.	21	Card 2: 5	LF-Intercomp Scale
7	Card 1: 7	RR-Axle Accelerom.	22	Card 2: 6	LR-Intercomp Scale
8	Card 1: 8	LF-Axle LVDT	23	Card 2: 7	RF-Intercomp Scale
9	Card 1: 9	LR-Axle LVDT	24	Card 2: 8	RR-Intercomp Scale
10	Card 1: 10	RF-Axle LVDT	25	Card 2: 9	LF-Actuator LVDT
11	Card 1: 11	RR-Axle LVDT	26	Card 2: 10	LR-Actuator LVDT
12	Card 1: 12	LF-Chassis Accel.	27	Card 2: 11	RF-Actuator LVDT
13	Card 1: 13	LR-Chassis Accel.	28	Card 2: 12	RR-Actuator LVDT
14	Card 1: 14	RF-Chassis Accel.			

Procedure:

1. Connect cables to computer, and cards to the cables.

2. Connect sensors to the cards according to the channel assignment table for the DYNTRAC Setup.

3. Connect the mouse to the Dolch.

4. Boot up the Dolch computer; if the optical drive is to be used, boot it up first.

5. Change to the ChartStream directory by typing: **cd CHRTSTRM** <return> at the C: prompt.

6. Start the ChartStream program by typing: **CSR** <return> at the prompt.

7. Select Acquire Data.

8. Select Test Setup: DYNTRAC.SET.

9. You may use the predefined Real-Time Display setup or modify it at this time.

10. The data collected will be saved as DYN.DAT; if this file already exists, the program will ask you to overwrite or rename the setup. Rename the setup to suit your needs. The setup will need to be renamed each time you collect data unless you rename the data file after data acquisition.

11. After taking care of how the data are to be saved, the real-time display graphs should begin. The graphs are displaying the signals, but they are not being saved to disk.

12. Check signals by looking at real-time graphs or tabular display and check to make sure the correct sampling frequency is active (see Real-Time Display Guide).

13. Data acquisition will be started when the DYNTRAC control computer sends a high value through the Digital 1 channel.

14. Data acquisition ends when the digital trigger changes to the LOW voltage or when **F10** is pressed.

15. You will be asked if you wish to save the data.

16. If you want the data saved, it will then ask if you want the DMA file converted to ChartStream format now or at a later date. It is usually best to convert it now; the process does not take long.
Note: Pay careful attention to the remaining disk space before running tests, a full or near-full hard drive will severely hamper data acquisition and could result in a crash. Use the magneto-optical drive as the data file directory or copy completed test runs to the magneto-optical drive to clear up space on the internal hard drive.

17. The data can now be loaded and displayed in the ChartStream Analyzer package. The data can also be converted to ASCII at this time using ChartStream Analyzer.

18. When many test runs are to be done and ASCII files are the desired end result, there is no easy and efficient way to do it. You have two options:
Option 1: Convert the current file to ASCII before moving on to the next test. This slows down the speed of running through test iterations and increases the disk space needed, but the data are immediately available for processing.
Option 2: Convert the ChartStream data files after testing. This is done

251

manually; depending on the amount of files, this process will be boring and time-consuming.

Real-Time Display Guide

The date and time are displayed at the bottom of the screen. When data are being stored, time elapsed and time remaining are also displayed at the bottom of the screen.

You can change through the real-time displays by holding down the **alt** key and pressing a function key. **F1** is for screen 1, **F2** is for screen 2 , etc. You can change to a tabular display by pressing **F1**. If the data sampling speed is too high or there are memory constraints the display may remain on tabular.

F3 will clear the real-time displays. **F4** begins actual data acquisition. **F5** will set a new sampling frequency, and **F6** will tell the computer to begin sampling at the new frequency. **F10** will exit out of the data acquisition.

F2 will exit from real-time display and enter the Real-Time Setup Screen. Options can be changed by selecting the parameter by clicking on the item with the mouse and entering the new setting. Check boxes can be turned on and off by clicking on them.

The Screen is divided into four sections: Data File Information, Operation Options, Real-Time Display Options, and Scanrate Settings. At the bottom of the screen are directions for help, canceling the action, and continue, which will return you to data acquisition.

Note: If the real-time display is modified after starting with the selection of Acquire Data, changes made will not be saved to the setup. Modifications to the real-time display will be saved during the Create Test Setup process, provided the changes are saved using the save setup menu.

Data File Information:

Saving raw data to disk is the normal setting. Using memory will improve recording performance and display speed. Data file directories are specified; raw files

252

are not available if raw data are saved to memory. The remaining options are for splitting large amounts of raw data into multiple files. This option is mainly for very long data acquisition times.

Operation Options:

These settings are for controlling the triggering options of ChartStream.

- MANUAL: indicates keyboard triggering of data storage.

- EVENT: ChartStream continually overwrites data until a specified trigger or event occurs that would stop data acquisition. The amount of data stored before the event is specified by the "Pre-Trigger Data Amount." Use the mouse or keyboard arrow keys to select the channel to monitor for the event. The value of the trigger is specified by the "Stop Trig" field.

- AUTO: This is similar to the EVENT mode except that a starting trigger is specified as well as a stopping trigger.

NOTE: For the triggering to work effectively, the trigger signal and/or trigger signal value must last at least on sample time. For example, if the scan rate is 200 Hz, the trigger signal must last at least 1/200th of a second.

Real-Time Display Options:

This section controls the graphics available to the operator during data acquisition. The first option turns real-time display on/off. The second option determines how and when the strip charts are cleared to display more data. The rest of the options control the 10 graphic pages that can be accessed by holding down the **alt** key and pressing the appropriate function key.

The check boxes following the page number indicate the type of graphs that will be displayed on the page. The check boxes can be checked or unchecked by the mouse. Selecting a data page and pressing **F5** will allow the user to select the channels to be graphed and the plotting limits. For plots, the axes are picked by selecting the parameters from the list at the top of the screen. For strip charts, the x-axis is already time, so only the y axes need to be selected. If the automatic scales are not adequate, they can be manually controlled on this screen.

253

Scanrate Settings:

The initial scanrate is specified on the first line; this is your desired scanrate for the test. The Autorate fields are for using trigger values to change the sampling rate. Alternate scanrates can be also specified, so the scanrate can be changed during data acquisition.

Creating New Setups

This section of the manual will give a brief description of how to develop a simple setup and will describe many of the features available. A more complete understanding of all the options and features that can be used in making a setup is best acquired through reading the manual and experimenting with the program.

Creating a Setup:

Select "Create a Test Setup" from the main menu of ChartStream. Either select "Load Setup" to modify an existing setup or start with the select analog option. The channels currently turned on as well as any calculated values or look-up values will be displayed on the screen.

Configuring the Analog Channels:

The option to select for configuring the analog channels is "Select Analog."

The voltage range for the setup is set by the **F8** key; this setting affects all channels. The options are ±5 V, ±10 V, and 0 to 10 V. The **F7** key changes the inputs from single-ended to double-ended inputs and vice versa. Each channel's characteristics can be changed by either selecting it by the mouse or by highlighting it via the arrow keys. Once highlighted the channel can be activated, the gain changed, or its label changed. To make a label for a channel, first select the channel, then press **F5** to clear the current label, and finally type your own label. Avoid the use of mathematical terms and functions as labels.

Channels that are turned on have their channel number highlighted. These activated channels are the only channels that will be recorded and displayed. Channels can be turned on or off by the **F3** or **F4** key. Each channel can have a different gain set

for it. The **F2** key changes the gain for the selected channel. The gain settings are 1, 10, 100, or 200. Gains of 100 or 200 will reduce the maximum scanrate to 50 kHz or 25 kHz, respectively.

Pressing **F10** will exit from this menu and return to the "Create Test Set Up" menu. At this point you should select **F10** again and save the setup.

Using Calculated and Table Parameters in the Setup:

Simple equations can be built from constants and channel inputs. These equations are stored in the Calculation Library. These equations can then be turned on and included in the displayed and recorded data. Look-up tables are created in the Table Library. A table of input and output values is created for the computer to use. To use the calculated and table values in the test setup select from the menu : "Select Calcs."

Two lists are presented on the screen. Turn the desired calculated or table parameters on by "clicking" on them with the mouse or by highlighting them with the arrow keys and pressing enter. Parameters turned on will have a ">" to the left of the item. A total of 12 parameters are permitted in a test setup.

You can access the Calculation and Table Libraries by pressing the **F4** or **F5** keys, respectively. While in the library, equations can be created and modified or look-up tables can be set up.

After finishing with this section, return to the setup menu by pressing **F10**. Do not forget to save your work by pressing **F10** again.

Changing the Default Scales for Real-Time Charts

Selecting **F4**: "Default Scales" will bring up a screen where the minimum and maximum values for the channel's strip chart can be individually set.

Configuring Real-Time Display Options:

Selecting **F5**: "Config RT" brings up the Data Acquisition Options screen. These options are described in the earlier section "Real-Time Display Guide."

255

Changes to these settings will become the default settings for the setup file being created, provided that the changes are saved. When the setup is run for data acquisition, the program will ask if the user wishes to use the default settings or configure a new display. The default settings are the configurations being created at this time, during "Create New Test Setup."

Once the user is finished creating the test setup make sure it is completely saved by selecting **F10**: "Save Setup" again. Once this is done, exit to the main menu by pressing the **Esc** key.

To collect data from the setup created, select "Acquire Data" from the main menu and then select the appropriately named setup from the list.

Other Features:

Table and Calculation Libraries are accessible through the Utilities in the main menu and in the "Create Test Set Up" menu. Once in these libraries, equations can be created and look-up tables can be set up. Alarms can be created, changed, turned on and off from the Utilities menu. Signals can be displayed for troubleshooting purposes as well as calibration of the channels. Special signal conditioning can be specified for different sensors. These features as well as others are explained in detail in the Users Manual.

Using Chartstream™ analyzer to convert and display data

This manual will not go into detail about the workings of ChartStream Analyzer. Directions will be given to load data, plot the data, and export the data into ASCII format.

Loading Data:

Select the "File Menu" from the Functions list on the right side of the screen.

Select "Load a New Primary File" from the menu and then select the appropriate ChartStream data file (with the extension .DAT). Note that the data collected during data acquisition must be converted to ChartStream format first before loading them into ChartStream Analyzer.

Exporting Data in ASCII:

After loading the desired ChartStream data file, select the "File Menu" again. Select "Export a Primary File" from the next menu. Select ASCII Column from the menu. Check "include time" to make the first column time in seconds followed by each channel in column format. The first row of each column is the label associated with that channel or parameter.

The width of each column and the method in which each column is separated can also be specified. Also, a portion of the file can be exported instead of the entire file.

Note: To use the ASCII file in MATLAB, the first row must be removed from the file. This is not possible within the ChartStream program.

Graphing Data:

The main screen of ChartStream Analyzer is divided into several sections.

The top section lists all the channels and parameters from the primary file available for plotting as well as a few special parameters in the upper-right corner. The middle section is a list of what parameters make up the current graph. The first column is a reference number. If the parameters in the X and Y columns are to be plotted, then the reference number must be highlighted. The second column contains the data file that contains the parameter. This file can be changed and new parameters picked for each reference number. This allows different data files to be compared for analysis. Columns for X and Y are for the parameters to be selected from the top section of the screen. This is accomplished through the mouse. Scaling and smoothing can also be set for each reference plot number. The lower-right corner lists the menu options available for ChartStream Analyzer. The bottom part of the screen controls what type of graph is being plotted. The scanrate, length of plot, and plot title are specified in this area.

Once the options for the graph are determined, select "Make Graph" from the menu.

Once plotted, the data file can be played to the end of the file using the play button. Other options include: zoom, pan, save, recall, print, add text, and stats.

257

TEST DATA STORAGE AND BACKUP

In most cases of DYNTRAC and road testing, the amount of data to be recorded will exceed the storage within the Dolch's hard drive. The magneto-optical drive should be used to download data from the Dolch for storage. During testing, the binary files should be converted to ASCII format before downloading. If it is also convenient, the header should be removed from the ASCII file before downloading. At no time should the data files be zipped or compressed in any way. The data files should be copied from the Dolch hard drive to optical disk using the following command:

XCOPY /V C:\path\filename.ext D:\path*.*

After copying the desired files, check that the copy file matches the original file by using the following command:

FC C:\path\filename.ext D:\path*.*

If any differences between files are detected, check the quality of the original file and then recopy the entire set.

This entire process should be done twice, producing two disks with the same files on each disk. Once both sets of files are checked with the originals in the Dolch, the Dolch disk space can be erased for the next set of data. If space permits, copy the binary files as well. If this cannot be done, after the ASCII files are backed up and checked, the raw data files can be removed as well. **This procedure is most important; do not remove any files without making two copies and verifying the accuracy of the copy!**

Make sure to note any changes in the setup or truck configuration during testing. Explain any problems encountered in detail and how they were overcome.

REFERENCES

[1]   D. A. Streit and B. T. Kulakowski, *Dynamic Vehicle Forces on Pavements, First Interim Report*. FHWA Contract No. DTFH61-90-C-00084, Pennsylvania Transportation Institute, Publication No. PTI 9437, The Pennsylvania State University, University Park, PA, January 1993.

[2]   D. A. Streit and B. T. Kulakowski, *Dynamic Vehicle Forces on Pavements, Second Interim Report*. FHWA Contract No. DTFH61-90-C-00084, Pennsylvania Transportation Institute, Publication No. PTI 9437, The Pennsylvania State University, University Park, PA, January 1994.

[3]   D. A. Streit and B. T. Kulakowski, *Dynamic Vehicle Forces on Pavements, Equipment Report*. FHWA Contract No. DTFH61-90-00084, Pennsylvania Transportation Institute, The Pennsylvania State University, PA, March 1991.

[4]   R. Wollyung, D. Streit, and B. Kulakowski, "Dynamic Wheel Scales for Heavy Vehicle Road Simulators." *International Journal of Vehicle Design* 3 (1-4): pp. 450-472 (1996).

[5]   D. J. Cole and D. Cebon, "Spatial Repeatability of Dynamic Tire Forces Generated by Heavy Vehicles." *Proceedings of the Institution of Mechanical Engineers*. 206, pp. 17-27 (1992).

[6]   D. J. Cole and D. Cebon, "Assessing the Road-Damaging Potential of Heavy Vehicles." *Proceedings of the Institution of Mechanical Engineers*. 205, Part D (1991).

[7]   D. Cebon, "Vehicle-Generated Road Damage: A Review." *Vehicle Systems Dynamics* 18 (1-3) (1989).

[8]   T. D. Gillespie and S. Karamihas, "Truck Factors Affecting Dynamic Loads and Road Damage." *Third International Symposium on Heavy Vehicle Weights and Dimensions*. Cambridge, UK (July 1992).

[9]   C. B. G. Mitchell and L. Gyenes, *Dynamic Pavement Loads Measured For a Variety of Truck Suspensions*. Transport and Road Research Laboratory, Crowthorne, Berkshire, England (May 1989).

[10]   P. F. Sweatman, "A Study of Dynamic Wheel Forces in Axle Group Suspensions." *ARRB*, Special Report No. 27 (1983).

[11]   L. Segel, T. E. Gillespie, et al., "The Mechanical and Kinematic Properties of Heavy Vehicle Suspensions." *Mechanics of Heavy-Duty Trucks and Truck Combinations*, Engineering Summer Conferences, The University of Michigan, College of Engineering (June 1984).

[12]   M. W. Sayers, T. D. Gillespie, and W. D. O. Paterson, "Guidelines for Conducting and Calibrating Road Roughness Measurements." *World Bank Technical Paper*, Paper No. 46, The World Bank, Washington, D.C. (1986).

259

[13] J. Anstrom and D. A. Streit, "Economical Longitudinal/Lateral Vehicle Tracking System." *Heavy Vehicle Systems, International Journal of Vehicle Design* 1 (4): pp. 445-448 (1994).

[14] S. Gore, "Performance and Tuning of Hydraulic Actuation Systems and a Modified Pavement Roughness Index for Heavy Vehicles." A Paper in Mechanical Engineering, The Pennsylvania State University, December 1994.

[15] N. Parikh, "Testing and Calibration of the Wheel Force Transducer." Master's Thesis, The Pennsylvania State University (1997).

[16] C. C. MacAdam, P. S. Fancher, G. T. Hu, and T. D. Gillespie, *A Computerized Dynamics of Trucks, Tractor Semi-Trailers, Doubles, and Triples Combinations: User Manual - Phase 4.* Report UMHSRI-80-58, University of Michigan Highway Safety Research Institute, Ann Arbor, Michigan (1980).

[17] W. J. Kenis and J. Hammouda, "A Sensitivity Study of Some Existing Truck Dynamic Simulation Programs." Presented at the Third Engineering Foundation Conference on Vehicle-Road and Vehicle-Bridge Interaction, Noordwijkerhout, Netherlands (June 5-10, 1994).

[18] K.B. Todd and B. T. Kulakowski, "Simple Computer Models for Predicting Ride Quality and Pavement Loading for Heavy Trucks." *Transportation Research Record* 1215, pp. 137-150 (1989).

[19] Y. R. Ho, "Identification of Linear and Nonlinear Models of Heavy Trucks." M.Sc. Paper in Mechanical Engineering, The Pennsylvania State University (1994).

[20] M. D. Casciani, "Identification of Certain Parameters of a Straight Truck Using a Dynamic Truck Actuator Simulator." M.Sc. Thesis, Department of Mechanical Engineering, The Pennsylvania State University, University Park, PA (1992).

[21] J. L. Shearer, B. T. Kulakowski, and J. F. Gardner, *Dynamic Modeling and Control of Engineering Systems.* Second Edition, Prentice Hall, Englewood, NJ (1997).

[22] D. Cebon, *Interaction Between Heavy Vehicles and Roads.* SAE SP-951, 930001 (1993).

[23] OECD Scientific Expert Group, *Dynamic Loading of Pavements.* OECD Road Transport Research. Final report, Paris (1992).

[24] D. J. Cole and D. Cebon, "Validation of an Articulated Vehicle Simulation." *Vehicle Systems Dynamics* 21 (4): pp. 197-224 (1992).

[25] S. M. Karamihas, T. D. Gillespie, and S. M. Riley, "Axle Tramp Contribution to the Dynamic Wheel Loads of a Heavy Truck." *Proceedings of the Fourth International Symposium on Heavy Vehicle Weights and Dimensions*, C. B. Winkler, Ed., University of Michigan, pp. 425-434 (1995).

[26] K. J. Hedrick, *The Simulation of Vehicle Dynamic Effects on Road Pavements.* Report to the Federal Highway Administration No. FHWA-RD90-108, University of California, Berkeley, CA (1992).

[27] M. W. Sayers, "Symbolic Computer Language for Multibody Systems." *Journal of Guidance, Control, and Dynamics* 14 (6): pp. 1153-1163 (1991).

[28] M. W. Sayers, "Symbolic Vector/Dyadic Multibody Formalism for Tree-Topology Systems." *Journal of Guidance, Control, and Dynamics* 14 (6): pp. 1240-1250 (1991).

[29] K. J. Hedrick, K. Yi, and M. Wargelin, *Advanced Suspensions for Heavy Vehicles.* Final Report, Vehicle Dynamics and Control Laboratory, Department of Mechanical Engineering, University of California, Berkeley, CA (1993).

[30] T. L. Ford and J. Zekoski, "Impact of Truck Tire Selection on Contact Pressures." Presented at the Paving and Transportation Conference, Symposium on Pavement Rutting, The University of New Mexico (January 1988).

[31] M. Huhtala and J. Phiajamaki, "Truck Tires and Pavements." *Proceedings of the Third International Conference on Bearing Capacity of Roads and Airfields,* vol.2, Trondheim, Norway (3-5 July, 1990).

[32] J. Krarup, This is the paper by J. Krarup presented at the 1992 Engineering Foundation Conference in Santa Barbara, *ASTM Proceedings,* ed. by B. T. Kulakowski.

[33] D. Cebon, "Vehicle-Generated Road Damage." *Vehicle System Dynamics* 18, pp.107-150 (1989).

[34] J. De Pont, "Experiences with Simulating On-Road Heavy Vehicle Suspension Behaviour Using Servo-Hydraulics." Presented at the Third Engineering Foundation Conference on Vehicle-Road and Vehicle-Bridge Interaction, Noordwijkerhout, Netherlands (June 1994).

[35] M. W. Sayers, "On the Calculation of IRI from Longitudinal Road Profile." In *Transportation Research Board, Annual Meeting.* Preprint No. 950842. Washington, D.C. (1995).

[36] J. Eisenmann, D. Birmann, and A. Hilmer, "Effects of Commercial Vehicle Design on Road Stress - Research Results Relating to the Roads." *Straße und Autobahn,* No. 6, pp. 238-244 (1986).

[37] E. B. Spangler and A. G. Girardi, "Measurement and Analysis of Airside Pavement Roughness at the Dallas/Forth Worth International Airport." *Proceedings of the Conference on Airport Pavement Innovations Theory to Practice,* American Society of Civil Engineers, Vicksburg, Mississippi, pp. 329-346 (1993).

[38] T. D. Gillespie, *Fundamentals of Vehicle Dynamics.* Society of Automotive Engineers, Warrendale, PA (1992).

[39]   A. C. Collop and D. Cebon, "A Model of Whole-Life Flexible Pavement Performance." *Proceedings of the Institution of Mechanical Engineers, Part C, Journal of the Mechanical Engineering Society* 6, pp. 389-407 (1995).